ACTIVE STRUCTURAL CONTROL

THEORY & PRACTICE

T T SOONG

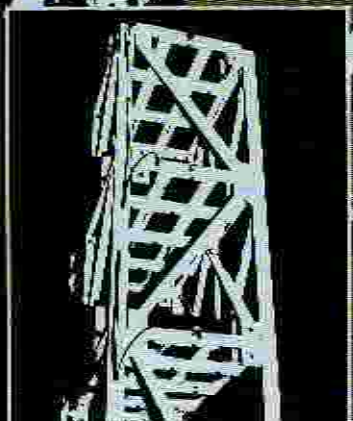

Active Structural Control: Theory and Practice

T T Soong
Department of Civil Engineering
State University of New York at Buffalo

Advisory Editor
W F Chen
School of Civil Engineering
Purdue University

Longman Scientific & Technical
Copublished in the United States with
John Wiley & Sons, Inc., New York

Longman Scientific & Technical
Longman Group UK Limited,
Longman House, Burnt Mill, Harlow,
Essex CM20 2JE, England
and Associated Companies throughout the world.

Copublished in the United States with
John Wiley & Sons, Inc., 605 Third Avenue, New York, NY 10158

First published 1990

British Library Cataloguing in Publication Data
Soong, T. T.
Active structural control.
1. Structures.Control
I. Title
624.1

ISBN 0-582-01782-3

Library of Congress Cataloging-in-Publication Data
Soong, T. T.
Active structural control : theory and practice / T.T. Soong ;
advisory editor, W. Chen.
p. cm.
Includes bibliographical references.
ISBN 0-470-21670-0
1. Structural engineering. 2. Control theory. I. Title.
TA636.S66 1990
624.1'771--dc20 89-13859
CIP

Typeset in 10/12 pt Monotype Times Roman

Printed and Bound in Great Britain
at the Bath Press, Avon

To Professor John L Bogdanoff

Teacher, Mentor, and Friend

Contents

Preface

Natural hazard mitigation is one of the most important issues facing civil engineers today. Many of us have experienced the feeling of helplessness when our homes or offices were shaken uncontrollably by earth tremors. All of us have witnessed through television and other news media the vast destruction of properties and tragic loss of lives caused by an earthquake, a hurricane, a fire or a flood. In structural engineering, one of the constant challenges is to find new and better means of protecting structures and constructed facilities from the damaging effects of destructive environmental forces. One avenue open to the researchers and designers is to introduce more conservative designs so that structures such as buildings and bridges are better able to cope with large external loads. This approach, however, can be untenable both technologically and economically. Another possible approach is to make structures behave more like machines, aircrafts, or human beings in the sense that they can be made adaptive or responsive to external forces. Structural muscles, so to speak, can be flexed when warranted, or appropriate adjustments can be made within the structure as environmental conditions change. This latter approach has led to active structural control research and has opened up a new field of investigation, which began more as an intellectual curiosity in the early 1970s but now is at the stage where large-scale experimentation is underway and actual active control systems have been designed and installed in full-scale structures.

Another reason that active structural control has been receiving an increasing amount of attention has to do with rapid advances that have been taking place in allied technologies. The development of the active control concept must go hand-in-hand with advances in areas such as computers, electronics, measurement techniques, instrumentation, controllers, actuators, materials, etc. Current phenomenal advances in all these areas have given added impetus to the development of active control technology. They also reflect favourably on the all-important cost factor.

On the basis of the analytical and experimental results obtained to date, it appears evident that, technologically, fully automated active systems are within sight of becoming a reality. At the same time, however, a large number of serious obstacles remain and they must be overcome before active structural

control can gain general acceptance by the civil engineering and construction professions at large. This brings us to the purpose of writing this book. It is intended to introduce to the interested reader basic principles involved in the theory of active structural control, to bring together in one volume a wealth of information documenting progress that has been made to date, and to address implementational issues. It is hoped that the material in this book will provide the reader with some added degree of understanding and maturity so that he or she may better delineate important issues involved and pursue further studies in this exciting and fast expanding field.

T T Soong
Buffalo, New York
August, 1989

Acknowledgements

My work in this research area has been supported since 1976 by the National Science Foundation. This continuing support is gratefully acknowledged. Since 1986, funding for my active control research has been shared by the National Science Foundation and the State of New York under the auspices of the National Center for Earthquake Engineering Research. I am also grateful to NATO, US–Spain Joint Committee for Science and Technological Cooperation, and Humboldt Foundation for their generous support of this work. This book first took shape when I was associated with the Curt-Risch-Institut, University of Hannover, under the Humboldt Foundation Senior US Scientist Award Program.

Industrial participation and contributions were also important to the success of this research effort, particularly during the large-scale experimental phase. It is a pleasure to acknowledge support received from the MTS Systems Corporation, the Takenaka Corporation of Japan and Kayaba Industry Ltd of Japan.

I am indebted to many of my colleagues with whom I have collaborated over many years. Professor James T P Yao of Texas A&M University introduced me to this research topic and provided invaluable guidance throughout. Professor A M Reinhorn has been my close associate at the State University of New York at Buffalo and has made invaluable contributions to our joint research programs. Professors J Rodellar and A H Barbat of the Technical University of Catalunya were kind enough to review earlier drafts of this book and made improvements. I have also learned a great deal about active control from the late Professor H H E Leipholz of the University of Waterloo and from Professor J N Yang of the George Washington University.

I have also had the good fortune of working with some of the most talented students on various active control projects. A vote of sincere thanks to C Martin, L L Chung, Z Prucz, R C Lin and S McGreevy.

My sincere thanks also go to my secretary, Mrs Carmella Gosden, who expertly and unflinchingly typed hundreds of pages of text and equations, and uncomplainingly made revision after revision.

Finally, I owe a special debt of gratitude to my wife, Dottie, who, for the fourth time, endured with good humour and provided unwavering support to this writing project.

Acknowledgements

We are indebted to the following for permission to reproduce copyright material:

American Society of Civil Engineering for figs 3.1 & 3.18–3.22 from figs 1, 2, 3, 6, 7, 11 (Yang, Akbarpour & Ghaemmaghami, 1987), figs 3.2, 3.5–3.7 & 4.6 from figs 1, 2 & 6–8 (Chung, Reinhorn & Soong, 1988), figs 3.8–3.12 from figs 2 & 5–8 (Yang, 1975), figs 3.13 & 3.14 from figs 3 & 4 (Martin & Soong, 1976), fig. 4.5 from fig. 5 (Pu, 1989), figs 4.22 & 4.23 from figs 1 & 2 (Pantelides & Cheng, 1989), figs 5.2–5.4 from figs 1 & 2 (Reinhorn & Soong, 1989), fig. 5.24 from fig. 3(a) (Yang, 1982), fig. 5.28a & b from figs 12 & 13 (Miller, Masri, Dehghanyar & Caughey, 1988), figs 5.32 & 5.33 from figs 5 & 6 (Soong & Skinner, 1981), figs 6.1–6.4 from figs 1–4 (Soong & Manolis, 1987) and figs 6.5–6.12 from figs 2–9 (Cha, Pitarresi & Soong, 1988); American Society of Mechanical Engineers for figs 3.24, 3.25, 3.27, 3.29 & 3.30 from figs 1–5 (Prucz, Soong & Reinhorn, 1985); Butterworth Scientific Ltd. and the author, Professor F Kozin for figs 3.15–3.17 from figs 2 & 4 (Wang, Kozin & Amini, 1983); Kajima Corporation for figs 5.22a & b, 5.26a & b & 5.27; E & F N Spon for fig. 4.33 from fig. 3 (Basharklah & Yao, 1984); Takaneka Corporation for figs 5.16, 5.19a & b and 5.25a & b; one of the authors, Professor S F Masri for figs 5.29, 5.30 & 5.31 from pp. 447–52 (Traina *et al.*, 1988).

1 Introduction

It is common knowledge that civil engineering structures must withstand ever-changing environmental loads, such as wind, earthquakes and waves, over the span of their useful lives. Yet, until very recently, buildings, bridges, and other constructed facilities have been built as passive structures that rely on their mass and solidity to resist outside forces, while being incapable of adapting to the dynamics of an ever-changing environment. Indeed, 'solidity' and 'massiveness' have often been equated to 'safety' and 'reliability'. In recent years, however, a number of factors have emerged that signal the need for considering structures with some degree of adaptability or responsiveness. These factors include the following:

1 *Increased flexibility*: With the trend towards taller, longer and more flexible structures, undesirable vibrational levels could be reached under large environmental loads, thus adversely affecting human comfort and even structural safety.
2 *Increased safety levels*: Higher safety levels are demanded as structures become more complex, more costly, and serve more critical functions. Examples are tall structures, deep-water offshore platforms, and nuclear power plants. In these cases, conventional reliability criteria are no longer adequate and failure is synonymous with disaster.
3 *Increasingly stringent performance requirements*: Within safety limits, conventional structures are allowed to deform and even sustain local damage if necessary. Structures are increasingly required, however, to operate within strict performance guidelines such as alignment or shape constraints. Examples in this area are radar tracking stations, radio telescope structures, and aerospace structures.
4 *Better utilization of material and lower cost*: Partly due to the considerations just given, and partly due to economic consideration, it is clear that savings in materials, weight, and cost are not only desirable but necessary. This is especially true for structures in space and for portable structures used in military applications.

As a result, new concepts of structural protection and structural motion control, such as supplemental damping, passive control and active control,

have been advanced and are at various stages of development. In the area of passive systems, they include base isolation systems against earthquake loads, tuned mass dampers and fluid sloshing damper systems against wind, and a variety of mechanical energy dissipaters such as bracing systems, friction dampers, viscoelastic dampers and other mechanical dampers. In the active system area, active mass dampers, active mass drivers, active tendon systems, pulse thrusters, and active variable stiffness systems are some of the devices being developed and tested both in the laboratory, and in some cases, in actual structural applications.

The operating principle of a passive protective system is now adequately understood; less so, however, for active systems. In structural engineering, 'active structural control' has become known as an area of research in which the motion of a structure is controlled or modified by means of the action of a control system through some external energy supply. Active systems are presently under close scrutiny in terms of their future structural applicability stemming from a number of motivating factors. They include the following:

1 As mentioned earlier, with the advent of new materials and new construction methods, structures are becoming taller, longer and more flexible. The application of active control is one of the options in safeguarding such structures against excessive vibrations. In fact, 'super-tall' buildings with up to 500 storeys are being considered as possibilities in the near future,[1,2] for which control systems, either active or passive, may become an integral part.

2 Active or hybrid active–passive systems can be attractive candidates for retrofitting or strengthening existing structures against, for example, earthquake hazards. Current passive means of using interior shear walls or base isolation systems are structurally invasive. Active systems, on the other hand, can be more effective and can be incorporated into an existing structure with less interference. In a report prepared for the National Research Council addressing research issues based on lessons learned from the 1985 Mexico earthquake,[3] research on retrofit of buildings using devices which 'might increase damping or modify the natural period' is recommended. This objective can be easily achieved using active or active–passive systems.

3 Civil engineering structures are not designed to withstand all possible external loads. However, extraordinary loading episodes do occur, resulting in structural damage or even failure. Active control in this context can mean a last resort attempt to save a structure which, without it, would not be able to survive. This extra protection is particularly attractive when one considers the high cost of some recent large structures such as deep-water offshore platforms, not even mentioning lives that might be lost otherwise. The same is true for structures which serve critical functions such as hospitals and nuclear power plants.

4 Some structures house valuable and sensitive equipment or secondary systems. Their operating safety is of paramount importance. Active control can thus be applied at the substructure level to ensure proper operating conditions for secondary systems.
5 Passive control devices such as base isolation systems, viscoelastic dampers and tuned mass dampers, have been installed in some existing structures, resulting in improved structural performance. Passive devices, however, have inherent limitations. Consider, for example, the tuned mass damper system installed in the Citicorp Center, New York.[4,5,6] Since it is tuned to the first modal frequency of the structure, it is basically designed to reduce only the first mode vibration. An active mass damper, on the other hand, can be effective over a much wider frequency range. Hence, the study of active structural control is a logical extension of passive control technology.
6 Finally, the idea of active control itself is not only attractive, but potentially revolutionary, since it elevates structural concepts from a static and passive level to one of dynamism and adaptability. One can envisage future structures having two types of load resisting members: the traditional passive members that are designed to support basic design loads, and active members whose function is to augment the structure's capability in resisting extraordinary loads. Their integration in an optimal fashion can conceivably result in better utilization of material and lower cost.[7-9]

Thus motivated, there has been a flurry of research activities in the area of active control of civil engineering structures over the last 20 years. In this book, an attempt is made to provide the reader with a working knowledge of this exciting and fast expanding field. Moreover, current research and development work in active control is brought up-to-date as much as possible.

1.1 Organization

The material of this book flows from theoretical background to practical considerations to implementational issues. Chapters 2 and 3 are concerned with the fundamental principles of active structural control and with the development of control algorithms suitable for structural control applications. Topics in these chapters are better understood when the reader has a working knowledge of elementary structural dynamics, random vibration, systems theory and control theory. Of the above knowledge areas, theoretical aspects of systems and control theory may not be familiar to some of the readers. Consequently, a brief introduction and a summary of results in linear control systems are given in Appendix A, together with a list of useful references.

Chapter 4 deals with practical considerations in control implementation. Issues addressed in this chapter include modelling errors, time delay in control execution, inelastic structural behaviour, and problems arising from hardware and computational limitations.

As mentioned earlier, several control devices are being actively considered for structural applications. In fact, large-scale testing is underway for some active structural control systems and, at least in one case, full-scale structural implementation has taken place. Discussions in Chapter 5 centre around some of these feasible control schemes with emphasis on their performance in the laboratory.

Actively controlled structures are a new strain of structural systems and their optimization takes on an added dimension in scale as well as in complexity. In Chapter 6, this optimization problem is addressed from one particular point of view. It is hoped that this brief exploration will lead to more serious investigations into many fascinating aspects of this challenging problem.

Finally, it should be pointed out that, since many references were used in the development of this book, no attempt was made to unify the units of quantities used in the text and in the examples. It was felt that, to leave them in their original units, easier reference to the original publications could be made. For convenience, a conversion table for English-unit to SI-unit conversion is provided in Appendix B.

References

1. Supertall Structures, the Sky's the Limit. *Engineering News Record* November 1983
2. Tucker J B 1985 Superskyscrapers: Aiming for 200 Storeys. *High Tech* **5** pp 50–63
3. NRC Committee on Earthquake Engineering *Research Agenda: Learning from the 19 September 1985 Mexico Earthquake* National Research Council, Washington DC 1986
4. Petersen N R 1980 Design of Large Scale Tuned Mass Dampers. In Leipholz H H E (ed) *Structural Control* North Holland, Amsterdam pp 581–96
5. Tuned Mass Damper Steady Sway of Skyscraper in Wind. *Engineering News Record* 28–9 August 1977
6. Wiesner K B 1979 Tuned Mass Dampers to Reduce Building Wind Motion Preprint 3510 ASCE Convention Boston
7. Soong T T and Manolis G D 1987 On Active Structures. *ASCE Journal of Structural Engineering* **113** pp 2290–301
8. Soong T T and Pitarresi J M 1987 On Optimal Design of Active Structures. In Jenkins D R (ed) *Computer Applications in Structural Engineering* ASCE NY pp 579–91
9. Cha J Z, Pitarresi J M and Soong T T 1988 Optimal Design Procedures for Active Structures. *ASCE Journal of Structural Engineering* **114** pp 2710–23

2 Actively Controlled Structures

Some early notions of an actively controlled structure are contained in work by Zuk[1,2] in which the notion of 'kinetic structures' is advanced. Zuk made the distinction between active controls which are designed to reduce structural motion and those which generate structural motion. The kinetic structures described by Zuk belong to the latter. Conceptually, Zuk visualizes all manner of buildings as being able to change form, shape, and configuration in order to make themselves adaptable to ever-changing forces and functional usages. For example, a building could be compactly prepackaged in a factory, and conveniently transported to the site. At the site, it would be energized, causing it to self-deploy or erect itself by means of control systems. Similarly, one can envisage structures which are self-collapsing, reversible, or are able to change shape, or control enclosed space through structural manipulation by means of control devices.

The topic addressed in this book, however, belongs to the first category, namely, controls designed to reduce structural motion. According to Zuk,[3] the earliest attempts in this direction were made in the 1960s when Eugene Freyssinet proposed in 1960 to use prestressing tendons as control devices to stabilize tall structures. Independently, Lev Zetlin in 1965 conceived the idea of designing tall buildings, whereby cables are fixed to the structural frame and attached to hydraulic jacks at the base. Sensors are used to detect movement at the top of the structure and to signal a control device which, in turn, directs the action of the jacks. Unfortunately, neither structure was built. Other early attempts include that of Kobori and Minai,[4] who advocated the concept of 'dynamic intelligent buildings' capable of executing active response control when they are subjected to severe earthquakes. Nordell[5] also suggested the use of active systems which can be activated to provide increased strength to a structure prior to any 'exceptional' overloading. Two examples of such systems are sketched in Figs 2.1 and 2.2. A movable diagonal bracing system is shown in Fig. 2.1. In its active state, the diagonal bracings would increase the lateral resistance of the structure in resisting exceptional loadings. As it was conceived, the bracing scheme would be manually activated. Similar concepts for movable columns, walls or trusses could also be envisaged and Fig. 2.2 provides such an example. The columns in their active state would increase both the lateral and vertical resistanee.

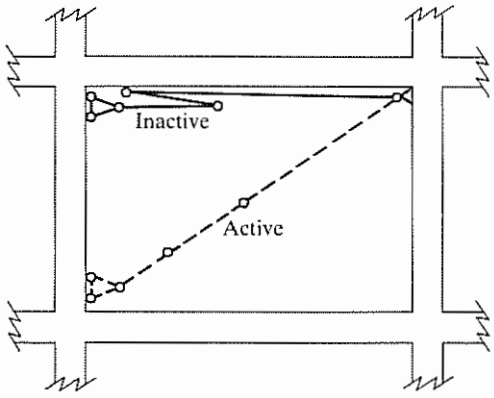

Figure 2.1 Hinged bar bracing system[5]

A systematic assault on active control research did not begin until 1972, when Yao laid down a more rigorous control-theory based concept of structural control.[6] In this an excessive-response triggered structural control system is suggested as an alternative approach to addressing the safety problem in structural engineering.

As described by Yao and in most of the subsequent research and development work, an active structural control system has the basic configuration as shown schematically in Fig. 2.3. It consists of:

1 Sensors located about the structure to measure either external excitations, or structural response variables, or both.

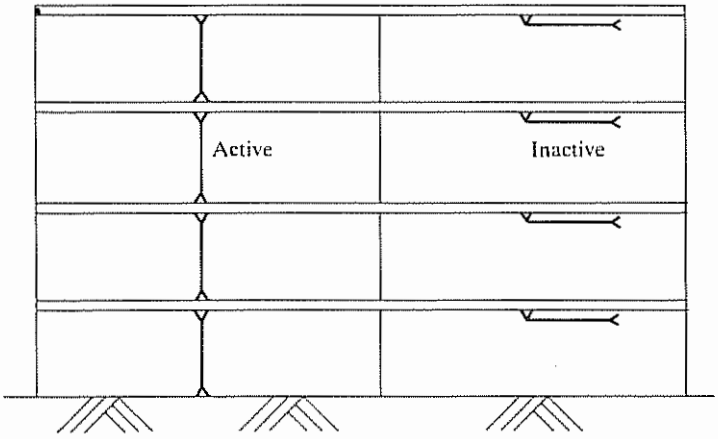

Figure 2.2 Movable columns[5]

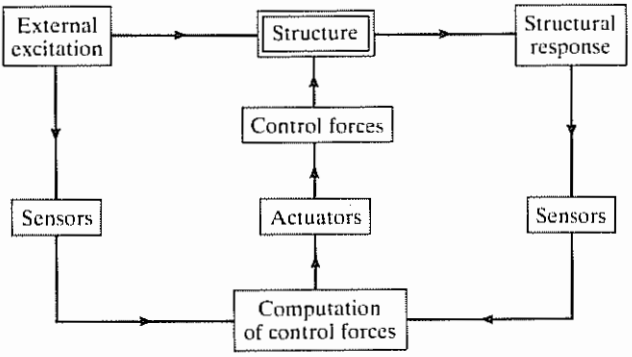

Figure 2.3 Schematic diagram of active control

2 Devices to process the measured information and to compute necessary control forces needed based on a given control algorithm.
3 Actuators, usually powered by external energy sources, to produce the required forces.

When only the structural response variables are measured, the control configuration is referred to as closed-loop control since the structural response is continually monitored and this information is used to make continual corrections to the applied control forces. An open-loop control results when the control forces are regulated only by the measured excitation. In the case where the information on both the response quantities and excitation are utilized for control design, the term closed–open-loop control is used in the literature.

To see the effect of applying such control forces to a structure under ideal conditions, consider a building structure modelled by an n-degree-of-freedom lumped mass-spring-dashpot system. The matrix equation of motion of the structural system can be written as

$$\boldsymbol{M}\ddot{\boldsymbol{x}}(t) + \boldsymbol{C}\dot{\boldsymbol{x}}(t) + \boldsymbol{K}\boldsymbol{x}(t) = \boldsymbol{D}\boldsymbol{u}(t) + \boldsymbol{E}\boldsymbol{f}(t) \tag{2.1}$$

where $\boldsymbol{M}$, $\boldsymbol{C}$ and $\boldsymbol{K}$ are, respectively, the $n \times n$ mass, damping and stiffness matrices, $\boldsymbol{x}(t)$ is the n-dimensional displacement vector, $\boldsymbol{f}(t)$ is an r-vector representing applied load or external excitation, and $\boldsymbol{u}(t)$ is the m-dimensional control force vector. The $n \times m$ matrix $\boldsymbol{D}$ and $n \times r$ matrix $\boldsymbol{E}$ are location matrices which define locations of the control force and the excitation, respectively.

Suppose that the closed–open-loop configuration is used in which the control force $\boldsymbol{u}(t)$ is designed to be a linear function of the measured displacement vector $\boldsymbol{x}(t)$, the velocity vector $\dot{\boldsymbol{x}}(t)$ and the excitation $\boldsymbol{f}(t)$. The

control force vector takes the form

$$u(t) = K_1 x(t) + C_1 \dot{x}(t) + E_1 f(t) \tag{2.2}$$

where K_1, C_1 and E_1 are respective control gains which can be time-dependent.

The substitution of Eq. (2.2) into Eq. (2.1) yields

$$M\ddot{x}(t) + (C - DC_1)\dot{x}(t) + (K - DK_1)x(t) = (E + DE_1)f(t) \tag{2.3}$$

Comparing Eq. (2.3) with Eq. (2.1) in the absence of control, it is seen that the effect of closed-loop control is to modify the structural parameters (stiffness and damping) so that it can respond more favourably to the external excitation. The effect of the open-loop component is a modification (reduction or total elimination) of the excitation. The choice of the control gain matrices K_1, C_1 and E_1 depends on the control algorithm selected.

We see that the concept of active control is immediately appealing and exciting. On one hand, it is capable of modifying properties of a structure in such a way as to react to external excitations in the most favourable manner. On the other hand, direct reduction of the level of excitation transmitted to the structure is also possible through active control.

In the development of an active structural control concept, one of the first tasks at hand is to develop suitable control laws such as that given by Eq. (2.2). Some of the commonly used control algorithms for structural applications are discussed in Chapter 3. For readers who are versed in control theory, it is readily apparent that the basic concepts of active control are not new; they have been the staple of electrical and control engineering for many decades. And they have been applied successfully in a variety of disciplines such as aerospace engineering and mechanical engineering. More recently, motion control of large space structures has also been a subject of intensive research. However, active control of civil engineering structures, as indicated above, has a more recent origin. While much of the theoretical basis is rooted in modern control theory, as we shall see, its application to civil engineering structures is unique in many ways and presents a host of new challenges.

References

1. Zuk W 1968 Kinetic Structures. *Civil Engineering* **39** pp 62–4
2. Zuk W and Clark R H 1970 *Kinetic Architecture* Van Nostrand Reinhold, New York
3. Zuk W 1980 The Past and Future of Active Structural Control Systems. In Leipholz H H E (ed) *Structural Control* North Holland, Amsterdam pp 779–94

4. Kobori T and Minai R 1960 Analytical Study on Active Seismic Response Control. *Transactions of the Architectural Institute of Japan* No. 66 (in Japanese)
5 Nordell W J 1969 *Active Systems for Elastic-Resistant Structure* Technical Report R-611, Naval Civil Engineering Laboratory, Port Hueneme, CA
6 Yao J T P 1972 Concept of Structural Control. *ASCE Journal of Structural Division* **98** pp 1567–74

3 Control Algorithms

Research efforts in active structural control have been focused on a variety of control algorithms based on several control design criteria. Some are considered classical as they are direct applications of modern control theory. Others, however, are specifically proposed for civil engineering structural control applications due to the fact that, as mentioned earlier, they give rise to some unique control problems.

To facilitate discussions, let us again use Eq. (2.1) to represent the structure under consideration which, using the state-space representation as discussed in Appendix A, can be written in the form

$$\dot{z}(t) = Az(t) + Bu(t) + Hf(t), \qquad z(0) = z_0 \tag{3.1}$$

where

$$z(t) = \begin{bmatrix} x(t) \\ \dot{x}(t) \end{bmatrix} \tag{3.2}$$

is the $2n$-dimensional state vector,

$$A = \begin{bmatrix} 0 & I \\ -M^{-1}K & -M^{-1}C \end{bmatrix} \tag{3.3}$$

is the $2n \times 2n$ system matrix, and

$$B = \begin{bmatrix} 0 \\ M^{-1}D \end{bmatrix} \quad \text{and} \quad H = \begin{bmatrix} 0 \\ M^{-1}E \end{bmatrix} \tag{3.4}$$

are $2n \times m$ and $2n \times r$ location matrices specifying, respectively, the locations of controllers and external excitations in the state-space. In Eqs (3.3) and (3.4), $\mathbf{0}$ and I denote, respectively, the null matrix and the identity matrix of appropriate dimensions. Matrices D and E in Eq. (3.4) are defined in Chapter 2.

3.1 Classical Linear Optimal Control

In classical linear optimal control, the control vector $u(t)$ is to be chosen in such a way that a performance index J, defined as

$$J = J_1[z(t_0), z(t_f), t_0, t_f] + \int_{t_0}^{t_f} J_2(z, \dot{z}, u, \dot{u}, t)\,dt \tag{3.5}$$

is minimized subject to the constraining equation (3.1). The performance index J has two terms. The first term, J_1, is an initial–terminal stage penalty function, which depends only on the initial and final times of the control interval $[t_0, t_f]$ and on the states evaluated at those two time instants. The second term of J is an integral evaluated over the control interval $[t_0, t_f]$.

In Eq. (3.5), J is a scalar functional which is to be minimized with respect to $u(t)$ while satisfying the constraint specified by the state-space equation (3.1). Other constraints, of course, can also be introduced. For example, bounds can be placed on the allowable range of the structure's position and velocity. One thus has

$$|z| \leqslant \mathbf{b} \tag{3.6}$$

as an additional (inequality) constraint.

The form of the performance index usually chosen for study in structural control is quadratic in $z(t)$ and $u(t)$. Setting $t_0 = 0$, it is written as

$$J = \int_0^{t_f} \left[z^{\mathrm{T}}(t) \boldsymbol{Q} z(t) + u^{\mathrm{T}}(t) \boldsymbol{R} u(t) \right] dt \tag{3.7}$$

In the above, the superscript $^{\mathrm{T}}$ indicates vector or matrix transpose, the time interval $[0, t_f]$ is defined to be longer than that of the external excitation, $\boldsymbol{Q}$ is a $2n \times 2n$ positive semi-definite matrix, and $\boldsymbol{R}$ is an $m \times m$ positive definite matrix. The matrices $\boldsymbol{Q}$ and $\boldsymbol{R}$ are referred to as weighting matrices, whose magnitudes are assigned according to the relative importance attached to the state variables and to the control forces in the minimization procedure. The assignment of large values to the elements of $\boldsymbol{Q}$ indicates that response reduction is given priority over the control forces required. The opposite is true when the elements of $\boldsymbol{R}$ are large in comparison with those of $\boldsymbol{Q}$. Hence, by varying the relative magnitudes of $\boldsymbol{Q}$ and $\boldsymbol{R}$, one can synthesize the controllers to achieve a proper trade off between control effectiveness and control energy consumption.

To solve the optimal control problem with J defined by Eq. (3.7) subject to the constraint represented by Eq. (3.1), the Lagrangian L is first formed by adjoining these two equations with a time-varying Lagrange multiplier

$\lambda(t)$,[1,2] giving

$$L = \int_0^{t_f} \{z^T(t)\boldsymbol{Q}z(t) + \boldsymbol{u}^T(t)\boldsymbol{R}\boldsymbol{u}(t) + \lambda^T(t)[\boldsymbol{A}z(t) + \boldsymbol{B}\boldsymbol{u}(t) + \boldsymbol{H}\boldsymbol{f}(t) - \dot{z}(t)]\}\,dt \tag{3.8}$$

The necessary conditions which define the optimal control can be found by taking the first variation of the Lagrangian with respect to the state and control variables and setting it to zero. Taking the first variation of Eq. (3.8) yields

$$\delta L = -\lambda^T(t_f)\delta z(t_f) + \lambda^T(0)\delta z(0) + \int_0^{t_f}\left[\left(\lambda^T + \frac{\partial \mathscr{H}}{\partial z}\delta z + \frac{\partial \mathscr{H}}{\partial \boldsymbol{u}}\delta \boldsymbol{u}\right)\right]dt \tag{3.9}$$

where $\mathscr{H}$ is the Hamiltonian defined as the integrand of Eq. (3.8).

Now, $\delta z(0) = \mathbf{0}$ since $z(0) = z_0$ is a given constant. By requiring $\delta L = 0$, one must have

$$\frac{\partial \mathscr{H}}{\partial \boldsymbol{u}} = 0, \qquad 0 \leqslant t \leqslant t_f \tag{3.10}$$

$$\dot{\lambda}^T + \frac{\partial \mathscr{H}}{\partial z} = \mathbf{0} \tag{3.11}$$

with boundary condition

$$\lambda^T(t_f) = \mathbf{0} \tag{3.12}$$

Equations (3.10–3.12) are the necessary conditions for optimal control. Upon carrying out the necessary partial derivatives of $\mathscr{H}$ with respect to $\boldsymbol{u}$ and z, one obtains

$$\dot{\lambda} = -\boldsymbol{A}^T\lambda - 2\boldsymbol{Q}z, \qquad \lambda(t_f) = \mathbf{0} \tag{3.13}$$

$$\boldsymbol{u} = -\tfrac{1}{2}\boldsymbol{R}^{-1}\boldsymbol{B}^T\lambda \tag{3.14}$$

The system of equations given by Eqs (3.1), (3.13), (3.14) provides the optimal solution for $z(t)$, $\boldsymbol{u}(t)$ and $\lambda(t)$. They define a two-point boundary value problem since $z(t)$ is specified at $t = 0$ and $\lambda(t)$ is specified at $t = t_f$.

3.1.1 Closed-loop Control

When the control vector is regulated by the state vector, one has

$$\lambda(t) = \boldsymbol{P}(t)z(t) \tag{3.15}$$

The unknown matrix $\boldsymbol{P}(t)$ can be determined by substituting Eq. (3.15) into Eqs (3.1,), (3.13), (3.14). One can show that it satisfies

$$[\dot{\boldsymbol{P}}(t) + \boldsymbol{P}(t)\boldsymbol{A} - \tfrac{1}{2}\boldsymbol{P}(t)\boldsymbol{B}\boldsymbol{R}^{-1}\boldsymbol{B}^{\mathrm{T}}\boldsymbol{P}(t) + \boldsymbol{A}^{\mathrm{T}}\boldsymbol{P}(t) + 2\boldsymbol{Q}]\boldsymbol{z}(t) + \boldsymbol{P}(t)\boldsymbol{H}\boldsymbol{f}(t) = \boldsymbol{0},$$
$$\boldsymbol{P}(t_{\mathrm{f}}) = \boldsymbol{0} \tag{3.16}$$

When $\boldsymbol{f}(t)$ is zero, Eq. (3.16) reduces to

$$\dot{\boldsymbol{P}}(t) + \boldsymbol{P}(t)\boldsymbol{A} - \tfrac{1}{2}\boldsymbol{P}(t)\boldsymbol{B}\boldsymbol{R}^{-1}\boldsymbol{B}^{\mathrm{T}}\boldsymbol{P}(t) + \boldsymbol{A}^{\mathrm{T}}\boldsymbol{P}(t) + 2\boldsymbol{Q} = 0, \qquad \boldsymbol{P}(t_{\mathrm{f}}) = \boldsymbol{0} \tag{3.17}$$

In optimal control theory, Eq. (3.17) is referred to as the matrix Riccati equation and $\boldsymbol{P}(t)$ is the Riccati matrix. Since $\boldsymbol{P}(t)$ is specified at t_{f}, Eq. (3.17) is solved backwards in time. Methods for solving the matrix Riccati equation are well documented in the literature.[2]

The substitution of Eq. (3.15) into Eq. (3.14) shows that the control vector $\boldsymbol{u}(t)$ is linear in $\boldsymbol{z}(t)$. The *linear optimal control law* is

$$\boldsymbol{u}(t) = \boldsymbol{G}(t)\boldsymbol{z}(t) = -\tfrac{1}{2}\boldsymbol{R}^{-1}\boldsymbol{B}^{\mathrm{T}}\boldsymbol{P}(t)\boldsymbol{z}(t) \tag{3.18}$$

where $\boldsymbol{G}(t) = -\frac{1}{2}\boldsymbol{R}^{-1}\boldsymbol{B}^{\mathrm{T}}\boldsymbol{P}(t)$ is the control gain. When $\boldsymbol{z}(t)$ is accessible through measurement, $\boldsymbol{u}(t)$ can be determined from Eq. (3.18) and it is known that the feedback controller determined in this way generates a stable closed-loop system.

We remark that, strictly speaking, the Riccati matrix $\boldsymbol{P}(t)$ obtained from Eq. (3.17) does not yield an optimal solution unless the excitation term $\boldsymbol{f}(t)$ vanishes within the control interval $[0, t_{\mathrm{f}}]$ as seen from Eq. (3.16), or it is a white noise stochastic process.[1,2] It is also mentioned that, in structural applications, numerical computations have shown that the Riccati matrix $\boldsymbol{P}(t)$ typically remains constant over the control interval, dropping to zero rapidly near t_{f}. For example, typical elements of $\boldsymbol{P}(t)$ for an eight-storey building structure with arbitrarily prescribed weighting matrices $\boldsymbol{Q}$ and $\boldsymbol{R}$ are shown in Fig. 3.1. Therefore, $\boldsymbol{P}(t)$ can in most cases be approximated by a constant matrix $\boldsymbol{P}$ and the Riccati equation (3.17) reduces to

$$\boldsymbol{P}\boldsymbol{A} - \tfrac{1}{2}\boldsymbol{P}\boldsymbol{B}\boldsymbol{R}^{-1}\boldsymbol{B}^{\mathrm{T}}\boldsymbol{P} + \boldsymbol{A}^{\mathrm{T}}\boldsymbol{P} + 2\boldsymbol{Q} = \boldsymbol{0} \tag{3.19}$$

The control gain $\boldsymbol{G}(t)$ is also a constant with

$$\boldsymbol{G} = -\tfrac{1}{2}\boldsymbol{R}^{-1}\boldsymbol{B}^{\mathrm{T}}\boldsymbol{P} \tag{3.20}$$

which can be precalculated for a given structure and with prescribed weighting matrices $\boldsymbol{Q}$ and $\boldsymbol{R}$.

Upon substituting Eq. (3.18) into Eq. (3.1), the behaviour of the optimally controlled structure is described by

$$\dot{\boldsymbol{z}}(t) = (\boldsymbol{A} + \boldsymbol{B}\boldsymbol{G})\boldsymbol{z}(t) + \boldsymbol{H}\boldsymbol{f}(t), \qquad \boldsymbol{z}(0) = \boldsymbol{z}_0 \tag{3.21}$$

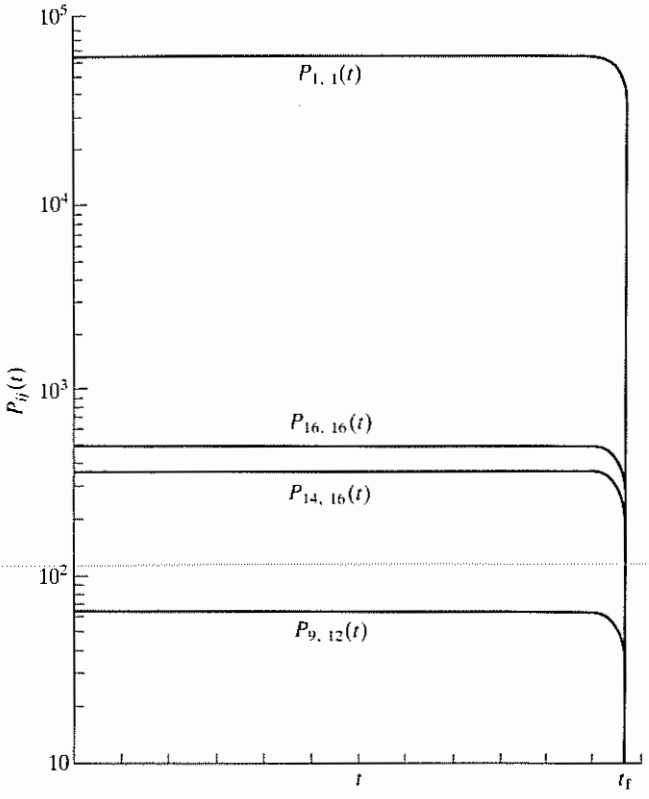

Figure 3.1 Some elements of Riccati matrix[3]

Again, we see that the effect of closed-loop control is one of structural modification where the system matrix is changed from A (open-loop system) to $A + BG$ (closed-loop system).

Finally, it is emphasized that the control law given in Eq. (3.18) requires knowledge of the entire state vector $z(t)$ of the structure (state feedback). Since the entire state can rarely be measured directly, it is often necessary to replace $z(t)$ by $\hat{z}(t)$, the state estimator determined from incomplete state measurements (output feedback).

Let $y(t)$ be the p-dimensional measurement (output) vector ($p \leqslant 2n$) with

$$y(t) = Cz(t) + \eta \tag{3.22}$$

where C is the $p \times 2n$ measurement matrix and η is the p-vector of possible output noise. The state estimator $\hat{z}(t)$ can be designed as a Luenberger observer when the signal-to-noise ratio for the output is sufficiently high and

as a Kalman filter otherwise.[2] It is given by

$$\dot{\hat{z}}(t) = A\hat{z}(t) + Bu(t) + G^*[C\hat{z}(t) - y(t)], \qquad \hat{z}(0) = z_0 \tag{3.23}$$

In the above, the estimator has an internal model of the system being estimated as indicated by the first two terms while the third term corrects the model by a linear feedback of the difference between the measurement output $y(t)$ and the computed output $\hat{y}(t) = C\hat{z}(t)$. In the Luenberger version, the estimator gain G^* is chosen so that the estimator error $\hat{z}(t) - z(t)$ decays exponentially at a prescribed rate.

3.1.2 Closed–open-loop Control and Open-loop Control

In some applications, the external excitation is also accessible to measurement. When this information is also used in control design, it leads to a closed–open-loop control law which should be superior to closed-loop control. For this case, we replace Eq. (3.15) by

$$\lambda(t) = P(t)z(t) + S(t)f(t) \tag{3.24}$$

Upon substituting Eq. (3.24) into Eqs (3.1), (3.13), (3.14), the Riccati equation (3.16) now takes the form

$$\begin{aligned}[\dot{P}(t) + P(t)A - \tfrac{1}{2}P(t)BR^{-1}B^{\mathrm{T}}P(t) + A^{\mathrm{T}}P(t) + 2Q]z(t) \\ + \dot{S}(t)f(t) + S(t)\dot{f}(t) - (\tfrac{1}{2}P(t)BR^{-1}B^{\mathrm{T}} - A^{\mathrm{T}})S(t)f(t) \\ + P(t)Hf(t) = 0, \qquad P(t_f) = 0, S(t_f) = 0\end{aligned} \tag{3.25}$$

The first part of this equation, upon using approximations as was done in Section 3.1.1, leads to the same closed-loop Riccati equation for the gain matrix $P(t)$. The remaining portion gives

$$[\dot{S}(t) - (\tfrac{1}{2}P(t)BR^{-1}B^{\mathrm{T}} - A^{\mathrm{T}})S(t) + P(t)H]f(t) + S(t)\dot{f}(t) = 0, \qquad S(t_f) = 0 \tag{3.26}$$

Unfortunately, the open-loop control gain $S(t)$ cannot be found in general. This is because Eq. (3.26) must be solved backwards from the terminal time t_f, requiring that $f(t)$ and $\dot{f}(t)$ over the entire control interval be known a priori. This is not possible for most structural control situations.

For open-loop control, Eq. (3.24) can be put in the form

$$\lambda(t) = S(t)f(t) \tag{3.27}$$

It can be readily seen that the same problem as encountered in closed–open-loop control exists and thus open-loop control is generally infeasible in structural control applications as well.

Example 3.1 As a demonstration of the closed-loop control principles presented above, let us study active control as applied to a simple single-degree-of-freedom structural system. Consider the horizontal motion of a one-storey structure subject to base acceleration $\ddot{x}_0(t)$. As shown in Fig. 3.2(a), the control force is applied to the structure through a set of tendons connected to an actuator placed at the base. The objective of control is to reduce the horizontal displacement of the first floor relative to the base for safety reasons, and to reduce its absolute acceleration for comfort reasons.

From the free-body diagram shown in Fig. 3.2(b), the equation of motion of the controlled system is

$$\ddot{x}(t) + 2\zeta\omega_0\dot{x}(t) + \omega_0^2 x(t) = -\ddot{x}_0(t) - \frac{4k_c \cos\alpha}{m}u(t), \qquad x(0) = \dot{x}(0) = 0 \tag{3.28}$$

where ζ and ω_0 are, respectively, the damping factor and undamped natural frequency of the uncontrolled (open-loop) structural system. The actuator displacement, denoted by $u(t)$, is considered here as the 'control force'. The quantities m, k_c and α denote, respectively, the system mass, tendon stiffness and inclination angle of the tendon with respect to the base.

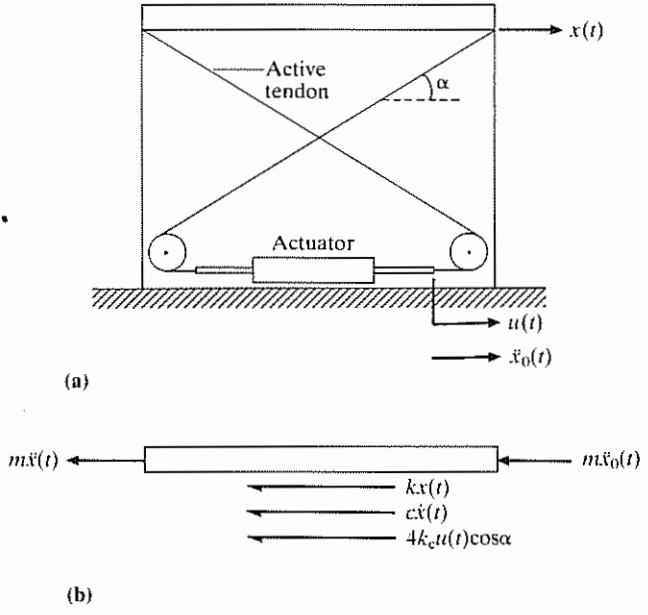

Figure 3.2 Structural system in Example 3.1 (a) schematic diagram; (b) free body diagram[4]

Introducing the state vector $z(t)$ with $z_1(t) = x(t)$ and $z_2(t) = \dot{x}(t)$, the state-space form of Eq. (3.28) is

$$\dot{z}(t) = Az(t) + bu(t) + h\ddot{x}_0(t), \qquad z(0) = \mathbf{0}$$

where

$$A = \begin{bmatrix} 0 & 1 \\ -\omega_0^2 & -2\zeta\omega_0 \end{bmatrix}$$

$$b = \begin{bmatrix} 0 \\ -\dfrac{4k_c \cos\alpha}{m} \end{bmatrix}$$

and

$$h = \begin{bmatrix} 0 \\ -1 \end{bmatrix}$$

Under the quadratic performance criterion, the actuator displacement $u(t)$ is to be found such that the integral J given by Eq. (3.7) is minimized. For simplicity, we shall use

$$Q = \begin{bmatrix} k & 0 \\ 0 & 0 \end{bmatrix} \qquad \text{and} \qquad R = \beta k_c$$

where k is structural stiffness as seen in Fig. 3.2(b).

The coefficient β determines the relative importance of control effectiveness (response reduction) and economy (control force requirements). When $\beta < 1$, control effectiveness is weighted more heavily and, when $\beta > 1$, economy is more important. They are equally important when $\beta = 1$. $\beta = \infty$ represents the uncontrolled case.

Let the system parameters take values as those given in Table 3.1. The computed control parameters and control effect on the structural behaviour are summarized in Table 3.2. It is seen that, as discussed earlier, substantial structural modification takes place as reflected by the changes in the natural frequency and the damping factor. In this case, there is a minor change in

Table 3.1 System parameter values in Example 3.1

Mass	$m = 16.69$ lb-sec^2/in
Structure stiffness	$k = 7934$ lb/in
Tendon stiffness	$k_c = 2124$ lb/in
Tendon angle	$\alpha = 36°$
Natural frequency	$\omega_0 = 3.47$ Hz
Damping factor	$\zeta = 1.24\%$

Table 3.2 Control parameters and controlled system behaviour

Parameter	$\beta = \infty$	$\beta = 5$	$\beta = 1$
Riccati matrix P	—	$\begin{bmatrix} 1926 & 16.15 \\ 16.15 & 3.780 \end{bmatrix}$	$\begin{bmatrix} 1035 & 14.51 \\ 14.51 & 1.660 \end{bmatrix}$
	—		
Natural frequency (Hz)	3.47	3.58	3.96
Damping factor (%)	1.24	17.8	34.0

natural frequency from uncontrolled to the controlled cases. The damping factor, however, is substantially increased from 1.25% in the uncontrolled case ($\beta = \infty$) to 34.0% in one of the controlled cases ($\beta = 1$). This is also demonstrated graphically in Fig. 3.3 by observing the change in magnitude of the input–output transfer function, the input being $\ddot{x}_0(t)$ and the output $\ddot{x}(t)$.

Consider the case in which $\ddot{x}_0(t)$ is a sample of a nonstationary stochastic process resembling an earthquake record as shown in Fig. 3.4. Numerical calculations can be carried out to determine the response behaviour of the structure under uncontrolled as well as controlled conditions.

The control effect in the time domain can be observed in Figs 3.5–3.7. Figure 3.5 shows reduction in the relative displacement for $\beta = 5$ and $\beta = 1$. As indicated earlier, a larger reduction is achieved for a smaller value of β as more weight is assigned to the control effectiveness. Corresponding reduction in the absolute acceleration is shown in Fig. 3.6. Figure 3.7 shows the required control force in the tendon which is obtained by multiplying tendon displacement $u(t)$ by tendon stiffness k_c. As expected, larger control forces are required for smaller values of β.

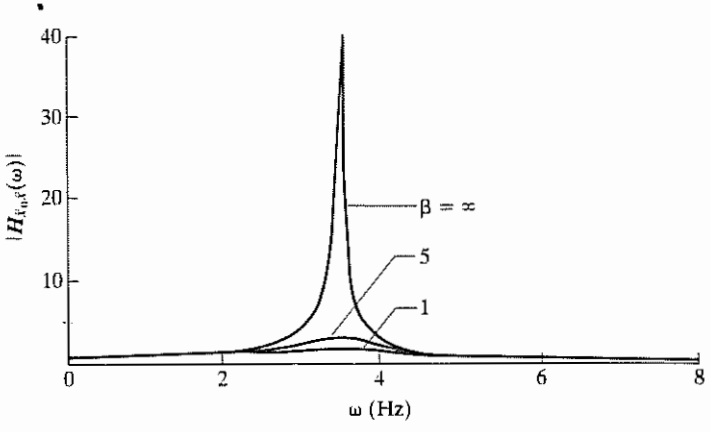

Figure 3.3 Magnitude of transfer function $\mathbf{H}_{\ddot{x}_0\ddot{x}}(\omega)$

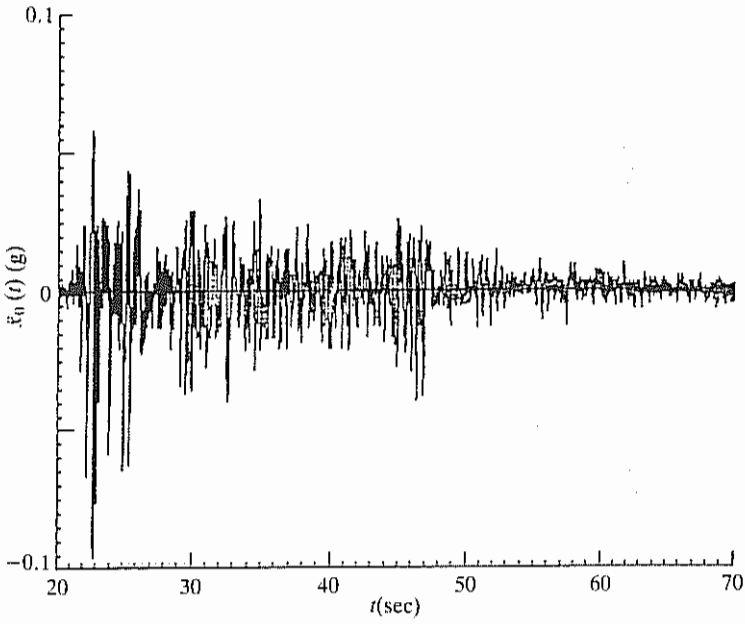

Figure 3.4 Base acceleration in Example 3.1

Example 3.2 Most of the environmental loads, such as wind and earthquakes, to which civil engineering structures are subjected are random in nature. Hence, the analysis of the behaviour of an actively controlled as well as an uncontrolled structure is based on the theory of random vibrations. We shall use this example to demonstrate some steps involved in such an analysis. Also, by using a two-degree-of-freedom structural system, relative merits of several different control configurations can be examined in an elementary way.

This example is taken from Yang.[5] The reader is referred to Appendix A for a review of some basic principles in random vibration analysis.

Consider a two-storey building as shown in Fig. 3.8, which is again excited by an earthquake-type ground acceleration $\ddot{X}_0(t)$. In this example, $\ddot{X}_0(t)$ is modelled by a nonstationary Gaussian shot noise with

$$\ddot{X}_0(t) = \psi(t)W(t) \tag{3.29}$$

in which $W(t)$ is a stationary zero-mean Gaussian white noise and $\psi(t)$ is a deterministic modulating function of the form

$$\psi(t) = g(e^{-\alpha t} - e^{-\beta t})h(t)$$

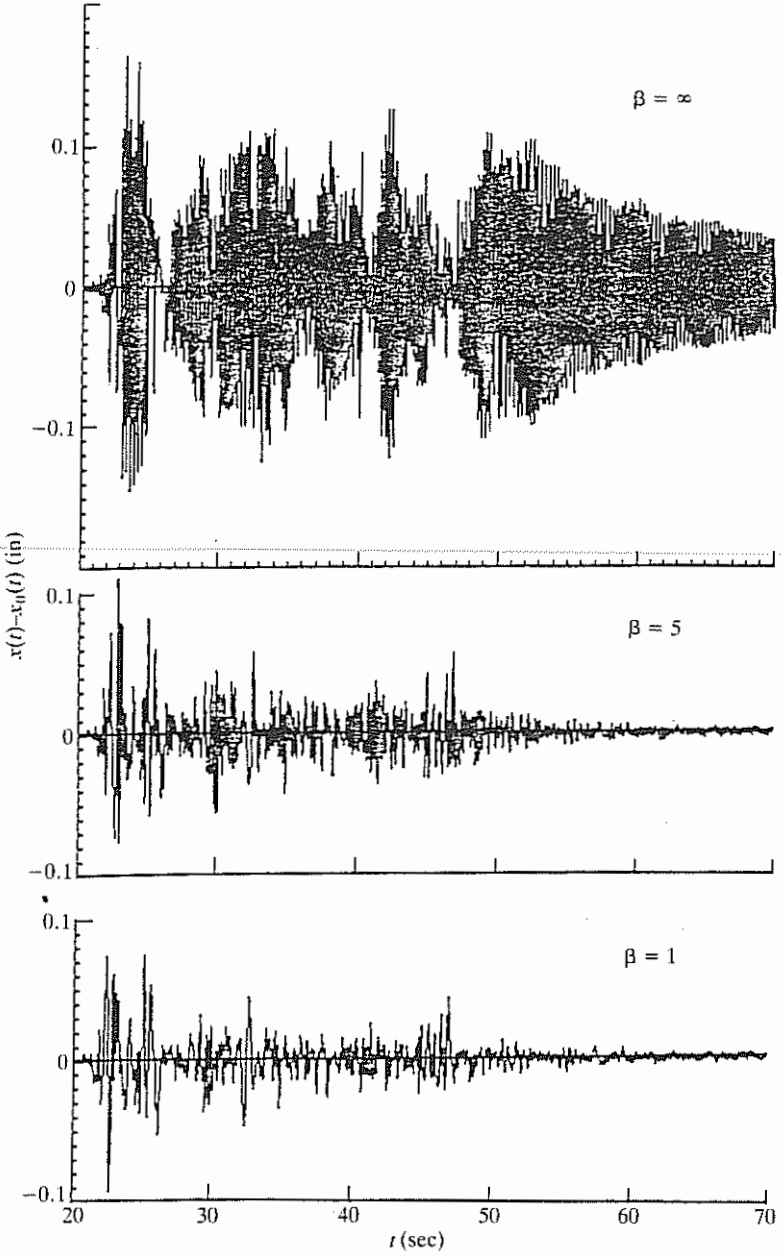

Figure 3.5 Relative displacement in Example 3.1[4]

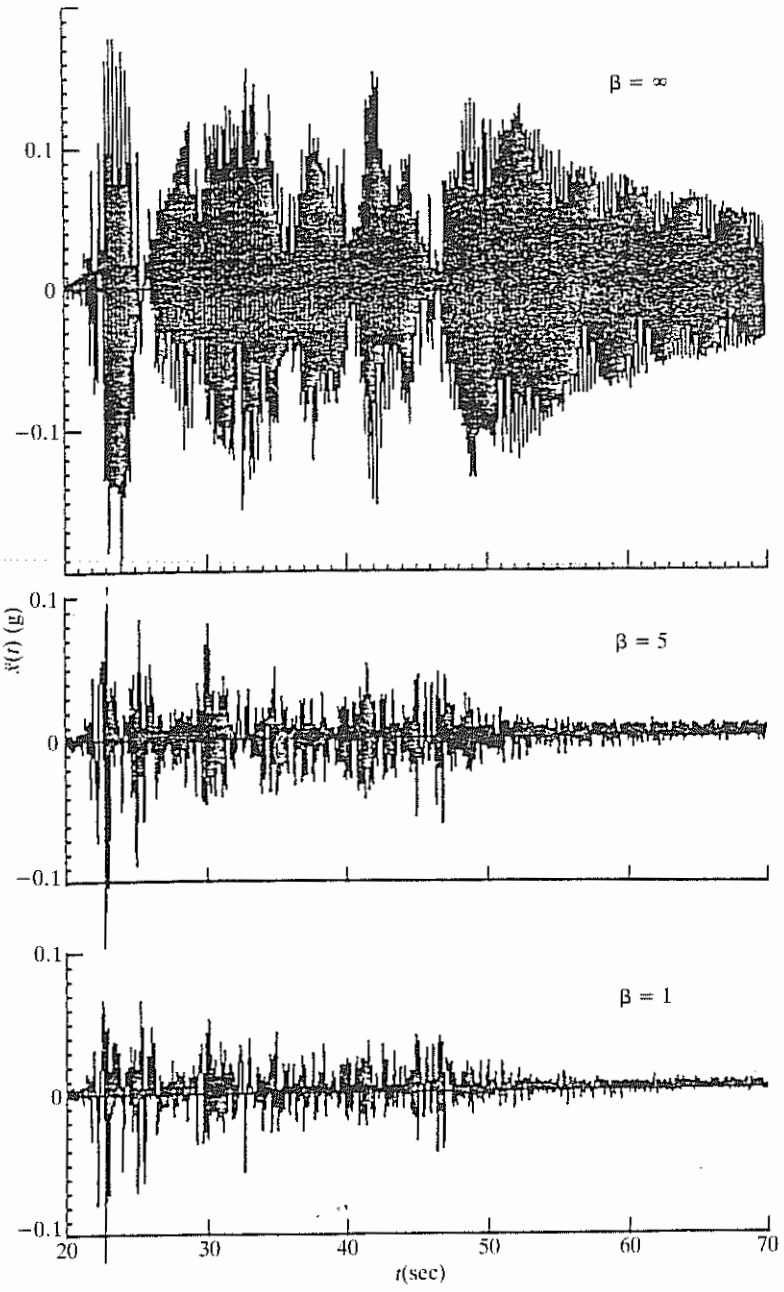

Figure 3.6 Absolute acceleration in Example 3.1[4]

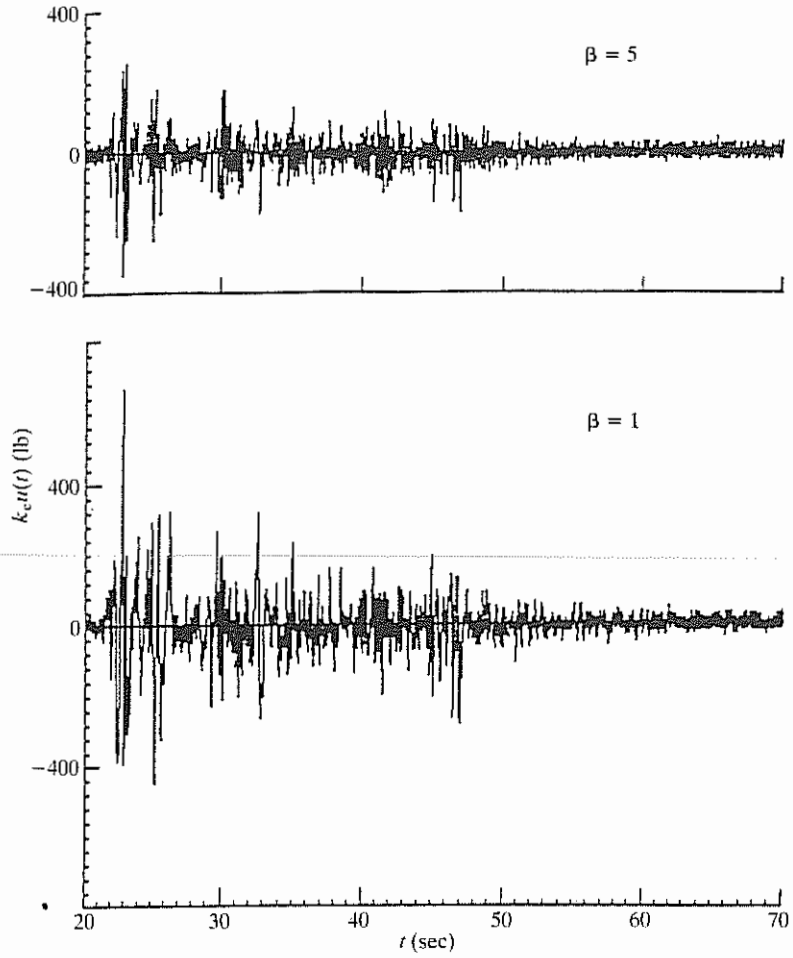

Figure 3.7 Control force in Example 3.1[4]

where $h(t)$ is the unit step function and g, α and β are constants. Accordingly, the mean of $\ddot{X}_0(t)$ is zero and its covariance is

$$E\{\ddot{X}_0(t)\ddot{X}_0(s)\} = g^2(e^{-\alpha t} - e^{-\beta t})^2 h(t) D\delta(t-s)$$

where D is the power spectral density of $W(t)$. For numerical calculations, we shall set $\alpha = 0.25/\text{sec}$, $\beta = 0.63/\text{sec}$, $g = 3.06$ and $D = 0.04\ \text{m}^2/\text{sec}^4$.

Since the excitation is random, the structural response is random and, as a consequence, the control as determined from Eq. (3.18) is also random. In what follows, these random quantities will be written in capital letters.

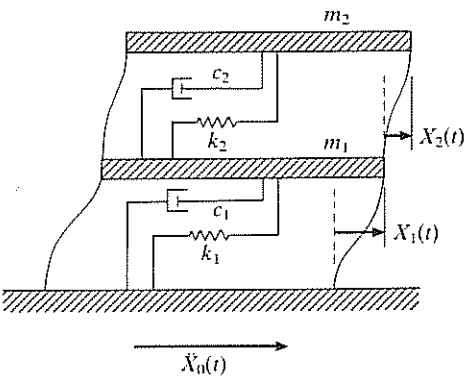

Figure 3.8 Structure in Example 3.2[5]

The state-space equation in this case has the form

$$\dot{\boldsymbol{Z}}(t) = \boldsymbol{A}\boldsymbol{Z}(t) + \boldsymbol{B}\boldsymbol{U}(t) + \boldsymbol{h}\ddot{X}_0(t), \qquad \boldsymbol{Z}(0) = \boldsymbol{0}$$

with

$$\boldsymbol{Z}(t) = \begin{bmatrix} X_1(t) \\ X_2(t) \\ \dot{X}_1(t) \\ \dot{X}_2(t) \end{bmatrix}$$

Note from Fig. 3.8 that $X_1(t)$ is the relative displacement of the first floor with respect to the foundation and $X_2(t)$ is the relative displacement of the second floor with respect to the first floor.

The system matrix $\boldsymbol{A}$ and vector $\boldsymbol{h}$ are

$$\boldsymbol{A} = \begin{bmatrix} 0 & 0 & 1 & 0 \\ 0 & 0 & 0 & 1 \\ -\omega_1^2 & \omega_2^2 \nu & -2\zeta_1\omega_1 & -2\zeta_2\omega_2\nu \\ \omega_1^2 & -\omega_2^2(1+\nu) & 2\zeta_1\omega_1 & -2\zeta_2\omega_2(1+\nu) \end{bmatrix}$$

and

$$\boldsymbol{h} = \begin{bmatrix} 0 \\ 0 \\ -1 \\ 0 \end{bmatrix}$$

Let us assume that control forces are applied at both floors. We have

$$\boldsymbol{U}(t)=\begin{bmatrix} U_1(t) \\ U_2(t) \end{bmatrix}, \qquad \boldsymbol{B}=\begin{bmatrix} 0 & 0 \\ 0 & 0 \\ \dfrac{1}{m_1} & 0 \\ -\dfrac{1}{m_1} & \dfrac{1}{m_2} \end{bmatrix}$$

For numerical computations, the following structural parameter values are used: $m_1 = m_2 = 40\,000$ kg, $\nu = m_2/m_1 = 1$, $\zeta_1 = \zeta_2 = 0.02$, $\omega_1 = 2$ Hz, and $\omega_2 = 1.5$ Hz.

Finally, the weighting matrices appearing in the performance index (Eq. 3.7) are assumed to be

$$\boldsymbol{Q}=\begin{bmatrix} 1 & 1 & 1 & 1 \\ 1 & 1 & 1 & 1 \\ 1 & 1 & 1 & 1 \\ 1 & 1 & 1 & 1 \end{bmatrix}, \qquad \boldsymbol{R}=\gamma\begin{bmatrix} 1 & 0 \\ 0 & 1 \end{bmatrix}$$

where γ is a parameter representing the relative importance between the covariances of the response and those of the control forces.

With the optimal control determined from Eq. (3.18), the mean of the controlled structural response is zero and its covariance matrix at $t = s$, defined by

$$\boldsymbol{R}_{ZZ}(t) = E\{\boldsymbol{Z}(t)\boldsymbol{Z}^{\mathrm{T}}(t)\}$$

satisfies the first-order matrix differential equation[2]

$$\dot{\boldsymbol{R}}_{ZZ}(t) = (\boldsymbol{A} + \boldsymbol{BG})\boldsymbol{R}_{ZZ}(t) + \boldsymbol{R}_{ZZ}(t)(\boldsymbol{A} + \boldsymbol{BG})^{\mathrm{T}} + 2\boldsymbol{h}\boldsymbol{R}_{X_0X_0}(t)\boldsymbol{h}^{\mathrm{T}}$$

with initial condition

$$\boldsymbol{R}_{ZZ}(0) = \boldsymbol{0}$$

The covariance matrix of the control vector at $t = s$ can be obtained from Eq. (3.18) as

$$\boldsymbol{R}_{UU}(t) = \boldsymbol{G}\boldsymbol{R}_{ZZ}(t)\boldsymbol{G}^{\mathrm{T}} \tag{3.30}$$

The variance, $\sigma^2_{X_1}(t)$, of the relative displacement between the foundation and the first floor under optimal control is plotted in Fig. 3.9(a) for various values of γ. Also plotted in Fig. 3.9(a) is $\sigma^2_{X_1}(t)$ without control. The variance, $\sigma^2_{X_2}(t)$, of the relative displacement between the first and second floors is plotted in Fig. 3.9(b). It can be observed that a significant reduction in the

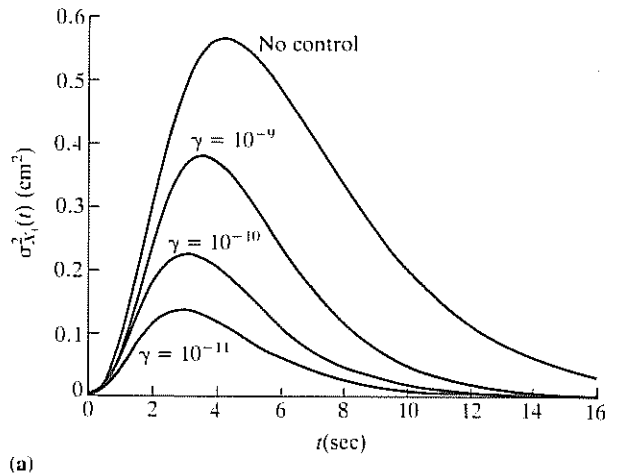

Figure 3.9 Variances of relative displacements in Example 3.2 (a) variance of $X_1(t)$; (b) variance of $X_2(t)$[5]

response variance is achieved by the use of active control. It is further observed that, the smaller the γ value is, the more reduction in response is achieved. However, as γ decreases, more control forces are required. The standard deviations $\sigma_{U_1}(t)$ and $\sigma_{U_2}(t)$ of the optimal control forces are computed from Eq. (3.30) and plotted in Fig. 3.10 to give an indication of required magnitudes of the control forces.

From a safety standpoint, the relative displacement between the first floor and the second floor is important, since $\sigma^2_{X_2}(t)$ is much greater than $\sigma^2_{X_1}(t)$.

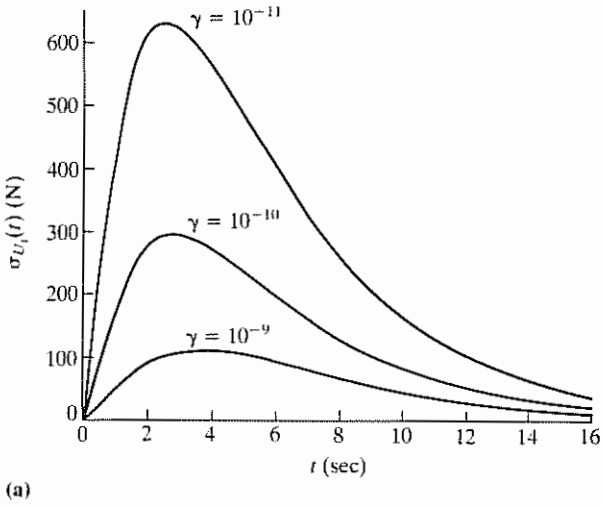

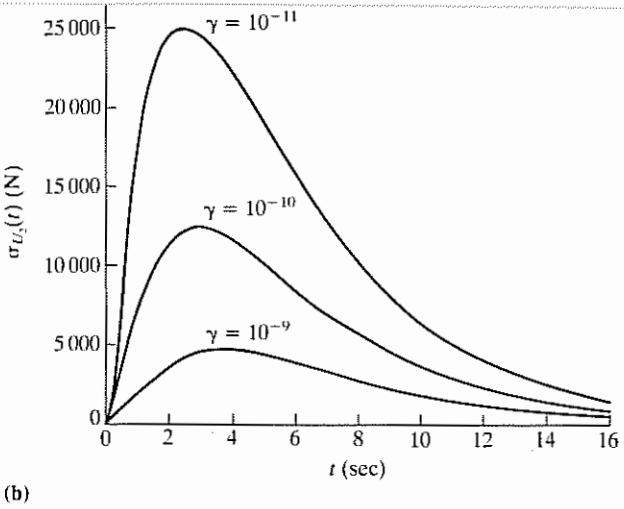

Figure 3.10 Standard deviations of control forces in Example 3.2 (a) standard deviation of $U_1(t)$; (b) standard deviation of $U_2(t)$[5]

As a result, it is more important to control or reduce $X_2(t)$. Supposing that we can only install one controller in the building, the question of whether it should be placed on the first floor or on the second floor is of practical importance. For the first case where only one controller is placed on the second floor, the response variance, $\sigma^2_{X_2}(t)$, and the standard deviation, $\sigma_{U_1}(t)$, of the control force are plotted in Figs 3.11 and 3.12 as solid curves. For the

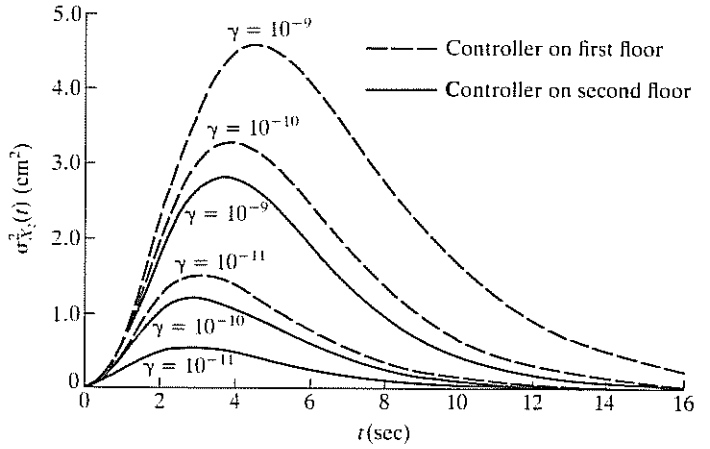

Figure 3.11 Variances of $X_2(t)$ in Example 3.2 – single-controller case[5]

second case where only one controller is placed on the first floor, the response variance, $\sigma^2_{X_2}(t)$, and the standard deviation, $\sigma_{U_1}(t)$, of the control force are plotted in Figs 3.11 and 3.12 as dashed curves.

It is observed from these figures that a controller on the second floor requires a smaller control force to achieve a larger reduction in the response variance, $\sigma^2_{X_2}(t)$, while a controller on the first floor requires a larger control force. Consequently, a controller installed on the second floor is more effective in response reduction in this case.

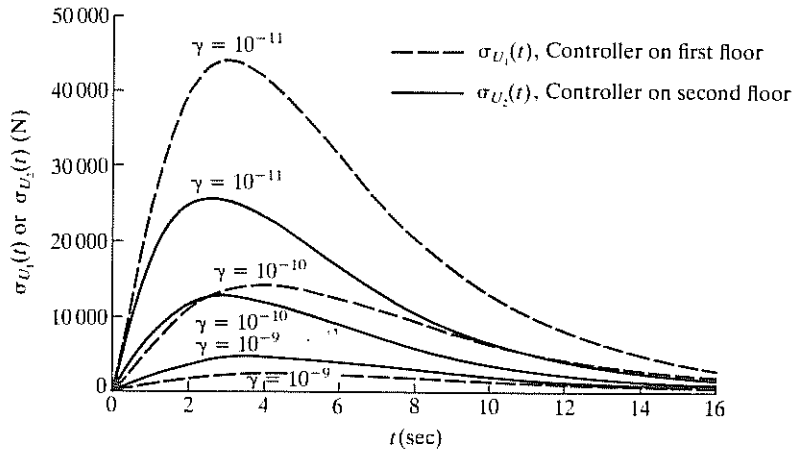

Figure 3.12 Standard deviations of control forces in Example 3.2 – single-controller case[5]

3.2 Pole Assignment

Consider again the state-space equation (3.1). The system matrix A defines the open-loop system dynamics and its eigenvalues provide modal damping and stiffness characteristics. Let the control force be determined by linear state feedback, i.e.

$$u(t) = Gz(t) \tag{3.31}$$

where G is a constant gain matrix. As Eq. (3.21) shows, the closed-loop system thus takes the form

$$\dot{z}(t) = (A + BG)z(t) + Hf(t), \qquad z(0) = z_0 \tag{3.32}$$

in which the system matrix becomes $A + BG$. As has been observed in Chapter 2, this modification of the system matrix through active control alters modal damping ratios and frequencies. This is reflected by the fact that the eigenvalues of $A + BG$ are generally different from those of A. For structural systems, these eigenvalues, which we shall denote by η_i, are related to the modal frequencies ω_i and damping ratios ζ_i in complex conjugate pairs by

$$\eta_i = \zeta_i\omega_i \pm j\omega_i\sqrt{1-\zeta_i^2}, \qquad j = \sqrt{-1} \tag{3.33}$$

Since these closed-loop eigenvalues define the controlled system behaviour, a feasible control strategy is to choose the control gain G in such a way that the η_is take a set of values prescribed by the designer. Control algorithms developed based on this procedure are generally referred to as *pole assignment* techniques. Successful application of these algorithms thus requires judicious placement of the closed-loop eigenvalues on the part of the designer as well as a good understanding of the uncontrolled structural modal behaviour.

Pole assignment algorithms have been studied extensively in the general control literature.[1,2] Its application to the study of civil engineering structural control has been fruitful when only a few vibrational modes contribute significantly to the response.[6,7] In these cases, attention needs to be paid only to these selected modes and a more clear choice of the closed-loop eigenvalues can be made.

In control design using the pole assignment approach, two questions need to be addressed. The first is, given the matrix pair (A, B), can one choose the feedback gain G so that the new (closed-loop) system matrix $A + BG$ possesses the prescribed eigenvalues? The second basic question has to do with finding an efficient method of generating the control gain G.

The answer to the first question is quite specific;[8] that is, the system must be completely controllable (see Appendix A). As for control design, a number of algorithms have been developed. The procedure described below is relatively simple and is due to Brogan.[9]

The eigenvalues η_is are the solutions of the determinantal equation

$$|\eta I - A - BG| = 0 \tag{3.34}$$

which can be written as

$$(|\eta I - A|)(|I - \psi(\eta)G|) = 0 \tag{3.35}$$

where

$$\psi(\eta) = (\lambda I - A)^{-1} B \tag{3.36}$$

Since η is not an eigenvalue of the original (open-loop) system,

$$|\eta I - A| \neq 0$$

and Eq. (3.35) leads to

$$|\Delta(\eta)| = |I_{2n} - \psi(\eta)G| = 0 \tag{3.37}$$

Making use of a determinantal identity, Eq. (3.37) can be written in the form

$$|\Delta(\eta)| = |I_m - G\psi(\eta)| = 0 \tag{3.38}$$

For the ith eigenvalue η_i, Eq. (3.38) is satisfied if a column or a row of $\Delta(\eta_i)$ consists entirely of zeros. Thus, suppose the jth column is selected and let e_j and $\psi_j(\eta_i)$ denote the jth columns of I_m and $\psi(\eta_i)$, respectively, then

$$e_j = G\psi_j(\eta_i)$$

defines m linear equations. The procedure described above is then repeated for each eigenvalue η_i, $i = 1, 2, \ldots, 2n$. The resulting equations can then be assembled into a single matrix equation of the form

$$E = G\Phi \tag{3.39}$$

where E is made up, column by column, of the vectors e_j and Φ is similarly made up of the vectors $\psi_j(\eta_i)$. Assuming that the eigenvalues η_i, $i = 1, 2, \ldots, 2n$, are distinct, Φ is invertible and the control gain matrix G can be determined as

$$G = E\Phi^{-1} \tag{3.40}$$

While G can be computed from the above, let us note that it is not unique since it depends upon the choice of the column of $\Delta(\eta)$. However, the resulting closed-loop system is guaranteed to have the required eigenvalues. Moreover, the control gain G does not alter the controllability of the open-loop system.

This nonuniqueness in the choice of G has also prompted many studies coupling pole assignment with other control objectives.[10] For example, one can require that a closed-loop system possess not only prescribed eigenvalues but also eigenvectors, thus allowing the designer to have some control over the influence of each eigenvalue on each state variable response.[11] Attempts

have also been made to use this design freedom to minimize a given performance index, thus combining the pole placement and optimal control.[12,13]

3.2.1 *The Case of Output Feedback*

The procedure described above is based on state feedback as indicated by Eq. (3.31). Consider now the case of output feedback with the p-dimensional output vector given by

$$y(t) = Cz(t) \tag{3.41}$$

where C is the $p \times 2n$ measurement matrix. The control vector is

$$u(t) = G'y(t) = G'Cz(t) \tag{3.42}$$

where G' is the output feedback gain matrix. The computational procedure for G' follows closely that just derived for the state feedback case.[14] Equations (3.37) and (3.38) in this case become

$$|\Delta'(\eta)| = |I_{2n} - \psi(\eta)G'C| = |I_p - C\psi(\eta)G'| = |I_m - G'C\psi(\eta)| = 0 \tag{3.43}$$

Let $\psi'_j(\eta_i)$ be the jth column of $C\psi(\eta)$, we have

$$e_j = G'\psi'_j(\eta_i)$$

and Eq. (3.39) becomes

$$E = G'\Phi' \tag{3.44}$$

where the columns of Φ' are made up of the vectors $\psi'_j(\eta_i)$. If Φ' is invertible, the output feedback control gain is found from

$$G' = E\Phi'^{-1} \tag{3.45}$$

It is important to point out that the number of linearly independent columns that can be obtained from $C\psi(\eta)$ will not exceed the rank of C. It is shown[14] that, if the open-loop system is controllable and the rank of C is p, $p \leqslant 2n$, then only p out of the $2n$ eigenvalues of the closed-loop system can be specified such that matrix Φ' is invertible. Thus, the control gain G' as found from Eq. (3.45) ensures the existence of only m out of the $2n$ specified closed-loop eigenvalues. However, if the open-loop system is completely controllable and observable (see Appendix A), it is always possible to transform the output feedback into a state feedback through the construction of an observer as discussed in Section 3.1.1.

Example 3.3 Consider a two-storey structure similar to that shown in Fig. 3.8. The state-space equation is of the form given by Eq. (3.1) where A is a 4×4 matrix. It is assumed that

$$A = \begin{bmatrix} 0 & 0 & 1 & 0 \\ 0 & 0 & 0 & 1 \\ -0.5 & 0.25 & -0.02 & 0.01 \\ 0.25 & -0.25 & 0.01 & -0.01 \end{bmatrix}$$

These numerical values are chosen to characterize a lightly damped system. Units for all physical quantities will not be specified since only comparative studies are performed here. The eigenvalues of the matrix A are

$$\lambda_{1,2} = -0.0019 \pm j0.3098$$

$$\lambda_{3,4} = -0.0134 \pm j0.8089$$

The uncontrolled two-storey structural system is assumed to be described by

$$\dot{z}(t) = Az(t) + hf(t)$$

where

$$h = \begin{bmatrix} 0 \\ 0 \\ 1 \\ 1 \end{bmatrix}$$

and

$$f(t) = 3 \sin \omega t + 5 \sin 2\omega t + 7 \sin 3\omega t + 4 \sin 4\omega t$$

which is a crude representation of a wind-type excitation acting on both floors. In the numerical calculations, the value of ω is chosen to be 0.309. This choice of ω (which is close to the first frequency of the structure) is deliberate. The intent is to dramatize the effect of control. It is further assumed that the control objective is to change the first frequency of the structure from 0.3098 to 4.0. Hence, the required closed-loop eigenvalues are

$$\eta_{1,2} = -0.0019 \pm j4.0$$

$$\eta_{3,4} = -0.0134 \pm j0.8089$$

The control to be applied to the structure is assumed to be of the form $\boldsymbol{b}u(t)$, where $u(t)$ is a scalar. The following modes of control are of practical interest:

Case A: $\boldsymbol{b}^{\mathrm{T}} = [0, 0, 1, 0]$, control applied at first floor only

Case B: $\boldsymbol{b}^{\mathrm{T}} = [0, 0, 0, 1]$, control applied at second floor only

Case C: $\boldsymbol{b}^{\mathrm{T}} = [0, 0, 1, 1]$, control applied at both floors with the same control force.

The numerical results for $x_1(t)$ and $x_2(t)$, the displacements of the first and second floors, are given in Figs 3.13 and 3.14 for the uncontrolled case and under the three modes of control as described above. The relative merits of the three control modes are also evaluated based upon their energy requirements, where the energy E is calculated according to

$$E = \int_0^T u^2(t)\boldsymbol{b}^{\mathrm{T}}\boldsymbol{b}\,\mathrm{d}t, \qquad T = 50$$

It is interesting to note that the case for which equal control forces being applied to both floors proved to be the most effective in terms of controlling the displacements (as well as the velocities) and energy required. The energy required for this case (case C) is $E_{\mathrm{C}} = 2.236$ while $E_{\mathrm{A}} = 7.664$ (first floor control only) and $E_{\mathrm{B}} = 2.927$ (second floor control only). Of the single-controller cases, no significant difference in displacement reduction is noted between case A and case B. However, in terms of energy requirement, it is more efficient to place the controller on the second floor than on the first.

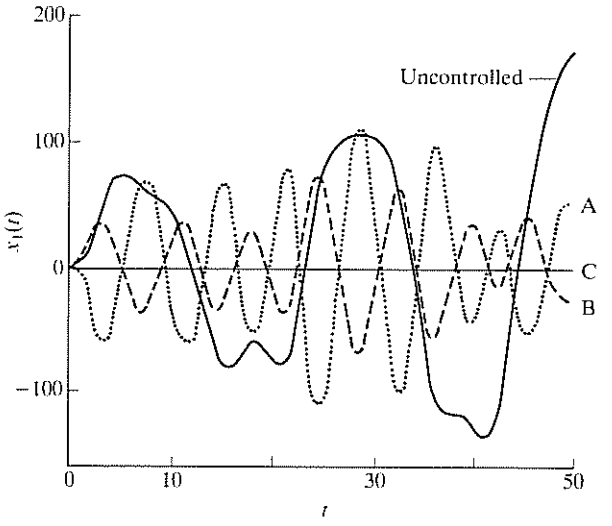

Figure 3.13 Displacement of first floor in Example 3.3[7]

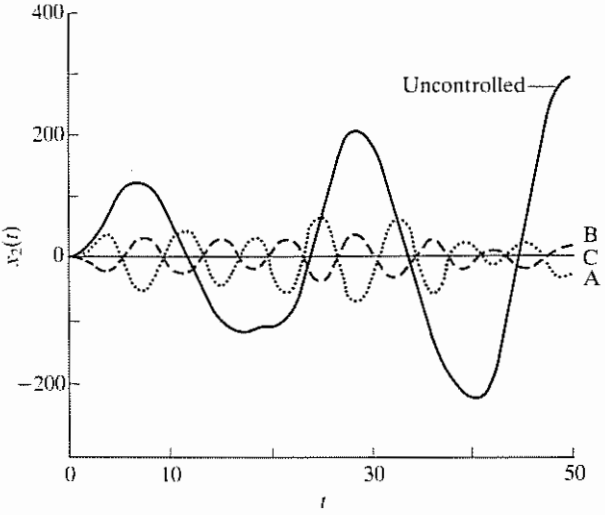

Figure 3.14 Displacement of second floor in Example 3.3[7]

Example 3.4 In this example, an extra dimension is added to the problem of pole assignment. Since exact locations of the closed-loop eigenvalues are not crucial, one may wish to perturb around the prescribed closed-loop eigenvalues so that some other control objectives can be met at the same time. In Wang *et al*[15] the pole assignment problem with the added requirement that the response be bounded by some permissible values is considered. To achieve this added objective, one may adopt the following iterative approach:[15]

1 The trial closed-loop eigenvalues are chosen first. With these trial values, the gain matrix $\boldsymbol{G}$ as well as the corresponding controlled system response can be computed.
2 Since the real parts of the eigenvalues play a more significant role in changing the response, these real parts are allowed to change so that the response can be limited to be below its permissible values. Let α be the absolute value of the real part of a given eigenvalue and x_p be the limiting value of a response quantity. After two successive trials, an improved value of α can be obtained by the approximation

$$\alpha_{i+1} = \alpha_i + \frac{x_i - x_p}{x_i - x_{i-1}}(\alpha_i - \alpha_{i-1})$$

where the subscripts $i-1$, i and $i+1$ represent successive iterations.

This procedure is demonstrated by considering a five-storey structure as shown in Fig. 3.15. The critical damping ratio and mass corresponding to each degree of freedom are assumed to be 3% and 750.0 k-sec^2/in,

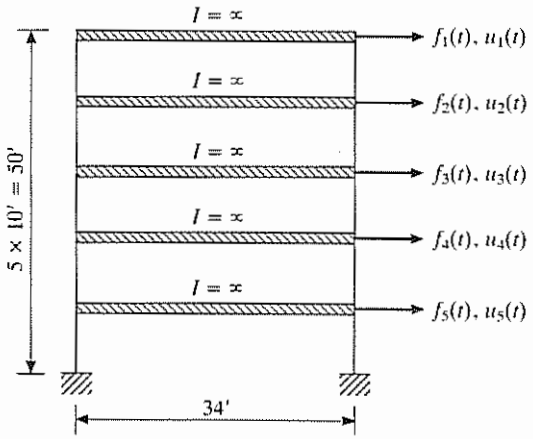

Figure 3.15 The rive-storey frame[15]

respectively. The stiffness matrix is

$$\boldsymbol{K} = \begin{bmatrix} 7400.0 & -1700.0 & 0.0 & 0.0 & 0.0 \\ -1700.0 & 6600.0 & -1600.0 & 0.0 & 0.0 \\ 0.0 & -1600.0 & 6000.0 & -1400.0 & 0.0 \\ 0.0 & 0.0 & -1400.0 & 4800.0 & -1000.0 \\ 0.0 & 0.0 & 0.0 & -1000.0 & 2000.0 \end{bmatrix} \text{k/in}$$

It is assumed that the excitation takes the form

$$f(t) = \boldsymbol{a}\cos 2\omega t + \boldsymbol{b}\cos 3\omega t + \boldsymbol{c}\sin 4\omega t + \boldsymbol{d}\sin 5\omega t$$

where $\omega = 1.1$ rad/sec and

$$\boldsymbol{a} = \begin{bmatrix} 950.1 \\ 11\,100.5 \\ 1230.3 \\ 1400.9 \\ 1350.9 \end{bmatrix} \quad \boldsymbol{b} = \begin{bmatrix} 30.2 \\ 350.6 \\ 569.0 \\ 750.0 \\ 0.6 \end{bmatrix}$$

$$\boldsymbol{c} = \begin{bmatrix} 37.2 \\ 1380.3 \\ 1128.9 \\ 1310.3 \\ 1471.0 \end{bmatrix} \quad \boldsymbol{d} = \begin{bmatrix} 1300.1 \\ 560.0 \\ 850.0 \\ 71.0 \\ 361.0 \end{bmatrix}$$

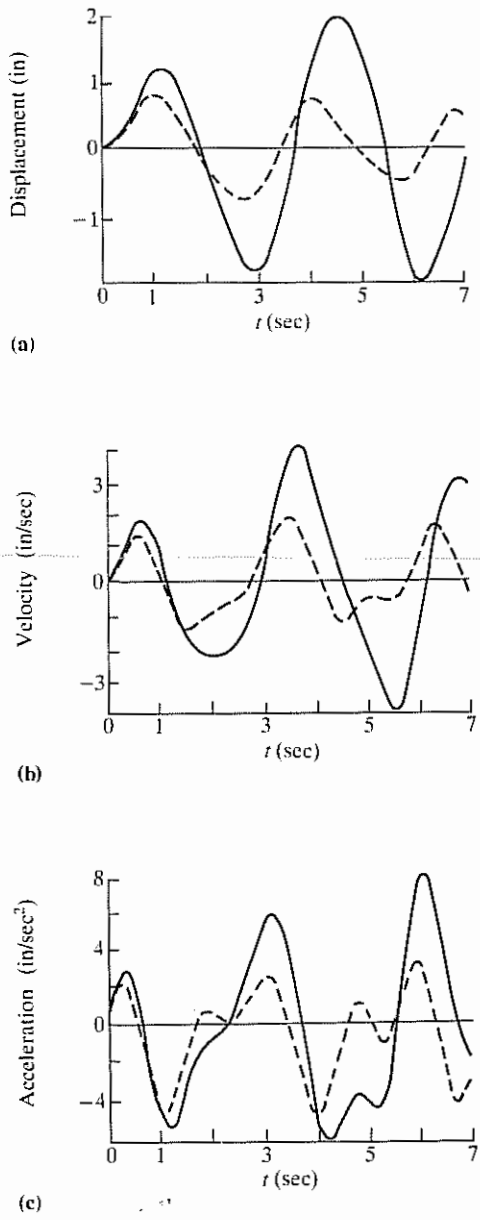

Figure 3.16 Responses at the fifth floor in Example 3.4 (a) displacement; (b) velocity; (c) acceleration[15]

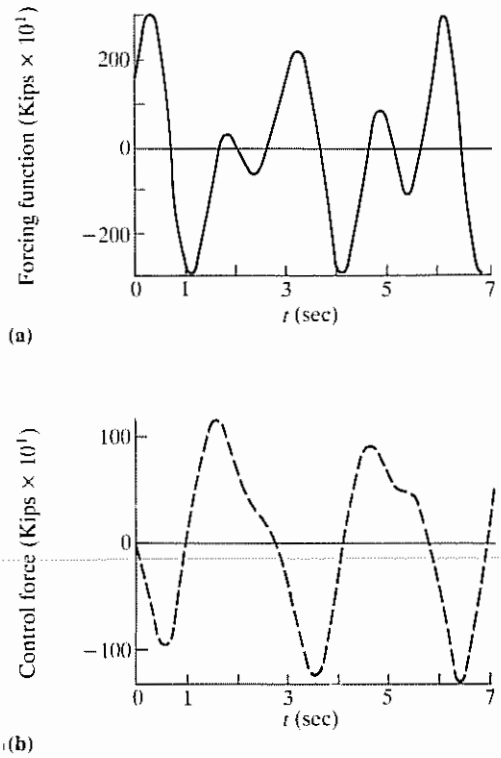

Figure 3.17 Excitation and control force at the fifth floor in Example 3.4 (a) excitation; (b) control force[15]

Beginning with the open-loop eigenvalues, the above-mentioned iterative procedure is used to obtain closed-loop eigenvalues such that some performance criteria are satisfied. In this case, the limit on displacement is taken to be 1/500 of the structural height, and the maximum permissible values for velocity and acceleration are, respectively, 4 in/sec and 4 in/sec^2.

The specified limitations are reached after nine iterations. The uncontrolled (solid line) and the controlled (dotted line) responses at the fifth floor are shown in Fig. 3.16. It is noted that the acceleration limit of 4 in/sec^2 controls the result. Also shown in Fig. 3.17 are the excitation together with the control force at the fifth floor.

3.3 Instantaneous Optimal Control

We have seen in Section 3.1 that classical optimal control is not truly optimum because the excitation term is ignored in the derivation of the Riccati matrix

$\boldsymbol{P}(t)$. Recognizing the fact that, at any particular time t, the knowledge of the external excitation may be available up to that time instant t, this knowledge can be utilized in arriving at improved control algorithms.

One of such attempts makes use of a time-dependent performance index $J(t)$ defined by[3]

$$J(t) = \boldsymbol{z}^{\mathrm{T}}(t)\boldsymbol{Q}\boldsymbol{z}(t) + \boldsymbol{u}^{\mathrm{T}}(t)\boldsymbol{R}\boldsymbol{u}(t) \tag{3.46}$$

Optimal control laws are derived by minimizing $J(t)$ at every time instant t for all $0 \leqslant t \leqslant t_f$. Hence, these control laws are referred to as instantaneous optimal control algorithms.

The starting point of the derivation of instantaneous optimal control algorithms is to consider the evolution of the state vector $\boldsymbol{z}(t)$ over a small time interval Δt. Consider again Eq. (3.1). Assuming that the open-loop system matrix $\boldsymbol{A}$ possesses distinct eigenvalues, this system of equations can be decoupled through the transformation (see Appendix A)

$$\boldsymbol{z}(t) = \boldsymbol{T}\boldsymbol{y}(t) \tag{3.47}$$

where $\boldsymbol{T}$ is the $2n \times 2n$ modal matrix whose columns are the eigenvectors of $\boldsymbol{A}$.

The decoupled state-space equation governing $\boldsymbol{y}(t)$ has the form, upon substituting Eq. (3.47) into Eq. (3.1),

$$\dot{\boldsymbol{y}}(t) = \boldsymbol{\Lambda}\boldsymbol{y}(t) + \boldsymbol{q}(t), \qquad \boldsymbol{y}(0) = \boldsymbol{0} \tag{3.48}$$

where

$$\boldsymbol{\Lambda} = \boldsymbol{T}^{-1}\boldsymbol{A}\boldsymbol{T} \tag{3.49}$$

is diagonal whose diagonal elements are the complex eigenvalues λ_j, $j = 1, 2, \ldots, 2n$, of matrix $\boldsymbol{A}$ and

$$\boldsymbol{q}(t) = \boldsymbol{T}^{-1}[\boldsymbol{B}\boldsymbol{u}(t) + \boldsymbol{H}\boldsymbol{f}(t)] \tag{3.50}$$

Over a small time interval Δt, the 'modal' state vector $\boldsymbol{y}(t)$ can be expressed as

$$\boldsymbol{y}(t) = \int_0^{t-\Delta t} \exp[\boldsymbol{\Lambda}(t-\tau)]\boldsymbol{q}(\tau)\,\mathrm{d}\tau + \int_{t-\Delta t}^{t} \exp[\boldsymbol{\Lambda}(t-\tau)]\boldsymbol{q}(\tau)\,\mathrm{d}\tau$$

$$\cong \exp(\boldsymbol{\Lambda}\Delta t)\boldsymbol{y}(t-\Delta t) + \frac{\Delta t}{2}[\exp(\boldsymbol{\Lambda}\Delta t)\boldsymbol{q}(t-\Delta t) + \boldsymbol{q}(t)] \tag{3.51}$$

For the state vector $\boldsymbol{z}(t)$, Eqs (3.47), (3.50) and (3.51) lead to

$$\boldsymbol{z}(t) = \boldsymbol{T}\boldsymbol{d}(t-\Delta t) + \frac{\Delta t}{2}[\boldsymbol{B}\boldsymbol{u}(t) + \boldsymbol{H}\boldsymbol{f}(t)] \tag{3.52}$$

where

$$\boldsymbol{d}(t-\Delta t)=\exp(\Lambda\Delta t)\,\boldsymbol{T}^{-1}\left\{\boldsymbol{z}(t-\Delta t)+\frac{\Delta t}{2}[\boldsymbol{B}\boldsymbol{u}(t-\Delta t)+\boldsymbol{H}\boldsymbol{f}(t-\Delta t)]\right\} \tag{3.53}$$

In the above, $\exp(\Lambda\Delta t)$ is a diagonal matrix with the jth diagonal element being $\exp(\lambda_j\Delta t)$. The vector $\boldsymbol{d}(t-\Delta t)$ contains all the dynamic quantities at time $t-\Delta t$.

With Eq. (3.52) as the motion constraint, the minimization of $J(t)$ given by Eq. (3.46) can be carried out in a similar fashion as was done in Section 3.1. In this case, the Hamiltonian is

$$\begin{aligned}\mathscr{H}=&\boldsymbol{z}^{\mathrm{T}}(t)\boldsymbol{Q}\boldsymbol{z}(t)+\boldsymbol{u}^{\mathrm{T}}(t)\boldsymbol{R}\boldsymbol{u}(t)\\&+\boldsymbol{\lambda}^{\mathrm{T}}(t)\left\{\boldsymbol{z}(t)-\boldsymbol{T}\boldsymbol{d}(t-\Delta t)-\frac{\Delta t}{2}[\boldsymbol{B}\boldsymbol{u}(t)+\boldsymbol{H}\boldsymbol{f}(t)]\right\}\end{aligned} \tag{3.54}$$

where $\boldsymbol{\lambda}(t)$ is the Lagrange multiplier.

The necessary conditions for minimization are

$$\frac{\partial\mathscr{H}}{\partial\boldsymbol{z}}=0,\qquad\frac{\partial\mathscr{H}}{\partial\boldsymbol{u}}=0,\qquad\frac{\partial\mathscr{H}}{\partial\boldsymbol{\lambda}}=0$$

which yield

$$\left.\begin{aligned}&2\boldsymbol{Q}\boldsymbol{z}(t)+\boldsymbol{\lambda}(t)=0\\&2\boldsymbol{R}\boldsymbol{u}(t)-\frac{\Delta t}{2}\boldsymbol{B}^{\mathrm{T}}\boldsymbol{\lambda}(t)=0\\&\boldsymbol{z}(t)=\boldsymbol{T}\boldsymbol{d}(t-\Delta t)+\frac{\Delta t}{2}[\boldsymbol{B}\boldsymbol{u}(t)+\boldsymbol{H}\boldsymbol{f}(t)]\end{aligned}\right\} \tag{3.55}$$

3.3.1 Closed-loop Control

Consider first closed-loop control when the control vector is regulated by the state vector. One has, as in Section 3.1.1,

$$\boldsymbol{\lambda}(t)=\boldsymbol{P}(t)\boldsymbol{z}(t) \tag{3.56}$$

The first of Eqs (3.55) immediately gives

$$\boldsymbol{P}(t)=-2\boldsymbol{Q}$$

and, using the second of Eqs (3.55),

$$\boldsymbol{u}(t)=-\frac{\Delta t}{2}\boldsymbol{R}^{-1}\boldsymbol{B}^{\mathrm{T}}\boldsymbol{Q}\boldsymbol{z}(t) \tag{3.57}$$

The response state vector $z(t)$ is, following Eqs (3.52) and (3.57),

$$z(t)=\left[I+\frac{\Delta t^2}{4}BR^{-1}B^{\mathrm{T}}Q\right]^{-1}\left[Td(t-\Delta t)+\frac{\Delta t}{2}Hf(t)\right] \tag{3.58}$$

If is of interest to compare Eq. (3.57) with Eq. (3.18), the closed-loop control law under classical optimal control criteria. We see that, in this case, ΔtQ plays the role of the Riccati matrix $P(t)$. It is thus a much simpler control design since it does not require solution of the Riccati equation. We also note that the choice of Q, which is a prescribed weighting matrix associated with the performance index, requires more careful consideration in the context of instantaneous optimal control.

3.3.2 *Closed–open-loop Control*

When the control vector is regulated by both the state vector and external excitation, the Lagrange multiplier has the form

$$\lambda(t)=Pz(t)+p(t) \tag{3.59}$$

where the second term, $p(t)$, represents open-loop control.

Using the second of Eqs (3.55), the control vector $u(t)$ in the third of Eqs (3.55) can be eliminated, resulting in

$$z(t)=Td(t-\Delta t)+\frac{\Delta t}{2}\left[\frac{\Delta t}{4}BR^{-1}B^{\mathrm{T}}\lambda(t)+Hf(t)\right] \tag{3.60}$$

Let us write the first of Eqs (3.55) in the form

$$\lambda(t)=-Q[z(t)+z(t)] \tag{3.61}$$

in which $2z(t)$ is somewhat arbitrarily divided into two equal parts to represent the closed-loop and open-loop contributions. Then, using Eq. (3.60) for the second $z(t)$ term, one has

$$Q\left\{z(t)+Td(t-\Delta t)+\frac{\Delta t}{2}\left[\frac{\Delta t}{4}BR^{-1}B^{\mathrm{T}}\lambda(t)+Hf(t)\right]\right\}+\lambda(t)=0$$

Upon substituting Eq. (3.59) into the equation above, we obtain

$$\left[Q+\left(I+\frac{\Delta t^2}{8}QBR^{-1}B^{\mathrm{T}}\right)P\right]z(t)+Q\left[Td(t-\Delta t)+\frac{\Delta t}{2}Hf(t)\right]$$
$$+\left(I+\frac{\Delta t^2}{8}QBR^{-1}B^{\mathrm{T}}\right)p(t)=0 \tag{3.62}$$

The solution for the unknown quantities $\boldsymbol{P}$ and $\boldsymbol{p}(t)$ can be found from the above equation. Since $\boldsymbol{z}(t) \neq \boldsymbol{0}$ and $\boldsymbol{p}(t) \neq \boldsymbol{0}$, the desired results are

$$\boldsymbol{P} = -\left(\boldsymbol{I} + \frac{\Delta t^2}{8}\boldsymbol{Q}\boldsymbol{B}\boldsymbol{R}^{-1}\boldsymbol{B}^{\mathrm{T}}\right)^{-1}\boldsymbol{Q} \tag{3.63}$$

$$\boldsymbol{p}(t) = \boldsymbol{P}\left[\boldsymbol{T}\boldsymbol{d}(t-\Delta t) + \frac{\Delta t}{2}\boldsymbol{H}\boldsymbol{f}(t)\right] \tag{3.64}$$

The substitution of Eqs (3.63) and (3.64) into Eq. (3.59) produces the desired closed–open-loop control law. It is in a recursive form in the sense that $\boldsymbol{u}(t)$ is not only a function of $\boldsymbol{z}(t)$ and $\boldsymbol{f}(t)$, but also a function of $\boldsymbol{z}(t-\Delta t)$, $\boldsymbol{u}(t-\Delta t)$ and $\boldsymbol{f}(t-\Delta t)$.

The closed-loop state vector is given by

$$\boldsymbol{z}(t) = \left[\boldsymbol{I} + \frac{\Delta t^2}{8}\boldsymbol{B}\boldsymbol{R}^{-1}\boldsymbol{B}^{\mathrm{T}}\boldsymbol{P}\right]^{-1}\left[\boldsymbol{T}\boldsymbol{d}(t-\Delta t) + \frac{\Delta t^2}{8}\boldsymbol{B}\boldsymbol{R}^{-1}\boldsymbol{B}^{\mathrm{T}}\boldsymbol{p}(t) + \frac{\Delta t}{2}\boldsymbol{H}\boldsymbol{f}(t)\right] \tag{3.65}$$

3.3.3 *Open-loop Control*

For open-loop control, $\boldsymbol{\lambda}(t)$ can be simply put in the form

$$\boldsymbol{\lambda}(t) = \boldsymbol{p}(t) \tag{3.66}$$

Following a procedure similar to that described above for the closed–open-loop control, one obtains

$$\boldsymbol{u}(t) = -\frac{\Delta t}{2}\left(\boldsymbol{R} + \frac{\Delta t^2}{4}\boldsymbol{B}^{\mathrm{T}}\boldsymbol{Q}\boldsymbol{B}\right)^{-1}\boldsymbol{B}^{\mathrm{T}}\boldsymbol{Q}\left[\boldsymbol{T}\boldsymbol{d}(t-\Delta t) + \frac{\Delta t}{2}\boldsymbol{H}\boldsymbol{f}(t)\right] \tag{3.67}$$

with $\boldsymbol{z}(t)$ given by

$$\boldsymbol{z}(t) = \left[\boldsymbol{I} - \frac{\Delta t^2}{4}\boldsymbol{B}\left(\frac{\Delta t^2}{4}\boldsymbol{B}^{\mathrm{T}}\boldsymbol{Q}\boldsymbol{B} + \boldsymbol{R}\right)^{-1}\boldsymbol{B}^{\mathrm{T}}\boldsymbol{Q}\right]\left[\boldsymbol{T}\boldsymbol{d}(t-\Delta t) + \frac{\Delta t}{2}\boldsymbol{H}\boldsymbol{f}(t)\right] \tag{3.68}$$

Example 3.5 It is instructive to examine numerically the control efficiencies associated with instantaneous optimal control algorithms and to compare them with those achievable under classical optimal control. The example given below is taken from Yang *et al.*[3]

An eight-storey structure in which every storey unit is identically constructed is considered for illustrative purposes. It is assumed that the structure is subjected to an earthquake-type ground acceleration $\ddot{x}_0(t)$ at the base, a sample function of $\ddot{x}_0(t)$ is shown in Fig. 3.18. The control is accomplished through an active mass damper system installed at the top of the structure as shown in Fig. 3.19.

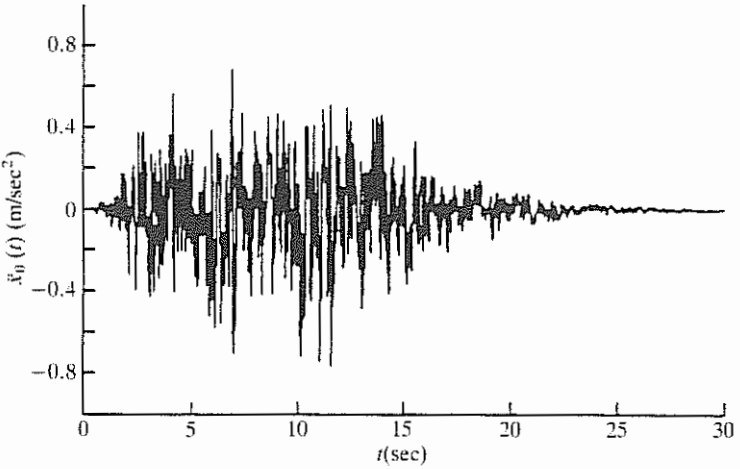

Figure 3.18 Simulated ground acceleration in Example 3.5[3]

Let $x_j(t)$, $j = 1, \ldots, 8$, be the relative displacement of the jth floor with respect to the ground and $x_d(t)$ be that associated with the active mass damper. Defining the state vector $z(t)$ as a nine-dimensional vector with

$$z^T(t) = [x_1(t), \ldots, x_8(t), x_d(t)]$$

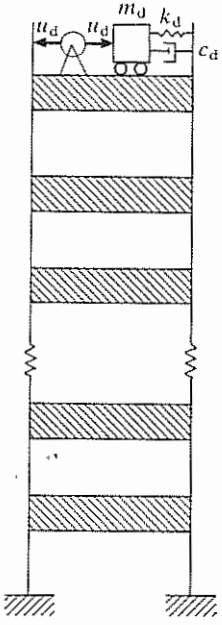

Figure 3.19 Structure with an active mass damper[3]

it is easy to show that the corresponding state-space equation has the usual form

$$\dot{z}(t) = Az(t) + bu_d(t) + h\ddot{x}_0(t), \qquad z(0) = 0 \tag{3.69}$$

where $u_d(t)$ is the control force generated by the active mass damper. It is noteworthy that all elements of vector b are zero except for the last two, i.e.

$$b^T = [0, \ldots, 0, -1, 1] \tag{3.70}$$

For the purpose of numerical calculations, the structural properties of each storey are taken to be: m = floor mass = 345.6 tons; k = elastic stiffness of each storey unit = 3.404×10^5 kN/m; and c = internal damping coefficient of each storey unit = 2937 tons/sec, which corresponds to a 2% damping for the first vibrational mode of the entire structure. The computed natural frequencies are 5.79, 17.18, 27.98, 37.82, 46.38, 53.36, 58.53, and 61.69 rad/sec. For the active mass damper, m_d = damper mass = 29.63 tons, c_d = damper

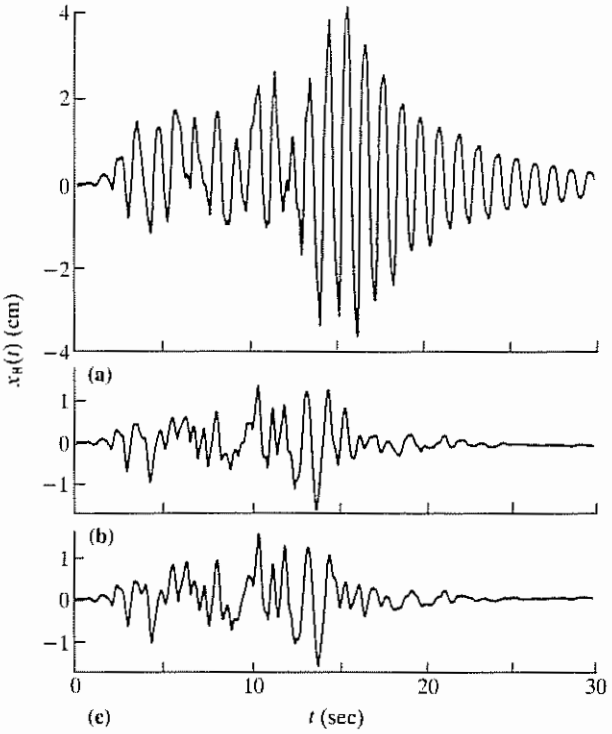

Figure 3.20 Top floor relative displacement in Example 3.5 (a) passive mass damper; (b) classical closed-loop control; (c) instantaneous optimal control[3]

damping = 25.0 tons/sec and k_d = damper stiffness = 957.2 kN/m. Thus, the damper mass is taken to be 2% of the first-mode generalized structural mass, the damper frequency is 98% of the first natural frequency of the structure, and the damping ratio of the damper is 7.3%.

The weighting matrix $\boldsymbol{R}$ in this case is a scalar and is assigned a value of 10^{-3}. The dimension of weighting matrix $\boldsymbol{Q}$ is 18 × 18. In view of the structure of vector $\boldsymbol{b}$ as given by Eq. (3.70), the active control force under instantaneous optimal control is influenced only by the last two rows of $\boldsymbol{Q}$. Hence, only the elements in the last two rows will be assigned with some values, i.e.

$$\boldsymbol{Q} = \alpha \begin{bmatrix} \mathbf{0} & \mathbf{0} \\ \hline \boldsymbol{Q}_{21} & \boldsymbol{Q}_{22} \end{bmatrix}$$

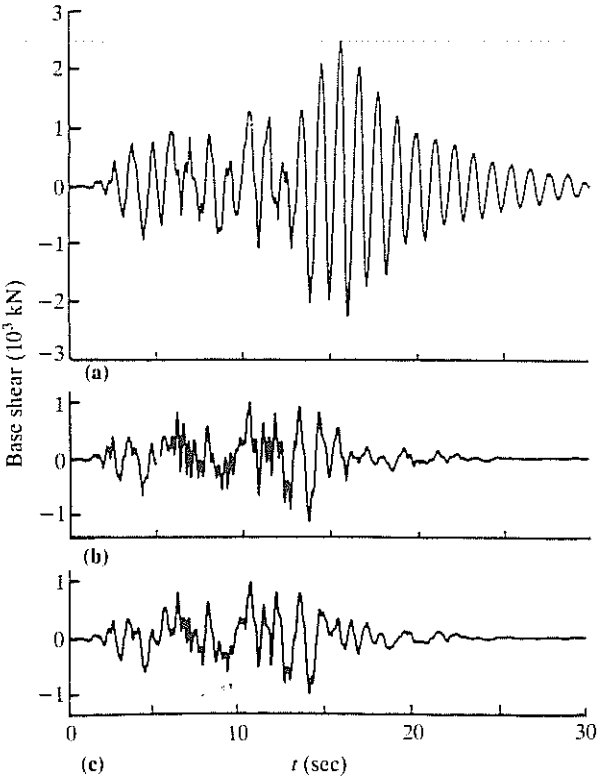

Figure 3.21 Base shear in Example 3.5 (a) passive mass damper; (b) classical closed-loop control; (c) instantaneous optimal control[3]

in which Q_{21} and Q_{22} are 2×9 matrices. For illustrative purposes these two matrices are given by

$$Q_{21} = \begin{bmatrix} -33.5 & -67 & -100.5 & -134 & -167.5 & -201 & -234.5 & -268 & 375.6 \\ -33.5 & -67 & -100.5 & -134 & -167.5 & -201 & -234.5 & -268 & 32.2 \end{bmatrix}$$

$$Q_{22} = \begin{bmatrix} 67.5 & 135 & 202.5 & 270 & 338.5 & 405 & 472.5 & 540 & 32.2 \\ 5.8 & 11.6 & 17.4 & 23.2 & 29 & 34.7 & 40.5 & 46.3 & 5.7 \end{bmatrix}$$

A value of 67.0 is chosen for α such that the top floor relative displacement is reduced by approximately 60%.

In the case of classical closed-loop control, the weighting matrix Q is considered to be diagonal with $Q_{jj} = 1.3 \times 10^5$, $j = 1, \ldots, 8$ and $Q_{jj} = 0$, $j = 9, \ldots, 18$.

Without the active control force, the mass damper is passive. The top floor relative displacement and the base shear are shown in Figs 3.20(a) and 3.21(a), respectively. The corresponding controlled results using instantaneous

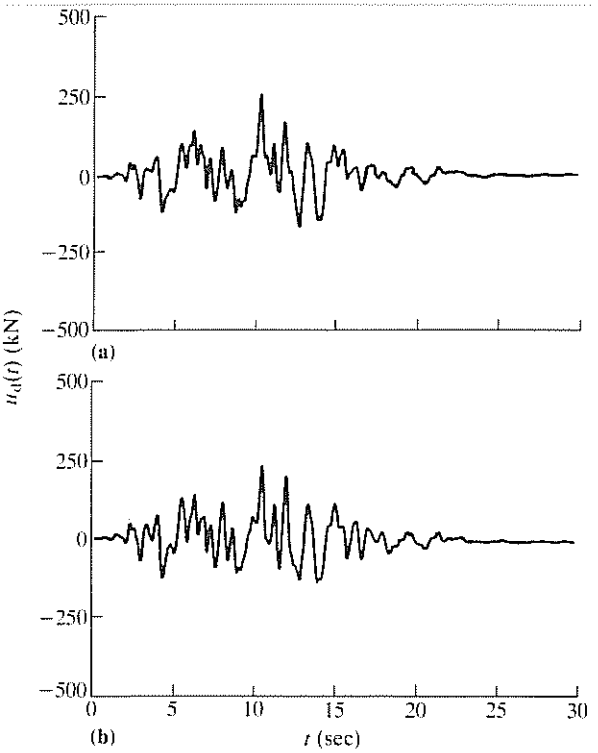

Figure 3.22 Required control force in Example 3.5 (a) classical closed-loop control; (b) instantaneous optimal control[3]

Table 3.3 Maximum response and required control force in Example 3.5

Control law	Top floor displacement (cm)	Base shear force (kN)	Active control force (kN)
Uncontrolled	4.10	2506	—
Classical closed-loop control	1.61	1075	250
Instantaneous optimal control	1.54	1045	232

control algorithms and the classical closed-loop control are also shown in Figs 3.20 and 3.21. They indicate that instantaneous optimal control algorithms are slightly more efficient than the classical closed-loop control. We note that all three instantaneous optimal control algorithms would produce identical results under the same simulated conditions.

A comparison of the required control forces is given in Fig. 3.22. The maximum required control forces and the maximum response quantities at the top floor are summarized in Table 3.3.

3.4 Independent Modal Space Control (IMSC)

As the name implies, control system design based on IMSC takes place in the modal space. To facilitate discussions, let us depart temporarily from the state-space representation and return to the traditional configuration space for this development.

Assuming that a structure possesses normal modes, it is well known that the equations of motion of an n-degree-of-freedom system can be decomposed into a system of n decoupled single-degree-of-freedom systems in modal coordinates. Thus, consider an n-degree-of-freedom structural system represented by (see Eq. 2.1)

$$\boldsymbol{M}\ddot{\boldsymbol{x}}(t)+\boldsymbol{C}\dot{\boldsymbol{x}}(t)+\boldsymbol{K}\boldsymbol{x}(t)=\boldsymbol{D}\boldsymbol{u}(t)+\boldsymbol{E}\boldsymbol{f}(t), \quad \boldsymbol{x}(0)=\boldsymbol{x}_0, \quad \dot{\boldsymbol{x}}(0)=\dot{\boldsymbol{x}}_0 \tag{3.71}$$

where $\boldsymbol{x}(t)$ is the n-dimensional displacement vector and $\boldsymbol{D}$ and $\boldsymbol{E}$ are, respectively, appropriate $n \times m$ and $n \times r$ control and external excitation location matrices. Let $\boldsymbol{\Phi}$ be the $n \times n$ modal matrix whose jth column is the jth mode shape vector. Then, applying the modal transformation

$$\boldsymbol{x}(t)=\boldsymbol{\Phi}\boldsymbol{y}(t) \tag{3.72}$$

and substituting it into Eq. (3.71), it is transformed into a system of second-order modal equations[16]

$$m_j\ddot{y}_j(t)+c_j\dot{y}_j(t)+k_jy_j(t)=v_j(t)+q_j(t), \qquad j=1,2,\ldots,n \tag{3.73}$$

where the subscript j is used to indicate quantities in the jth mode. In particular, the vector $\boldsymbol{v}(t)$, defined by

$$\boldsymbol{v}^{\mathrm{T}}(t)=[v_1(t),\ldots,v_n(t)] \tag{3.74}$$

is the control vector in the modal space and is related to the physical control vector $\boldsymbol{u}(t)$ through the modal participation matrix by[16]

$$\boldsymbol{v}(t)=\boldsymbol{\Phi}^{\mathrm{T}}\boldsymbol{D}\boldsymbol{u}(t)=\boldsymbol{L}\boldsymbol{u}(t) \tag{3.75}$$

Equations (3.73) have the appearance of a set of traditional decoupled modal equations except for the fact that they are in general coupled through the modal control forces $v_j(t)$, since each $v_j(t)$ usually depends on all the modal coordinates. If, however, each $v_j(t)$ is designed to depend on $y_j(t)$ and $\dot{y}_j(t)$ alone, e.g.

$$v_j(t)=g_{1j}y_j(t)+g_{2j}\dot{y}_j(t) \tag{3.76}$$

Equations (3.73) then become mutually independent, thus permitting independent control design of n second-order systems. Control algorithms based on this design procedure have been referred to as control by modal synthesis[17] or, more commonly, independent modal space control.[18–20] The procedure essentially shifts the problem of control design from a coupled $2n$-order structural system to n second-order systems, a considerably simpler problem with substantial savings in computational efforts. It is particularly attractive when only a few critical modes need to be controlled.

The modal control forces $\boldsymbol{v}(t)$ can be determined by using any method of control. For example, if optimal control is desired, they can be determined by minimizing a quadratic performance index J of the form

$$J=\sum_{j=1}^{n}J_j \tag{3.77}$$

where J_j are the modal performance indices taking, for example, the form

$$J_j=\int_0^{t_f}[q_{1j}y_j^2(t)+q_{2j}\dot{y}_j^2(t)+r_jv_j^2(t)]\,\mathrm{d}t \tag{3.78}$$

Upon determination of the modal control forces, the physical controller forces can be synthesized subsequently via Eq. (3.75).

Let us examine Eq. (3.75) more closely. Note that the dimension of modal participation matrix $\boldsymbol{L}$ is $n\times m$, where n is the number of controlled modes

and m is the number of controllers. If $m = n$, $\boldsymbol{L}$ is a square matrix and, if it is invertible, the physical control vector $\boldsymbol{u}(t)$ is simply found from Eq. (3.75) as

$$\boldsymbol{u}(t) = \boldsymbol{L}^{-1}\boldsymbol{v}(t) \tag{3.79}$$

If $m \neq n$, the inverse of $\boldsymbol{L}$ does not exist but $\boldsymbol{u}(t)$ can be approximated by performing a pseudo-inverse of $\boldsymbol{L}$ or by employing a least square procedure, giving

$$\boldsymbol{u}(t) = \boldsymbol{L}^{+}\boldsymbol{v}(t) \tag{3.80}$$

where

$$\begin{aligned} \boldsymbol{L}^{+} &= \boldsymbol{L}^{\mathrm{T}}(\boldsymbol{L}\boldsymbol{L}^{\mathrm{T}})^{-1}, \qquad m > n \\ &= (\boldsymbol{L}^{\mathrm{T}}\boldsymbol{L})^{-1}\boldsymbol{L}^{\mathrm{T}}, \qquad m < n \end{aligned} \tag{3.81}$$

if the indicated inverses exist.

The effect of $m \neq n$ on the controlled system performance can be assessed by comparing the design modal control vector $\boldsymbol{v}(t)$ with the actual modal control vector $\boldsymbol{v}_a(t)$ applied to the structure. As seen from Eq. (3.75), the actual modal control vector is

$$\boldsymbol{v}_a(t) = \boldsymbol{L}\boldsymbol{u}(t)$$

with $\boldsymbol{u}(t)$ given by Eqs (3.80) and (3.81). Hence, for $m > n$,

$$\boldsymbol{v}_a(t) = \boldsymbol{L}\boldsymbol{u}(t) = \boldsymbol{L}\boldsymbol{L}^{\mathrm{T}}(\boldsymbol{L}\boldsymbol{L}^{\mathrm{T}})^{-1}\boldsymbol{v}(t) = \boldsymbol{v}(t) \tag{3.82}$$

and, for $m < n$,

$$\boldsymbol{v}_a(t) = \boldsymbol{L}\boldsymbol{u}(t) = \boldsymbol{L}(\boldsymbol{L}^{\mathrm{T}}\boldsymbol{L})^{-1}\boldsymbol{L}^{\mathrm{T}}\boldsymbol{v}(t) \tag{3.83}$$

Equation (3.82) shows that, when the number of controllers is larger than the number of controlled modes, $\boldsymbol{v}_a(t) = \boldsymbol{v}(t)$ and the excess controllers result in redundant control forces which do not alter the controlled system behaviour. Thus, there is no practical purpose served by having more controllers than the number of modes to be controlled. On the other hand, it is seen from Eq. (3.83) that, when the number of controllers is smaller than the number of controlled modes $\boldsymbol{v}_a(t) \neq \boldsymbol{v}(t)$ and a degradation of the controlled system behaviour is possible. As the following example shows, control efficiency deteriorates as the number of controllers decreases.

Example 3.6 Consider the control of bending vibration of a tapered bar of length $d = 5$ clamped at one end. The displacement $w(x, t)$ as a function of the spatial variable x and time t satisfies the partial differential equation

$$\frac{\partial^2}{\partial x^2}\left[EI(x)\frac{\partial^2 w}{\partial x^2} \right] + M(x)\frac{\partial^2 w}{\partial t^2} = u(x, t) \tag{3.84}$$

where the mass and stiffness distributions are

$$M(x) = EI(x) = 1.0 - 0.2x/d$$

It is assumed that the control forces are point forces equally spaced along the beam.

Using the expansion theorem, $w(x, t)$ can be represented by a linear function of modal coordinates $y_j(t)$, each of which satisfying an ordinary differential equation similar in form to Eq. (3.73).

We wish to control the lowest 20 modes ($n = 20$) based on IMSC using a varying number of controllers. The performance index given by Eqs (3.77) and (3.78) is used with

$$q_{1j} = \omega_j^2, \quad q_{2j} = 1, \qquad \text{and} \qquad r_j = 20, \quad j = 1, 2, \ldots, n$$

where ω_j is the jth modal frequency.

The control gain for each of the modal control forces can be found by solving a second-order Riccati equation. Assuming a constant Riccati matrix, a closed form solution of the Riccati equation is available and the optimal modal control force $v_j(t)$ is[19]

$$v_j(t) = \omega_j(\omega_j - \sqrt{\omega_j^2 + 1/r_j})y_j(t) - [2\omega_j(-\omega_j + \sqrt{\omega_j^2 + 1/r_j}) + 1/r_j]^{1/2}\dot{y}_j(t)$$

Table 3.4 Closed-loop Eigenvalues for different numbers of actuators[20]

	Number of actuators					
	5	10	15	19	20	
Mode no.	Real part	Real part	Real part	Real part	Real part	Imag. part
1	−0.033	−0.116	−0.127	−0.132	−0.146	0.138
2	−0.039	−0.106	−0.137	−0.142	−0.158	0.900
3	−0.043	−0.107	−0.140	−0.143	−0.158	2.486
4	−0.043	−0.073	−0.142	−0.145	−0.158	4.845
5	−0.048	−0.075	−0.143	−0.146	−0.158	8.013
6	−0.059	−0.073	−0.145	−0.147	−0.158	11.96
7	−0.010	−0.076	−0.146	−0.147	−0.158	16.70
8	−0.027	−0.077	−0.148	−0.148	−0.158	22.23
9	−0.039	−0.080	−0.149	−0.149	−0.158	28.54
10	−0.044	−0.088	−0.148	−0.150	−0.158	35.65
11	−0.051	−0.122	−0.149	−0.151	−0.158	43.55
12	−0.076	−0.022	−0.118	−0.152	−0.158	52.44
13	−0.010	−0.056	−0.119	−0.152	−0.158	61.72
14	−0.035	−0.064	−0.092	−0.153	−0.158	71.99
15	−0.041	−0.068	−0.099	−0.154	−0.158	83.06
16	−0.042	−0.070	−0.129	−0.155	−0.158	94.92
17	−0.048	−0.072	−0.028	−0.155	−0.158	107.6
18	−0.059	−0.073	−0.060	−0.157	−0.158	121.0
19	−0.010	−0.075	−0.068	−0.157	−0.158	135.3
20	−0.027	−0.078	−0.070	−0.158	−0.158	150.4

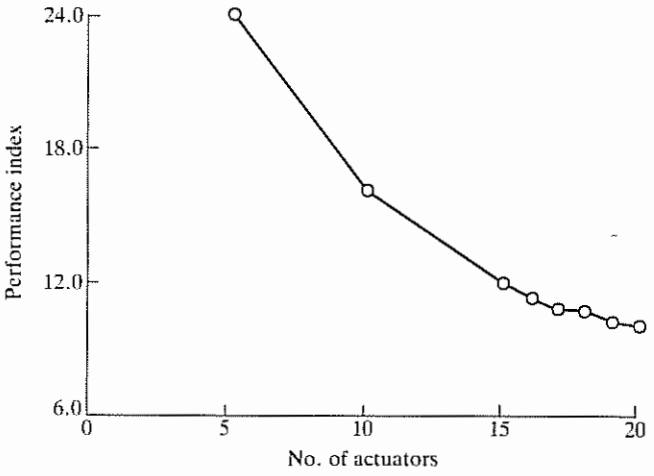

Figure 3.23 Performance index for different numbers of actuators[20]

The effect of using a varying number of actuators to implement IMSC has been studied.[20] Table 3.4 compares the closed-loop eigenvalues as functions of the number of actuators. It is seen that, as the number of actuators decreases, the stability margin decreases due to degradation of the accuracy in carrying out the pseudo-inverse given by the second of Eqs (3.81).

The value of the performance index is expected to increase as the number of actuators decreases. This trend is shown in Fig. 3.23 with $t_f = 20$. It is noted that, when computing the performance index, one must replace $v_j(t)$ in Eq. (3.78) by $v_{aj}(t)$, the actual jth modal control force. Larger values of the performance index indicate poorer closed-loop system performance and lower control efficiency.

3.5 Bounded State Control

In general, the purpose of active control is served when a set of structural response variables are maintained within an allowable region determined by the requirements of structural safety and human comfort. Under safety considerations, relative displacements at selected locations of the structure are of central concern and, for human comfort, the absolute accelerations. Thus, active control algorithms designed to limit the state variables within prescribed bounds, or bounded state control, are of practical importance when applied to civil engineering structures.

An approach to bounded state control is discussed[21,22] using linear state feedback laws. Based on an extension of the Lyapunov function methods, it

follows, in a sense, the pole assignment concept to achieve bounded state control. In addition, all pulse control strategies proposed in the literature fall into this category.[23–34] The objective of pulse control advanced by Masri *et al*[23–25] and by Udwadia and Tabaie[32,33] is to destroy the gradual rhythmic build-up of the structural response in the case of resonance by means of short-interval high-energy pulses. A continuous monitoring of the system state variables is required. To conserve energy, control is activated only when some prespecified threshold has been exceeded. The pulse magnitudes are determined analytically[24,32,33] so as to minimize a non-negative cost function. The control procedure proposed[23,25] consists of application of pulses every time a zero crossing of the response variable is detected. The magnitudes of the pulses are functions of the instantaneous velocities.

In Prucz and Soong[26] and in Reinhorn *et al*[31], the pulse control design is anticipatory, namely, pulses are applied a short time interval prior to an anticipated threshold crossing. These algorithms require state prediction but cover the case of non-resonant as well as resonant response.

Generally speaking, pulse control procedures are relatively simple to implement; they require less on-line computational efforts when compared with other modern control techniques. They are also suited for treatment of inelastic structures. Another advantage has to do with possible savings of control energy required. In the pulse control mode, since small vibrational levels are tolerated, control forces need to be applied only when necessary and a relatively small amount of energy may be sufficient for periodic corrective actions.

In what follows, the development of a pulse control strategy based on work by Prucz *et al*[28] is briefly described for a simple case.

The basic idea used in pulse control design is that a train of force pulses applied to a structure can produce a response which matches the response produced by a continuous loading of arbitrary nature within specified error bounds. Consider a single-degree-of-freedom linear system. One pure pulse applied to the system will cause a free vibration with an initial velocity which depends on the impulse magnitude, at a frequency equal to the natural frequency. If the system experiences a forced vibration, its response after pulse application can be regarded as the resultant of the response due to the pulse alone and the system response to the forcing function alone. The response to a pulse of finite duration $\Delta t (\Delta t = T_0/10, T_0$ is the natural period) is illustrated in Fig. 3.24. Suppose the frequency of the forcing function is lower than the natural frequency of the system. A pure pulse applied in the proper direction can reduce the response of the system during a time period of one half of the natural period, where maximum reduction is achieved after one fourth the natural period and no reduction at half the natural period. After a time longer than half the natural period, the response of the system can be increased by the pulse. Therefore, in order to control the system

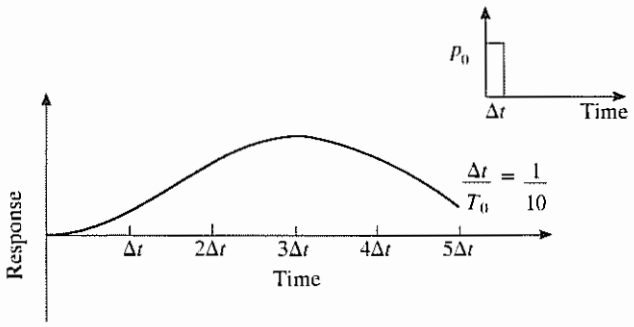

Figure 3.24 Typical response to a rectangular pulse[28]

response, a second pulse should be applied with a period Δt_p smaller than half the natural period (Fig. 3.25).

Let us consider the interpulse interval (t_i, t_j) and choose its length to be of the order of one fourth the natural period. The response expected in this time interval has to be reduced, if necessary, to a value below the safety limit. Suppose the expected maximum response exceeds the allowable value and it is at time t_j. A proper pulse applied at time t_i can reduce the response at time t_j to any desired value. The information needed is the system state at time t_i which defines the 'initial conditions' and contains the system response prior to time t_i, the systen dynamic characteristics and the external forcing function in the time interval (t_i, t_j). The block diagram of the control procedure is shown in Fig. 3.26.

Next, a procedure to determine the required pulse $p(t_i)$, based only on the sensed system state at time t_i and the system dynamic characteristics, is derived. The system response at time t_j can be considered as a superposition of the contributions of the initial conditions at time t_i, the pulse applied at time t_i and the external forcing function during the time interval (t_i, t_j). This is true for nonlinear systems as well if we assume that the system characteristics

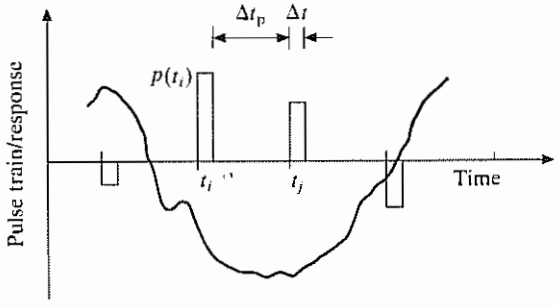

Figure 3.25 Schematic representation of a pulse train[28]

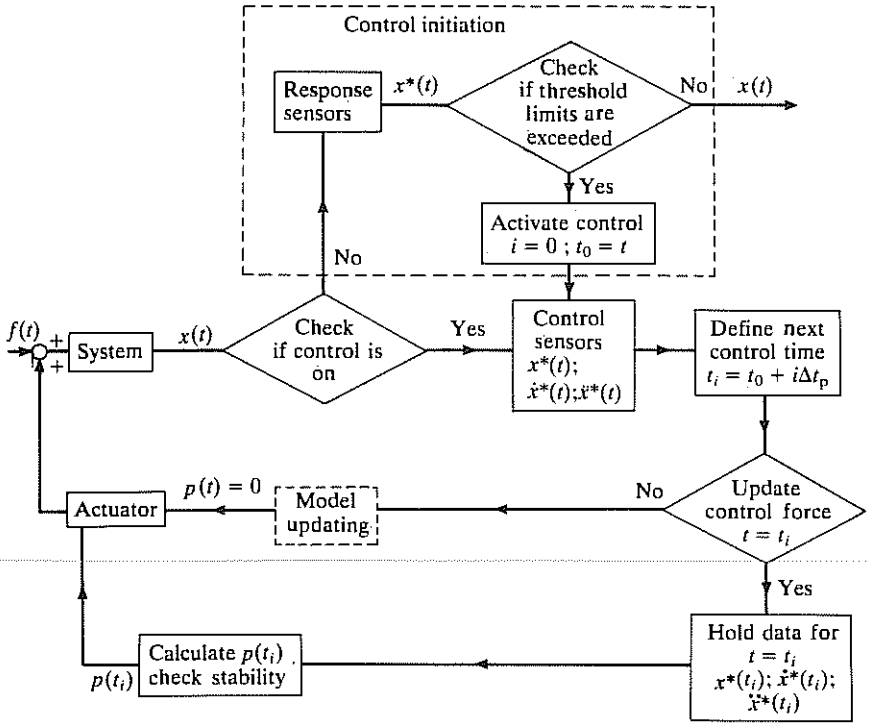

Figure 3.26 Block diagram of control procedure

are constant during this time interval. Thus, if rectangular pulses of width Δt are considered, the system response to an excitation of the form

$$f(t) = f_o \sin \omega t \tag{3.85}$$

is

$$x(t_j) = Z_X x(t_i) + Z_V \dot{x}(t_i) + Z_p p(t_i) + Z_{EF} f_o \tag{3.86}$$

where, for zero damping,

$$\left.\begin{aligned} Z_X &= \cos(\omega_o \Delta t_p) \\ Z_V &= \frac{1}{\omega_o} \sin(\omega_o \Delta t_p) \\ Z_p &= \frac{1}{k}\{\cos[\omega_o(\Delta t_p - \Delta t)] - \cos(\omega_o \Delta t_p)\} \\ Z_{EF} &= \frac{\omega_o}{k}\left[\frac{\omega_o \sin(\omega t_j)}{\omega_o^2 - \omega^2} - \frac{\sin(\omega t_i - \omega_o \Delta t_p)}{2(\omega_o + \omega)} - \frac{\sin(\omega t_i + \omega_o \Delta t_p)}{2(\omega_o - \omega)}\right] \end{aligned}\right\} \tag{3.87}$$

In the above, ω_o and k are the natural frequency and the stiffness of the system, respectively. Coefficients Z_X, Z_V, Z_p and Z_{EF} define the contributions to the response of the displacement, velocity, pulse at time t_i and of the forcing function, respectively. More general expressions for these coefficients for a damped system can be similarly derived.

In most cases, the forcing function in the interval (t_i, t_j) is unknown and difficult to predict. Its contribution to the response in Eq. (3.86) may be significant and cannot be ignored. However, over a small time interval (t_i, t_j), the external force is not expected to change in a significant way. Therefore, as a first approximation, the external force will be assumed to be constant in the interval (t_i, t_j) and equal to the external force at time t_i, $f(t_i)$. This force, in turn, can be estimated from the monitored state variables at time t_i as

$$f(t_i) = \left(\frac{k}{\omega_0^2}\right)\ddot{x}(t_i) + kx(t_i) \tag{3.88}$$

With this approximation, Eq. (3.86) becomes

$$x(t_j) = Z_X x(t_i) + Z_V \dot{x}(t_i) + Z_p p(t_i) + Z_{AF} f(t_i) \tag{3.89}$$

where Z_{AF} is the coefficient of the approximated forcing function

$$Z_{AF} = \frac{1}{k}[1 - \cos(\omega_o \Delta t_p)] \tag{3.90}$$

The pulse magnitude $p(t_i)$ is designed such that, if the expected response during interval (t_i, t_j) exceeds a maximum permissible level x_L, it will be reduced to x_L and, if the expected maximum response, x_{max}, is below the limiting values, no pulse is to be triggered. Thus, the required pulse magnitude can be expressed as

$$p(t_i) = \frac{1}{Z_p} x_L + \alpha x(t_i) + \beta \dot{x}(t_i) + \gamma f(t_i), \qquad x_{max} > x_L \tag{3.91}$$

where

$$\left.\begin{aligned}
\alpha &= -\frac{Z_X}{Z_p} = -\frac{k\cos(\omega_o \Delta t_p)}{\cos[\omega_o(\Delta t_p - \Delta t)] - \cos(\omega_o \Delta t_p)} \\
\beta &= -\frac{Z_V}{Z_p} = -\frac{k\sin(\omega_o \Delta t_p)/\omega_o}{\cos\omega_o(\Delta t_p - \Delta t) - \cos(\omega_o \Delta t_p)} \\
\gamma &= -\frac{Z_{AF}}{Z_p} = -\frac{1 - \cos(\omega_o \Delta t_p)}{\cos[\omega_o(\Delta t_p - \Delta t)] - \cos(\omega_o \Delta t_p)}
\end{aligned}\right\} \tag{3.92}$$

and

$$p(t_i) = 0, \qquad x_{max} \leqslant x_L \tag{3.93}$$

Coefficients α, β and γ define the contribution of the initial conditions at time t_i and of the approximated external force to the required pulse magnitude, respectively. They are functions of pulse width, interpulse interval and system dynamic characteristics only. Thus, for a linear system, α, β and γ remain constant during control and can be calculated off-line.

When the frequencies of dominant components of the forcing function are close to or above the system natural frequencies, the maximum response during interval (t_i, t_j) can occur at some time within this interval and not at time t_j, as previously assumed. The pulse can be designed to limit 'local' maximum by changing Δt_p used in the equations for α, β and γ to

$$\Delta t'_p = t_{max} - t_i \tag{3.94}$$

where $t_{max}(t_i \leqslant t_{max} < t_j)$ is the time instant at which the response to be reduced requires a maximum pulse magnitude, $p(t_i)_{max}$. Values for α, β, and γ for different time intervals $\Delta t'_p(\Delta t < \Delta t'_p < \Delta t_p)$ can also be calculated off-line, so that this improvement does not increase on line computations. Nevertheless, it may lead to instability. While the value of the response is decreased at some time within interval (t_i, t_j), the pulse may increase the value of the response at time t_j if it is of the opposite sign. This can happen when the external force has a dominant high frequency component. Therefore, an additional condition has to be added that will exclude this possibility, but will still keep the response below safety limits. It is suggested that, in this case, the pulse $p(t_i)$ will still be applied but the interpulse interval will be decreased such that the next pulse $p(t_j)$ will be applied before the response at the end of interval (t_i, t_j) exceeds its permitted value. The decreased interpulse interval will continue to be used throughout the control period. No additional computations are required since values for α, β and γ for different time intervals $\Delta t'_p$ are already stored. Thus, the pulse algorithm adjusts itself to high frequency dominant loading and response, thus avoiding instability while controlling peak response values.

Example 3.7 An example that illustrates the control procedure presented is given in Fig. 3.27 for a system with a natural frequency of 3.14 sec^{-1} and a damping ratio of 0.01. The frequency of the forcing function is 0.34 sec^{-1} and the parameters Δt and Δt_p used are 0.10 sec and 0.50 sec, respectively. A 20% reduction in the response is desired. Fig. 3.28 shows the acceleration of the system before and after control. The acceleration level is generally decreased except during time intervals when pulses are applied, and peak acceleration values are induced. Control of 40% of maximum response for

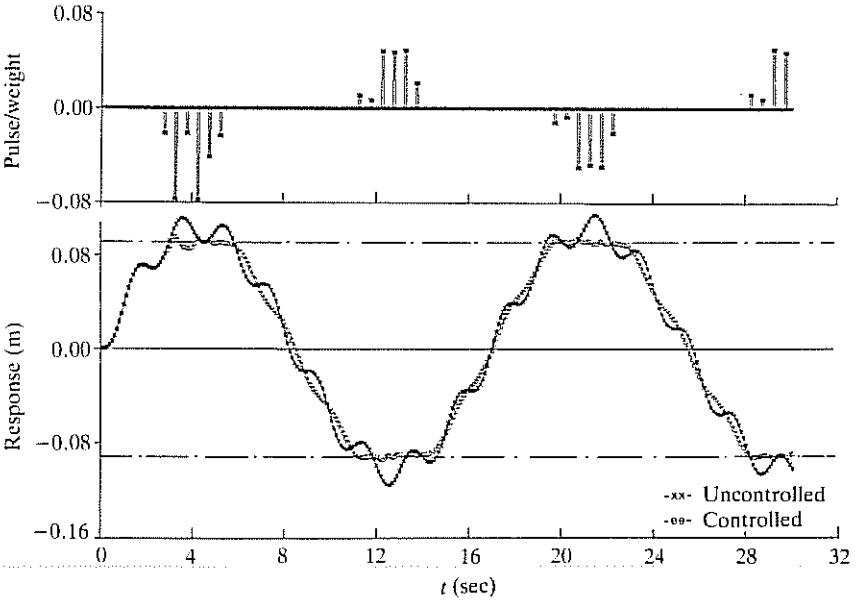

Figure 3.27 Pulse train, controlled and uncontrolled displacement response (20% reduction)[28]

the same system and the required pulse train are illustrated in Fig. 3.29. The controlled response shows that, at the beginning of the pulse train when the forcing function is increasing and therefore 'underestimated', the reduction is less than desired and, when the forcing function is decreasing and thus 'overestimated', more reduction is achieved. The error involved is of the order of 3%.

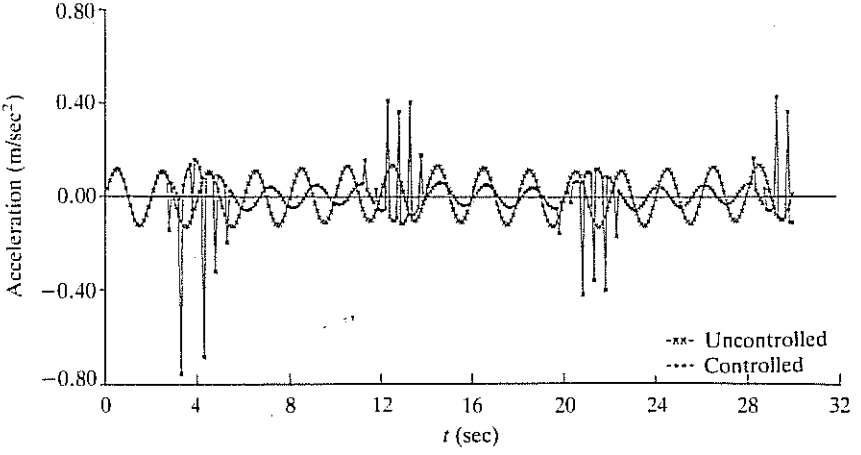

Figure 3.28 Controlled and uncontrolled acceleration response (20% reduction)

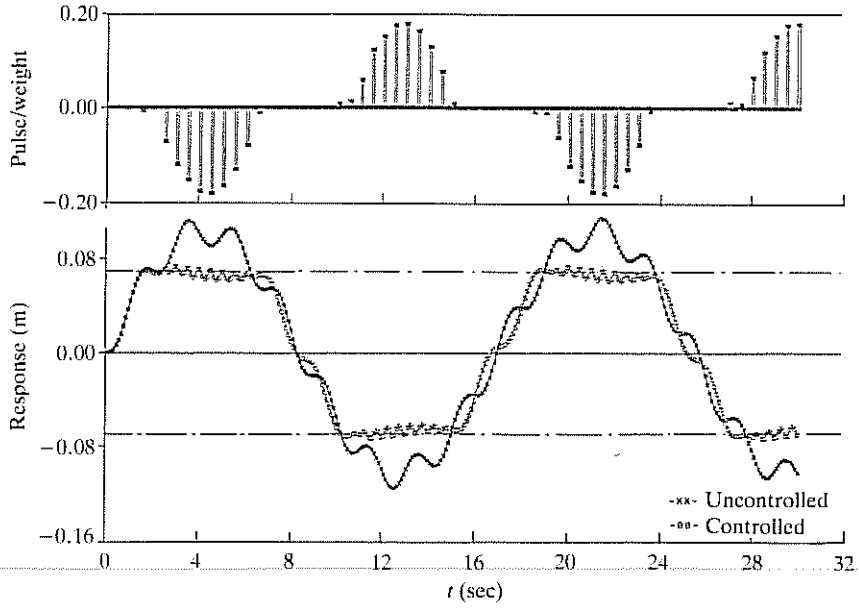

Figure 3.29 Pulse train, controlled and uncontrolled displacement response (40% reduction)[28]

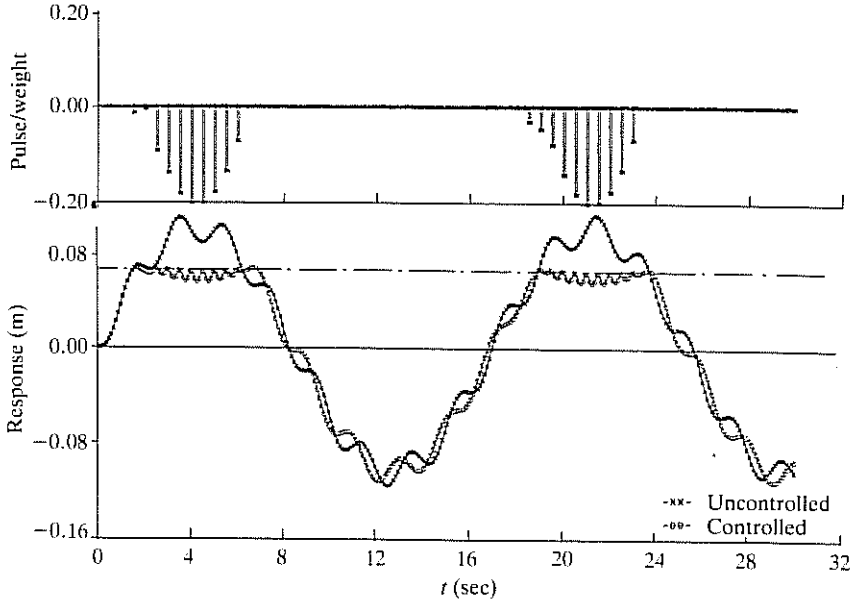

Figure 3.30 Unidirectional pulse train, controlled and uncontrolled displacement response (40% reduction)[28]

3.5.1 Unidirectional Pulses

The control algorithm is designed to reduce the response to a safety level if its value is expected to exceed this safety level. No pulse is applied if the expected response is below the limiting value. The stability check of the algorithm ensures that a pulse applied for correcting one direction of the response will not increase the response in the opposite direction above its safety level. Thus, the control algorithm allows the use of pulses in only one direction to ensure only one limit of the response. This can result in a considerable simplification in pulse supply hardware and its installation. There is no change in the algorithm, but the requirement to trigger a pulse only when the expected response in the direction considered exceeds its limit. An example of the feasibility of this procedure is given in Fig. 3.30, where a 40% response reduction is considered. The previous system and control parameters are used.

3.6 Other Control Algorithms

Not included in the discussion above are a wide variety of sub-optimal or ad hoc control techniques, most of which are tailored to specific structural environments or specific sensor-controller specifications. More recent work includes discussions on predictive control[34,35] and fuzzy control[36,37] as possible control philosophies. Simultaneous control and structural parameter optimization is another topic receiving increasing attention at present.[39,40] This topic will be discussed in more detail in Chapter 6.

References

1. Sage A P and White C C III 1977 *Optimum Systems Control* 2nd edn Prentice-Hall, Englewood Cliffs NJ
2. Kwakernaak H and Sivan R 1972 *Linear Optimal Control Systems* Wiley, New York NY
3. Yang J N, Akbarpour A and Ghaemmaghami P 1987 New Control Algorithms for Structural Control. *ASCE Journal of Engineering Mechanics* **113** pp 1369–86
4. Chung L L, Reinhorn A M and Soong T T 1988 Experiments on Active Control of Seismic Structures. *ASCE Journal of Engineering Mechanics* **114** pp 241–56
5. Yang J N 1975 Application of Optimal Control Theory to Civil Engineering Structures. *ASCE Journal of Engineering Mechanics* **101** pp 818–38
6. Abdel-Rohman M and Leipholz H H E 1978 Structural Control by Pole Assignment Method. *ASCE Journal of Engineering Mechanics* **104** pp 1157–75
7. Martin C R and Soong T T 1976 Modal Control of Multistorey Structures. *ASCE Journal of Engineering Mechanics* **102** pp 613–23

8. Wonham W M 1974 Linear Multivariable Control. *Lecture Notes on Economics and Mathematical Systems* No. 101 Springer-Verlag, New York
9. Brogan W L 1974 Applications of a Determinant Identity to Pole-Assignment and Observer Problems. *IEEE Transactions on Automatic Control* **AC-19** pp 612–14
10. Moore B C 1976 On the Flexibility Offered by State Feedback in Multivariable Systems Beyond Closed Loop Eigenvalue Assignment. *IEEE Transactions on Automatic Control* **AC-21** pp 689–92
11. Kimura H 1975 Pole Assignment by Gain Output Feedback. *IEEE Transactions on Automatic Control* **AC-20** pp 509–16
12. Solheim O A 1972 Design of Optimal Control Systems with Prescribed Eigenvalues. *International Journal of Control* **15** pp 143–60
13. Sebakhy O A and Sorial N N 1979 Optimization of Linear Multivariable Systems with Prespecified Closed-loop Eigenvalues. *IEEE Transactions on Automatic Control* **AC-24** pp 355–7
14. Davison E J 1970 On Pole Assignment in Linear Systems with Incomplete State Feedback. *IEEE Transactions on Automatic Control* **AC-15** pp 348–51
15. Wang P C, Kozin F and Amini F 1983 Vibration Control of Tall Buildings. *Engineering Structures* **5** pp 282–9
16. Clough R W and Penzien J 1975 *Dynamics of Structures* McGraw-Hill, New York
17. Meirovitch L and Oz H 1980 Active Control of Structures by Modal Synthesis. In Leipholz H H E (ed) *Structural Control* North Holland, Amsterdam pp 505–21
18. Meirovitch L and Oz H 1980 Modal Space Control of Distributed Gyroscopic Systems. *Journal of Guidance, Control and Dynamics* **3** pp 140–50
19. Meirovitch L and Baruh H 1982 Control of Self-Adjoint Distributed Parameter Systems. *Journal of Guidance, Control and Dynamics* **5** pp 60–66
20. Baruh H and Meirovitch L 1982 Implementation of the IMSC Method by Means of a Varying Number of Actuators, Paper No. 82-1035, AIAA/AAS/ Astrodynamic Conference, San Diego CA
21. Lee S K and Kozin F 1986 Bounded State Control of Structures with Uncertain Parameters. In Hart G C and Nelson R B (eds) *Dynamic Response of Structures* ASCE, New York pp 788–94
22. Lee S K and Kozin F 1987 Bounded State Control of Linear Structures. In Leipholz H H E (ed) *Structural Control* Martinus Nijhoff, Amsterdam pp 387–407
23. Masri S F, Bekey G A and Udwadia F E 1980 On-line Pulse Control of Tall Buildings. In Leipholz H H E (ed) *Structural Control* North Holland, Amsterdam pp 471–92
24. Masri S F, Bekey G A and Caughey T K 1981 Optimal Pulse Control of Flexible Structures. *ASME Journal of Applied Mechanics* **48** pp 619–26
25. Masri S F, Bekey G A and Caughey T K 1982 On-line Control of Nonlinear Flexible Structures. *ASME Journal of Applied Mechanics* **49** pp 877–84
26. Miller R K, Masri S F, Dehghanyar T J and Caughey T K 1988 Active Vibration Control of Large Civil Structures. *ASCE Journal of Engineering Mechanics* **114** pp 1542–70

27. Prucz Z and Soong T T 1983 On Reliability and Active Control of Tension Leg Platforms. In Chen W F and Lewis A D M (eds) *Recent Advances in Engineering Mechanics and Their Impact on Civil Engineering Practice* **2** pp 903–6
28. Prucz Z, Soong T T and Reinhorn A M 1985 An Analysis of Pulse Control for Simple Mechanical Systems. *ASME Journal of Dynamic Systems Measurement Control* **107** pp 123–31
29. Reinhorn A M, Soong T T and Manolis G D 1986 Disaster Prevention of Deep Water Offshore Structures by Means of Active Control. *Procedures of ASME Fifth International OMAE Conference* Tokyo, Japan pp 39–44
30. Reinhorn A M, Manolis G D and Wen C Y 1987 Active Control of Inelastic Structures. *ASCE Journal of Engineering Mechanics* **113** pp 315–33
31. Reinhorn A M, Soong T T and Wen C Y 1987 Base Isolated Structures With Active Control. *Proceedings of ASME PVD Conference* San Diego CA pp 413–20
32. Udwadia F E and Tabaie S 1981 Pulse Control of a Single-Degree-of-Freedom System. *ASCE Journal of Engineering Mechanics* **107** pp 997–1010
33. Udwadia F E and Tabaie S 1981 Pulse Control of Structural and Mechanical Systems. *ASCE Journal of Engineering Mechanics* **107** pp 1011–28
34. Barbat A H, Rodellar J and Martin-Sanchez J M 1986 Pulse Control of the Earthquake Response of Elevated Water Tanks. *Proceedings of 8th European Conference on Earthquake Engineering* **8.5** pp 49–56
35. Rodellar J, Barbat A H and Martin-Sanchez J M 1987 Predictive Control of Structures. *ASCE Journal of Engineering Mechanics* **113** pp 797–812
36. Rodellar J, Chung L L, Soong T T and Reinhorn A M 1989 Experimental Digital Predictive Control of Structures. *ASCE Journal of Engineering Mechanics* **115** pp 1245–61
37. Yao J T P and Abdel-Rohman M 1987 Research Topics for Practical Implementation of Structural Control. In Leipholz H H E (ed) *Structural Control* Martinus Nijhoff, Amsterdam pp 762–67
38. Yao J T P 1987 Uncertainties in Structural Control. *Proceedings of ASME Vibrations Conference* Boston MA
39. Soong T T and Manolis G D 1987 On Active Structures, *ASCE Journal of Structural Engineering* **113** pp 2290–301
40. Cha J Z, Pitarresi J M and Soong T T 1988 Optimal Design Procedures for Active Structures. *ASCE Journal of Structural Engineering* **114** pp 2710–23

4 Practical Considerations

While most of the results reported in the preceding chapter are encouraging, it is important to recognize that they are largely based on idealized system descriptions under ideal conditions. In terms of real-time application, it has been pointed out that a number of important problems must be addressed from a practical standpoint.[1] The importance of taking these practical considerations into account in the algorithm development has been stressed and some of these issues are discussed in this chapter.

4.1 Modelling Errors and Spillover Effects

Civil engineering structures are distributed-parameter systems. With a very few exceptions, analytical and simulation control results obtained to date are based on greatly simplified structural models. In fact, as indicated in Fig. 4.1, a two-stage model reduction procedure is generally carried out whereby the distributed-parameter system is first reduced to a many-degree-of-freedom system discretized in space, which we shall refer to as a full-order system (FOS); it is then further reduced to a discrete-parameter system with a small number of degrees of freedom, referred to here as the reduced-order system (ROS). As shown in Fig. 4.1, control design is generally carried out

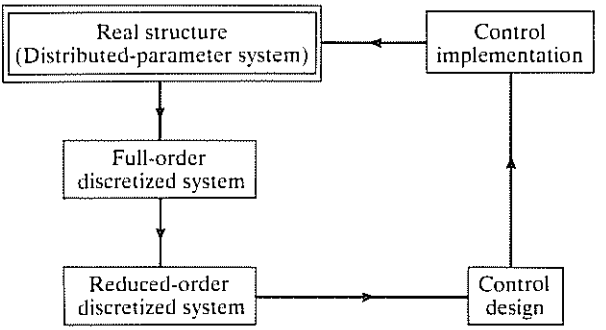

Figure 4.1 Model reduction and control design

based on the reduced-order system, necessitated by practical limitations as well as computational considerations.

When an ROS-based control design is synthesized and applied to a real structure, inevitable errors such as control and observation spillovers and possible instability are introduced.[2-4] In order to see the effect of spillovers, let us start with an FOS represented by the matrix equation (3.1) without the excitation term

$$\dot{z}(t) = Az(t) + Bu(t), \qquad z(0) = z_0 \tag{4.1}$$

with the observation equation Eq. (3.41)

$$y(t) = Cz(t) \tag{4.2}$$

where, as before, $z(t)$ is the $2n$-dimensional state vector of the structural system (large n), $u(t)$ is the m-dimensional control vector and $y(t)$ is the p-dimensional observation vector.

A reduced-order model (ROS) can be generated through aggregation or modal eigenfunction expansion techniques by retaining only the controlled modes of the system, giving

$$\dot{z}_c(t) = A_c z_c(t) + B_c u(t) + E_c(t) \tag{4.3}$$

with the observation equation

$$y(t) = C_c z_c(t) + R_c(t) \tag{4.4}$$

In the above, $z_c(t)$ is the controlled portion of the state vector $z(t)$ whose dimension is in general much smaller than that of $z(t)$. $E_c(t)$ and $R_c(t)$ are error terms introduced through the truncation process; they can be represented by

$$E_c(t) = A_{cr} z_r(t) \qquad \text{and} \qquad R_c(t) = C_r z_r(t) \tag{4.5}$$

where $z_r(t)$ is the state vector associated with the residual (or uncontrolled) modes of the FOS. It is governed by

$$\dot{z}_r(t) = A_r z_r(t) + B_r u(t) + E_r(t) \tag{4.6}$$

The error term $E_r(t)$ in the residue equation has the form

$$E_r(t) = A_{rc} z_c(t) \tag{4.7}$$

The error term $E_c(t)$ in Eq. (4.3) represents the modelling error due to the model reduction process. The term $B_r u(t)$ in Eq. (4.6) shows the effect of control $u(t)$ entering the residue subsystem, or *control spillover* to the residual modes. The contamination of observations in Eq. (4.4) with residue information $R_c(t)$ produces *observation spillover*. Thus, the controller imparts energy to the residual modes through the interaction term $B_r u(t)$ and the resulting residual mode excitation is in turn detected by the sensors through

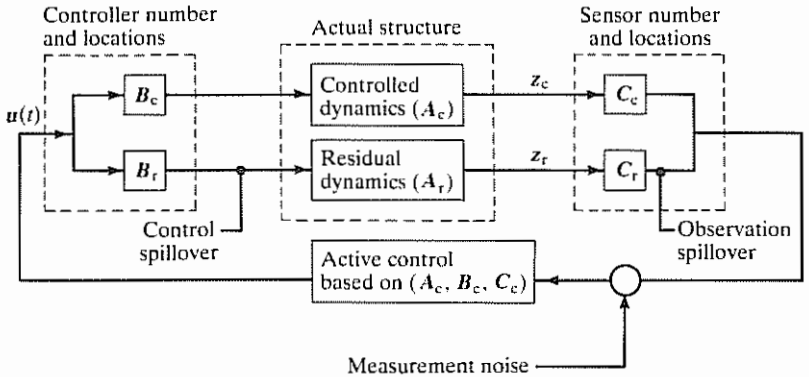

Figure 4.2 Interaction among model reduction, spillover, and sensor and controller placement

the term $\boldsymbol{R}_c(t)$ for control design, resulting in an escalating performance degradation. These interactions are shown graphically in Fig. 4.2. It can be shown that spillovers can reduce stability margins of the actual structure and are at the heart of the control problem based on the reduced-order models.[2,3]

Clearly, the magnitude of control and observation spillover is a function of the model reduction process. It is also a function of controller and sensor locations and their effects on the residual modes. We are interested in the spillover effect when the control design is carried out based on the ROS by assuming that $\boldsymbol{E}_c(t) = \boldsymbol{0}$ and $\boldsymbol{R}_c(t) = \boldsymbol{0}$, but is applied to the full-order system given by Eqs (4.1) and (4.2).

4.1.1 Effect of Spillover

Let $\hat{z}_c(t)$ be an estimate of the state vector $z_c(t)$ based on the sensor measurement $y(t)$ and designed either as a Luenberger observer or as a Kalman filter (see Section 3.1.1). Using a Luenberger observer, for example, the state estimator has the form [see Eq. (3.23)]

$$\dot{\hat{z}}_c(t) = \boldsymbol{A}_c\hat{z}_c(t) + \boldsymbol{B}_c\boldsymbol{u}(t) + \boldsymbol{G}^*[\boldsymbol{C}_c\hat{z}_c(t) - \boldsymbol{y}(t)] \tag{4.8}$$

$$\hat{z}_c(0) = z_0$$

Following a linear control law, the control design based on the error-free ROS gives

$$\boldsymbol{u}(t) = \boldsymbol{G}\hat{z}_c(t) \tag{4.9}$$

where the control gain G is determined as though the true state $z_c(t)$ were available instead of $\hat{z}_c(t)$. The substitution of Eq. (4.9) into Eq. (4.1) yields

$$\begin{aligned}\dot{z}(t) &= Az(t) + BG\hat{z}_c(t) \\ &= Az(t) + BGz_c(t) + BG[\hat{z}_c(t) - z_c(t)]\end{aligned} \tag{4.10}$$

Let

$$e(t) = \hat{z}_c(t) - z_c(t) \qquad \text{and} \qquad z_c(t) = Dz(t) \tag{4.11}$$

We then have

$$\dot{z}(t) = (A + BGD)z(t) + BGe(t) \tag{4.12}$$

For the error term $e(t)$, the derivative of the first of Eqs (4.11) leads to

$$\dot{e}(t) = G^*(C - C_cD)z + (A_c - G^*C_c)e(t) \tag{4.13}$$

Define the composite closed-loop system state by

$$w(t) = \begin{bmatrix} z(t) \\ e(t) \end{bmatrix} \tag{4.14}$$

Then,

$$\dot{w}(t) = Qw(t) = \begin{bmatrix} Q_{11} & Q_{12} \\ Q_{21} & Q_{22} \end{bmatrix} w(t) \tag{4.15}$$

with

$$\left.\begin{aligned} Q_{11} &= A + BGD \\ Q_{12} &= BG \\ Q_{21} &= G^*(C - C_cD) \\ Q_{22} &= A_c - G^*C_c \end{aligned}\right\} \tag{4.16}$$

It is seen that the sensor output is contaminated by the residue modes through the term $(C - C_cD)z(t)$, which can be identified as $C_rz_r(t)$, the observation spillover. Thus, while the poles of $A + BGD$ and $A_c - G^*C_c$ can be designed with substantial stability margin, the presence of observation spillover can lead to instabilities in the residue modes. This is especially true in the lightly damped system.

4.1.2 Spillover Compensation

In view of the fact that spillover can cause serious system performance degradation, it is important that conventional design procedures be modified in order to eliminate or minimize spillover effects. The most obvious method

of spillover reduction is to locate the controllers and sensors at or very near the zeros of the affected modes. However, this is difficult if not impossible to do as the freedom of locating sensors and controllers is rarely available to the control designer. Other attempts include the introduction of a 'comb' filter between the sensor output and state estimator for the purpose of 'combing out' the residue modes,[2,3,5] implementation of an orthogonal filter in an attempt to counteract spillover as an unmodelled disturbance,[6,7] and addition of measurements for more complete state feedback.[8] However, these procedures are indirect and can become ineffective when the residue modes are closely spaced or when it becomes impractical to add the required number of sensors.

The control design procedure proposed by Soong and Chang[4] is a direct modification of the spillover-free control law as indicated in Chapter 3 by requiring that the controlled modes of the system stay close to the designed values and that the stability of the uncontrolled modes be preserved. This procedure is briefly described below.

Let the dimension of $z_c(t)$ in Eq. (4.3) be $2n'$ and consider the $2(n+n') \times 2(n+n')$ matrix $\boldsymbol{Q}$ defined in Eqs (4.15) and (4.16). For structural systems, the eigenvalues of $\boldsymbol{Q}$ consist of complex conjugate pairs (λ_1, λ_1^*), (λ_2, λ_2^*), $\ldots$, $(\lambda_{n+n'}, \lambda_{n+n'}^*)$ and, for convenience, we shall assume that they are distinct at least in the controlled modes. Using pole assignment, for example, the control objective is to affect changes in the controlled modes so that they take prescribed eigenvalue pairs (η_1, η_1^*), (η_2, η_2^*), $\ldots$, $(\eta_{n'}, \eta_{n'}^*)$.

In the absence of spillover, it is straightforward to determine the control gain $\boldsymbol{G}$ as indicated in Eq. (4.9). In the presence of spillover, the proposed procedure calls for a modification of the value of $\boldsymbol{G}$ by minimizing the cost function

$$J = \sum_{j=1}^{n'} r_j |\lambda_j - \eta_j|^2 = \boldsymbol{\omega}_c^{\mathrm{T}} \boldsymbol{R} \boldsymbol{\omega}_c^* \tag{4.17}$$

where

$$\boldsymbol{\omega}_c = \begin{bmatrix} \lambda_1 - \eta_1 \\ \vdots \\ \lambda_{n'} - \eta_{n'} \end{bmatrix} \tag{4.18}$$

and

$$\boldsymbol{R} = \mathrm{diag.}[r_1, \ldots, r_{n'}] \tag{4.19}$$

while a set of inequality constraints is satisfied. These inequality constraints arise from stability requirements in the uncontrolled modes and can be written in the form

$$\mathrm{Re}(\lambda_j) + \varepsilon_j \leqslant 0, \qquad j = n'+1, \ldots, n \tag{4.20}$$

where ε_j are some prescribed small positive numbers.

The optimization problem with the cost function defined by Eq. (4.17) and inequality constraints given by Eq. (4.20), although highly nonlinear, can be numerically carried out using the method of Lagrange multipliers with the help of carefully defined slack variables. It can be shown that the problem reduces to that of finding the solution of a set of $(r+n-n')$ simultaneous nonlinear equations, where r is the number of unknown parameters in the optimization problem. While the dimension $(r+n-n')$ is in general large due to large n, the procedure can be facilitated by seeking the control gain $\boldsymbol{G}$ sequentially by incorporating into the solution procedure the inequality constraints given by Eq. (4.20) sequentially. Numerical simulations show that the solution for control gain stabilizes at a rate proportional to the number of inequality constraints considered at each stage.

Example 4.1 Let us illustrate the procedure presented above with a simple example in which all modal data are readily obtained. Consider a structural system whose FOS is described by Eqs (4.1) and (4.2) with $n=5$, $p=1$, $m=1$ and

$$\boldsymbol{A}=\begin{bmatrix} \boldsymbol{0} & \boldsymbol{I} \\ \boldsymbol{A}_{21} & \boldsymbol{A}_{22} \end{bmatrix} \tag{4.21}$$

$$\boldsymbol{B}^T=[0,\ 0,\ 0,\ 0,\ 0,\ 0,\ 0,\ 0,\ 0,\ 1.0] \tag{4.22}$$

$$\boldsymbol{C}=[0,\ 0,\ 0,\ 0,\ 1,\ 0,\ 0,\ 0,\ 0,\ 20.0] \tag{4.23}$$

in which the matrices $\boldsymbol{A}_{21}$ and $\boldsymbol{A}_{22}$ take values so that FOS represents a lightly damped five-degree-of-freedom mass-spring-damper system. Equation (4.22) indicates that a single controller is applied at the fifth mass and Eq. (4.23) shows that a single sensor is located at the same mass with its displacement and velocity observed. The eigenvalues of $\boldsymbol{A}$ are

$$\lambda_1,\ \lambda_1^* = -0.0036 \pm j12.679$$

$$\lambda_2,\ \lambda_2^* = -0.0055 \pm j37.011$$

$$\lambda_3,\ \lambda_3^* = -0.0012 \pm j58.344$$

$$\lambda_4,\ \lambda_4^* = -0.0458 \pm j74.950$$

$$\lambda_5,\ \lambda_5^* = -0.0941 \pm j85.484$$

In this example, the critical modes are taken to be the first three structural modes (the first three pairs of eigenvalues) and the fourth and fifth modes are the residue modes. Thus, the reduced-order system is one of order six $(n'=3)$ with

$$\boldsymbol{B}_c^T=[0,\ 0,\ 0,\ 0.12,\ -0.16,\ 0.86]$$

$$\boldsymbol{C}_c=[0,\ 0,\ 1,\ 0,\ 0,\ 20.0]$$

The control objective is to apply active control to the uncontrolled system so that the three controlled modes take the following desired values:

$$\eta_1, \eta_1^* = -1.370 \pm j16.679$$

$$\eta_2, \eta_2^* = -1.888 \pm j40.011$$

$$\eta_3, \eta_3^* = -2.583 \pm j61.344$$

In the control design, the following cases are of interest:

Case A: The conventional modal control design based upon the ROS while ignoring the uncontrolled modes.
Case B: The modified modal control design where the control gain is determined by minimizing the cost function given by Eq. (4.17) with inequality constraints given by Eq. (4.20). The matrix $\boldsymbol{R}$ in Eq. (4.17) is taken to be $\boldsymbol{I}$ and $\varepsilon_1 = \varepsilon_2 = 0.00001$ in Eq. (4.20).
Case C: The same as Case B but with $\varepsilon_1 = \varepsilon_2 = 0.1$.

The pole shifting characteristics for all three cases are summarized in Table 4.1. It is shown that conventional modal control design (Case A) can lead to instabilities in the residue modes in the presence of spillover. On the other hand, the modified procedure (Cases B and C) ensures stability in the residue modes while the controlled modes are kept close to their desired

Table 4.1 Pole shifting characteristics[4]

Mode	Uncontrolled	Controlled without spillover	Controlled with spillover
Case A			
1	$-0.0036 \pm j12.68$	$-1.370 \pm j16.68$	$-1.376 \pm j16.67$
2	$-0.0055 \pm j37.01$	$-1.888 \pm j40.01$	$-1.876 \pm j39.93$
3	$-0.0012 \pm j58.34$	$-2.583 \pm j61.34$	$-2.107 \pm j60.91$
4	$-0.0458 \pm j74.95$	$-0.0458 \pm j74.95$	$+0.189 \pm j75.61$
5	$-0.0941 \pm j85.48$	$-0.0941 \pm j85.48$	$-0.033 \pm j85.59$
Case B			
1		$-1.404 \pm j16.68$	$-1.410 \pm j16.67$
2		$-1.974 \pm j40.05$	$-1.971 \pm j39.97$
3	Same as	$-4.118 \pm j61.27$	$-3.038 \pm j60.79$
4	Case A	$-0.046 \pm j74.95$	$-0.00001 \pm j75.81$
5		$-0.094 \pm j85.48$	$-0.054 \pm j85.64$
Case C			
1		$-2.105 \pm j16.32$	$-2.109 \pm j16.29$
2		$-3.143 \pm j38.24$	$-2.937 \pm j38.26$
3	Same as	$-0.807 \pm j58.84$	$-0.778 \pm j58.85$
4	Case A	$-0.046 \pm j74.95$	$-0.100 \pm j75.26$
5		$-0.094 \pm j85.48$	$-0.100 \pm j85.55$

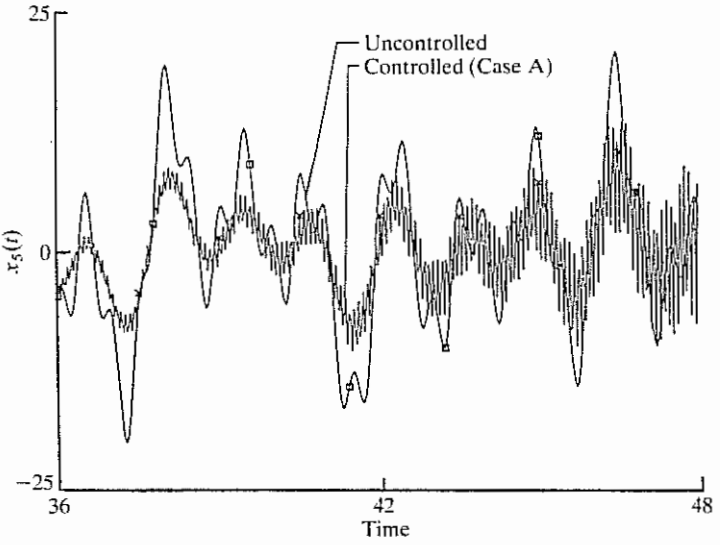

Figure 4.3 Displacement $x_5(t)$ (Case A)[4]

values. Results for Cases B and C also show that varied stability margins in the residue modes can be achieved but modal accuracy in the controlled modes is somewhat sacrificed.

A more dramatic difference in results between Cases A and B is shown in Figs 4.3 and 4.4 when the system is subjected to a somewhat arbitrary forcing

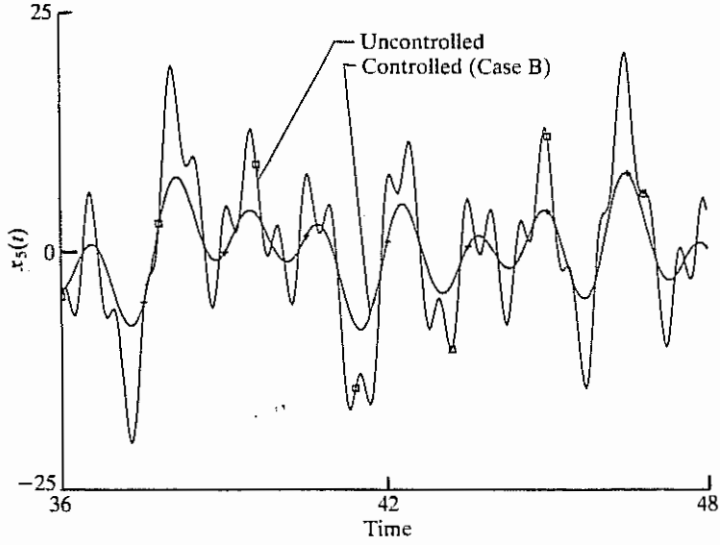

Figure 4.4 Displacement $x_5(t)$ (Case B)[4]

function. Figure 4.3 shows $x_5(t)$, the displacement of the fifth mass, as a function of time under uncontrolled conditions and under conventional control (Case A). While a reduction of displacement magnitude is affected by Case A control, instabilities in the residue modes cause oscillation with increasing magnitude. In contrast, Case B leads to stable results as shown in Fig. 4.4.

4.2 Time Delay

In treating ideal systems, the assumption is made that all operations in the control loop as shown in Fig. 2.1 can be performed instantaneously. In reality, however, time has to be consumed in processing measured information, in performing on-line computation, and in executing the control forces as required. Thus, time delay causes unsynchronized application of the control forces and this unsynchronization can not only render the control ineffective, but may also cause instability in the system.[9,10]

In order to see the effect of time delay on control effectiveness, let us consider a simple single-degree-of-freedom structural system with active control as represented by the equation of motion

$$m\ddot{x}(t) + c\dot{x}(t) + kx(t) = u(t) + f(t), \quad x(0) = 0, \quad \dot{x}(0) = 0 \tag{4.24}$$

where all the quantities in Eq. (4.24) are defined as usual. Assuming a linear control law, we write

$$u(t) = g_1 x(t) + g_2 \dot{x}(t) \tag{4.25}$$

It is easy to show that the frequency response function of the closed-loop system is (see Appendix A)

$$h(j\omega) = [1 + h_o(j\omega)v(j\omega)]^{-1} h_o(j\omega) \tag{4.26}$$

in which

$$h_o(j\omega) = [-m\omega^2 + jc\omega + k]^{-1}$$

is the open-loop transfer function and

$$v(j\omega) = g_1 + jg_2\omega$$

is the transfer function associated with the feedback gain. As discussed in Appendix A, the magnitude of $h(j\omega)$ gives a measure of the dynamic reduction of the system response and thus a measure of control efficiency.

Suppose now that time delay exists in the execution of control with an amount equal to τ. The modified equation of motion takes the form

$$m\ddot{x}(t) + c\dot{x}(t) + kx(t) = u(t-\tau) + f(t), \quad x(0) = 0, \quad \dot{x}(0) = 0 \tag{4.27}$$

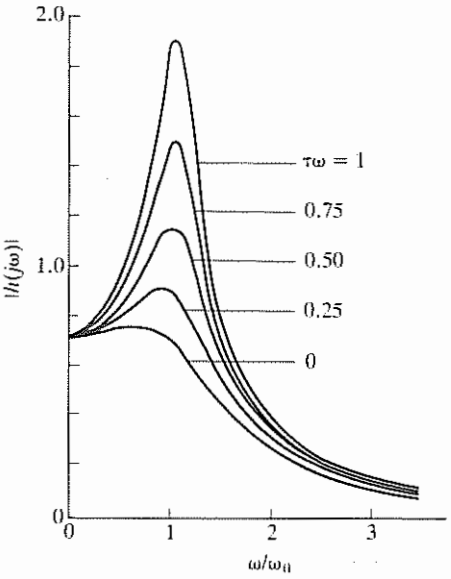

Figure 4.5 Time delay effect on control efficiency[10]

and Eq. (4.26) becomes

$$h(j\omega) = [1 + e^{-j\tau\omega} h_o(j\omega) v(j\omega)]^{-1} h_o(j\omega) \tag{4.28}$$

Typical time delay effects on the magnitude of $h(j\omega)$ can be seen in Fig. 4.5, where ω_o is the undamped natural frequency of the system with arbitrary values assigned to m, c, k, g_1 and g_2. It clearly shows deterioration of the controlled system response as a function of time delay.

As mentioned earlier, time delay can also lead to instability in the controlled system. The stability problem can be investigated by sketching the Bode plot of the loop transfer function $h_o(j\omega)v(j\omega)$. It is noted from Eq. (4.28), however, that time delay enters in the loop transfer function as a coefficient in the form of $\exp(-j\tau\omega)$. Since $|\exp(-j\tau\omega)| = 1$ for all ω, the time delay affects the phase but not the magnitude of the Bode plot. The control system can thus become unstable when $\tau\omega$ takes such values as to cause the phase margin to become negative. A more detailed discussion of this phenomenon can be found in Pu.[10]

4.2.1 Time Delay Compensation

Equation (3.1) gives the state-space representation of the basic controlled system dynamics, i.e.

$$\dot{z}(t) = Az(t) + \boldsymbol{B}u(t) + \boldsymbol{H}f(t) \tag{4.29}$$

When time delays are taken into account, time retardations can occur in both $z(t)$ and $\boldsymbol{u}(t)$ appearing on the right-hand side of Eq. (4.29). Let τ_{zi} be the time delay in $z_i(t)$, the ith component of $z(t)$ and τ_{ui} be that associated with $u_i(t)$, the ith component of $\boldsymbol{u}(t)$. Equation (4.29) now becomes a differential-difference matrix equation of the form

$$\dot{z}(t) = \sum_{i=1}^{2n} \boldsymbol{A}_i z_i(t-\tau_{zi}) + \sum_{i=1}^{m} \boldsymbol{B}_i u_i(t-\tau_{ui}) + \boldsymbol{H}f(t) \tag{4.30}$$

where $\boldsymbol{A}_i$ and $\boldsymbol{B}_i$ are, respectively, the ith columns of $\boldsymbol{A}$ and $\boldsymbol{B}$.

The problem of control design for systems represented by Eq. (4.30) has been studied extensively in the control literature and, more recently, in connection with control of civil engineering structures. In what follows, two simple methods are described which have shown success in structural control applications.

Taylor Series Expansion One of the simple methods of time delay compensation,[11-14] is based on Taylor series expansion of time-retarded variables in Eq. (4.30). Consider, for example, $z_i(t-\tau_{zi})$. Its Taylor series expansion about t gives

$$z_i(t-\tau_{zi}) = z_i(t) - \tau_{zi}\dot{z}_i(t) + \frac{\tau_{zi}^2}{2!}\ddot{z}_i(t) - \dots \tag{4.31}$$

For practicality, the series is truncated after a few terms and the truncation error depends upon whether the time delay is small as compared with the system's natural periods.

One can also use the Taylor series in reverse, namely,

$$\begin{aligned} z_i(t) = z_i(t-\tau_{zi}+\tau_{zi}) &= z_i(t-\tau_{zi}) + \tau_{zi}\dot{z}_i(t-\tau_{zi}) \\ &+ \frac{\tau_{zi}^2}{2!}\ddot{z}_i(t-\tau_{zi}) + \dots \end{aligned} \tag{4.32}$$

Upon substituting either Eq. (4.31) or Eq. (4.32) into Eq. (4.30), one can then form an augmented state-space system containing the state variables $z_i(t)$, $z_i(t-\tau_{zi})$, $u_i(t)$, $u_i(t-\tau_{ui})$, ... The state-space equation of the augmented system again takes the standard form of Eq. (4.29) except that the dimension of the state vector is increased. Conventional control design algorithms such as those described in Chapter 3 can again be applied.

As an example, consider Eq. (4.27) again. Time delay compensation in $u(t)$ can be accomplished in this simple case using the Taylor series expansion approach in the form given by Eq. (4.32). Retaining only the first three terms, we have

$$u(t) = u(t-\tau) + \tau\dot{u}(t-\tau) + \frac{\tau^2}{2}\ddot{u}(t-\tau) \tag{4.33}$$

which is another second-order differential equation governing $u(t-\tau)$. The augmented system encompassing Eqs (4.27) and (4.33) can be established by defining a four-dimensional state variable $z(t)$ as

$$z(t) = \begin{bmatrix} x(t) \\ \dot{x}(t) \\ u(t-\tau) \\ \dot{u}(t-\tau) \end{bmatrix}$$

with the associated state-space equation

$$\dot{z}(t) = Az(t) + Bu(t) + Hf(t) \tag{4.34}$$

where

$$A = \begin{bmatrix} 0 & 1 & 0 & 0 \\ -\frac{k}{m} & -\frac{c}{m} & \frac{1}{m} & 0 \\ 0 & 0 & 0 & 1 \\ 0 & 0 & -\frac{2}{\tau^2} & -\frac{2}{\tau} \end{bmatrix}$$

$$B = \begin{bmatrix} 0 \\ 0 \\ 0 \\ -\frac{2}{\tau^2} \end{bmatrix}$$

and

$$H = \begin{bmatrix} 0 \\ \frac{1}{m} \\ 0 \\ 0 \end{bmatrix}$$

The additional initial conditions are

$$z_3(t) = z_4(t) = 0, \quad t \leqslant \tau \tag{4.35}$$

Equation (4.34) now has the state-space form for a structural system free of time delays and conventional control algorithms can be used for control design.

The application of the Taylor series expansion technique to the study of distributed-parameter structures with time delay can be found in Abdel-Rohman.[15]

Phase Compensation Consider a linear control law such as that given by Eq. (4.25). Due to time delays, the displacement feedback control and the velocity feedback control can be resolved into displacement and velocity components as shown in Fig. 4.6, where $\omega\tau_x$ and $\omega\tau_{\dot{x}}$ are the phase lags for displacement delay time τ_x and velocity delay time $\tau_{\dot{x}}$, respectively, ω being the dominant system frequency.

Possible detrimental effect of time delay on the controlled system behaviour can also be seen from this phase space interpretation. With the phase shift, the displacement feedback vector may be resolved to produce positive active stiffness but negative active damping while the velocity feedback vector may be resolved to produce positive active stiffness and positive active damping. Due to the existence of negative active damping, control effects are diminished for the real system as compared to the ideal one. Even worse, time delay will cause instability if the resultant damping force is negative. Since phase lags are proportional to the delay time and dominant frequency, the effect of time delay can be serious for higher modes even with small amounts of time delay. This phenomenon has been observed earlier when the Bode plot of the loop transfer function was discussed.

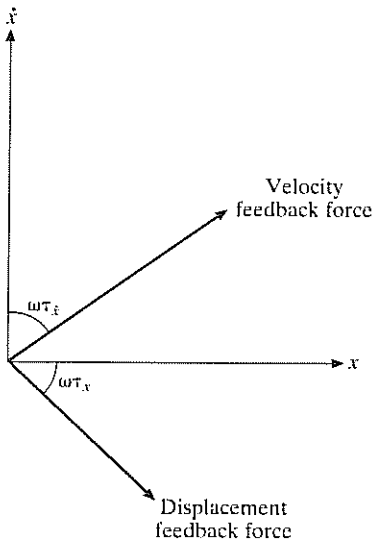

Figure 4.6 Displacement and velocity feedback vectors in phase space[17]

The idea behind phase compensation, first discussed by Roorda,[16] is to modify the time-delay-free control gains, g_1 and g_2 in Eq. (4.25), in order to take into account these rotations in the phase space. Let g_1' and g_2' be the modified displacement and velocity control gains, respectively. The relationship between (g_1', g_2') and (g_1, g_2) can be established as follows.

As seen from Fig. 4.6, the displacement feedback vector can be resolved into two components, $g_1' x\cos\omega\tau_x$ and $g_1' \dot{x}\sin\omega\tau_x/\omega$, in the displacement and velocity directions, respectively. Similarly, the velocity feedback vector has component $g_2'\omega x\sin\omega\tau_{\dot{x}}$ in the displacement direction and $g_2'\dot{x}\cos\omega\tau_{\dot{x}}$ in the velocity direction. On the other hand, for the ideal case with no time delay, the displacement and velocity feedback vectors are simply $g_1 x$ and $g_2\dot{x}$ in the displacement and velocity directions, respectively. Hence

$$g_1 x = g_1' x\cos(\omega\tau_x) + g_2'\omega x\sin(\omega\tau_{\dot{x}})$$

$$g_2\dot{x} = g_1'\dot{x}\sin(\omega\tau_x)/\omega + g_2'\dot{x}\cos(\omega\tau_{\dot{x}})$$

giving

$$\begin{bmatrix} g_1 \\ g_2 \end{bmatrix} = \begin{bmatrix} \cos(\omega\tau_x) & \omega\sin(\omega\tau_{\dot{x}}) \\ \sin(\omega\tau_x)/\omega & \cos(\omega\tau_{\dot{x}}) \end{bmatrix} \begin{bmatrix} g_1' \\ g_2' \end{bmatrix} \tag{4.36}$$

The modified control gains are thus

$$\begin{bmatrix} g_1' \\ g_2' \end{bmatrix} = \begin{bmatrix} \cos(\omega\tau_x) & \omega\sin(\omega\tau_{\dot{x}}) \\ \sin(\omega\tau_x)/\omega & \cos(\omega\tau_{\dot{x}}) \end{bmatrix}^{-1} \begin{bmatrix} g_1 \\ g_2 \end{bmatrix} \tag{4.37}$$

For multi-degree-of-freedom structural systems, the control gain correction as indicated in Eq. (4.37) can be applied to each mode in the modal domain and, through modal transformation to the physical domain, the necessary modification to the control gain matrix due to time delays can be determined.[17]

The technique of phase compensation has been applied to the study of active structural control and it has been shown to be effective in both computer simulation and in laboratory experiments.[16–19] Some of these results will be discussed in Chapter 5 where these experiments will be described.

4.3 Structural Nonlinearities

Our development of active structural control has been restricted to the consideration of linear structures. In reality, however, many civil engineering structures may undergo large deformation or yielding when subjected to strong environmental loads, and hence exhibit inelastic or nonlinear

behaviour. Consequently, active control systems may operate in the nonlinear range of structural motion, and it is of practical interest to extend active control concepts to the case of nonlinear or inelastic structures.

Several control algorithms developed in Chapter 3 have been studied in the context of control of nonlinear structures. For example, the application of several pulse control strategies discussed in Section 3.5 to the control of nonlinear systems has been investigated.[20-23] Similar extensions have also been made of the instantaneous control algorithms derived in Section 3.3.[24,25] We shall follow Yang *et al*[25] in our development, showing only one possible procedure in treating structural control problems involving structural nonlinearities.

Consider an n-degree-of-freedom nonlinear structural system described by (see Eq. 2.1)

$$\boldsymbol{M}\ddot{\boldsymbol{x}}(t)+\boldsymbol{f}_{\mathrm{d}}(t)+\boldsymbol{f}_{\mathrm{s}}(t)=\boldsymbol{D}\boldsymbol{u}(t)+\boldsymbol{E}\boldsymbol{f}(t), \quad \boldsymbol{x}(0)=\boldsymbol{x}_0, \quad \dot{\boldsymbol{x}}(0)=\dot{\boldsymbol{x}}_0 \tag{4.38}$$

where $\boldsymbol{x}(t)$ is the n-dimensional displacement vector and $\boldsymbol{D}$ and $\boldsymbol{E}$ are, respectively, appropriate $n\times m$ and $n\times r$ control and external excitation location matrices. The structural nonlinearities are reflected in the damping and stiffness terms in which $\boldsymbol{f}_{\mathrm{d}}(t)$, the n-dimensional damping force vector and $\boldsymbol{f}_{\mathrm{s}}(t)$, the n-dimensional stiffness force vector, are nonlinear functions of $\dot{\boldsymbol{x}}(t)$ and $\boldsymbol{x}(t)$, respectively, i.e.

$$\boldsymbol{f}_{\mathrm{d}}(t)=\boldsymbol{f}_{\mathrm{d}}[\dot{\boldsymbol{x}}(t)] \quad \text{and} \quad \boldsymbol{f}_{\mathrm{s}}(t)=\boldsymbol{f}_{\mathrm{s}}[\boldsymbol{x}(t)]. \tag{4.39}$$

For a sufficiently small step size Δt in the step-by-step numerical integration procedure, the nonlinear terms in Eq. (4.38) can be approximated by

$$\left.\begin{aligned}\boldsymbol{f}_{\mathrm{d}}(t)&=\boldsymbol{f}_{\mathrm{d}}(t-\Delta t)+\boldsymbol{C}^*(t-\Delta t)[\dot{\boldsymbol{x}}(t)-\dot{\boldsymbol{x}}(t-\Delta t)]\\ \boldsymbol{f}_{\mathrm{s}}(t)&=\boldsymbol{f}_{\mathrm{s}}(t-\Delta t)+\boldsymbol{K}^*(t-\Delta t)[\boldsymbol{x}(t)-\boldsymbol{x}(t-\Delta t)]\end{aligned}\right\} \tag{4.40}$$

in which $\boldsymbol{C}^*(t-\Delta t)$ and $\boldsymbol{K}^*(t-\Delta t)$ are influence coefficient matrices whose ijth elements are given[26,27] as

$$\left.\begin{aligned}c_{ij}^*(t-\Delta t)&=\frac{\partial f_{\mathrm{d}i}(t-\Delta t)}{\partial \dot{x}_j(t-\Delta t)}\\ k_{ij}^*(t-\Delta t)&=\frac{\partial f_{\mathrm{s}i}(t-\Delta t)}{\partial x_j(t-\Delta t)}\end{aligned}\right\} \tag{4.41}$$

where $f_{\mathrm{d}i}(t-\Delta t)$ and $f_{\mathrm{s}i}(t-\Delta t)$ are the ith components of $\boldsymbol{f}_{\mathrm{d}}(t-\Delta t)$ and $\boldsymbol{f}_{\mathrm{s}}(t-\Delta t)$, respectively, whereas $\dot{x}_j(t-\Delta t)$ and $x_j(t-\Delta t)$ are jth components of the response vectors $\dot{\boldsymbol{x}}(t-\Delta t)$ and $\boldsymbol{x}(t-\Delta t)$, respectively. In Eqs (4.41), the influence coefficients $c_{ij}^*(t-\Delta t)$ and $k_{ij}^*(t-\Delta t)$ represent the tangent damping and tangent stiffness at $t-\Delta t$, respectively.

Upon substituting Eqs (4.40) into Eq. (4.38), the equation of motion for the nonlinear structural system can be expressed in the form

$$\begin{aligned} &\boldsymbol{M}\ddot{\boldsymbol{x}}(t)+\boldsymbol{f}_{\mathrm{d}}(t-\Delta t)+\boldsymbol{C}^{*}(t-\Delta t)[\dot{\boldsymbol{x}}(t)-\dot{\boldsymbol{x}}(t-\Delta t)] \\ &\quad+\boldsymbol{f}_{\mathrm{s}}(t-\Delta t)+\boldsymbol{K}^{*}(t-\Delta t)[\boldsymbol{x}(t)-\boldsymbol{x}(t-\Delta t)]=\boldsymbol{D}\boldsymbol{u}(t)+\boldsymbol{E}\boldsymbol{f}(t) \end{aligned} \tag{4.42}$$

whose solution can be found following, for example, the Wilson-θ numerical procedure.[27] Let $\boldsymbol{z}(t)$ be the $2n$-dimensional state vector with

$$\boldsymbol{z}(t)=\begin{bmatrix}\boldsymbol{x}(t)\\ \dot{\boldsymbol{x}}(t)\end{bmatrix} \tag{4.43}$$

It can be expressed in terms of the response state vector $\boldsymbol{z}(t-\Delta t)$, damping force vector $\boldsymbol{f}_{\mathrm{d}}(t-\Delta t)$, stiffness force vector $\boldsymbol{f}_{\mathrm{s}}(t-\Delta t)$, external excitation $\boldsymbol{f}(t-\Delta t)$ and the control vector $\boldsymbol{u}(t-\Delta t)$, all at time $t-\Delta t$, as well as the control vector $\boldsymbol{u}(t)$ and the excitation $\boldsymbol{f}(t)$ at time t. It can be written as

$$\boldsymbol{z}(t)=\boldsymbol{d}^{*}(t-\Delta t)+\boldsymbol{A}_1\boldsymbol{u}(t)+\boldsymbol{A}_2\boldsymbol{f}(t) \tag{4.44}$$

where

$$\begin{aligned} \boldsymbol{d}^{*}(t-\Delta t)=&\boldsymbol{A}_3\boldsymbol{x}(t-\Delta t)+\boldsymbol{A}_4[\boldsymbol{f}_{\mathrm{d}}(t-\Delta t)+\boldsymbol{f}_{\mathrm{s}}(t-\Delta t)] \\ &+\boldsymbol{A}_5\boldsymbol{u}(t-\Delta t)+\boldsymbol{A}_6\boldsymbol{f}(t-\Delta t) \end{aligned} \tag{4.45}$$

In the above, $\boldsymbol{A}_j$, $j=1,\ldots,6$, are matrices defined by

$$\boldsymbol{A}_1=\theta^{-2}\begin{bmatrix}\boldsymbol{T}_1\\ 3\boldsymbol{T}_1/\Delta t\end{bmatrix}$$

$$\boldsymbol{A}_2=\theta^{-2}\begin{bmatrix}\boldsymbol{T}_2\\ 3\boldsymbol{T}_2/\Delta t\end{bmatrix}$$

$$\boldsymbol{A}_3=\theta^{-2}\begin{bmatrix}\theta^2\boldsymbol{I} & \boldsymbol{F}\boldsymbol{T}_3\\ 0 & \theta^2\boldsymbol{I}+\boldsymbol{F}\boldsymbol{T}_4\end{bmatrix}$$

$$\boldsymbol{A}_4=\theta^{-2}\boldsymbol{F}\begin{bmatrix}\boldsymbol{T}_5\\ \boldsymbol{T}_6\end{bmatrix}$$

$$\boldsymbol{A}_5=\theta^{-2}\boldsymbol{F}\begin{bmatrix}\boldsymbol{T}_7\\ \boldsymbol{T}_8\end{bmatrix}\boldsymbol{D}$$

$$\boldsymbol{A}_6=\theta^{-2}\boldsymbol{F}\begin{bmatrix}\boldsymbol{T}_7\\ \boldsymbol{T}_8\end{bmatrix}\boldsymbol{E}$$

with $\theta > 1.37$ and

$$\boldsymbol{T}_1 = \boldsymbol{FE}$$

$$\boldsymbol{T}_2 = \boldsymbol{FD}$$

$$\boldsymbol{T}_3 = (6/\Delta t)\boldsymbol{M} + 3\theta\boldsymbol{C}^* + \Delta t(\theta^2 - 1)\boldsymbol{K}^*$$

$$\boldsymbol{T}_4 = -3\boldsymbol{K}^*$$

$$\boldsymbol{T}_5 = -(3\boldsymbol{I} + \boldsymbol{S}_1)$$

$$\boldsymbol{T}_6 = -(6/\Delta t)\boldsymbol{I} - \boldsymbol{S}_2$$

$$\boldsymbol{T}_7 = 2\boldsymbol{I} + \boldsymbol{S}_1$$

$$\boldsymbol{T}_8 = (3/\Delta t)\boldsymbol{I} + \boldsymbol{S}_2$$

$$\boldsymbol{F} = \left[\frac{6\boldsymbol{M}}{(\theta\Delta t)^2} + \frac{3\boldsymbol{C}^*}{\theta\Delta t} + \boldsymbol{K}^*\right]^{-1}$$

$$\boldsymbol{S}_1 = [\Delta t(1.5\theta - 1)\boldsymbol{C}^* + 0.5\Delta t^2(\theta^2 - \theta)\boldsymbol{K}^*]\boldsymbol{M}^{-1}$$

$$\boldsymbol{S}_2 = [3(\theta - 1)\boldsymbol{C}^* + \theta\Delta t(\theta - 1.5)\boldsymbol{K}^*]\boldsymbol{M}^{-1}$$

In the above, θ is the parameter defined in the Wilson-θ procedure. The argument $t - \Delta t$ for $\boldsymbol{C}^*$ and $\boldsymbol{K}^*$ has been omitted for simplicity. Thus, all $\boldsymbol{A}_j$s, being functions of $\boldsymbol{C}^*$ and $\boldsymbol{K}^*$, are also functions evaluated at $t - \Delta t$.

Equation (4.44) for the state vector $z(t)$ is seen to have the same form as Eq. (3.52) for a linear structure when the following replacements are made:

$$\boldsymbol{Td}(t - \Delta t) \rightarrow \boldsymbol{d}^*(t - \Delta t), \quad \Delta t\boldsymbol{B}/2 \rightarrow \boldsymbol{A}_1, \quad \Delta t\boldsymbol{H}/2 \rightarrow \boldsymbol{A}_2$$

Hence, instantaneous optimal control design for the nonlinear structure can be determined from the linear results with appropriate substitutions indicated above. For example, for closed-loop instantaneous optimal control, it follows from Eqs (3.57) and (3.58) that, for the nonlinear structure under consideration,

$$\boldsymbol{u}(t) = -\boldsymbol{R}^{-1}\boldsymbol{A}_1^{\mathrm{T}}\boldsymbol{Q}\boldsymbol{z}(t) \tag{4.46}$$

and the controlled response state vector $z(t)$ is

$$\boldsymbol{z}(t) = [\boldsymbol{I} + \boldsymbol{A}_1\boldsymbol{R}^{-1}\boldsymbol{A}_1^{\mathrm{T}}\boldsymbol{Q}]^{-1}[\boldsymbol{d}^*(t - \Delta t) + \boldsymbol{A}_2\boldsymbol{f}(t)] \tag{4.47}$$

Two numerical examples using the closed-loop instantaneous optimal control law given in Eq. (4.46) are discussed below.

Example 4.2 Following an example discussed in Yang *et al*,[25] a single-degree-of-freedom structure similar to the one presented in Example 3.1 is considered. The stiffness is now assumed to be bilinear elastic–plastic with an elastic translational stiffness $k_1 = 8.53 \times 10^4$ kN/m and a post elastic

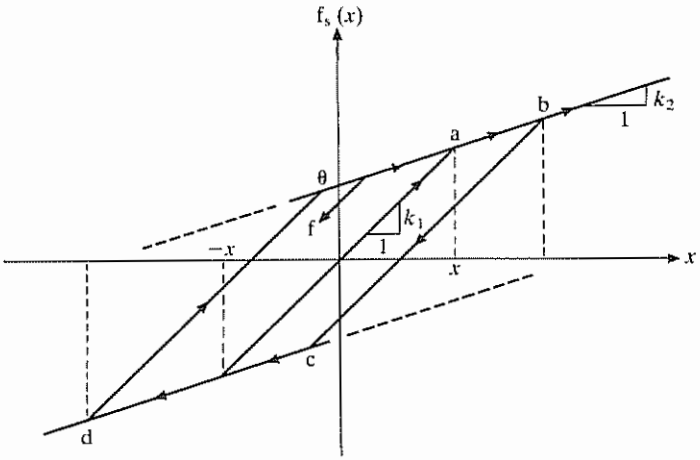

Figure 4.7 Nonlinear stiffness characteristics

translational stiffness $k_2 = 9.75 \times 10^3$ kN/m as shown in Fig. 4.7, where x denotes the lateral relative displacement and $f_s(x)$ is the stiffness restoring force. The floor mass m is 345.5 tons and the linear viscous damping coefficient is 54.29 kN-sec/m which corresponds to a damping ratio of 0.5%. The natural frequency of the structure is 2.5 Hz and yielding occurs at a lateral relative displacement of 2.4 cm. The angle of inclination of active tendons with respect to the ground is $\alpha = 25°$ (see Fig. 3.2). A simulated earthquake ground acceleration time history shown in Fig. 4.8 is considered as the input excitation, where the maximum ground acceleration is 0.4 g.

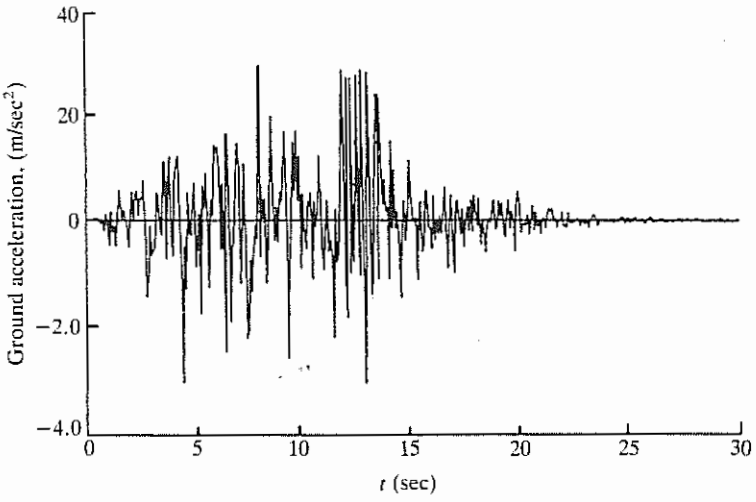

Figure 4.8 Ground acceleration

Without active control, the relative displacement of the top floor and the base shear force are displayed in Figs 4.9(a) and 4.10(a), respectively. The hysteresis loop of the inelastic restoring force is shown in Fig. 4.11(a), in which significant yielding occurs in the structure. With an active tendon control system, the structural response and active control force depend on the weighting matrices $\boldsymbol{Q}$ and $\boldsymbol{R}$. In this example, $\boldsymbol{Q}$ is a 2×2 matrix and $\boldsymbol{R}$

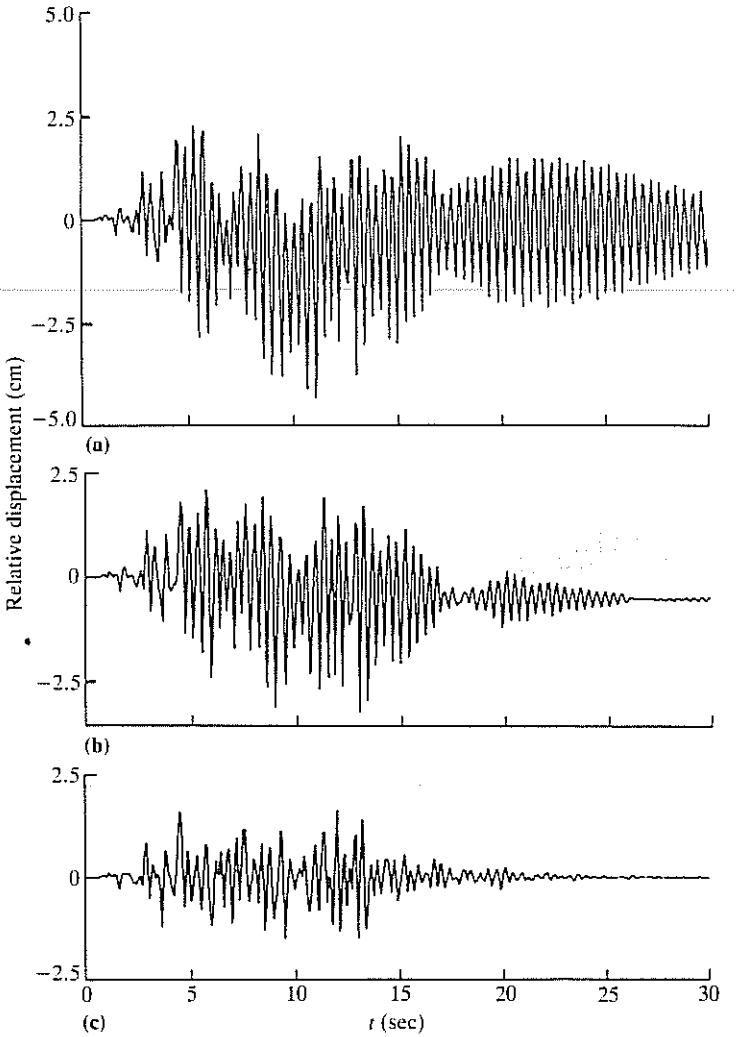

Figure 4.9 Relative displacement (a) without control; (b) $q/r = 0.15 \times 10^8$; (c) $q/r = 0.8 \times 10^8$

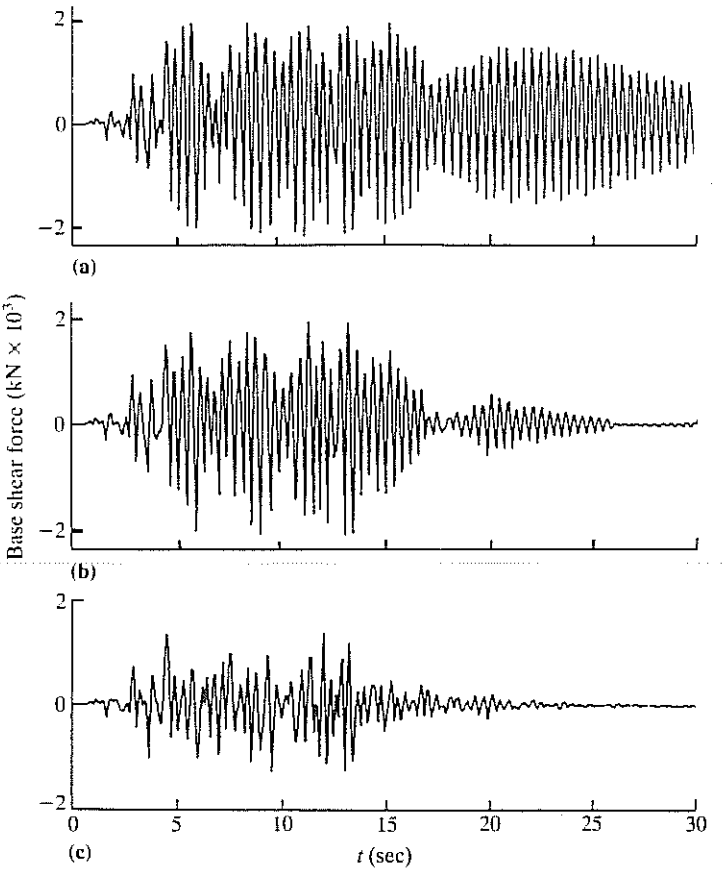

Figure 4.10 Base shear (a) without control; (b) $q/r = 0.15 \times 10^8$; (c) $q/r = 0.8 \times 10^8$

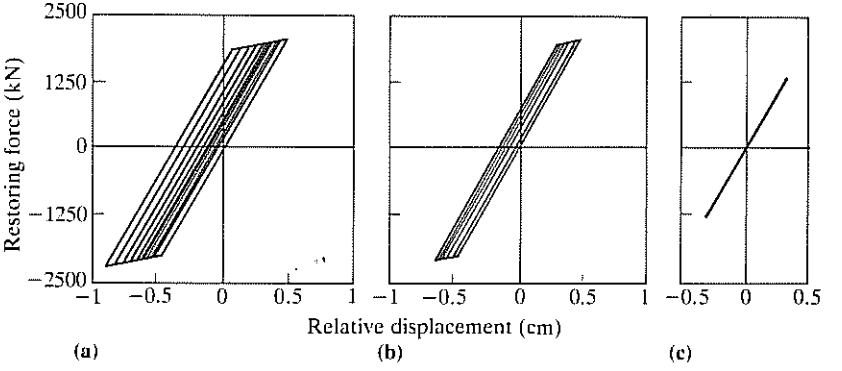

Figure 4.11 Hysteresis loop of inelastic restoring force (a) without control; (b) $q/r = 0.15 \times 10^8$; (c) $q/r = 0.8 \times 10^8$

is a scalar. For simplicity, we shall assume that

$$\boldsymbol{Q} = \begin{bmatrix} q & 0 \\ 0 & q \end{bmatrix} \quad , \quad \boldsymbol{R} = r$$

Numerical results on relative displacement, base shear, the hysteresis loop of inelastic restoring force, and the required control force are presented in Figs 4.9–4.12 for $q/r = 0.15 \times 10^8$ and $q/r = 0.8 \times 10^8$. In the first case, the maximum relative displacement is reduced by 27%, whereas the maximum base shear force is reduced by 5%. In the second case, it is seen that these reductions increase to 63.8% and 38.5%, respectively, and the response is entirely well within the elastic range. To examine the effect of weighting matrices on active control, the maximum floor relative displacement and maximum control force in the entire earthquake episode of 30 seconds are presented in Fig. 4.13 as functions of q/r. It is observed that, as the ratio q/r increases, the structural response quantities decrease with a corresponding increase of the required active control force. The structural oscillation is completely within the elastic range when $q/r > 0.35 \times 10^8$. Thus, the active

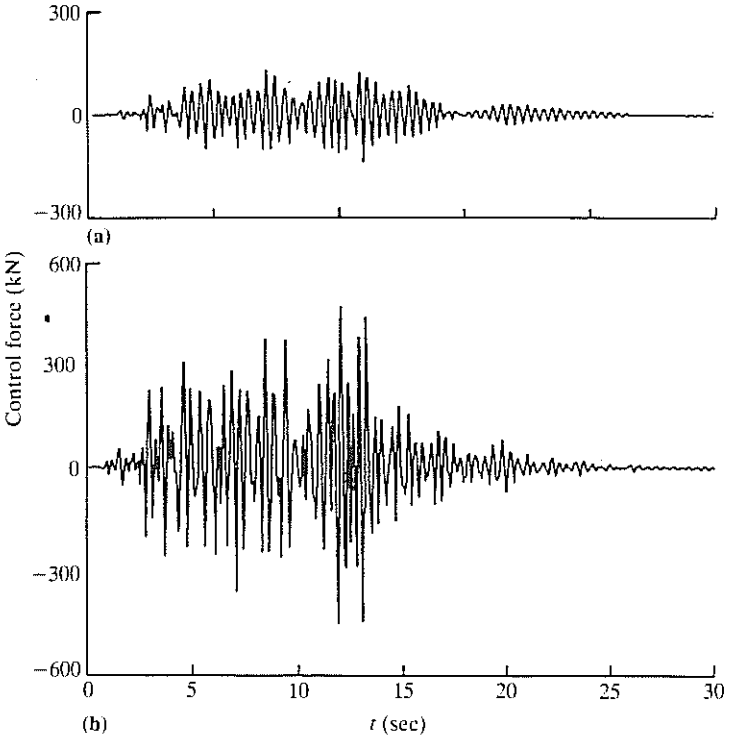

Figure 4.12 Required active control force (a) $q/r = 0.15 \times 10^8$; (b) $q/r = 0.8 \times 10^8$

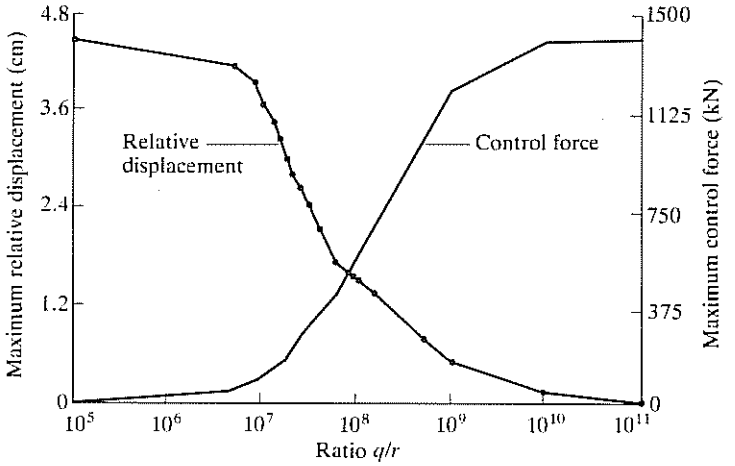

Figure 4.13 Maximum relative displacement and maximum control force as functions of q/r

tendon control system is capable of preserving the structural response within the elastic range provided that the level of the required control force is achievable.

Example 4.3 The eight-storey structure with an active mass damper installed on the top floor, first discussed in Example 3.5, is reconsidered here when the stiffness of each storey unit is assumed to be bilinear elastic–plastic. Again, the results presented here are extracted from Yang *et al.*[25]

All the structural and control parameters used in this example are the same as those given in Example 3.5 except for the following:

Elastic stiffness (each storey): 3.404×10^5 kN/m
Post elastic stiffness (each storey): 3.404×10^4 kN/m
Yielding level: 2.4 cm
First mode damping ratio: 0.5%
Damper mass: 36.3 tons
Damper damping: 31.0 kN-sec/m
Damper stiffness: 1173 kN/m
r: 10^5
α: 5.12
Excitation: Fig. 4.8 modified to 0.3 g maximum

Without any control system, the top floor relative displacement with respect to the ground and the base shear force of the structure are shown in Figs 4.14(a) and 4.15(a), respectively. Hysteresis loops for the shear force in

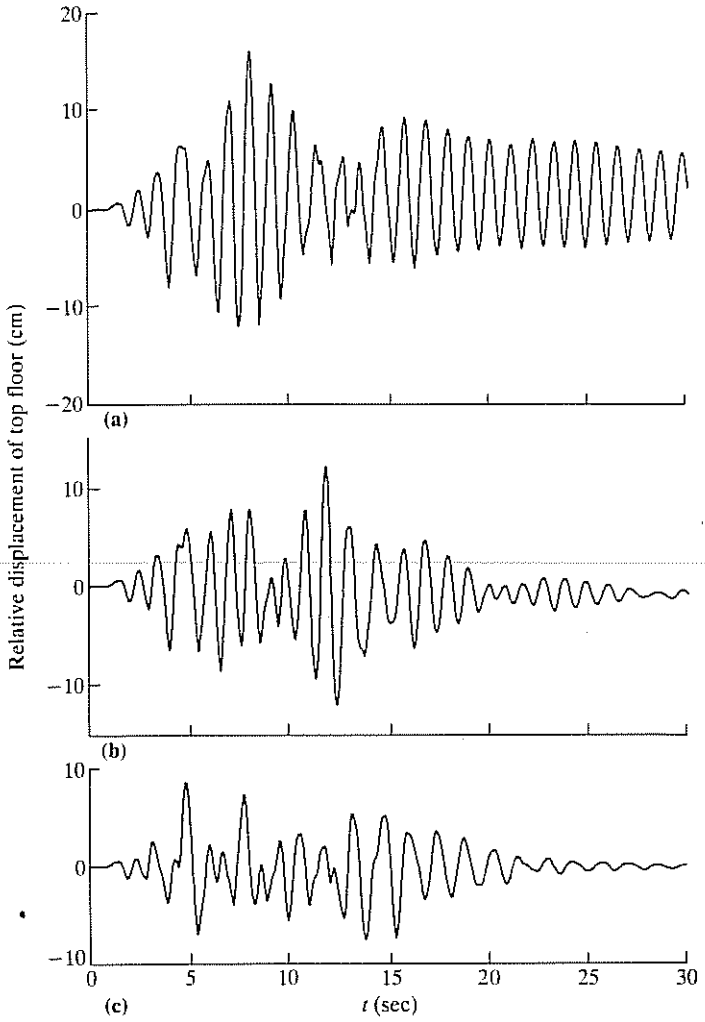

Figure 4.14 Top floor relative displacement (a) without control; (b) with passive mass damper; (c) with active mass damper

each storey unit are displayed in Fig. 4.16(a), in which '*i*' signifies the *i*th storey unit. As observed from Fig. 4.16, yielding occurs in the lower three storey units.

Without the active control force but with the mass damper in place, the mass damper is passive. In this case, the response quantities, including the top floor relative displacement with respect to the ground and the base shear force, are shown in Figs 4.14(b) and 4.15(b), respectively. It is observed from these two figures that the passive mass damper is not effective.

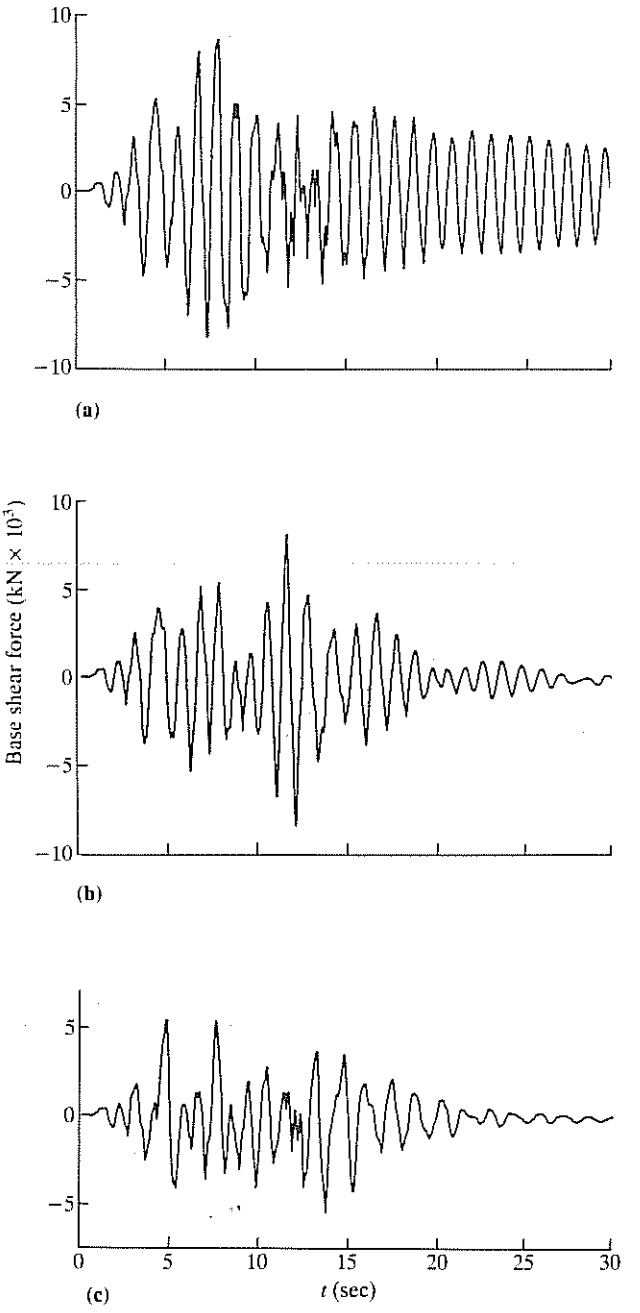

Figure 4.15 Base shear (a) without control; (b) with passive mass damper; (c) with active mass damper

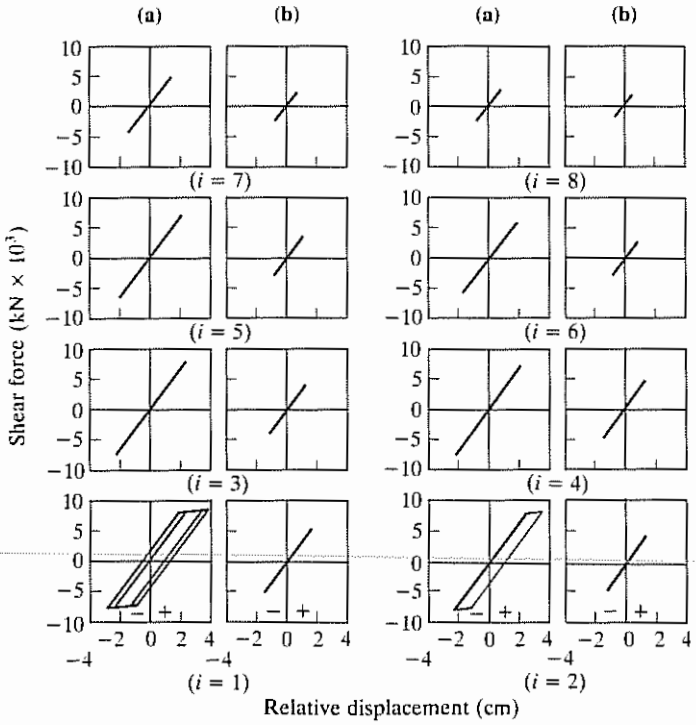

Figure 4.16 Hysteresis loops for shear force in each storey unit (a) without control; (b) with active mass damper

With the active mass damper, the response quantities and the required active control force from the controller are presented in Figs 4.14(c), 4.15(c) and 4.17(a). The relative displacement of the mass damper with respect to the top floor is displayed in Fig. 4.17(b). Also, hysteresis loops for the shear

Table 4.2 Maximum response quantities[25]

Floor no. (i)	Without control			Passive mass damper $y_d = 0.60$ m			Active mass damper $u_{max} = 820.7$ kN $y_d = 1.64$ m		
	x_i (cm)	y_i (cm)	s_i (kN)	x_i (cm)	y_i (cm)	s_i (kN)	x_i (cm)	y_i (cm)	s_i (kN)
1	3.89	3.89	8677	2.99	2.99	8369	1.62	1.62	5529
2	7.04	3.22	8447	5.32	2.47	8195	3.11	1.48	5042
3	9.26	2.49	8200	7.44	2.21	7509	4.41	1.32	4497
4	11.16	2.30	7812	9.22	1.79	6089	5.52	1.27	4310
5	12.84	2.11	7184	10.49	1.48	5026	6.55	1.14	3877
6	14.28	1.84	6274	11.30	1.30	4426	7.45	0.93	3169
7	15.36	1.45	4951	11.82	0.99	3360	8.11	0.68	2327
8	16.00	0.80	2722	12.26	0.53	1810	8.46	0.60	2043

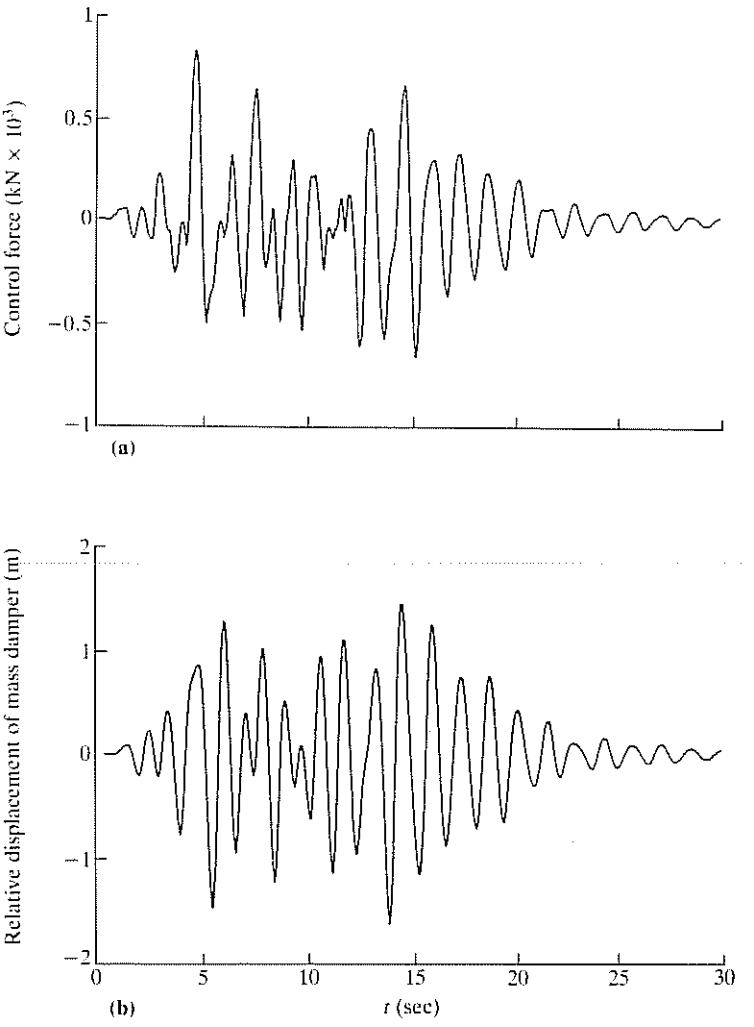

Figure 4.17 Required active control force and relative displacement of mass damper

force in each storey unit are depicted in Fig. 4.16(b). Within 30 seconds of the earthquake episode, the maximum response quantities, including the relative displacement of each floor with respect to the ground, $x_i (i = 1, 2, \ldots, 8)$, the interstorey drift, $y_i (i = 1, 2, \ldots, 8)$, and the shear force S_i, in each storey unit are presented in Table 4.2 for comparison. The maximum control force is 820.7 kN. It is observed from Figs 4.14–4.17 that, with the active mass damper, the response of the entire building is well within the elastic range.

4.4 Uncertainties in Structural Parameters

We have seen in Chapter 3 that the control laws and the resulting controlled system performance are in general functions of structural parameters such as masses, stiffnesses and damping ratios. In reality, structural parameters of as-built structures cannot be identified precisely and the parameter values used in control design may deviate significantly from their actual values. Thus, parameter uncertainties are another practical concern. More recent work in structural control has begun to address the problem of control sensitivity to structural parameter uncertainties.[28-30]

The effect of parameter uncertainties on control effectiveness can be investigated at several levels. At a fundamental level, the problem is one of robustness of control.[31] An important feature in feedback control theory, a robust control design is one which satisfactorily meets control specifications even in the presence of parameter uncertainties and other modelling errors. Two aspects of control specifications can be discussed: stability robustness and performance robustness. Most of the work on stability robustness has been done in the frequency domain using singular value decomposition, while many of the recent results on performance robustness were obtained using sensitivity approaches in the time domain. A more detailed discussion of stability robustness is beyond the scope of this book. In what follows, an elementary sensitivity approach is described which addresses the performance robustness issue.

Consider again the basic controlled system dynamics described by Eq. (3.1), i.e.

$$\dot{z}(t) = A(p)z(t) + B(p)u(t) + H(p)f(t) \tag{4.48}$$

with a linear control law given by

$$u(t) = G(p)z(t) \tag{4.49}$$

In the above, the dependence of the coefficient matrices on a set of parameter values, denoted by p, is explicitly noted. Let the actual parameter values be represented by p_a. It is expected that $u(t)$ and $z(t)$ as given by Eqs (4.48) and (4.49) will be adversely affected when p deviates from p_a. In order to study control sensitivity to parameter variations, let us write $u(t)$ as $u(p, t)$ to show its dependence on p. Then, assuming small parameter variations, $u(p, t)$ can be expanded in a Taylor series around p_a retaining only first-order terms, giving

$$u(p, t) = u(p_a, t) + \frac{\partial u(p_a, t)}{\partial p_a^T}(p - p_a) \tag{4.50}$$

where $\partial \boldsymbol{u}/\partial \boldsymbol{p}_a^T$ is the Jacobian defined by

$$\frac{\partial \boldsymbol{u}(\boldsymbol{p}_a, t)}{\partial \boldsymbol{p}_a^T} = \begin{bmatrix} \dfrac{\partial u_1}{\partial p_{a1}} & \dfrac{\partial u_1}{\partial p_{a2}} & \cdots & \dfrac{\partial u_1}{\partial p_{as}} \\ \vdots & & & \vdots \\ \dfrac{\partial u_m}{\partial p_{a1}} & & \cdots & \dfrac{\partial u_m}{\partial p_{as}} \end{bmatrix} \tag{4.51}$$

In the above, m and s are, respectively, the dimensions of $\boldsymbol{u}(t)$ and $\boldsymbol{p}_a$. The quantities u_i and p_{ai} are the ith elements of $\boldsymbol{u}(t)$ and $\boldsymbol{p}_a$, respectively.

Equation (4.51) defines the sensitivity matrix associated with the feedback control design with respect to parameter variations. The magnitudes of its elements dictate the degree of control sensitivity to parameter variations. These elements can be derived directly if the solution $\boldsymbol{u}(\boldsymbol{p}_a, t)$ is known explicitly, or they can be determined by solving the sensitivity matrix equation

$$\frac{\mathrm{d}}{\mathrm{d}t}\left[\frac{\partial \boldsymbol{u}(\boldsymbol{p}_a, t)}{\partial \boldsymbol{p}_a^T}\right] = \boldsymbol{A}(\boldsymbol{p}_a)\frac{\partial \boldsymbol{u}(\boldsymbol{p}_a, t)}{\partial \boldsymbol{p}_a^T} + \boldsymbol{B}(\boldsymbol{p}_a), \tag{4.52}$$

with the initial condition

$$\frac{\partial \boldsymbol{u}(\boldsymbol{p}_a, 0)}{\partial \boldsymbol{p}_a^T} = \boldsymbol{0}$$

Another approach to addressing the parameter variation problem for a specific control design is one of direct numerical simulation. The values of $\boldsymbol{z}(t)$ and $\boldsymbol{u}(t)$ as given by Eqs (4.48) and (4.49) can be numerically generated and they can be compared with those obtained when $\boldsymbol{p}$ is replaced by possible values of $\boldsymbol{p}_a$. This type of simulation permits an estimate of the amount of parameter variability that can be tolerated for a prescribed level of performance robustness. This approach is followed by Yang and Akbarpour[29,30] and possible information that can be derived from it is illustrated numerically in the following example.[30]

Example 4.4 Consider again the eight-storey structure with an active mass damper as discussed in Example 3.5. All structural and control parameters stay unchanged but various degrees of variability in stiffness and damping are introduced here to illustrate the effect of structural parameter uncertainties on control system performance. The variations in stiffness and damping in every storey unit are expressed as percentages of their actual values and denoted by Δk and Δc, respectively. The variations in the fundamental frequency and in the first-mode damping ratio, denoted respectively by $\Delta\omega$ and $\Delta\zeta$, are similarly defined.

Table 4.3 Maximum response and control force under parameter uncertainties

Estimation error				Top floor displacement (cm)	Difference in % of 1.61 cm	Base shear force (kN)	Difference in % of 1070 kN	Control force (kN)	Difference in % of 20 kN
Δk (%)	$\Delta\omega$ (%)	Δc (%)	$\Delta\zeta$ (%)						
0	0	0	0	1.61	—	1070	—	250	—
40	18.3	0	0	1.71	6.2	1047	−2.1	254	1.6
20	9.6	0	0	1.65	2.5	1052	−1.7	255	2.0
−20	−10.5	0	0	1.59	−1.2	1096	2.4	253	1.2
−40	−22.6	0	0	1.58	−1.8	1096	2.4	278	11.2
0	0	40	40	1.64	1.8	1085	1.4	240	−4.0
0	0	−40	−40	1.59	−1.2	1054	−1.4	259	3.6

The system response and control force for various values of Δk, Δc, $\Delta\omega$ and $\Delta\zeta$ can be calculated based on Eqs (4.48) and (4.49). Using the classical closed-loop control as an example, the maximum values of these quantities are tabulated in Table 4.3 for several parameter variation combinations. It is seen that the classical closed-loop control algorithm is rather insensitive to parameter variations. A variation of 40% in stiffness leads to a maximum of 5.2% change in the maximum top-floor relative displacement and base shear. Moreover, damping variations have a negligible effect on the control force and the response quantities.

In closing, let us remark that, as seen in Section 3.3.1, a special property possessed by the instantaneous closed-loop control is that its control gain is not a function of the structural parameters. Hence, the control efficiency in this case is not affected by structural parameter variations.

4.5 Limited Number of Sensors and Controllers

From the viewpoint of practicality and economy, the number of sensors and controllers will be severely limited for real structural applications, and this is particularly true in the case of controllers. To be sure, the development of control algorithms in Chapter 3 has been based on an arbitrary number of controllers and has included the case of an arbitrary number of sensors (output feedback) as long as the structural system is completely controllable and observable. However, there are still a number of pertinent questions that remain. They include (a) what are the minimum numbers of sensors and controllers required for the structure to be completely controllable and observable? and (b) where should these sensors and controllers be positioned to produce maximum control benefit?

The answer to the first question can be obtained by testing the ranks of the controllability matrix [Eq. (A.60) in Appendix A] and the observability matrix [Eq. (A.62) in Appendix A]. It can be shown that, for structural systems with no repeated modal frequencies, they can be made controllable and observable by a single properly located sensor and a single properly located controller.[8,32,33] It should be emphasized, however, that practical considerations and computational requirements often require more sensors and controllers to be used than these minimum numbers.

4.5.1 Optimal Placement of Sensors and Controllers

Given the number of sensors to be placed, the problem of determining their optimal locations can be formulated relatively easily. Conceptually, a criterion of optimality should be related to maximum state information, i.e. sensor

locations should be chosen in such a way that they produce maximum information on the state of the structural system. For example, this approach is taken by Juang and Rodriguez[33] where the optimal sensor locations are defined as those points where the absolute minimum of the state estimation error occurs. Let us recall that the state estimator $\hat{z}(t)$ is defined in Eq. (3.23). When the observation error η in Eq. (3.22) is random, $\hat{z}(t)$ is also random. Denoting the random state estimator by $\hat{Z}(t)$, a plausible definition of the state estimation error ε is

$$\varepsilon = E\{[\hat{Z}(t) - z(t)]^{\mathrm{T}}[\hat{Z}(t) - z(t)]\} \tag{4.53}$$

Thus, one possible approach is to determine sensor locations so that the error ε is minimized.

The following example, discussed by Juang and Rodriguez,[33] is presented here in order to gain insight into the minimization problem of state estimation error and optimal sensor locations. It also serves to show the interesting relationship that exists between optimal sensor locations and structural mode shapes.

Example 4.5 Consider the sensor location problem associated with the free transverse vibration of a simply supported beam of unit length as shown in Fig. 4.18. The beam dynamics is governed by

$$\frac{\partial^4 w}{\partial x^4} + \frac{\partial^2 w}{\partial t^2} = \delta(x - 0.7)u(t) \tag{4.54}$$

where $w(x, t)$ is the transverse beam displacement at distance x from the left end point and $u(t)$ is the control force located at $x = 0.7$. The modal frequencies for this case are

$$\omega_j = j^2\pi^2, \quad j = 1, 2, \ldots$$

and the corresponding normalized mode shapes are

$$\phi_j = \sqrt{2}\sin j\pi x, \quad j = 1, 2, \ldots$$

Only a single point sensor is considered and we begin with the case where the simply-supported beam is characterized by one mode only.

Figure 4.18 A simply supported beam

Case A (one mode only): For this case, an analytical solution is possible. Let the sensor location be denoted by x_s, the error ε as defined by Eq. (4.53) is a function of x_s with, under some simplifying assumptions on the control parameters,

$$\varepsilon(x_s) = 2\sigma^2(\rho + \rho^3)\cos(\alpha/2)$$

where σ^2 is the variance of the measurement noise and

$$\rho = (\pi^4 + \omega_0^4)^{1/4}$$

$$\omega_0^2 = 2\sin 0.7\pi \sin \pi x_s$$

$$\alpha = \cos^{-1}(-\pi^2/\rho^2)$$

The optimal sensor location, denoted by x_s^*, is then found by finding the absolute minimum of $\varepsilon(x_s)$, $0 \leqslant x_s \leqslant 1$. It is easy to show that it occurs in this case at the midpoint of the beam, i.e.

$$x_s^* = 0.5$$

which, as shown in Fig. 4.19(a), coincides with the peak of the mode shape. Figure 4.19(b) shows the state estimation error as a function of the sensor

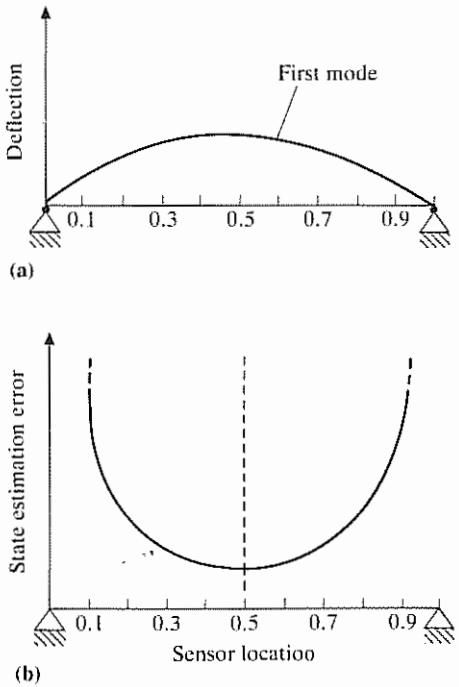

Figure 4.19 Sensor location for one-mode case (a) mode shape; (b) state estimation error

location. Infinite estimation error occurs at the end points which correspond, in fact, to the case of nonobservability.

Case B (*two modes*): For this case, the best sensor location is found to be

$$x_s^* = 0.3 \quad \text{or} \quad 0.7$$

It is seen from Fig. 4.20(a) that the peaks of the mode shapes occur at $x = 0.25$, 0.5 and 0.75. Intuitively, we can interpret the best sensor location as a result of a compromise between the peaks of the mode shapes.

The state estimation error as a function of the sensor location is shown in Fig. 4.20(b), which shows nonobservability at the midpoint as well as at the ends since the second mode is not observable at these points. It also shows two relative minima at $x = 0.3$ and 0.7 due to anti-symmetry of the second mode relative to the middle of the beam.

Case C (*three modes*): The best sensor location in this case is

$$x_s^* = 0.25 \quad \text{or} \quad 0.75$$

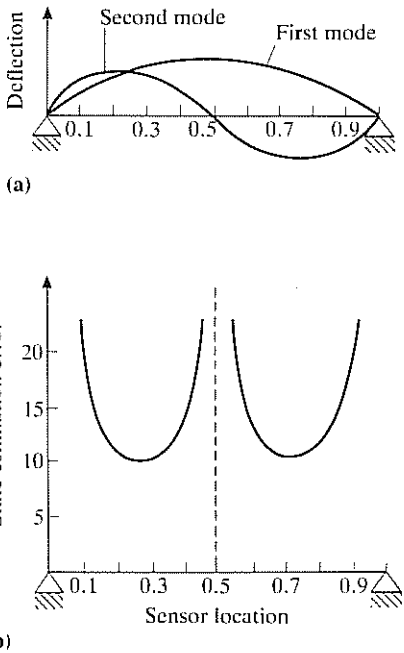

Figure 4.20 Sensor location for two-mode case (a) mode shapes; (b) state estimation error

Figure 4.21(b) shows that there exist four relative minima of the state estimation error resulting from additional peaks of the mode shapes considered as shown in Fig. 4.21(a).

The problem of optimal controller placement has received considerable attention. In comparison with the sensor location problem, this topic is more complex since a number of issues must be addressed to arrive at a meaningful optimality criterion. These include not only structural and control parameters but also the type of controllers and external excitations.

A wide variety of optimality criteria have been considered. An energy performance index is used.[34,35] Another method developed[36] uses a scalar measure, the degree of controllability, as a criterion for controller placement on large structural systems. The use of a controllability index is another possible criterion.[37,38] Other criteria that have been considered include those based on actual control effort,[39] structural failure modes[40] and structural mode shapes.[41] In what follows, the methodology developed by Cheng and

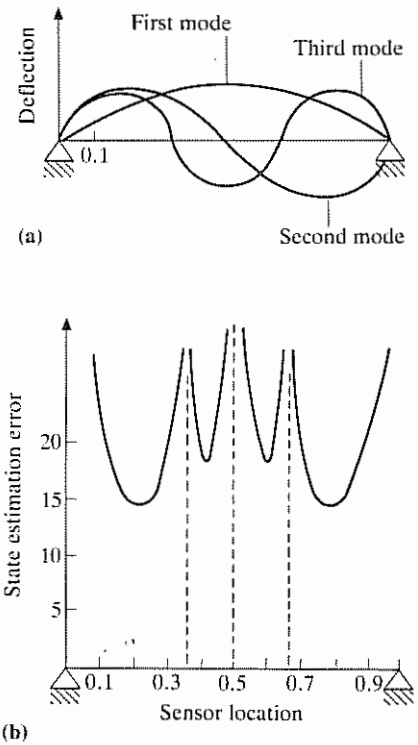

Figure 4.21 Sensor location for three-mode case (a) mode shapes; (b) state estimation error

Pantelides[37,38] will be briefly described. Based on a scalar measure of controllability, the basic idea behind the method is that a controller is optimally placed where the displacement response of the uncontrolled structure is largest due to the action of an externally applied disturbance. In this study, an earthquake-type load is considered.

The controllability index criterion developed[37,38] for seismic structures is based on the following considerations.

1 Lower modes are dominant in the response of earthquake excited structures.
2 The control objective is to reduce the structural response and stabilize the seismic structure.
3 The control effort in terms of control power available is limited.
4 The structural response should not exceed certain thresholds for safety and serviceability of the structure.

Based on these premises, a controllability index can be defined as

$$\rho(x)=\left[\sum_{j=1}^{n}\{g[\phi_j(x)]y_{j(\max)}(t)\}^2\right]^{1/2} \tag{4.55}$$

where

x = percent of total height of structure $(0 \leqslant x \leqslant 1)$

n = number of modes considered

$\phi_j(x)$ = jth mode shape

$y_{j(\max)}(t)$ = maximum jth modal response spectrum

The functional form of $g[\ ]$ depends upon the type of controllers considered. For example, for active tendons, it may take the form

$$g[\phi_j(x)]=\Delta\phi_j(x)/\Delta x$$

where $\Delta\phi_j(x)$ is the jth mode-shape difference over a height increment of Δx. The algebraic difference of the mode shapes is taken in this case since the relative displacement between floors is a critical parameter for active tendons.

In Eq. (4.55), the modal contributions are weighted in a root-mean-square fashion since the modal response maxima do not occur at the same time. It is also noted that the modal response spectra are functions of the applied load.

According to the stipulations outlined above, the optimal controller location is defined to be the value of x for which $\rho(x)$ is maximum. The next best location is one for which $\rho(x)$ has the second largest value, etc.

Example 4.6 A 15-storey shear building, as shown in Fig. 4.22, is studied for optimal location of active tendon controllers on two of its floors. The structural properties of the building are assumed to be as follows: floor stiffness $k = 3000$ k/in and floor mass $m = 2$ k-sec^2/in for all floors; damping = 3% critical. The first two natural frequencies of the uncontrolled structure are 3.92 rad/sec and 11.73 rad/sec; these frequencies correspond to periods of 1.60 sec and 0.54 sec, respectively.

The instantaneous closed-loop control algorithm as discussed in Section 3.3 is used for control design. The weighting matrix $\boldsymbol{Q}$ is assumed to be diagonal with $q_{ii} = 15\,000$ and the $\boldsymbol{R}$ matrix is varied in order to achieve different levels of control forces.

The controllability index of Eq. (4.55) is used to establish optimal locations of the two active tendons. Using response spectra for the 1940 N–S El-Centro earthquake record, the first two maximum modal response values are $y_{1(\max)} = 0.439$ ft and $y_{2(\max)} = 0.265$ ft. The first two modes are considered in evaluating Eq. (4.55) and the values for each term of the controllability index are given in Table 4.4.

A plot of $\rho(x)$ for the present example is shown in Fig. 4.23. It is seen that the two largest values of $\rho(x)$ occur at the first and second floors. Hence, according to the controllability index criterion, they are optimal locations for the active tendon controllers.

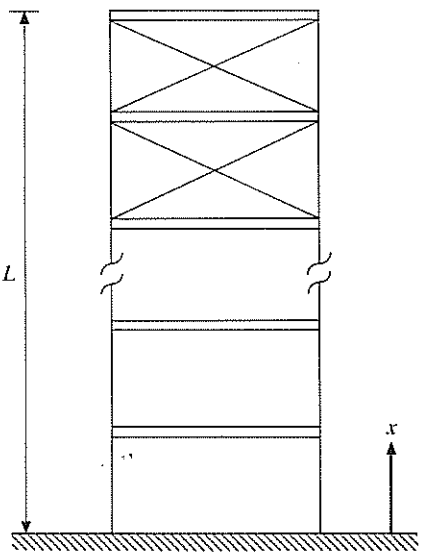

Figure 4.22 The 15-storey structure[38]

Table 4.4 The controllability index

Floor	x	1st mode $\phi_1(x)$	2nd mode $\phi_2(x)$	$\Delta\phi_1/\Delta x$	$\Delta\phi_2/\Delta x$	$\rho(x)$
1	0.067	0.026	−0.076	0.390	1.140	10.60
2	0.133	0.051	−0.145	0.375	1.035	9.76
3	0.200	0.076	−0.201	0.375	0.840	8.45
4	0.267	0.100	−0.238	0.360	0.555	6.59
5	0.333	0.123	−0.254	0.345	0.240	5.01
6	0.400	0.145	−0.246	0.330	0.120	4.52
7	0.467	0.165	−0.216	0.300	0.450	5.42
8	0.533	0.184	−0.165	0.285	0.765	7.27
9	0.600	0.201	−0.100	0.255	0.975	8.60
10	0.667	0.216	−0.026	0.225	1.110	9.47
11	0.733	0.228	0.051	0.180	1.155	9.65
12	0.800	0.238	0.123	0.150	1.080	8.97
13	0.867	0.246	0.184	0.120	0.915	7.57
14	0.933	0.251	0.228	0.075	0.660	5.43
15	1.000	0.254	0.251	0.045	0.345	2.86

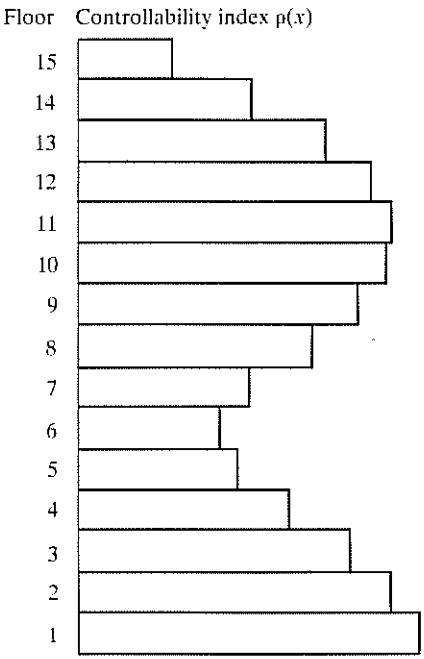

Figure 4.23 Optimal locations of active tendons[38]

4.6 Discrete Time Control

Another important consideration in real-time control implementation is the discrete-time nature in the application of a control algorithm. Strictly speaking, continuous-time control algorithms such as those developed in Chapter 3 can only be executed in discrete time since a digital computer is usually used for on-line computation and control execution. Digital computers are better suited for real-time control because of their flexibility, reliability and speed. As a consequence, response measurements are digitized as feedback signals and control forces are applied in the form of piecewise step functions through the use of analogue-digital converters. Hence, they are not continuous functions as called for by continuous-time control algorithms.

With this in mind, discrete time formulation of active structural control has been a topic of some recent investigations.[42-44] As shown by Chung and Soong,[42] there are actually some inherent advantages in using discrete time formulations. For example, time delay can be compensated in a straightforward fashion by modifying only the feedback gain without demanding extra on-line computation. Output feedback can also be accommodated with resulting savings in the number of sensors required. Moreover, it is shown[43,44] that predictive control can be easily developed using the discrete time approach.

We shall first develop in this section a discrete-time analogue of the continuous version of the classical optimal control algorithm given in Chapter 3, into which time delay will be incorporated. This will be followed by a derivation of predictive control developed by Rodeller et al.[43,44]

Consider again structural systems governed by Eq. (3.1). The solution of $z(t)$ at some time $t_2 (t_2 \geqslant t_1)$ can be written as

$$z(t_2) = \exp[A(t_2 - t_1)]z(t_1) + \int_{t_1}^{t_2} \exp[A(t_2 - t)][Bu(t) + Hf(t)]\,dt \quad (4.56)$$

Suppose that the state vector $z(t)$ and the external excitation $f(t)$ are sampled with period τ for on-line calculation. Between two consecutive sampling instants $k\tau$ and $(k+1)\tau$, the best available information about the excitation is $f(k\tau)$. Thus, excitation is sampled as zero-order hold and is thus assumed to be constant between two consecutive sampling instants. In real-time control, the calculated discrete-time control signal is converted into a zero-order-hold analogue signal, which is a piecewise step function over sampling intervals. Therefore, the system can be described in a discrete-time fashion by

$$z(k+1) = A'z(k) + B'u(k) + H'f(k), \quad k = 0, 1, \ldots \quad (4.57)$$

where

$$A' = \exp(A\tau), \quad B' = A^{-1}(A' - I)B, \quad H' = A^{-1}(A' - I)H$$

The discrete-time system is also shift-invariant and stability of the uncontrolled system is preserved under sampling. Provided the sampling rate is two times larger than the highest controlled modal frequency, the discrete-time system given by Eq. (4.57) is controllable if and only if the corresponding continuous-time system is controllable.[45]

Inevitable time delay in control execution makes it necessary to consider appropriate modifications to the control algorithm. In the presence of time delay $m\tau$, Eq. (4.57) becomes

$$z(k+1) = A'z(k) + B'u(k-m) + H'f(k) \tag{4.58}$$

Under classical optimal control criteria, the active control force, $u(t)$, is found such that the summation

$$J = \frac{1}{2}\sum_{k=m}^{n-1} [z^{\mathrm{T}}(k)Qz(k) + u^{\mathrm{T}}(k-m)Ru(k-m)] \tag{4.59}$$

is minimized, where n is defined such that $f(k) = 0$ for $k > n$, and Q and R are weighting matrices as before. By introducing the costate vector $\lambda(k)$, the constraint equation (4.58) can be incorporated into the performance index as

$$J = \sum_{k=m}^{n-1} \left\{ \frac{1}{2} z^{\mathrm{T}}(k)Qz(k) + \frac{1}{2} u^{\mathrm{T}}(k-m)Ru(k-m) \right.$$
$$\left. + \lambda^{\mathrm{T}}(k+1)[A'z(k) + B'u(k-m) + H'f(k) - z(k+1)] \right\} \tag{4.60}$$

The solution of the optimization problem described above can be obtained using variational procedures as described in Section 3.1. In addition to the constraint equation (4.58), the Euler–Lagrange equations are

$$\lambda(k) = Qz(k) + A'^{\mathrm{T}}\lambda(k+1) \tag{4.61}$$

and

$$u(k-m) = -R^{-1}B'^{\mathrm{T}}\lambda(k+1), \quad k = m, \ldots, n \tag{4.62}$$

Under linear optimal feedback control, the costate vector, $\lambda(k)$, has the form

$$\lambda(k+1) = P(k+1)z(k+1) \tag{4.63}$$

and the control force vector is linearly related to the state variables as

$$u(k-m) = R^{-1}B'^{\mathrm{T}}P(k+1)z(k+1), \quad k = m, \ldots, n-1 \tag{4.64}$$

where $P(k)$ satisfies the discrete-time matrix Riccati equation

$$P(k) = Q + A'^{\mathrm{T}}P(k+1)[I + B'R^{-1}B'^{\mathrm{T}}P(k+1)]^{-1}A' \tag{4.65}$$

with boundary condition

$$\boldsymbol{P}(n) = \boldsymbol{0} \tag{4.66}$$

As discussed in Section 3.1, $\boldsymbol{P}(k)$ can in most cases be approximated by a constant matrix $\boldsymbol{P}$.

With Eqs (4.61) and (4.63), the state variables over a sampling period are related by

$$z(k+1) = \boldsymbol{T}z(k) \tag{4.67}$$

where

$$\boldsymbol{T} = (\boldsymbol{A}'^{\mathrm{T}}\boldsymbol{P})^{-1}(\boldsymbol{P} - \boldsymbol{Q}) \tag{4.68}$$

By repeated application of Eq. (4.67), the control force under linear state feedback with time delay compensation can be expressed as

$$\boldsymbol{u}(k-m) = \boldsymbol{G}(m)z(k-m) \tag{4.69}$$

where

$$\boldsymbol{G}(m) = -\boldsymbol{R}^{-1}\boldsymbol{B}'^{\mathrm{T}}\boldsymbol{P}\boldsymbol{T}^{m+1} \tag{4.70}$$

As we have seen in Section 4.2, the dynamic equation of a continuous-time system with time delay becomes a differential-difference one which makes the stability problem of feedback control difficult. However, the dynamic equation of a discrete-time system remains a difference one in the presence of time delay. The stability problem is just the eigenvalue problem of the augmented effective system matrix. The effect of time delay without compensation can be investigated through the corresponding poles and frequency response functions with $\boldsymbol{G} = \boldsymbol{G}(0)$. How well time delay is compensated can be studied with $\boldsymbol{G} = \boldsymbol{G}(m)$.

Example 4.7 In this example, the discrete-time control algorithm developed above is applied to the study of the structural system discussed in Example 3.1 with special attention paid to the time delay effect. The poles of the controlled system transfer function with uncompensated and compensated time delay are listed in Table 4.5 for different amounts of delay. For the uncompensated case, it is seen that one of the poles is approaching a unit circle of the complex plane as time delay increases. If time delay is further increased, the control system will become unstable. The corresponding relative displacement frequency response functions are plotted in Fig. 4.24. The peak amplitude increases rapidly as a function of time delay and it shifts to the right as time delay increases.

For the compensated case, the pole that is closest to the unit circle in the complex plane remains the same for different time delays (Table 4.5), but the

Table 4.5 Poles of system transfer function

Time delay (m)	Poles of uncompensated transfer function	Poles of compensated transfer function
0	$0.8940 \pm j0.2130$	$0.8940 \pm j0.2130$
1	$0.8841 \pm j0.2357$ 0.1792 0.0	$0.8940 \pm j0.2130$ 0.1595 0.0
2	$0.8865 \pm j0.2722$ 0.5138 -0.3395 $\pm 3.765 \times 10^{-9}$	$0.8940 \pm j0.2130$ 0.4558 -0.2963 $\pm j2.5 \times 10^{-9}$
3	$0.9164 \pm j0.3016$ 0.6792 $-0.2823 \pm j0.3971$ $(-1.1989 \pm j2.077) \times 10^{-6}$ 0.2398×10^{-6}	$0.8940 \pm j0.2130$ 0.6359 $-0.2382 \pm j0.3334$ $(1.750 \pm j3.031) \times 10^{-6}$ 3.50×10^{-6}
4	$0.9508 \pm j0.3068$ 0.7495 -0.5619 $-0.07087 \pm j0.5933$ $(\pm 3.599 \pm j3.599) \times 10^{-5}$	$0.8940 \pm j0.2130$ 0.7348 $-0.06197 \pm j0.4774$ -0.4514 $\pm 1.168 \times 10^{-4}$ $-3.4 \times 10^{-10} \pm j1.168 \times 10^{-4}$

number of poles increases by two as time delay increases by one time interval. Although the effect of time delay cannot be perfectly compensated, the peak amplitude is now less sensitive to time delay and system stability is ensured (Fig. 4.24). The peak frequency shifts slightly to the left as time delay increases.

The effect of time delay compensation is illustrated by comparing the frequency response functions for various values of m (Fig. 4.24). When $m = 1$ and 2, the delay uncompensated case is even slightly better than the delay compensated case as far as peak amplitude is concerned. But when $m = 3$ and 4, the contribution of time delay compensation becomes apparent.

In order to gain more insight into the problem in time domain, results of a computer simulation are presented in Figs 4.25–4.29 with the north-south component of the 1940 El Centro earthquake acting as the base excitation. When no time delay is introduced, the uncontrolled and controlled relative displacements are shown in Fig. 4.25. From Fig. 4.29, it is seen that the control effect without time delay compensation is even worse than the uncontrolled case when $m = 4$. By comparing Figs 4.26–4.29, it is found that the uncompensated case is slightly better than the compensated one for $m = 1$ and 2 as far as peak response is concerned, but it is much worse for $m = 4$. The results match those obtained from the frequency response functions.

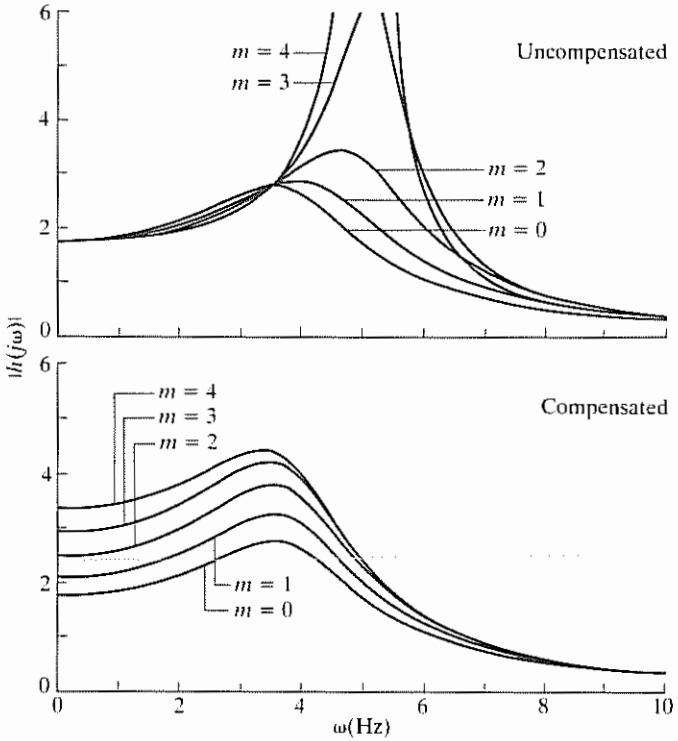

Figure 4.24 Relative displacement frequency transfer functions

4.6.1 Predictive Control

The basic issues in formulating a discrete-time predictive control algorithm can be summarized as follows:[43,44] (1) at each sampling instant $k\tau$, a prediction horizon is defined over a finite number of steps ahead and a discrete-time model is used to predict the response over this horizon as a function of the control sequence; and (2) the control computed at instant $k\tau$ is a part of the control sequence that produces a desired response trajectory over the prediction horizon; this trajectory verifies a performance criterion.

Consider here the predictive horizon $[k\tau, (k+\lambda)\tau]$ over which the response can be predicted by a state-space model of the form

$$\hat{z}(k+j|k) = \hat{A}\hat{z}(k+j-1|k) + \hat{B}\hat{u}(k+j-1|k) \tag{4.71}$$

where $\hat{z}(k+j-1|k)$ is the state vector predicted at instant k for instant $k+j-1$, $\hat{u}(k+j-1|k)$ is the corresponding control sequence, and $\hat{A}$ and $\hat{B}$ are the discrete-time system and control matrices, respectively. This model is

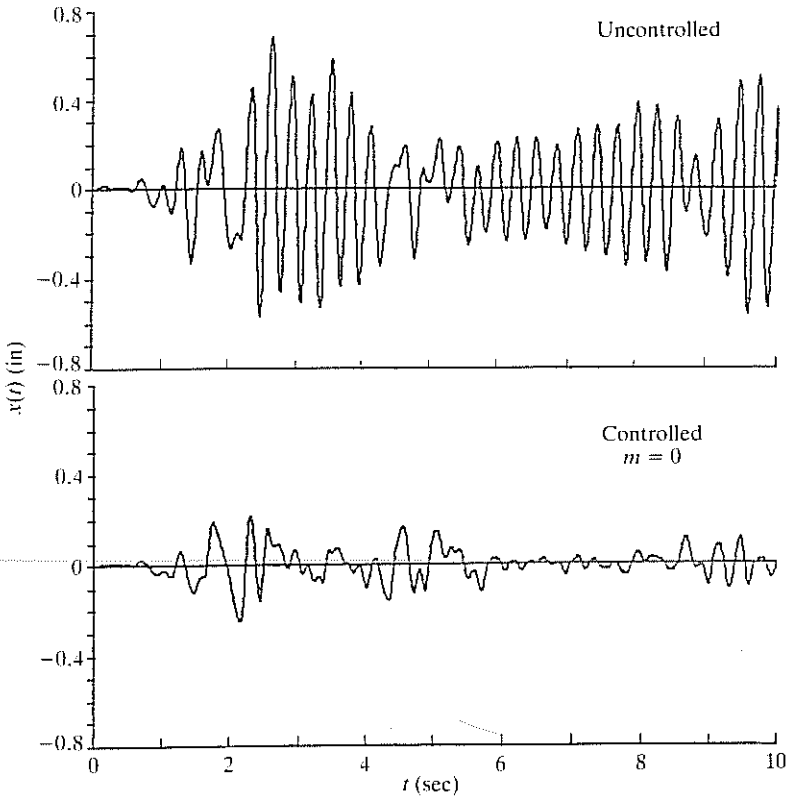

Figure 4.25 Relative displacement ($m = 0$)

redefined at each sampling instant k in the form

$$\left.\begin{aligned}\hat{z}(k|k) &= z(k)\\ \hat{u}(k|k) &= u(k)\end{aligned}\right\} \tag{4.72}$$

where $z(k)$ and $u(k)$ are the state vector and the control signal at instant k.

A general performance criterion to define the desired trajectory and the control vector $u(k)$ may consist of minimization of the cost function

$$J = \frac{1}{2}\sum_{j=0}^{\lambda}[\hat{z}(k+j|k) - z_r(k+j|k)]^T Q(j)[\hat{z}(k+j|k) - z_r(k+j|k)]$$

$$+ \frac{1}{2}\sum_{j=0}^{\lambda-1}\hat{u}(k+j|k)^T R(j)\hat{u}(k+j|k) \tag{4.73}$$

where the weighting matrices $Q(j)(j = 0, 1, \ldots, \lambda)$ and $R(j)(j = 0, 1, \ldots, \lambda - 1)$ are real positive semi-definite and $R(j)$ is also non-singular. z_r is a reference trajectory which may be redefined at each sampling instant k starting

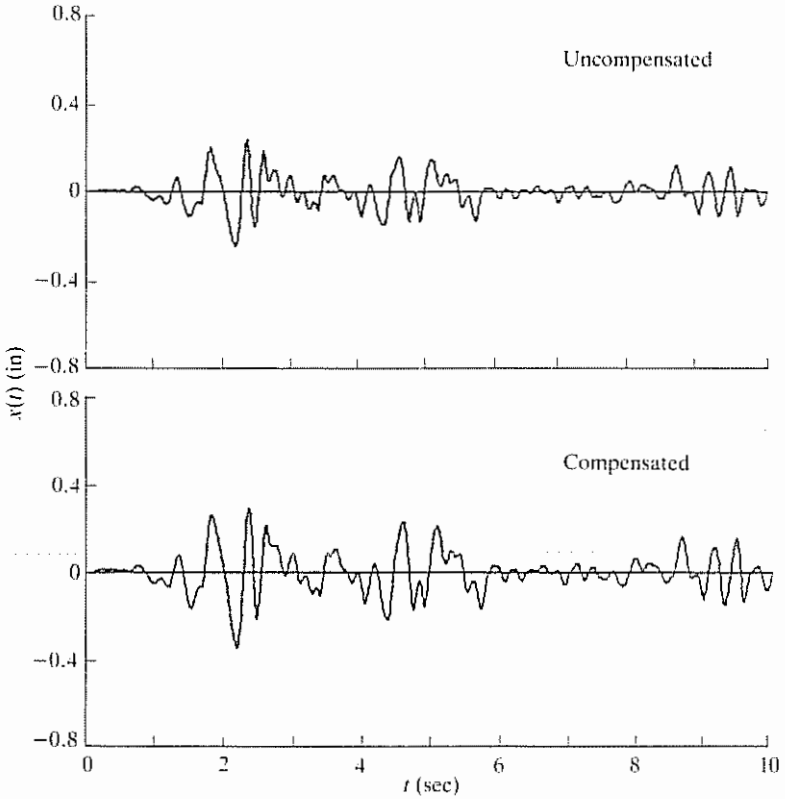

Figure 4.26 Relative displacement ($m = 1$)

from the current output and evolves towards a target state according to a chosen dynamics.

This cost function can be minimized by following standard optimization techniques like those described in Chapter 3. Within the predictive control strategy, a more intuitive and direct solution can be found which requires less computational effort. This solution is based on imposing some specified shapes to the control sequence on the prediction horizon, which allows a reduction in the number of unknowns in the minimization of the cost function.

A particular choice of the shape of the control sequence may be that of a step or of a pulse. One may consider, as an example, the following index:

$$J = \frac{1}{2}\sum_{j=1}^{\lambda} [\hat{z}(k+j|k) - z_r(k+j|k)]^{\mathrm{T}} \boldsymbol{Q}(j) [\hat{z}(k+j|k) - z_r(k+j|k)]$$

$$+ \frac{1}{2}\hat{\boldsymbol{u}}(k|k)^{\mathrm{T}} \boldsymbol{R}\hat{\boldsymbol{u}}(k|k) \qquad (4.74)$$

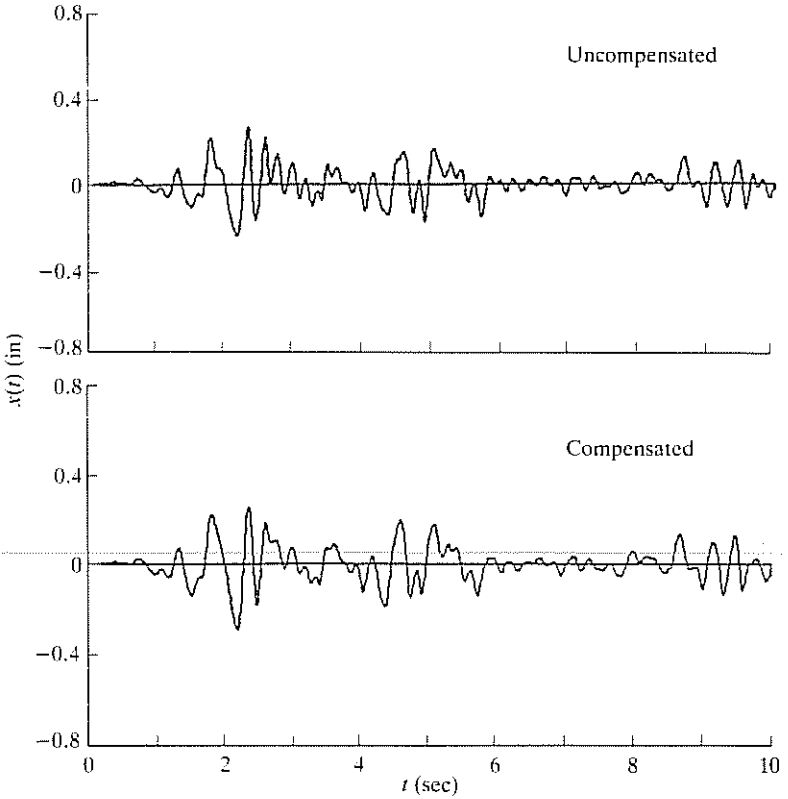

Figure 4.27 Relative displacement ($m = 2$)

In the case of a step-shaped control sequence, the minimization of index (4.74) is performed by using the condition

$$\hat{\boldsymbol{u}}(k+j|k) = \hat{\boldsymbol{u}}(k|k) = \boldsymbol{u}(k), \quad j = 1, \ldots, \lambda - 1 \tag{4.75}$$

By using Eqs (4.71), (4.72) and (4.75), the process output predicted at instant k for consecutive instants $k + j (j = 1, \ldots, \lambda)$ can be expressed as a function of the current state vector $\boldsymbol{z}(k)$ and the control vector $\boldsymbol{u}(k)$ as

$$\hat{\boldsymbol{z}}(k+j|k) = \boldsymbol{T}(j)\boldsymbol{z}(k) + \boldsymbol{S}(j)\boldsymbol{u}(k) \tag{4.76}$$

where $\boldsymbol{T}(j)$ and $\boldsymbol{S}(j)$ are matrices given by

$$\left.\begin{aligned} \boldsymbol{T}(j) &= \hat{\boldsymbol{A}}^j \\ \boldsymbol{S}(j) &= (\boldsymbol{I} + \hat{\boldsymbol{A}} + \hat{\boldsymbol{A}}^2 + \ldots + \hat{\boldsymbol{A}}^{j-2} + \hat{\boldsymbol{A}}^{j-1})\hat{\boldsymbol{B}} \end{aligned}\right\} \tag{4.77}$$

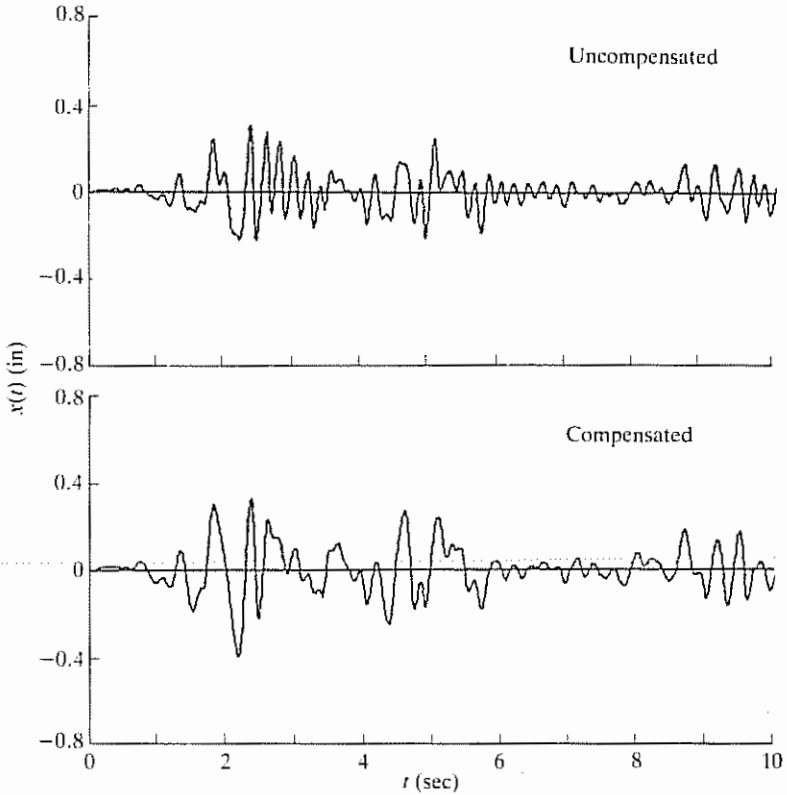

Figure 4.28 Relative displacement ($m = 3$)

The substitution of Eq. (4.76) into Eq. (4.74) gives

$$J = \frac{1}{2} \sum_{j=1}^{\lambda} [\boldsymbol{T}(j)\boldsymbol{z}(k) + \boldsymbol{S}(j)\boldsymbol{u}(k) - \boldsymbol{z}_r(k+j|k)]^T \boldsymbol{Q}(j)$$

$$\times [\boldsymbol{T}(j)\boldsymbol{z}(k) + \boldsymbol{S}(j)\boldsymbol{u}(k) - \boldsymbol{z}_r(k+j)] + \frac{1}{2}\boldsymbol{u}^T(k)\boldsymbol{R}\boldsymbol{u}(k) \quad (4.78)$$

Since $\boldsymbol{u}(k)$ is the only unknown in Eq. (4.78), it can be obtained by imposing the following condition on the gradient of J:

$$\frac{\partial J}{\partial \boldsymbol{u}(k)} = \boldsymbol{0} \quad (4.79)$$

The application of condition (4.79) to Eq. (4.78) results in

$$\boldsymbol{A}'\boldsymbol{z}(k) + \boldsymbol{B}'\boldsymbol{u}(k) = \boldsymbol{\mu}(k) \quad (4.80)$$

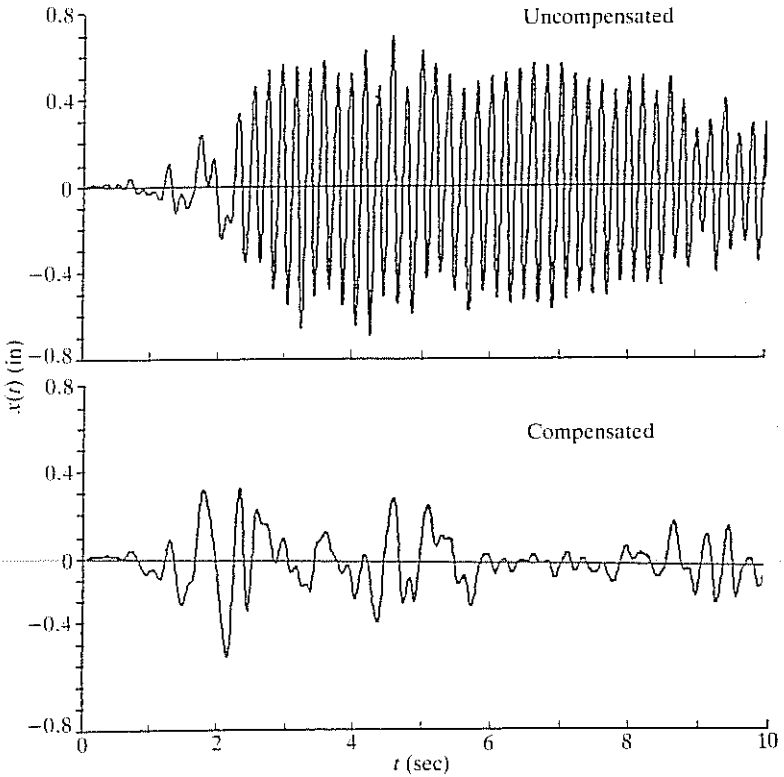

Figure 4.29 Relative displacement ($m = 4$)

where A' and B' are matrices given by

$$\left.\begin{aligned} A' &= \sum_{j=1}^{\lambda} S^{\mathrm{T}}(j)Q(j)T(j) \\ B' &= \sum_{j=1}^{\lambda} S^{\mathrm{T}}(j)Q(j)S(j) \end{aligned}\right\} \tag{4.81}$$

and $\mu(k)$ is a vector defined by

$$\mu(k) = \sum_{j=1}^{\lambda} S^{\mathrm{T}}(j)Q(j)z_{\mathrm{r}}(k+j|k) \tag{4.82}$$

which represents a weighted average of the reference trajectory in $[k, k+\lambda]$. The control vector is finally reduced from Eq. (4.80), resulting in the following control law:

$$u(k) = -B'^{-1}[A'z(k) - \mu(k)] \tag{4.83}$$

The computation of the control gain matrix $B'^{-1}A'$ is significantly simpler than that of the gain matrix in the optimal control law which requires the solution of a Riccati equation. A particular choice of weighting matrices $Q(j)$ and R which further simplifies the computation of matrices A' and B' is

$$R = 0$$
$$Q(j) = 0, \quad j = 1, \ldots, \lambda - 1$$
$$Q(\lambda) = Q$$

In this case, the control law reduces to

$$u(k) = -B'^{-1}A'z(k) + B'^{-1}C'z_r(k+\lambda|k) \tag{4.84}$$

where now

$$\left.\begin{aligned} A' &= S^T(\lambda)QT(\lambda) \\ B' &= S^T(\lambda)QS(\lambda) \\ C' &= S^T(\lambda)Q \end{aligned}\right\} \tag{4.85}$$

With this particular choice of matrices $Q(j)$ and R, index (4.74) is reduced to

$$J = \frac{1}{2}\,[\hat{z}(k+\lambda|k) - z_r(k+\lambda|k)]^T Q[\hat{z}(k+\lambda|k) - z_r(k+\lambda|k)] \tag{4.86}$$

The minimization of this index implies that the desired output at instant $k+\lambda$ will be as close as possible to the reference trajectory. In the special case in which the input and output vectors have the same dimension, the minimum value for J is zero. This case means imposing the criterion that the desired output at instant $k+\lambda$ should be equal to a given value $z_r(k+\lambda|k)$.

Example 4.8 To illustrate the main features of predictive control, it is applied to a one-degree-of-freedom system subjected to the horizontal ground acceleration $\ddot{x}_0(t)$ shown in Fig. 4.30 and to a horizontal control force $u(t)$. The equation of motion takes the form

$$m\ddot{x}(t) + c\dot{x}(t) + kx(t) = -m\ddot{x}_0(t) + u(t)$$

with $m = 866.5$ tons, $c = 346$ tons/sec and $k = 128 \times 10^6$ N/m. The matrices $\hat{A}$ and $\hat{B}$ in Eq. (4.71) are defined through the discretization procedure using a sampling period $\tau = 0.05$ sec. The predictive control law (4.84) is used to compute the control force at each sampling instant. The value of the reference trajectory $z_r(k+j)$ is obtained by the discrete-time equation

$$z_r(k+j|k) = A_r z_r(k+j-1|k), \quad j = 1, \ldots, \lambda \tag{4.87}$$

where A_r is chosen in such a way that Eq. (4.87) represents the free vibration of a harmonic oscillator with critical damping and frequency ω. The initial

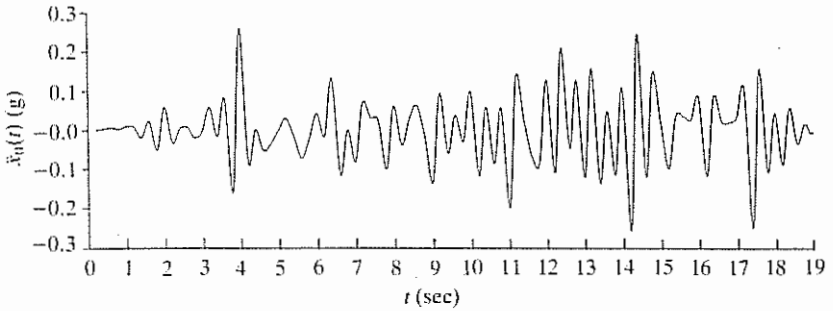

Figure 4.30 Seismic ground acceleration in Example 4.8

condition is $z_r(k|k) = z(k)$ where $z(k)$ is the state vector measured at sampling instant k.

As illustrated in Fig. 4.31, a faster trajectory corresponds to a higher frequency. In a limiting case, a null trajectory may be considered, thus resulting in a discontinuous jump from the displacement $x_r(k)$ to a null value. The weighting matrix $\boldsymbol{Q}$ reduces, in this single-degree-of-freedom case, to a positive scalar and it has been fixed as equal to one. Consequently, the parameters to be chosen in each application are the value of λ defining the prediction horizon and that of frequency ω of the referenced trajectory.

Numerical simulations were carried out in which the predictive control was used by varying the value of λ for different values of ω. In Fig. 4.32, the maximum displacement and the control force are shown for these cases. For the purpose of comparison, the maximum displacement without control is 9.7 cm.

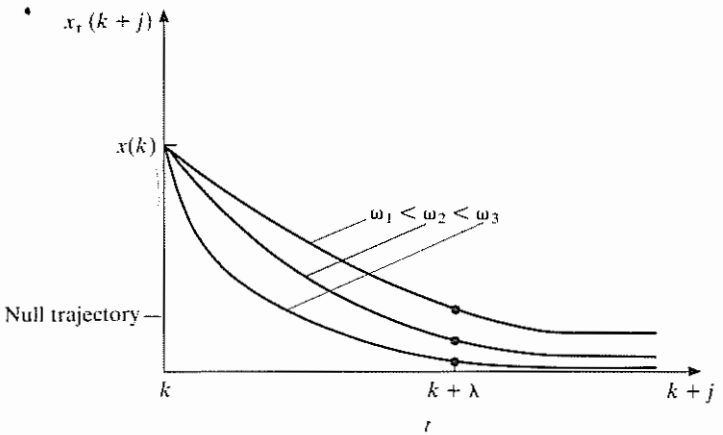

Figure 4.31 Reference displacement trajectories

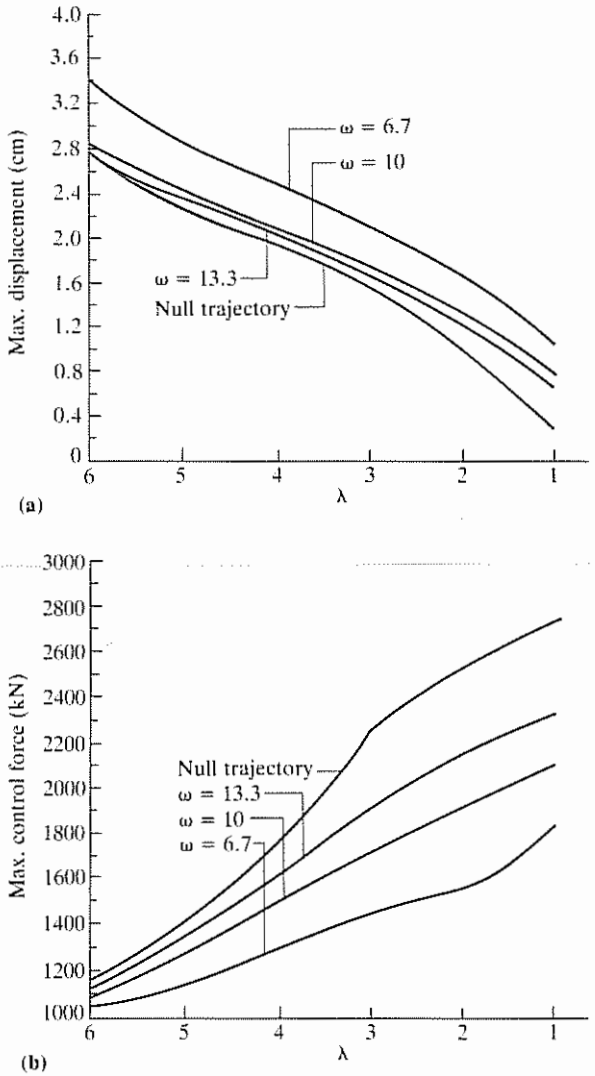

Figure 4.32 Numerical simulation[43] (a) maximum displacement; (b) maximum control force

Some important features of predictive control can be observed from Fig. 4.32. For a given reference trajectory, a decrease in parameter λ results in a decrease in the displacement together with an increase in the control force. At the same time, by comparing the graphs for different reference trajectories, it can be seen that, for a larger value of ω, displacements are smaller and control forces are greater. These comments may be interpreted

according to the physical significance of parameters λ and ω. A smaller value of λ implies a shorter prediction horizon and, according to the strategy of predictive control, it determines a desired output closer to the equilibrium position. On the other hand, a higher value of ω results in a faster reference trajectory, which also imposes a desired output closer to equilibrium. Consequently, the smaller the value of λ or the greater the value of ω is, the more demanding the control action is.

4.7 Reliability

While reliability is of central importance in all areas of system analysis, design and synthesis, it takes on an added dimension of complexity, both technologically and psychologically, when an active control system is relied upon to ensure safety of a structure. First of all, when active control is only used to counter large environmental forces, it is likely that the control system will be infrequently activated. The reliability of a system operating largely in a standby mode and the related problems of maintenance and performance qualification become an important issue. Furthermore, active systems rely on external power sources which, in turn, rely on all the support utility systems. These systems, unfortunately, are most vulnerable at the precise moment when they are most needed. The scope of the reliability problem is thus considerably enlarged if all possible ramifications are considered.

Not to be minimized is the psychological side of the reliability problem. There may exist a significant psychological barrier on the part of the occupants of a structure in accepting the idea of an actively controlled structure, leading to perhaps perceived reliability-related concerns.

The reliability problem can be addressed by identifying important factors influencing the control system performance. Methodologies are well developed and one of the approaches is discussed here for a simple case.[9] For the sake of simplicity, only the effect of time constant, i.e. time required for generation of the required full control force, on the reliability of structural control is considered.

Example 4.9 Consider a single-degree-of-freedom structural system described by

$$\dot{z}(t)=\begin{bmatrix} 0 & 1 \\ -16.67 & -1.67 \end{bmatrix} z(t)+\begin{bmatrix} 0 \\ 1 \end{bmatrix} u(t)+\begin{bmatrix} 0 \\ 1 \end{bmatrix} f(t) \qquad (4.88)$$

and suppose the control law is given by

$$u(t)=-[5.0 \quad 0]z(t) \qquad (4.89)$$

With the presence of a random time constant T in the control loop, the transfer function of the controller, $H_c(s)$, has the form

$$H_c(s) = \frac{g}{1 + Ts} \tag{4.90}$$

where g is a constant gain which is determined by the control law. Let us assume a uniform distribution in the interval [0, 0.1] for T. The effect of this time constant on the reliability of structural control can be important since the displacement of the controlled system can increase significantly with increasing values of the time constant. Hence, the failure probability at a given limiting displacement will be increased.

For the purpose of this study, failure is said to occur when the maximum displacement of the structural system exceeds a certain level. To study the time constant effect, 12 sample values of T are chosen from the assumed uniform distribution. For each sample, the maximum displacements to 20 artificial earthquakes are computed. These data points are then plotted on an extreme-value probability paper as shown in Fig. 4.33. These results show that, while ideal control systems (with zero time constant) are effective in reducing the structural response, relatively large values of T may cause adverse effect.

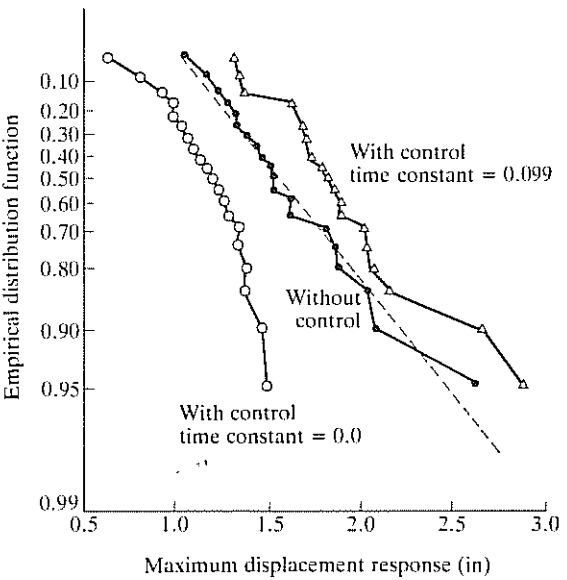

Figure 4.33 Empirical distribution function of maximum displacement[9]

Assuming that the distribution function for the maximum displacement conditional upon the time constant has the extreme-value form

$$F_{X|T}(x|t) = \exp\{-\exp[a(t)x + b(t)]\}, \quad x \geqslant 0 \tag{4.91}$$

the parameters of the distribution can be estimated based on the data generated above, resulting in

$$a(t) = -4.87 + 10.91t + 121.2t^2$$

$$b(t) = 4.92 + 18.04t - 227.7t^2$$

The probability distribution function of the maximum displacement may be found from

$$F_X(x) = \int_0^\infty F_{X|T}(x|t) f_T(t) \mathrm{d}t \tag{4.92}$$

where $f_T(t)$ is the probability density function of T. In this case,

$$f_T(t) = 10, \quad 0 \leqslant t \leqslant 0.1$$

$$= 0, \quad \text{elsewhere}$$

It can be seen from Fig. 4.33 that $F_X(x)$ lies to the right of that for the structure with an ideal control system. In other words, for a given limiting displacement value, the probability of failure is higher in the presence of time constant than that for ideally controlled structures. By increasing the distribution interval of the time constant or by changing the shape of $f_T(t)$, it is even possible to obtain a higher failure probability for the controlled structure than for an uncontrolled structure.

4.8 Other Considerations

We have touched upon only a few topics which may become important from the point of view of control implementation. In addition, eventual implementability of an active control system will depend on the solution or resolution of a number of key problems dealing with hardware development and its cost-effectiveness when compared with other means of structural control. Active control requires the generation of large control forces, for which a new generation of actuators and control systems will be required. Furthermore, appropriate control devices must be developed not only based on technological considerations, but also on economic, aesthetic and structural integration grounds. Above all, cost-effectiveness must be carefully assessed for various specific structural applications.

References

1. Yao J T P and Abdel-Rohman M 1987 Research Topics for Practical Implementation of Structural Control. In Leipholz H H E (ed) *Structural Control* Martinus Nijhoff, Amsterdam pp 762–7
2. Balas M 1978 Feedback Control of Flexible Systems. *IEEE Transactions on Automatic Control* **AC-23** pp 673–9
3. Balas M 1980 Active Control of Large Engineering Structures: A Naive Approach. In Leipholz H H E (ed) *Structural Control* North Holland, Amsterdam pp 107–25
4. Soong T T and Chang J C H 1982 Active Vibration Control of Large Flexible Structures. *Shock Vibration Bulletin* **52** Part IV pp 47–54
5. Gustafson D E and Speyer J L 1976 Linear Minimum Variance Filters Applied to Carrier Tracking. *IEEE Transactions on Automatic Control* **AC-21** pp 65–73
6. Skelton R E and Likins P W 1978 Orthogonal Filters for Model Error Compensation in the Control of Nonrigid Spacecrafts. *Journal of Guidance and Control* **1** pp 41–9
7. Skelton R E 1979 Adaptive Orthogonal Filters for Compensation of Truncated Modes and Other Modal Data Uncertainty in Spacecraft. *Proceedings of AIAA 17th Aerospace Science Meeting* New Orleans
8. Wu Y W, Rice R B and Juang J N 1979 Sensor and Actuator Placement for Large Flexible Space Structures. *Preprint Joint Automatic Control Conference*
9. Basharkhah M A and Yao J T P 1984 Reliability Aspects of Structural Control. *Civil Engineering Systems* **1** pp 224–9
10. Pu J P 1989 Frequency Response Design of Controlled Structure. In Nelson J K Jr (ed) *Computer Utilization in Structural Engineering* ASCE, NY pp 131–41
11. Hammerstrom L G and Gros K S 1980 Adaptation of Optimal Control Theory to Systems with Time Delays. *International Journal of Control* **32** pp 320–57
12. Mutharasan R and Luus R 1975 Analysis of Time-Delay Systems by Series Approximations. *American Institute of Chemical Engineers Journal* **21** pp 567–72
13. Soliman M A and Ray W H 1972 Optimal Feedback Control for Linear-Quadratic Systems Having Time Delays. *International Journal of Control* **15** pp 609–15
14. Abdel-Rohman M 1985 Structural Control Considering Time Delay Effect. *Transactions of the Canadian Society of Mechanical Engineers* **9** pp 224–7
15. Abdel-Rohman M 1987 Time Delay Effects on Actively Damped Systems. *ASCE Journal of Engineering Mechanics* **113** pp 1709–19
16. Roorda J 1980 Experiments in Feedback Control of Structures. In Leipholz H H E (ed) *Structural Control* North Holland, Amsterdam pp 629–61
17. Chung L L, Reinhorn A M and Soong T T 1988 Experiments on Active Control of Seismic Structures. *ASCE Journal of Engineering Mechanics* **114** pp 241–56
18. Chung L L, Lin R C, Soong T T and Reinhorn A M 1989 Experimental Study of Active Control for MDOF Seismic Structures. *ASCE Journal of Engineering Mechanics* **115** pp 1609–27
19. McGreevy S, Soong T T and Reinhorn A M 1988 An Experimental Study of

Time Delay Compensation in Active Structural Control. *Proceedings of International Modal Analysis Conference* Orlando FL pp 733–9
20. Masri S F, Bekey G A and Caughey T K 1981 Optimal Pulse Control of Flexible Structures. *ASME Journal of Applied Mechanics* **48** pp 619–26
21. Masri S F, Bekey G A and Caughey T K 1982 On-line Control of Nonlinear Flexible Structures. *ASME Journal of Applied Mechanics* **49** pp 877–84
22. Miller R K, Masri S F, Dehghanyar T J and Caughey T K 1988 Active Vibration Control of Large Civil Structures. *ASCE Journal of Engineering Mechanics* **114** pp 1542–70
23. Reinhorn A M, Manolis G D and Wen C Y 1987 Active Control of Inelastic Structures. *ASCE Journal of Engineering Mechanics* **113** pp 315–33
24. Yang J N, Long F X and Wong D 1988 Optimal Control of Nonlinear Structures. *ASME Journal of Applied Mechanics* **55** pp 931–9
25. Yang J N, Long F X and Wong D 1988 *Optimal Control of Nonlinear Flexible Structures* Technical Report NCEER-88-0002, National Center for Earthquake Engineering Research, Buffalo NY
26. Clough R W and Penzien J 1975 *Dynamics of Structures* McGraw-Hill, NY
27. Wilson E L and Fahoomand L 1973 Nonlinear Dynamic Analysis of Complex Structures. *Journal of Earthquake Engineering Structural Dynamics* **1** pp 241–52
28. Yao J T P 1987 Uncertainties in Structural Control. In Inman D J and Simonis J C (eds) *Vibration Control and Active Vibration Suppression* ASME, New York pp 197–200
29. Yang J N and Akbarpour A 1987 Effect of System Uncertainty on Active Structural Control. *Proceedings of ASCE 6th Structural Congress* Orlando FL
30. Yang J N and Akbarpour A 1987 *Practical Considerations for Structural Control Technical Report* NCEER-87-0018, National Center for Earthquake Engineering Research, Buffalo NY
31. Leitmann G 1985 Feedback and Adaptive Control for Uncertain Systems. In Batten D F and Lesse P F (eds) *New Mathematical Advances in Economic Dynamics* Croom Helm, London
32. Juang J N and Balas M 1978 Dynamics and Control of Large Spinning Spacecraft. *Proceedings of AIAA/AAS Astrodynamics Conference* Palo Alto CA
33. Juang J N and Rodriguez G 1979 Formulation and Applications of Large Structure Actuator and Sensor Placements. *Proceedings of Second VPI&SU/AIAA Symposium on Dynamics and Control of Large Flexible Spacecraft* Blacksburg VA
34. Martin C R and Soong T T 1976 Modal Control of Multistory Structures. *ASCE Journal of Engineering Mechanics Division* **102** pp 613–23
35. Chang M I J and Soong T T 1980 Optimal Control Placement in Modal Control of Complex Systems. *Journal of Mathematical Analysis and Applications* **75** pp 340–58
36. Laskin R A 1982 *Aspects of the Dynamics and Controllability of Large Flexible Structures* Ph.D. Dissertation Columbia University NY
37. Cheng F Y and Pantelides C P 1988 *Optimal Placement of Actuators for Structural Control.* Technical Report NCEER-88-0037, National Center for Earthquake Engineering Research, Buffalo NY
38. Pantelides C P and Cheng F Y 1989 Optimal Location of Active Controllers

Subjected to Seismic Excitations. In Nelson J K Jr (ed) *Computer Utilization in Structural Engineering* ASCE, NY pp 111–20

39. Lindberg R E Jr. and Longman R W 1984 On the Number and Placement of Actuators for Independent Modal Space Control. *Journal of Guidance* **7** pp 215–21
40. Vander Velde W E and Carignan C R 1984 Number and Placement of Control System Components Considering Possible Failures. *Journal of Guidance* **7** pp 703–9
41. Ibidapo-Obe O 1985 Optimal Actuators Placements for the Active Control of Flexible Structures. *Journal of Mathematical Analysis and Applications* **105** pp 12–25
42. Chung L L and Soong T T 1987 Practical Considerations in Discrete Time Structural Control. In Inman D and Simonis J (eds) *Vibration Control and Active Vibration Suppression* ASME, NY **DE4** pp 201–7
43. Rodellar J, Barbat A H and Martin-Sanchez J M 1987 Predictive Control of Structures. *ASCE Journal of Engineering Mechanics* **113** pp 797–812
44. Rodellar J, Chung L L, Soong T T and Reinhorn A M 1989 Experimental Digital Predictive Control of Structures. *ASCE Journal of Engineering Mechanics* **115** pp 1245–61
45. Kalman R E, Ho Y C and Narendra K S 1962 Controllability of Linear Dynamical Systems. *Contributions to Differential Equations* **1** pp 189–213

5 Control Mechanisms and Experimental Studies

As in all other new technological innovations, experimental verification constitutes a crucial element in the maturing process as active structural control progresses from conceptualization to actual implementation. Experimental studies are particularly important in this area since hardware requirements for the fabrication of a feasible active control system for structural applications are in many ways unique. As an example, control of civil engineering structures requires the ability on the part of the control device to generate large control forces with high velocities and fast reaction times. Experimentation on various designs of possible control devices is thus necessary to assess the implementability of theoretical results in the laboratory and in the field.

In order to perform feasibility studies and to carry out control experiments, investigations on active structural control have focused on several control mechanisms. In this chapter, some of these control schemes are introduced with emphasis on their performance in the laboratory.

5.1 Active Tendon Control

Active control using structural tendons, proposed as early as 1960 by Freyssinet, has been one of the most studied mechanisms both on paper and in the laboratory. The system generally consists of a set of prestressed tendons connected to a structure whose tensions are controlled by electrohydraulic servomechanisms. One of the reasons for favouring such a control mechanism has to do with the fact that tendons are already existing members of many structures. Thus, active tendon control can make use of existing tendons and thus minimize extensive additions or modifications of an as-built structure. This is attractive, for example, in the case of retrofitting or strengthening an existing structure. Another attractive feature is that active tendons can operate in the pulsed mode as well as in the continuous-time mode. Thus, active tendon control can accommodate both continuous-time and pulse control algorithms.

Active tendon control has been studied analytically in connection with control of slender structures,[1,2] tall buildings,[3-10] bridges[11-13] and offshore structures.[14-16] Early experiments involving the use of tendons were performed on a series of small-scale structural models,[17] which included a simple cantilever beam, a king-post truss and a free-standing column while control devices varied from tendon control with manual operation to tendon control with servovalve-controlled actuators. Actuator dynamics and placement of sensors and controllers were studied. The influence of time delay was demonstrated by varying the phase of the feedback control force.

More recently, a comprehensive experimental study was designed and carried out in order to study the feasibility of active tendon control using a series of carefully calibrated structural models. As Fig. 5.1 shows, the model structures increased in weight and complexity as the experiments progressed from stage 1 to stage 3 so that more control features could be incorporated into the experiments. Figure 5.2(a) shows the model structure studied during the first stage. It is a three-storey steel frame modelling a shear building by the method of mass simulation; the top two floors are rigidly braced to simulate a single-degree-of-freedom system.[18] The model is similar in geometry, material properties and boundary conditions to a structural model extensively tested in several laboratories[19,20] and it is approximately a 1:4 scaled model of a prototype structure (1:2 scaled model), which has also been extensively tested.

The model was mounted on a shaking table which supplied the external load. The control force was transmitted to the structure through two sets of diagonal prestressed tendons mounted on the side frames as indicated in Fig. 5.2(b). In the experiment, the classical optimal closed-loop control algorithm, discussed in Section 3.1, was employed with time delay compensation based on the procedure developed in Section 4.2.

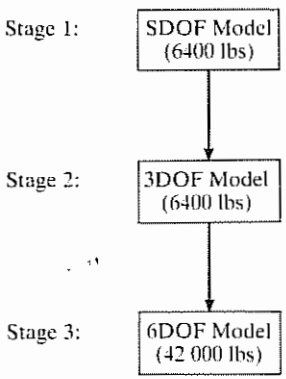

Figure 5.1 Active tendon control experiments

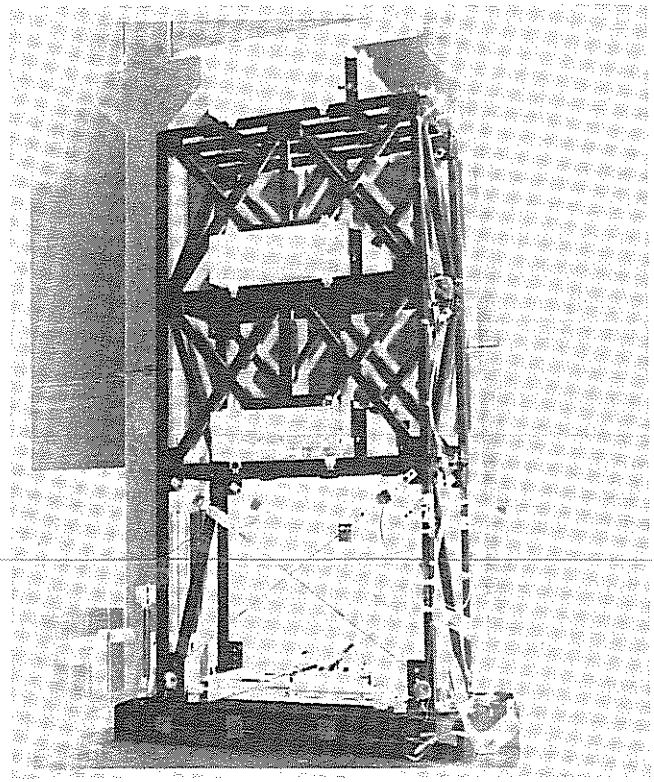

(a)

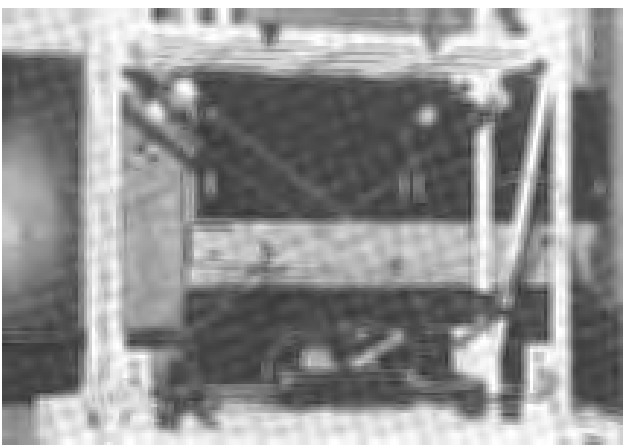

(b)

Figure 5.2 Stage 1 modal structure (a) view of the model; (b) tendon arrangement[26]

Results obtained from this series of experiments are reported.[21,22] Several significant features of these experiments are noteworthy. First, they were carefully designed in order that a realistic structural control situation could be investigated. Efforts made towards this goal included making the model structure dynamically similar to a real structure, working with a carefully calibrated model, using realistic base excitation, and requiring more realistic control forces.

Secondly, these experiments permitted a realistic comparison between analytical and experimental results, which made it possible to perform extrapolation to real structural behaviour. Furthermore, important practical considerations such as time delay, robustness of control algorithms, modelling errors and structure-control system interactions could be identified and realistically assessed.

At stage 2, rigid bracings on the top two floors of the model structure shown in Fig. 5.2(a) were removed in order to simulate a three-degree-of-freedom system. This multi-degree-of-freedom model provided opportunities for study and verification of a number of control features which were not possible in the earlier stage 1 study. These included modal control, time delay in the modal space and control and observation spillover compensation. Moreover, further verification of simulation procedures could be carried out which gave added confidence in using simulation for extrapolating active control results to more complex situations. The control algorithms tested in this series of experiments included instantaneous optimal control and discrete-time control algorithms as well as the classical closed-loop optimal control.[23–25] Experimental results compared favourably with analytical results obtained under the same conditions, and they showed that the motion of all three floors can be effectively controlled using a single actuator when control design is carefully carried out by taking into account the above-mentioned practical considerations.

As a further step in this direction, a substantially larger and heavier six-storey model structure was fabricated for stage 3 of this experimental undertaking. As shown in Fig. 5.3, it is also a welded space frame utilizing artificial mass simulation. Some of the model's properties are given in Table 5.1.

Multiple tendon control was possible in this case and the following arrangements were included in this phase of the experiments:

1 A single actuator is placed at the base with diagonal tendons connected to a single floor.
2 A single actuator is placed at the base with tendons connected simultaneously to two floors, thus applying proportional control to the structure.
3 Two actuators are placed at different locations of the structure with two sets of tendons acting independently.

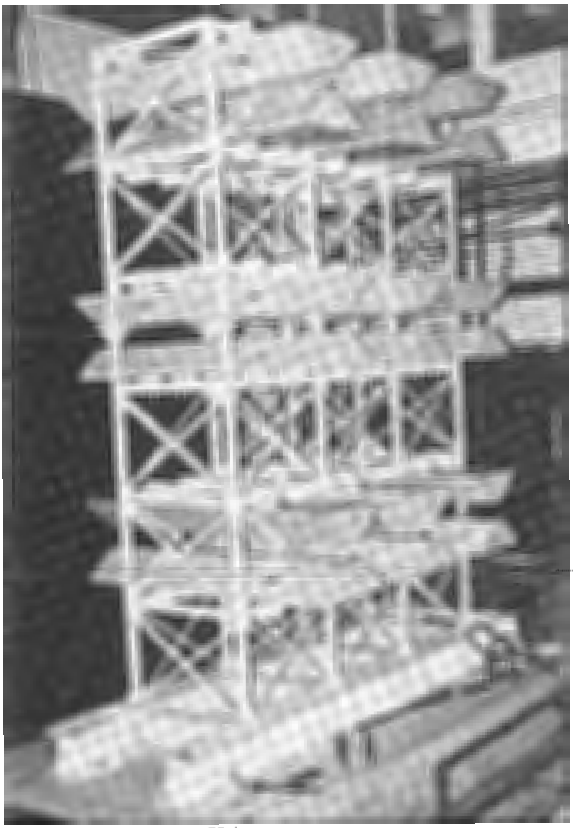

Figure 5.3 Stage 3 model structure[26]

Table 5.1 Properties of Stage 3 model structure

Height (ft)	18
Weight (kips)	42
Modal frequency (Hz)	$\begin{bmatrix} 2.34 \\ 7.71 \\ 13.28 \\ 19.04 \\ 24.80 \\ 28.91 \end{bmatrix}$
Modal damping factor (%)	$\begin{bmatrix} 1.3 \\ 0.5 \\ 0.7 \\ 1.1 \\ 0.2 \\ 0.4 \end{bmatrix}$

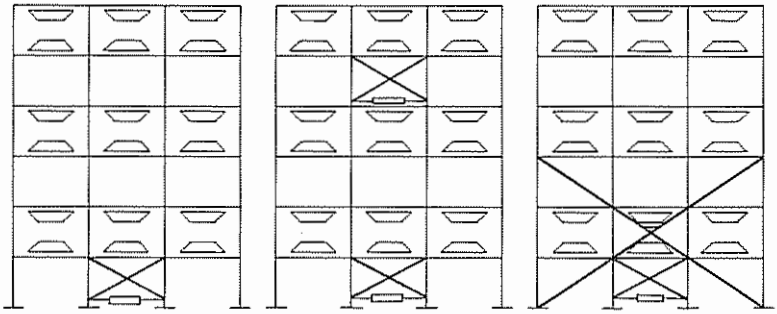

Figure 5.4 Examples of tendon arrangements[26]

Several typical actuator–tendon arrangements are shown in Fig. 5.4. Attachment details of the tendon system are similar to those shown in Fig. 5.2(b).

Another added feature at this stage was the testing of a second control system, an active mass damper, on the same model structure, thus allowing a performance comparison of these two systems. The active mass damper will be discussed in more detail in the next section.

For the active tendon systems, experimental as well as simulation results have been obtained based upon the tendon configurations stipulated above. Using the N–S component of the El-Centro acceleration record as input, but

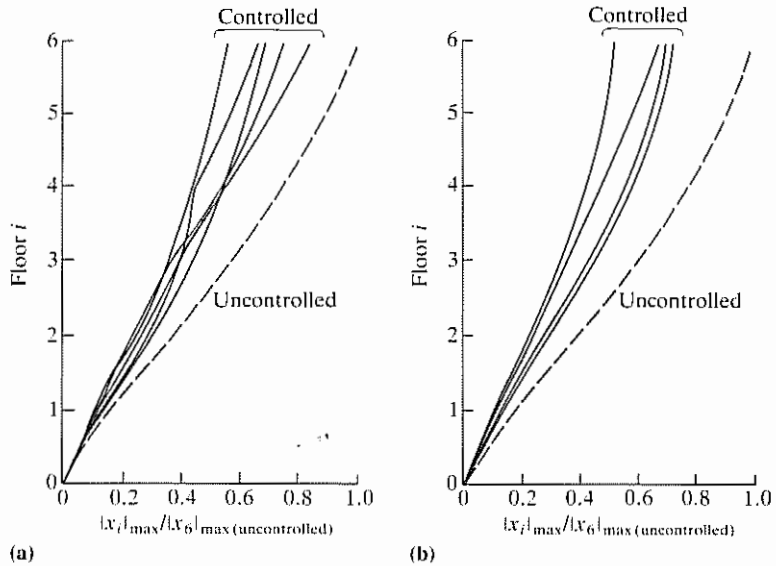

Figure 5.5 Reduction of maximum response normalized to uncontrolled top displacement (a) experimental results; (b) simulation results

scaled to 25% of its actual intensity, control effectiveness was demonstrated. For example, in terms of reduction of maximum relative displacements, results under all actuator–tendon arrangements tended to cluster within a narrow range as shown in Fig. 5.5. At the top floor, a reduction of 45% could be achieved. Figure 5.5 further shows that there was reasonably good agreement between experimental and simulation results. Control force and power requirements were also found to be well within practical limits when extrapolated to the full-scale situation.[26]

It is instructive to give more details of the experimental set-up, results obtained and their implications with regard to all the experiments described above. To conserve space, however, this will be done only for the experiments performed at stage 2.

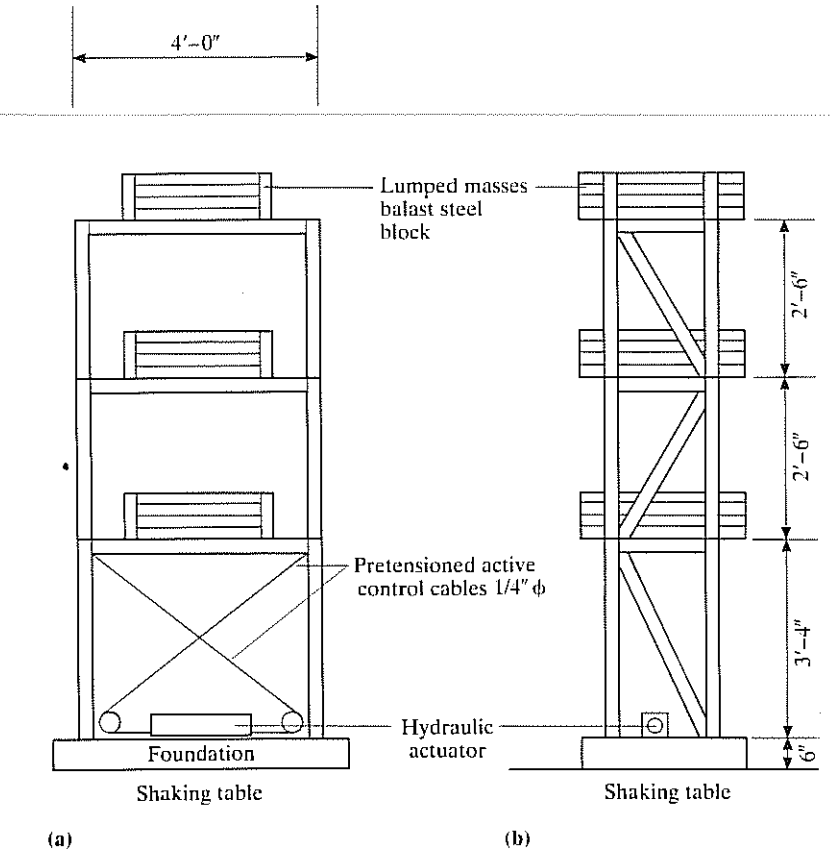

Figure 5.6 Configuration of model structure for MDOF system (total weight 6250 lbs) (a) front view; (b) side view

5.1.1 *Stage 2 Experiments*

As described above, the basic experimental set-up used in this study consisted of a three-storey 1:4 scale frame with one tendon control device implemented to the first floor (Fig. 5.6). The control was supplied by a servocontrolled hydraulic actuator through a system of tendons.

The state variable measurements were made by means of strain gauge bridges installed on the columns just below each floor slab. For each set of the strain gauge bridges, the signal from one strain gauge bridge was used as the signal of measured storeydrift displacement between adjoining storeys, while the signal from the second set was further passed through an analogue differentiator to yield measured storeydrift velocity. The base acceleration and the absolute acceleration of each floor were directly measured by the use of accelerometers installed at the base of the structure and on the floor slabs. The transducers and instrumentation system are shown in Fig. 5.7. A

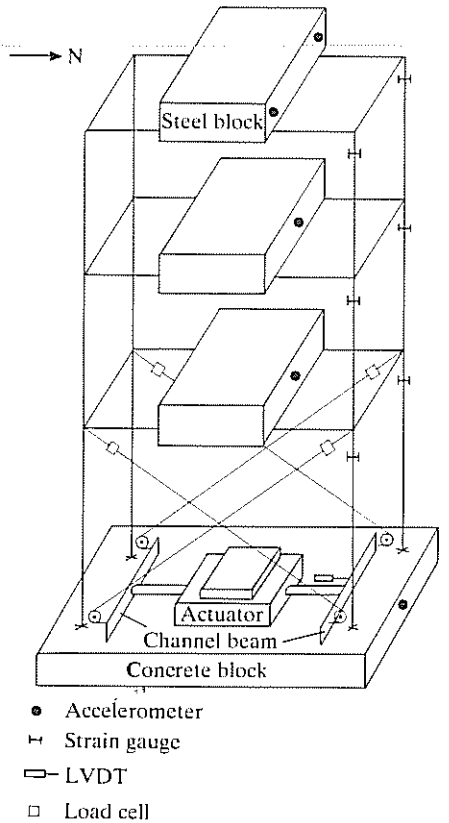

Figure 5.7 Transducers used in instrumentation system

block diagram showing the measurement system and the control procedure is given in Fig. 5.8.

The model was shaken by means of a shaking table with banded white noise and an earthquake accelerogram. Under white noise excitation, modal properties were identified from the frequency response functions for system identification. Moreover, it provided a preliminary examination of the system performance including structural, sensor and controller dynamics for more realistic inputs that were to follow. The N–S component of the El-Centro acceleration record was used in the experiment; however, it was scaled to 25% of its actual intensity to prevent inelastic deformations in the model structure during uncontrolled vibrations. The reproduced time history and the frequency distribution of the scaled down El Centro excitation are shown in Fig. 5.9.

The classical closed-loop optimal control with time delay compensation was first studied with all three modes under control. After carrying out the variational procedure, it was found that there was only a slight increase in natural frequencies (stiffness) but damping factors were increased from 1.62%, 0.39% and 0.36% to 12.77%, 12.27% and 5.45% (Tables 5.2 and 5.3).

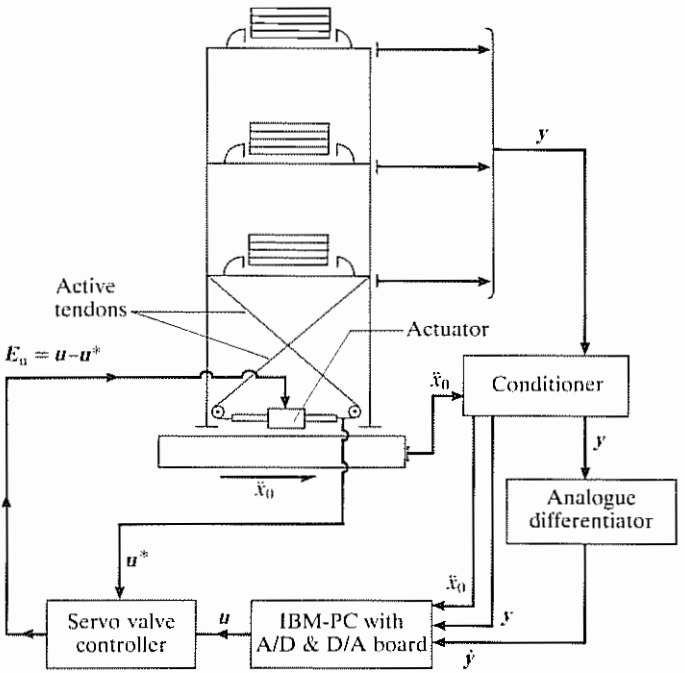

Figure 5.8 Block diagram of control system

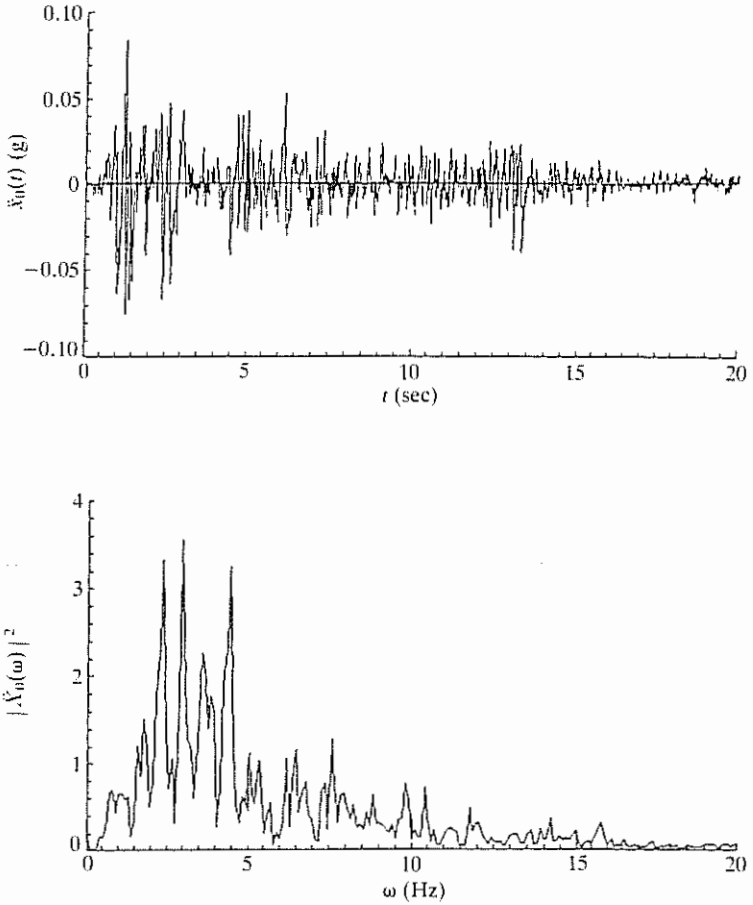

Figure 5.9 Scaled-down El Centro excitation

The spillover was investigated by selecting the first fundamental mode as the controlled critical mode. The critical modal quantities were reconstructed from the measurements at all floors. The effect of spillover to the residual modes was studied. When fewer output measurements were available, the estimated critical modal quantities were actually affected by the observation spillover to the residual modes. Even worse, time delay was compensated as if the outputs were contributed by the critical modes alone. The combined effect of observation spillover and time delay made the system unstable.

When the first fundamental mode was the only controlled critical mode, the modal quantities were recovered from measurements at all three floors. In the presence of modelling errors (mode shapes were not exactly orthogonal)

Table 5.2 Parameters of the model structure

Mass matrix M (lb-sec^2/in)	$\begin{bmatrix} 5.6 & 0 & 0 \\ 0 & 5.6 & 0 \\ 0 & 0 & 5.6 \end{bmatrix}$
Stiffness matrix K (lb/in)	$\begin{bmatrix} 15\,649 & -9\,370 & 2107 \\ -9\,370 & 17\,250 & -9274 \\ 2\,107 & -9\,274 & 7612 \end{bmatrix}$
Damping matrix C (lb-sec/in)	$\begin{bmatrix} 2.185 & -0.327 & 0.352 \\ -0.327 & 2.608 & -0.015 \\ 0.352 & -0.015 & 2.497 \end{bmatrix}$
Modal frequency ω (Hz)	$\begin{bmatrix} 2.24 \\ 6.83 \\ 11.53 \end{bmatrix}$
Modal damping factor ζ (%)	$\begin{bmatrix} 1.62 \\ 0.39 \\ 0.36 \end{bmatrix}$
Tendon stiffness k_c (lb/in)	2124
Tendon inclination α (°)	36
Modal matrix Φ	$\begin{bmatrix} 0.262 & 0.743 & 0.583 \\ 0.568 & 0.373 & -0.728 \\ 0.780 & -0.555 & 0.360 \end{bmatrix}$

and measurement noise, the first modal quantities could not be reconstructed perfectly and a small contribution of the residual modes to the feedback signal was unavoidable. Because of small stability margins (small damping factors) for the second and third modes, the model structure was very sensitive to these errors. To circumvent this problem, the command control signal was passed through a low-pass filter before driving the actuator in order to eliminate the effect of the residual modes. However, no perfect filter exists; the higher the order of the filter, the sharper is the cutoff frequency, but the longer is the time delay. As a compromise, a third-order Butterworth filter with a cutoff frequency of 5 Hz was selected, but time delay was increased from 35 msec to 88 msec.

Acceleration frequency response functions as shown in Figs 5.10–5.12 were constructed by using banded white noise excitation. For the three controlled modes, significant damping effect (large active damping) was reflected from

Table 5.3 Parameters of control system

Parameters	Three controlled modes	One controlled mode
Response weighting matrix $Q^{[1]}$	$\begin{bmatrix} K & 0 \\ 0 & 0 \end{bmatrix}$	
Control weighting matrix $R^{[2]}$	$20\ k_c$	
Modal frequency ω (Hz)	$\begin{bmatrix} 2.28 \\ 6.94 \\ 11.56 \end{bmatrix}$	$\begin{bmatrix} 2.28 \\ 6.83 \\ 11.53 \end{bmatrix}$
Modal damping factor ζ (%)	$\begin{bmatrix} 12.77 \\ 12.27 \\ 5.45 \end{bmatrix}$	$\begin{bmatrix} 1.62 \\ 0.39 \\ 0.36 \end{bmatrix}$
Time delay $\tau_x, \tau_{\dot{x}}$ (msec)	35	88
Feedback gain matrix G^T	$\begin{bmatrix} 0.1857 \\ -0.1571 \\ 0.0641 \\ 0.0171 \\ 0.0021 \\ 0.0055 \end{bmatrix}$	$\begin{bmatrix} 0.0056 \\ 0.0123 \\ 0.0157 \\ 0.0027 \\ 0.0059 \\ 0.0076 \end{bmatrix}$

[1] K is structural stiffness matrix
[2] k_c is tendon stiffness

a decrease in peak magnitudes, but peak frequencies shifted to the right due to small active stiffness. It was shown that all three modes were under control with one controller in the presence of time delay. For the case of one controlled mode, the peak of the first mode was decreased but the peaks of the second and third modes were increased. Due to the effect of control spillover, the performance of the controlled system was not better than that of the uncontrolled one.

Under El Centro excitation, significant reduction in acceleration was achieved with three controlled modes. In addition to the reduction in peak magnitudes, the effect of active damping was clearly evident due to control execution but the excitation frequency was distributed over all three modes. Due to control spillover, the control effect was greatly degraded (Figs 5.13–5.15).

The instantaneous optimal control algorithms were also studied with all three modes under control using the seismic excitation. With carefully chosen weighting matrices, similar control effects could also be achieved.

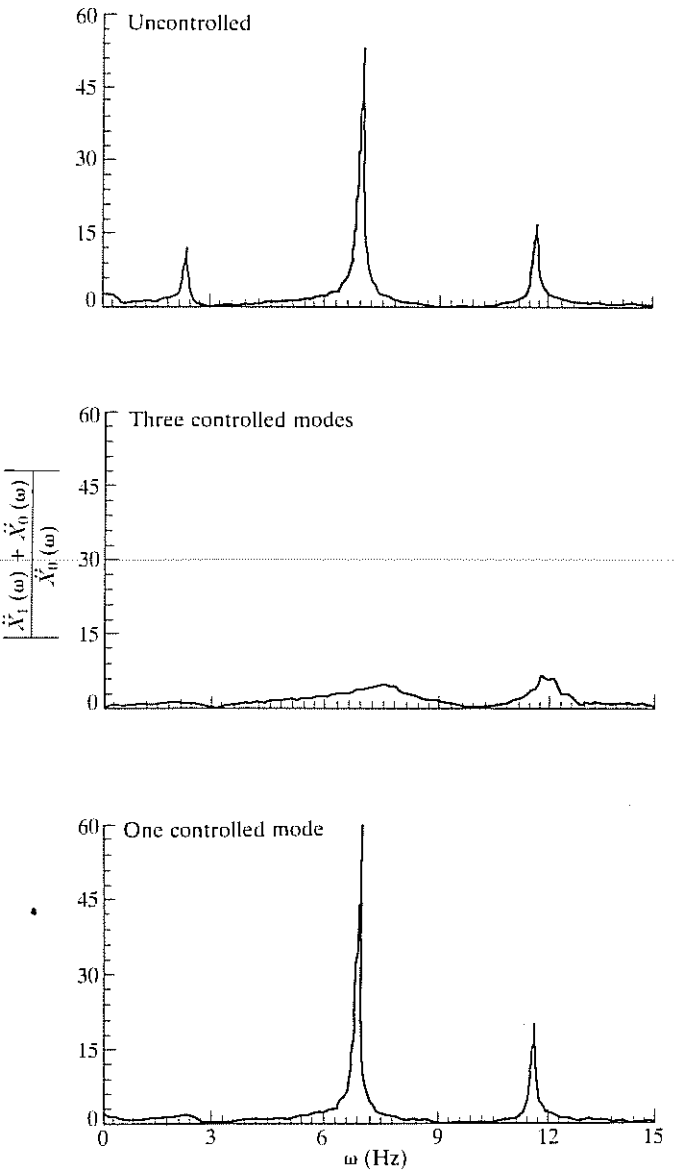

Figure 5.10 First-floor acceleration frequency response functions

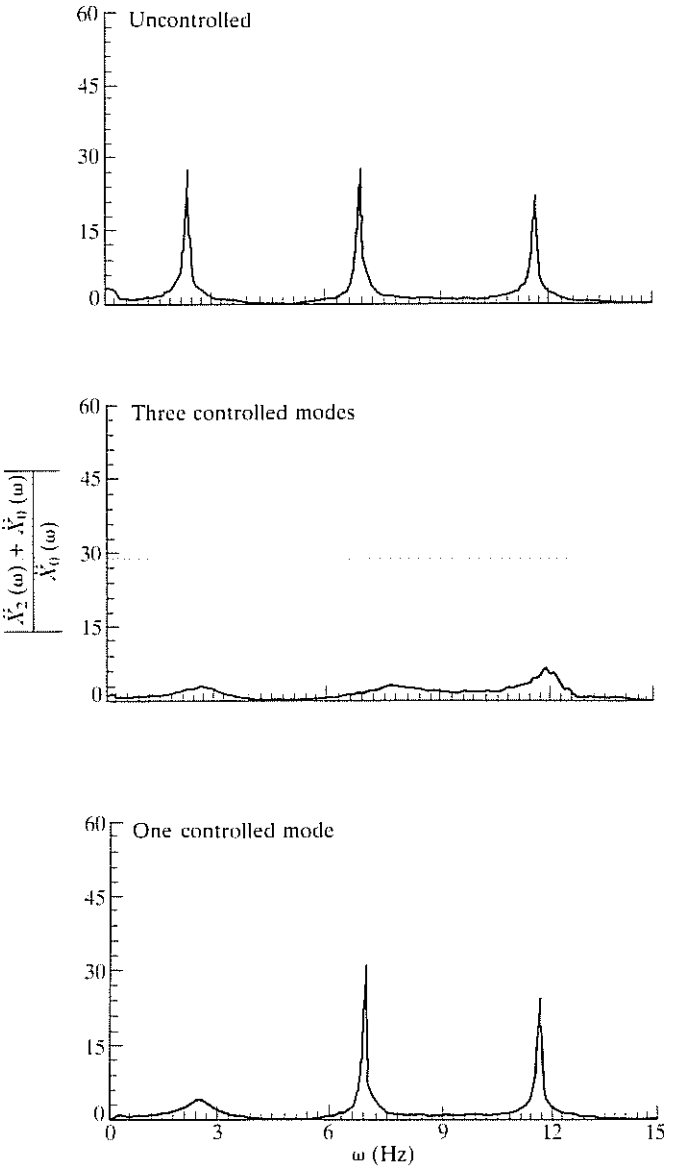

Figure 5.11 Second-floor acceleration frequency response functions

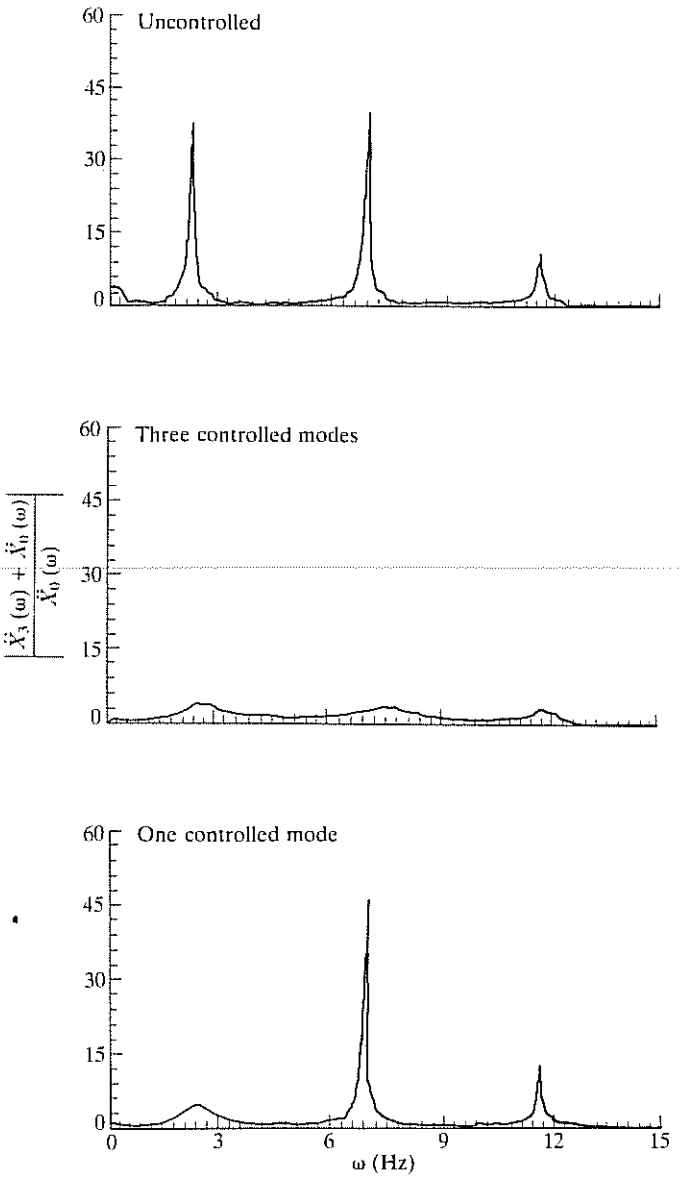

Figure 5.12 Third-floor acceleration frequency response functions

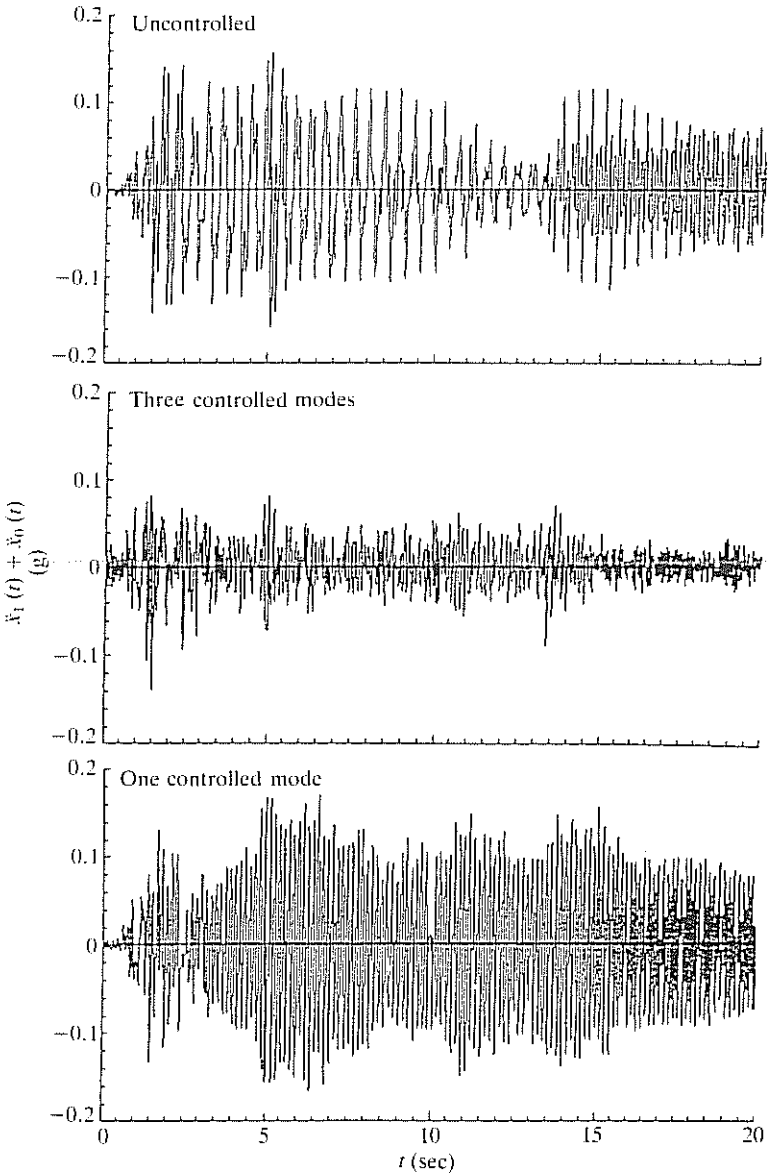

Figure 5.13 First-floor accelerations under El Centro excitation

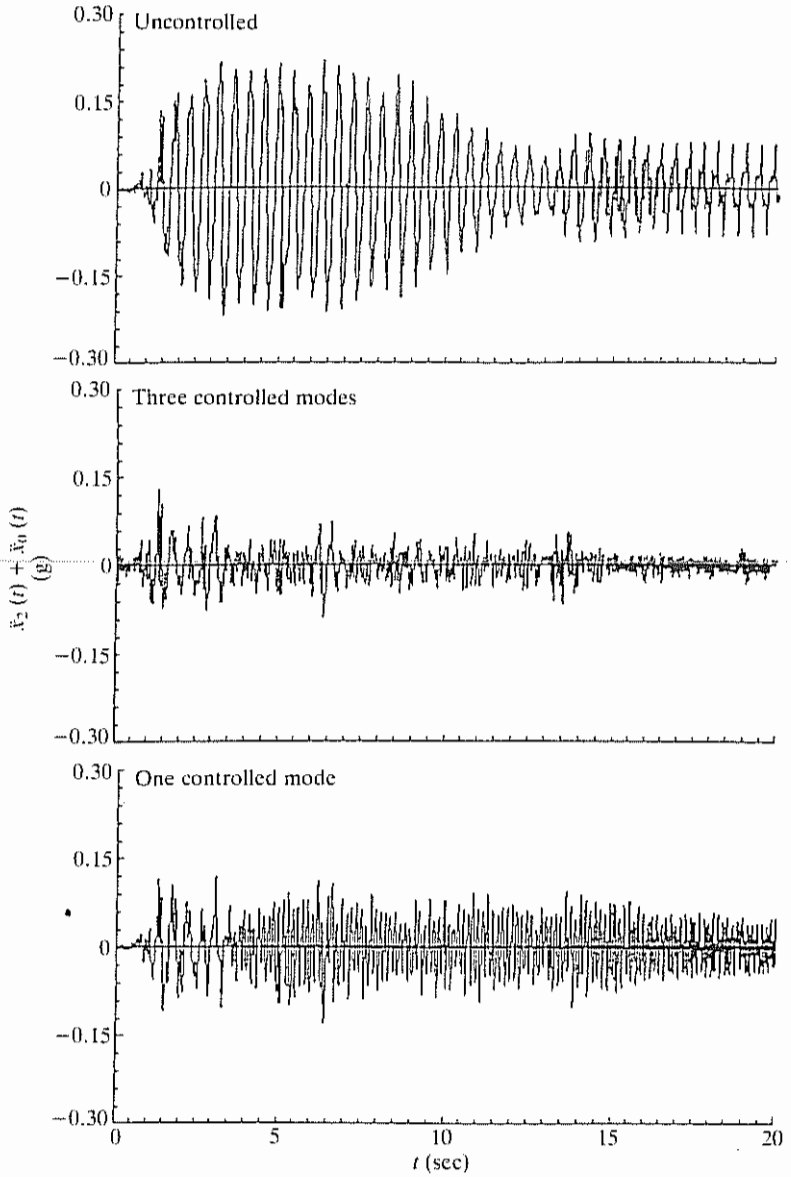

Figure 5.14 Second-floor accelerations under El Centro excitation

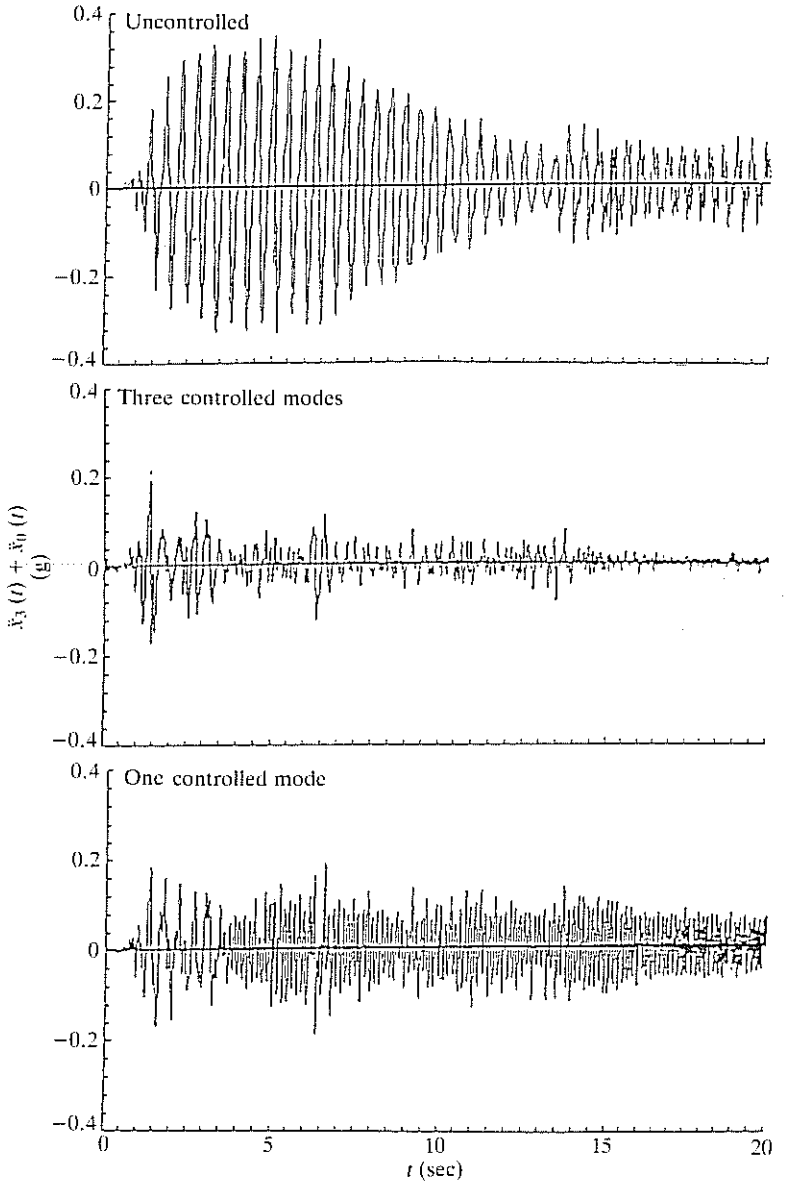

Figure 5.15 Third-floor accelerations under El Centro excitation

Good agreement was achieved between analytical and experimental results. The discrepancies were larger in the uncontrolled test due to the servocontrolled system. The actuator was kept stationary by this system during uncontrolled tests. However, slight actuator movement was induced by the structural motion and the actuator movement was continuously corrected to reduce the error to zero. This interaction between the controller and the structure made the damping force a complicated function of the structural response. For the case of El Centro excitation, some discrepancies resulted from the fact that the equivalent viscous damping was different from the calibrated one measured in the banded white noise tests. However, for the controlled cases, most of the damping was contributed by the feedback force. Therefore, the influence of actuator–structure interaction was negligible and excellent agreement was observed. With one controlled mode, the control force was of a lower magnitude and of a lower frequency, leading to a better performance of the actuator and hence excellent agreement between experimental and analytical results.

The results presented above are encouraging in that they show simple control systems can be effective for response control of complex structures. In addition, extrapolations show that tendon control can be feasible for full-scale structural applications in terms of force and power requirements.

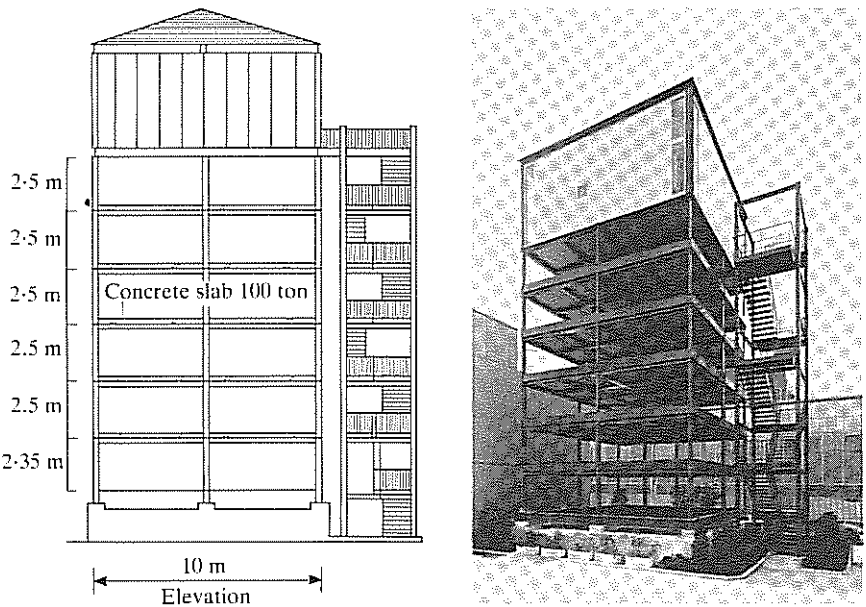

Figure 5.16 Full-scale test structure (courtesy of Takenaka Corporation, Tokyo, Japan)

5.1.2 *Full-scale Testing*

In closing, it is noted that plans are underway for full-scale testing and demonstration of an active tendon system. A six-storey, 600-ton symmetric building as shown in Fig. 5.16 has been erected in Tokyo, Japan. In fact, two control systems will be tested on the structure: a biaxial active mass damper system and a biaxial active tendon system.

As shown in Figs 5.17 and 5.18, the active tendon system consists of four actuators attached to bracings on the first floor. It is designed to provide motion control in either of the two directions.

The planned research tasks upon completion of the installation are:

1 Calibration of the control systems by using one of the systems as motion inducer and the other as motion controller. Even without actual seismic

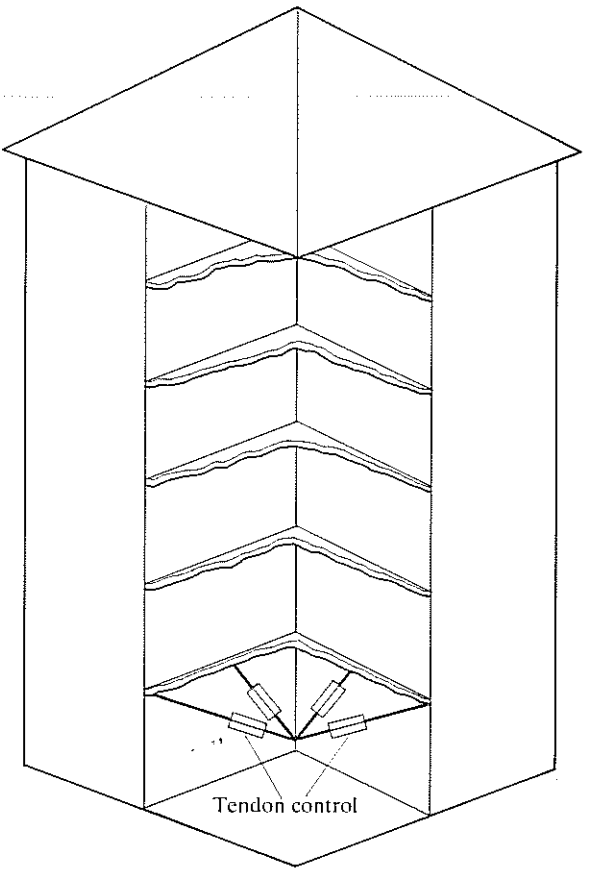

Figure 5.17 Active tendon configuration (isometric view of test structure)

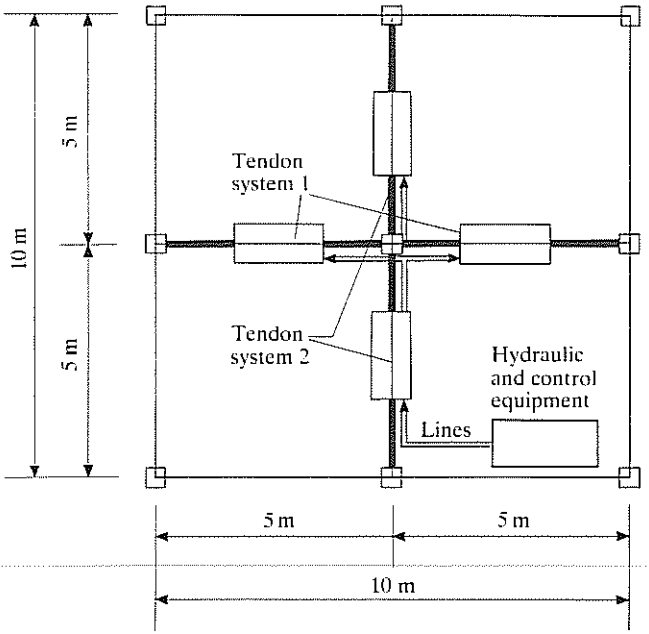

Figure 5.18 Plane view of active tendon system

motion, much of the performance characteristics can be assessed using this calibration method. During the calibration period, several feasible control algorithms will be evaluated and control parameters refined on the basis of knowledge gained in the laboratory.

2 One of the systems will be deactivated for a period of six months in order to allow the assessment of the other system under actual ground excitation. This activation–deactivation phase will be rotated between the two control systems. A total five-year observation period is planned.

5.2 Active Mass Damper and Active Mass Driver

The study of this control mechanism was in part motivated by the fact that tuned mass dampers for motion control of tall buildings, operating in a passive mode, are already in existence.[27–29] Passive tuned mass dampers are in general tuned to the first fundamental frequency of the structure, thus only effective for building control when the first mode is the dominant vibrational mode. This may not be the case, however, when a structure is subjected to, for example, earthquake-type loads when vibrational energy is spread over a wider frequency band. It is thus natural to ask what additional benefits

can be derived when they function according to active control principles. Indeed, a series of feasibility studies of active and semi-active mass dampers has been made along these lines[4,30–33] and they show, as expected, enhanced effectiveness for tall buildings under either strong earthquakes or severe wind loads.

Recently, experimental studies of active tuned mass damper systems have been carried out in the laboratory using scaled-down building models.[34–36] In the work by Kuroiwa and Aizawa[34] an active mass damper (AMD) was placed on top of a four-storey model frame as shown in Fig. 5.19. The moving mass was a variable, ranging from approximately 1% to 2% of the structural weight. The model structure, 1 m (width) × 1 m (depth) × 2 m (height) and weighing 970 kg, was placed on a shaking table which provided simulated earthquake-type base motion. The overall experimental set-up is shown in Fig. 5.20 and a schematic diagram of the AMD is shown in Fig. 5.21. Following the closed-loop control algorithm and using three representative earthquake inputs, experimental results show that the maximum relative displacement reduction at the top floor could be as high as 50%; however, only 5–7% reduction was possible for the maximum absolute acceleration of the top floor.

The control strategy used in Kobori *et al*[35,36] is based on expressing the acceleration vector $\ddot{x}(t)$ in the incremental form

$$\ddot{x}(t) = E^{-1}(t)[g_1(t) + g_2(t - \Delta t)] \tag{5.1}$$

where

$$E(t) = M + 0.5Ct + 0.25Kt^2$$

$$g_1(t) = M\ddot{x}_0(t)$$

$$g_2(t - \Delta t) = [M - E(t)]\ddot{x}(t - \Delta t) - (C + 0.5Kt)\dot{x}(t - \Delta t) - Kx(t - \Delta t)$$

where M, C and K are, respectively, the mass, damping and stiffness matrices. Considering $\ddot{x}(t)$ as a function of a 'transfer function', $E^{-1}(t)$, and an 'instantaneous force', $g_1(t) + g_2(t - \Delta t)$, the control objective using a moving mass is to minimize $\ddot{x}(t)$ by adjusting the transfer function and by reducing the instantaneous force. The moving mass, termed an 'active mass driver', is then designed to generate the necessary counter force in order to reduce the resonant force. In the experimental study, the active mass driver was placed on a 0.5 m (width) × 3 m (height) three-storey steel frame as shown in Fig. 5.22. The structure was mounted on a shaking table while an electro-magnetic force generator was adopted as the active controller. Experimental results indicated that a two-thirds reduction of the maximum acceleration and displacement could be achieved.

At a much larger scale, an active mass damper system was tested in conjunction with an active tendon system as described in Section 5.1. Using

(a)

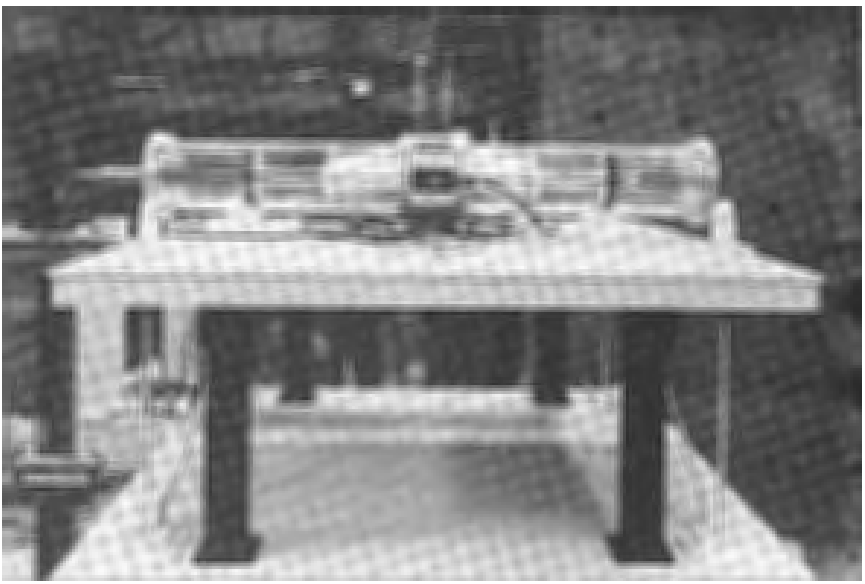

(b)

Figure 5.19 The four-storey model frame with AMD (courtesy of Takenaka Corporation, Tokyo, Japan) (a) model structure; (b) close-up view of AMD

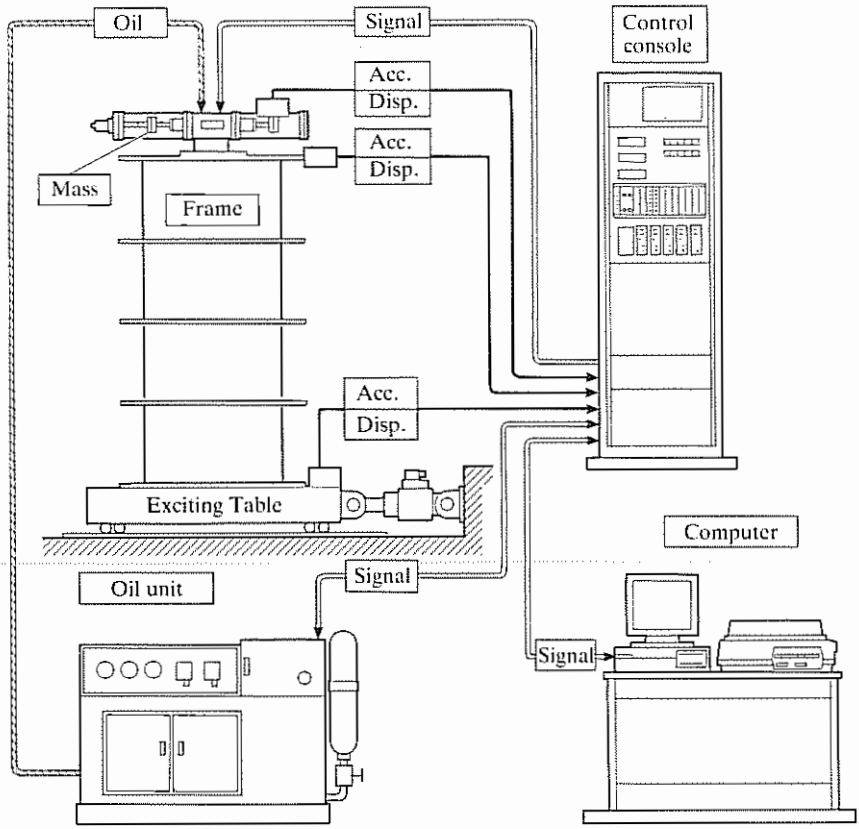

Figure 5.20 Experimental set-up

the same six-storey 42 000-lb structure as shown in Fig. 5.3, the AMD system was placed on top of the structure as shown in Fig. 5.23, which could be operated under different conditions by changing its added mass, its stiffness and the state of the regulator. A total of 12 cases were performed in the experiment.

Extensive experimental results were obtained under various simulated earthquake excitations. A summary of results obtained under the 25%-intensity El Centro excitation is given below:

Percent Reduction of Maximum Top-floor Relative Displacement:	43.3–57.2
Percent Reduction of Maximum Top-floor Acceleration:	5.5–30.7
Percent Reduction of Maximum Base Shear:	31.4–44.4
Maximum Control Force Required (kips):	0.68–2.56
Maximum Mass Peak-to-Peak Stroke (in):	3.23–10.1
Maximum Control Power Required (Kw):	0.82–5.73

Specification

1. Dimension	Piston dia.	41.6 mm
	Rod dia.	40.0 mm
	Stroke	± 129 mm
	Piston area	1.025 cm^2
2. Power	Max 30 kg	
3. Moving mass	9, 12, 15, 18 kg	
4. Weight	55 kg	

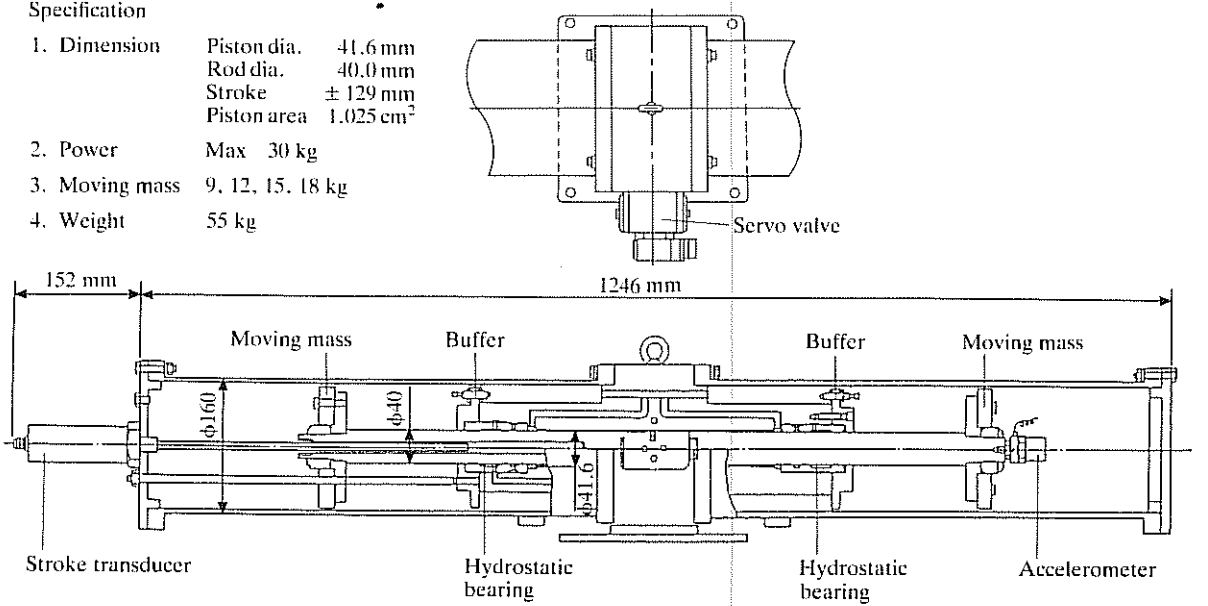

Figure 5.21 Schematic diagram of AMD

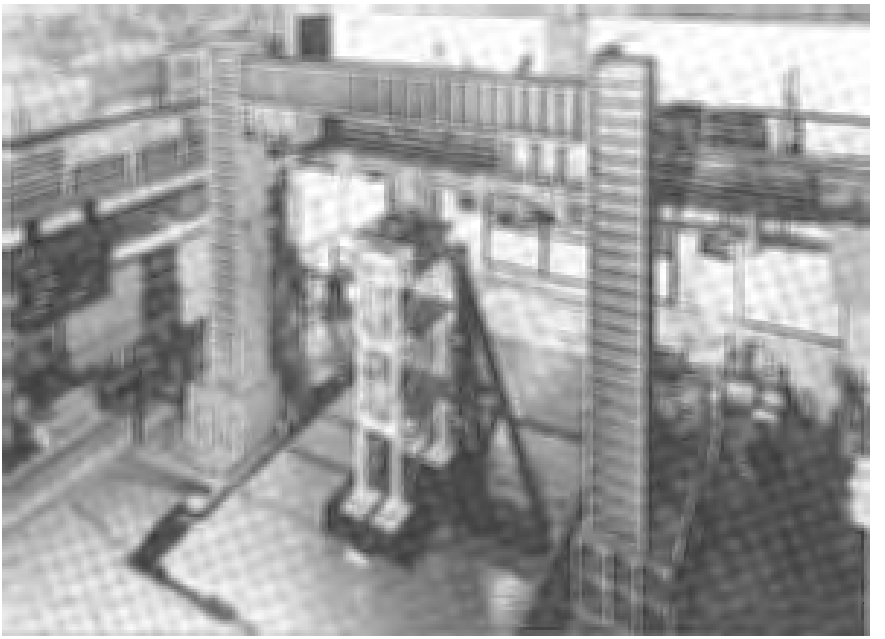

(a)

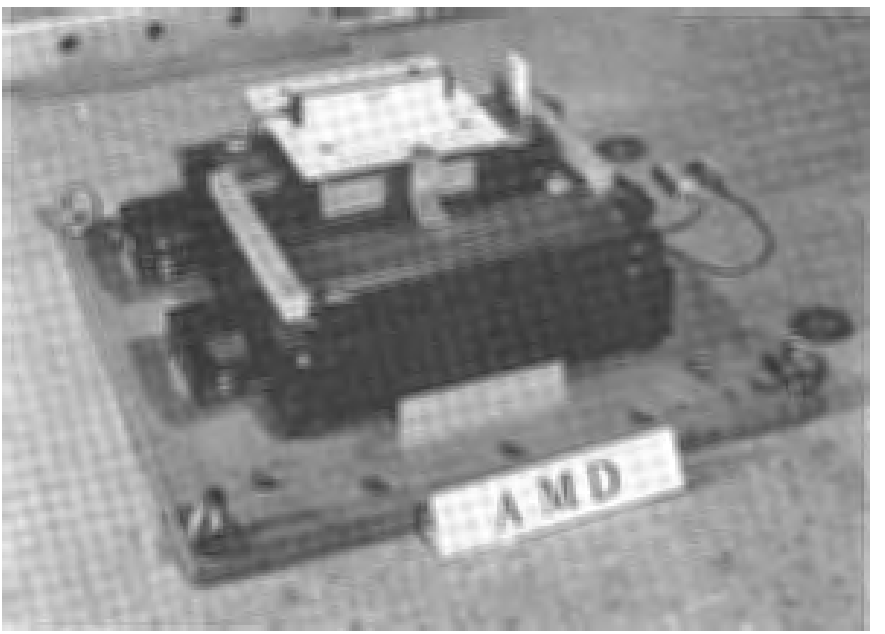

(b)

Figure 5.22 The three-storey model frame with active mass driver (courtesy of Kajima Corporation, Tokyo, Japan) (a) model structure; (b) close-up view of active mass driver

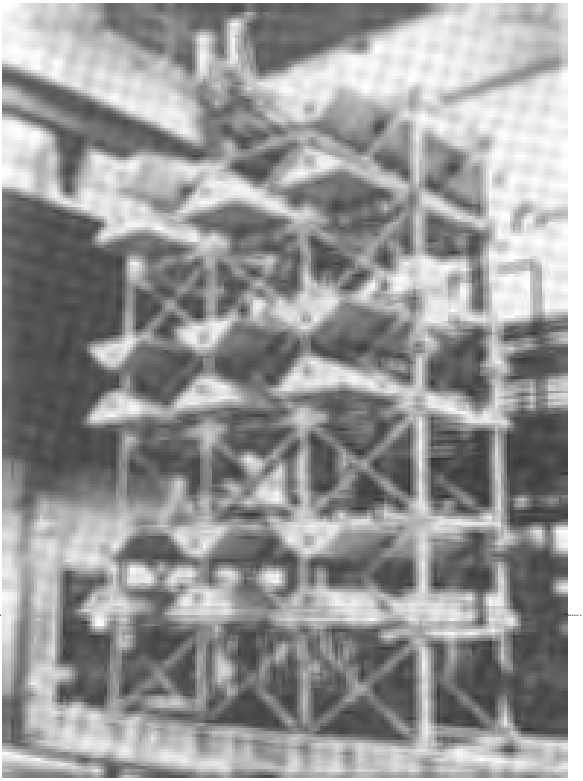

(a)

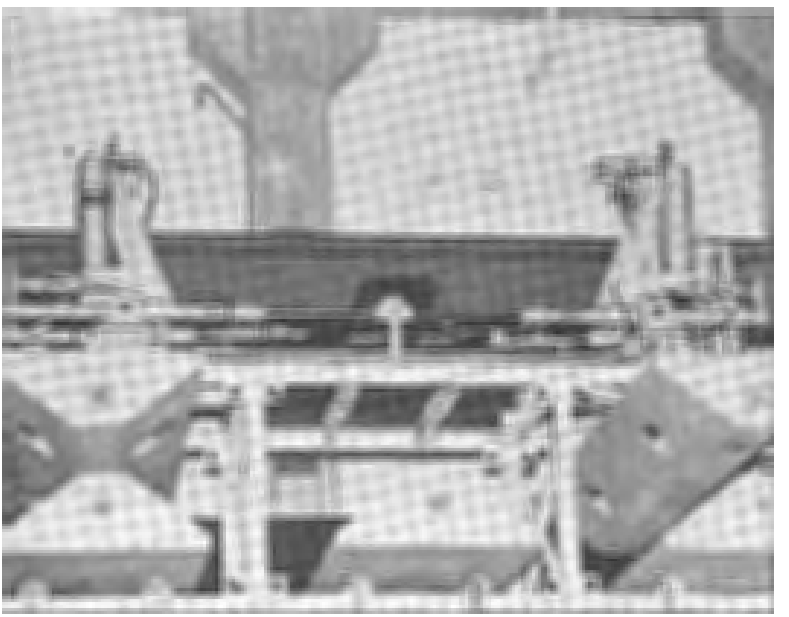

(b)

Figure 5.23 The six-storey model structure with AMD (a) model structure; (b) close-up view of AMD

5.2.1 *AMD vs. Active Tendon System*

One of the advantages of testing two different active systems using the same model structure is that their performance characteristics can be realistically compared. Extensive simulation and experimental results obtained based on the six-storey, 42 000-lb model structure show that both AMD and tendon systems display similar control effectiveness in terms of reduction in maximum top-floor relative displacement, in maximum top-floor absolute acceleration, and in maximum base shear. They also have similar control requirements such as maximum control force and maximum power. Other information which may shed more light on their relative merits but is not considered here includes cost, space utilization, maintenance and other practical observations.

It should be noted that a number of analytical comparative studies have been carried out concerning relative merits associated with active tuned mass dampers and active tendons for specific applications.[4,5,7,8,37,38] As indicated in Yang,[8] one of the inherent limitations associated with an active mass damper is that, since only one is likely to be used for economical reasons, it provides only a single point of control action and it usually acts at the top of a structure. Simulation results show that, under practical constraints, its effectiveness is mostly felt at the first fundamental frequency but less so at higher frequencies. A comparative study was made between an active tendon system and an active mass damper using the eight-storey structure described in Example 3.5 under an earthquake-like ground excitation. Figure 5.24 shows their respective spectral densities of top-floor relative displacement. It is seen that, while the active tendon system is capable of suppressing peak amplitudes at several model frequencies, the effect of the active mass damper is only felt at the first frequency.

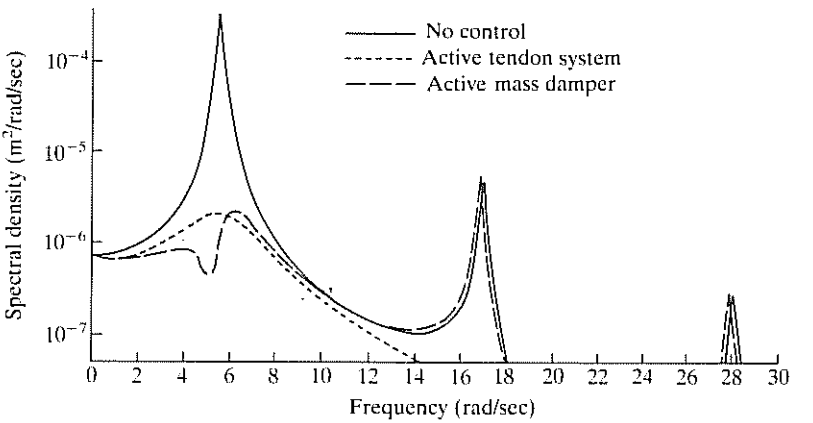

Figure 5.24 Spectral densities of top-floor relative displacement[8]

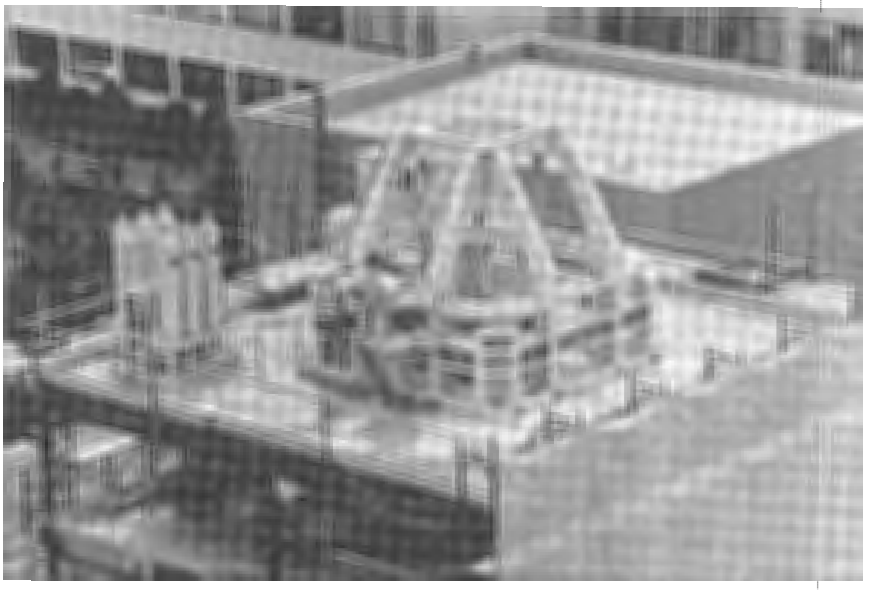

(a)

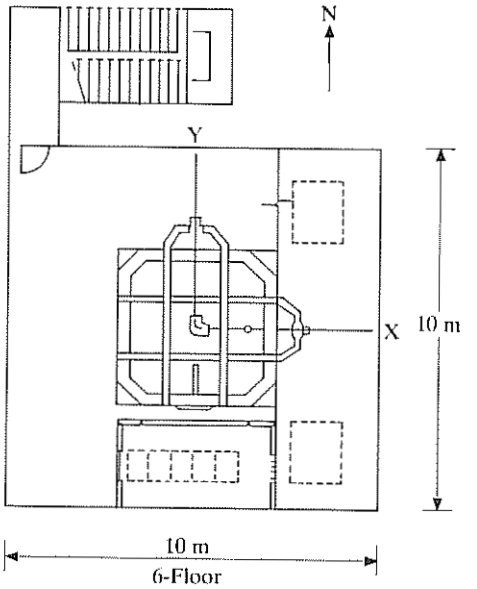

(b)

Figure 5.25 Full-scale AMD (courtesy of Takaneka Corporation, Tokyo, Japan) (a) view of AMD on top of structure; (b) AMD placement in structure

5.2.2 *Full-scale Testing and Implementation*

As described in Section 5.1.2, plans for testing a full-scale AMD system together with an active tendon system are underway. The AMD system, shown in Fig. 5.25, has been placed at the top of the dedicated test structure depicted in Fig. 5.16. The biaxial AMD system is of the pendulum type with a fail-safe regulator. It weighs 6 tons, approximately 1/100 of the structural weight, and has a maximum stroke of ± 1.0 m with a maximum control force of 10 tons.

Additionally, a full-scale active mass driver system has been installed on the top floor of the eleven-storey Kyobashi Seiwa building in Tokyo, Japan (Fig. 5.26). The active mass driver, shown in Fig. 5.27, is a pendulum-type dual-mass system capable of controlling torsional as well as lateral vibration of the slender structure due to strong wind or moderate earthquakes. The

(a)

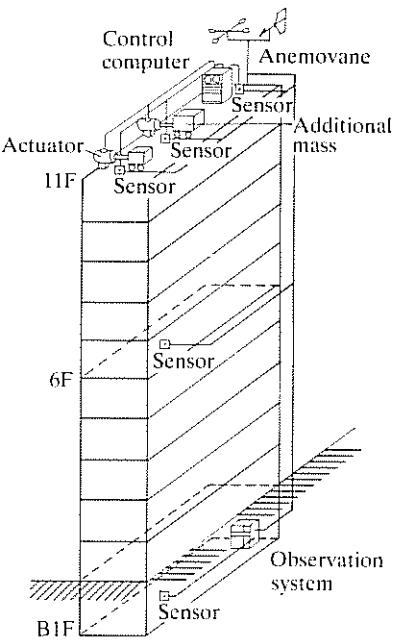

(b)

Figure 5.26 Kyobashi Seiwa Building with AMD (courtesy of Kajima Corporation, Tokyo, Japan) (a) Kyobashi Seiwa Building; (b) AMD system

Figure 5.27 View of active mass driver in Kyobashi Seiwa building (courtesy of Kajima Corporation, Tokyo, Japan)

first mass, weighing approximately four tons, is used for lateral motion control and the second mass, weighing approximately one ton, is used for torsional control. The system represents one of the first active control systems installed in an actual structure in the world.

5.3 Pulse Generators

Pulse control, discussed in Section 3.5, has also been a subject of experimental study in the laboratory. The experimental work was based on a simple control strategy described below.[39,40]

Consider a vibrating structural system. Assuming that relative motions at several locations within the structure are to be limited in magnitude, a simple control procedure is to have pulse generators positioned at these locations; a control pulse is applied at a given location whenever the relative velocity at this location reaches a maximum, but in the direction which opposes this velocity. Thus, an actuator is triggered each time a zero-crossing of the relative displacement at a point of interest is detected. The magnitude of the control pulse at location i, $p_i(t)$, is given by

$$\begin{aligned} p_i(t) &= -c_i \operatorname{sgn}(v_i)|v_i|^{n_i}, \qquad t_{0_i} < t < t_{0_i} + \Delta t_i \\ &= 0, \qquad\qquad\qquad \text{otherwise} \end{aligned} \tag{5.2}$$

where c_i is a pulse scaling coefficient at location i, sgn( ) indicates the algebraic sign of its argument, v_i is the relative velocity at location i, t_{0_i} is the zero-crossing time at location i, and Δt_i is the pulse width at location i. The exponent n_i in Eq. (5.2) is to be chosen appropriately. When $n_i = 0$, the control force acts as a Coulomb friction force with magnitude $\pm c_i$. The $n_i = 1$ case corresponds to active viscous damping with coefficient c_i and, when $n_i > 1$, nonlinear velocity damping is introduced.

This control algorithm was tested in the laboratory using a six-storey frame weighing approximately 159 kg and measuring six feet in height.[40,41] Figure 5.28 shows the model structure together with the test apparatus which includes vibration exciter, instrumentation, pneumatic power supply, and the minicomputer used for digital control. As shown in Fig. 5.29, the electrodynamic exciter, sensor, and pneumatic actuators were located at the top of the structure. The actuators consisted of two solenoids which metered the flow of compressed air at 125 psi through eight nozzles, thus generating the required control pulses. A sample measurement from a thruster is shown in Fig. 5.30, showing delay time elapsed between the control signal and the actuator response and inevitable deviations from an ideal rectangular pulse shape.

Figure 5.31 shows sample measurements of the control pulse train and top-floor relative displacement when the structure was subjected to a harmonic excitation at a frequency close to the fundamental frequency. It is seen that, within ten periods of onset of control, the response is reduced to approximately 15% of its uncontrolled value. The control pulse magnitude used in the experiment correspond to that given in Eq. (5.2) with $n_i = 0$. Thus, it is not surprising to see that the oscillation decay at control initiation follows that associated with Coulomb friction, i.e. straight-line decay envelope. On the other hand, at the end of control duration, the envelope of free vibration approximates an exponential decay curve, which corresponds to the well-known viscously damped behaviour.

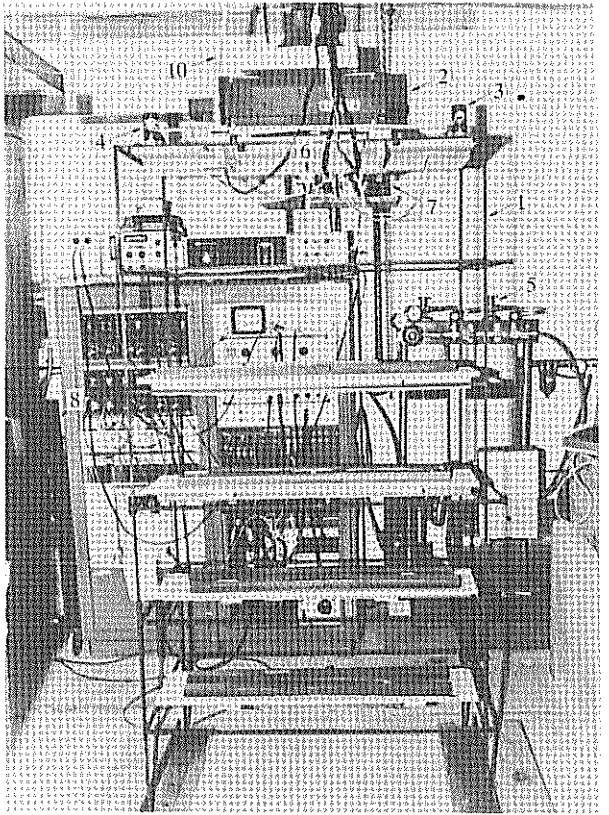

(a)

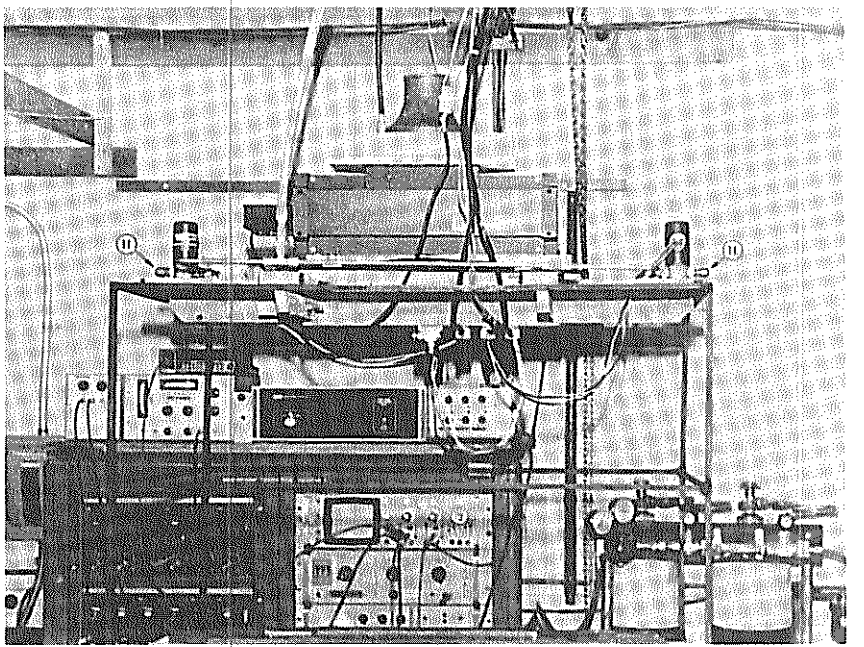

(b)

LEGEND:
1 – FRAME; 2 – EXCITER; 3 – RHS THRUSTER; 4 – LHS THRUSTER; 5 – COMPRESSED GAS; 6 – ACCELEROMETER; 7 – DISPLACEMENT FOLLOWER; 8 – MICROCOMPUTER; 9 – VIDEO TERMINAL; 10 – PNEUMATIC SUPPLY LINE; 11 – NOZZLE

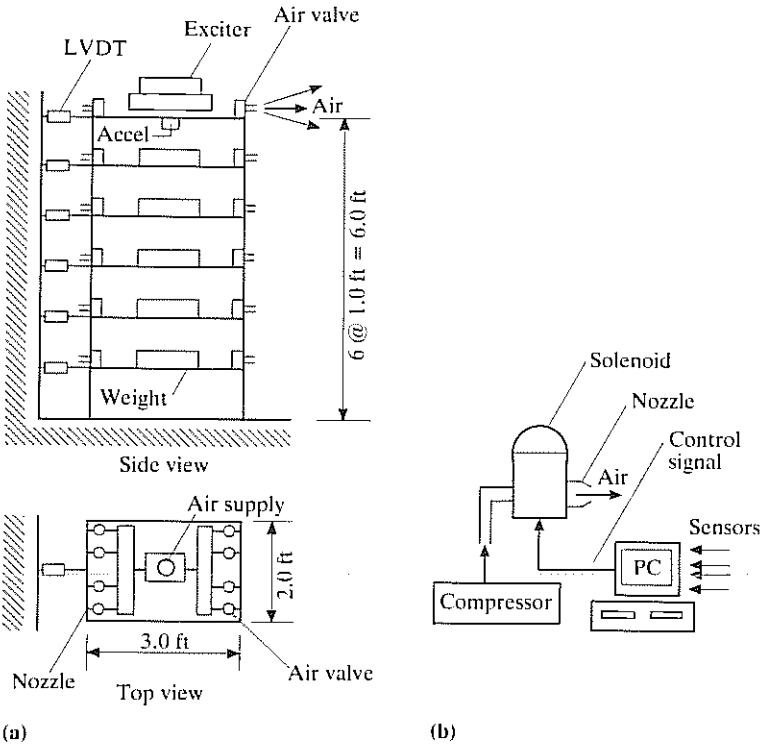

Figure 5.29 Schematic diagram of control configuration[41] (a) control configuration; (b) pneumatic active control

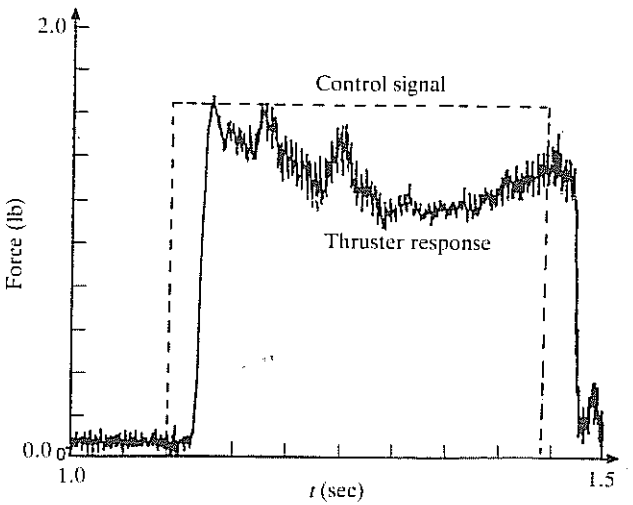

Figure 5.30 Experimental control pulse[41]

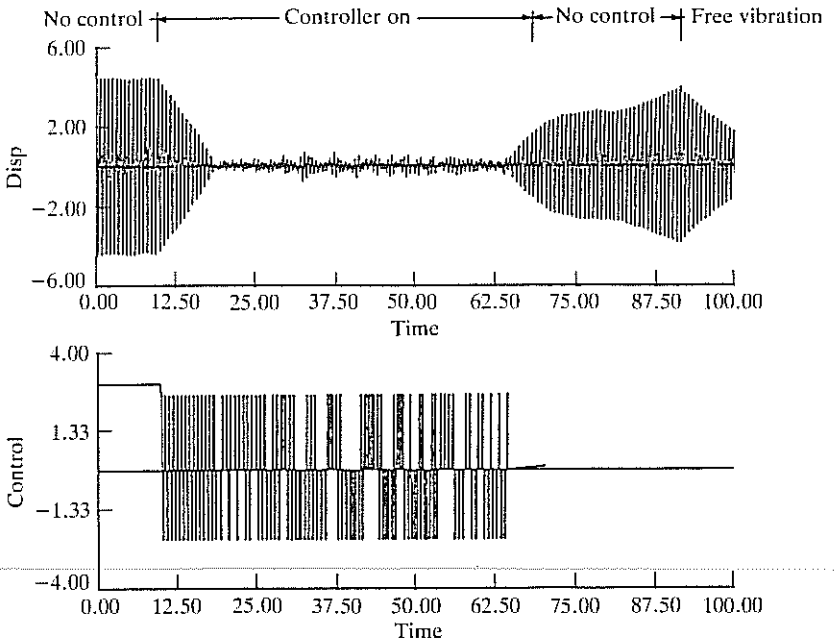

Figure 5.31 Experimental results on control pulse and top-floor relative displacement[41]

Discussions on some of the recently developed cold-gas generators having potential structural control applications can be found in [42,43]. In addition, pulse control experiments involving hydraulic and electromagnetic actuators have also been conducted in the laboratory.[41,42]

Finally, suggestion has been made to use semi-active auxiliary mass dampers as an alternate pulse-control mechanism.[44] Hence, instead of using cold-air jets or other mass ejection techniques to provide directly the required control forces, control objectives are accomplished through internal momentum transfer between the structure and the auxiliary masses. An on-line control procedure is used to optimize the parameters of the auxiliary mass dampers located about the structure.

5.4 Aerodynamic Appendages

The use of aerodynamic appendages as active control devices to reduce wind-induced motion of tall buildings was first proposed by Klein *et al*[45] and by Klein and Salhi.[46] Its main attractive feature is that the control designer is able to exploit the energy in the wind to control the structure,

which is being excited by the same wind. Thus, it eliminates the need for an external energy supply to produce the necessary control force; the only power required is that needed to operate the appendage positioning mechanism.

Additional analytical studies of aerodynamic appendages using optimal control algorithms were carried out[47,48] as well as a wind-tunnel experimental study.[49] The experiment was conducted using an elastic model at a geometric scale of roughly 1:400. This is schematically presented in Fig. 5.32(a). Its stiffness was provided by a steel plate fixed at the structure core, as shown, and its length was adjusted so that under planned wind conditions in the wind tunnel used in the experiment, the first mode was dominant and was observed to be approximately 5 Hz.

The full-scale (prototype) building frequency corresponding to 5 Hz in the model depends on the scaling of frequency, or time, between model and prototype. If the ground roughness and building are scaled in the same ratio, then a characteristic frequency of the wind eddies can be written in terms of, say, the geostrophic wind speed and a characteristic length. Thus,

$$\frac{\omega_p}{\omega_m} = \frac{\bar{v}_p \lambda_m}{\bar{v}_m \lambda_p} \tag{5.3}$$

in which ω = frequency; $\bar{v}$ = mean wind velocity (say geostrophic); and λ = characteristic length. The subscripts p and m denote, respectively, prototype and model. The model data were taken with $\bar{v}_m = 2.0$ m/sec. With the scale at 1:400, the building frequency corresponding to, say, $\bar{v}_p =$ 160 kmph would be 0.26 Hz. Thus, this is a realistic representation of the phenomenon.

For simplicity, the control algorithm used in the experiment is a suboptimal one,[45,46] i.e.

$$\begin{aligned} u(t) &= 1, \quad v(t) \leqslant 0 \\ &= 0, \quad v(t) > 0 \end{aligned} \tag{5.4}$$

In other words, it is on–off control with the appendage fully extended when the velocity at the top of the model structure is opposite to the wind, and fully retracted otherwise.

The aerodynamic appendage consisted of a metal plate. It was controlled by means of a 24 VDC solenoid, activated by the sign of structural velocity as sensed by a linear differential transformer, followed by appropriate carrier and signal amplifications and a differentiator. The appendage area normal to the wind direction was roughly 2% of the structural frontal area when fully extended.

A boundary layer wind tunnel was used to generate the necessary wind forces. An inside view, looking upstream and with the model in place, is shown in Fig. 5.32(b).

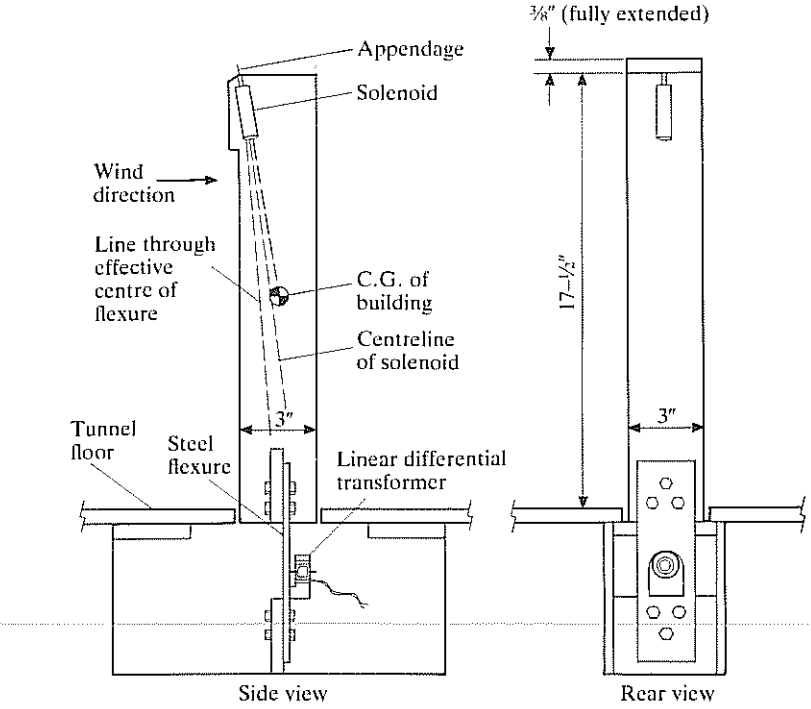

(a)

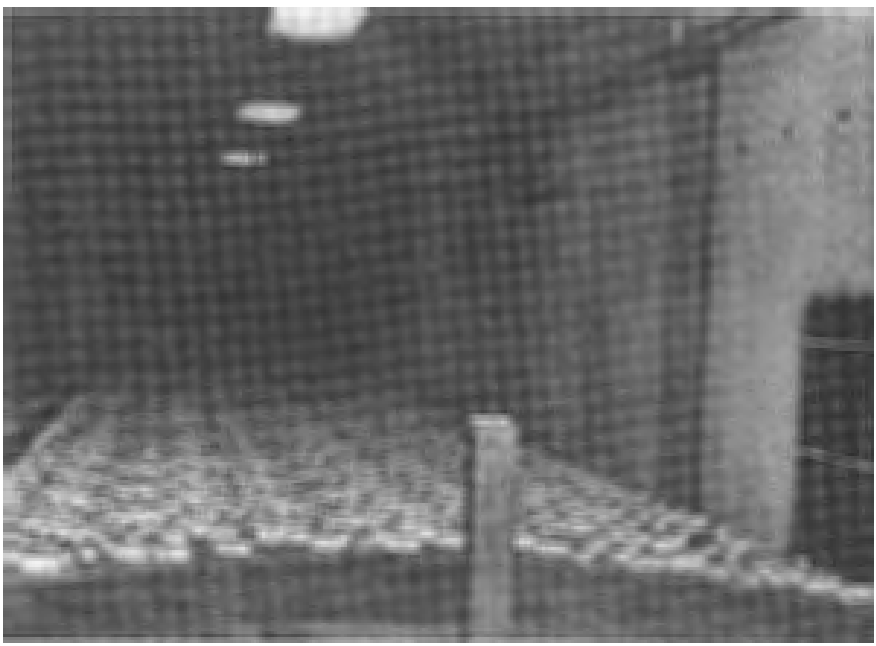

(b)

Figure 5.32 Model structure and test apparatus[49] (a) schematic diagram of model structure; (b) inside-tunnel view of model structure

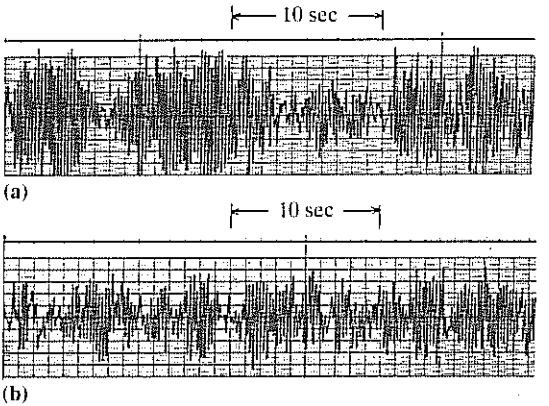

Figure 5.33 Typical displacement record (arbitrary scale) (a) without control; (a) with control[49]

The active control experiment was performed under various wind conditions. Some typical structural response characteristics are shown in Figs 5.33 and 5.34. Figure 5.33 gives the structural displacement without and with control; the corresponding velocities are shown in Fig. 5.34. Both show a peak amplitude reduction of approximately 50%.

More recent publications related to appendages include a comparative study of appendages, active mass dampers and active tendons for wind-excited tall building control,[4] a more detailed design study of optimal appendage mechanisms on the basis of force or power needed for their operation,[50] and a discussion on their aesthetic aspects when appendages are deployed in an urban setting.[51]

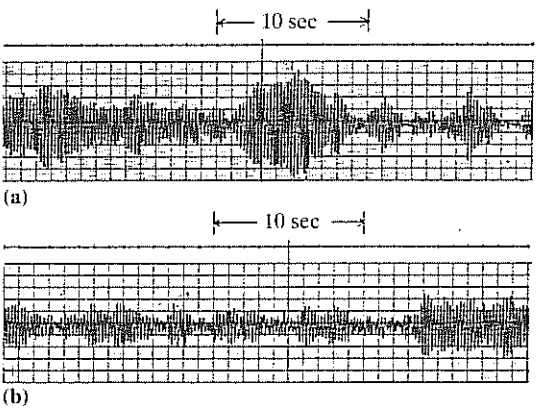

Figure 5.34 Typical velocity record (arbitrary scale) (a) without control; (b) with control

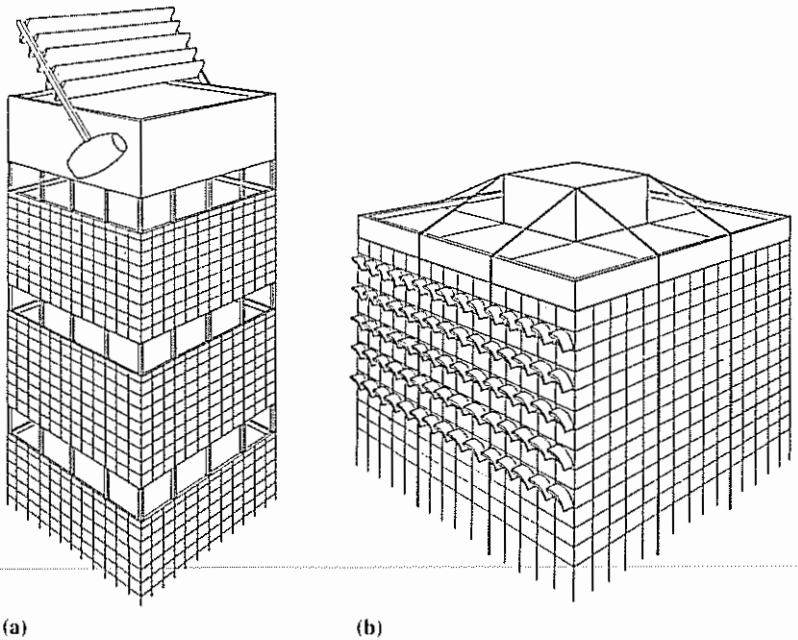

Figure 5.35 Examples of appendage design (a) venetian blind-type appendage; (b) symmetrically placed appendages

Two examples of appendage design are shown in Fig. 5.35. Figure 5.35(a) shows a venetian blind-type appendage whose elements can be operated independently or in a synchronized fashion by means of an electro-hydraulic control system. A system of appendages situated on opposite sides of a structure is shown in Fig. 5.35(b); they can be used for translational-motion control when both sides move in phase and for rotational-motion control when they move out-of-phase.

It should be mentioned that aerodynamic appendages can also serve useful secondary functions. For example, those in the form of venetian blinds as depicted in Fig. 5.35(a) can be used as solar panels for power generation. The system shown in Fig. 5.35(b) is ideally suited for use as sun screens with great effectiveness since their orientation can be controlled as a function of time.

5.5 Other Control Mechanisms

Discussed in the preceding sections are some of the most studied control mechanisms for structural applications. Many others have been proposed.

These include the use of a gyroscope for reducing wind-induced vibration of a suspension bridge,[52] the development of a variable stiffness controller capable of steering the natural frequencies of a structure away from resonant frequencies,[36] and the use of actively controlled air chambers for controlling wave-induced motion of an offshore platform.[53] In Sirlin *et al*[53] an open-bottom structural model floating in a water-filled tank was used to simulate the response of a floating platform under wave loads. The air pressure in the air chamber trapped between the water and the platform was actively servocontrolled to reduce the structural response under simple harmonic waves. Experiments gave encouraging results in correcting heave motion of the platform.

Finally, the combined use of two active control systems and hybrid active–passive systems have also been suggested for some specific structural applications.[4,54–56]

References

1. Roorda J 1975 Tendon Control in Tall Structures. *ASCE Journal of Structural Division* **101** pp 505–21
2. Yang J N and Giannopoulos F 1978 Active Tendon Control of Structures. *ASCE Journal of Engineering Mechanics Division* **104** pp 551–68
3. Abdel-Rohman M and Leipholz H H E 1983 Active Control of Tall Buildings. *ASCE Journal of Structural Engineering* **109** pp 628–45
4. Abdel-Rohman M 1987 Feasibility of Active Control of Tall Buildings Against Wind. *ASCE Journal of Structural Engineering* **113** pp 349–62
5. Juang J N, Sae-Ung S and Yang J N 1980 Active Control of Large Building Structures. In Leipholz H H E (ed) *Structural Control* North Holland, Amsterdam pp 663–76
6. Samali B, Yang J N and Yeh C T 1985 Control of Coupled Lateral-Torsional Motion of Wind-Excited Buildings. *ASCE Journal of Engineering Mechanics* **111** pp 779–96
7. Samali B, Yang J N and Liu S C 1985 Control of Lateral-Torsional Motion of Buildings Under Seismic Load. *ASCE Journal of Structural Engineering* **111** pp 2165–80
8. Yang J N 1982 Control of Tall Buildings Under Earthquake Excitations. *ASCE Journal of Engineering Mechanics Division* **108** pp 50–68
9. Yang J N and Lin M J 1983 Building Critical-Mode Control: Nonstationary Earthquakes. *ASCE Journal of Engineering Mechanics Division* **109** pp 1375–89
10. Yang J N and Samili B 1983 Control of Buildings in Along-Wind Motion. *ASCE Journal of Structural Division* **109** pp 50–68
11. Yang J N and Giannopoulos F 1979 Active Control and Stability of Cable-Stayed Bridge. *ASCE Journal of Engineering Mechanics Division* **105** pp 677–94
12. Yang J N and Giannopoulos F 1979 Active Control of Two-Cable-Stayed Bridge. *ASCE Journal of Engineering Mechanics Division* **105** pp 795–810

13. Carotti A, DeMiranda M and Turci E 1987 An Active Protection System for Wind Induced Vibrations on Pipeline Suspension Bridges. In Leipholz H H E (ed) *Structural Control* Martinus Nijhoff, Amsterdam pp 76–104
14. Prucz Z and Soong T T 1983 On Reliability and Active Control of Tension Leg Platforms. In Chen W F and Lewis A D M (eds) *Recent Advances in Engineering Mechanics and Their Impact on Civil Engineering Practice* **2** pp 903–6
15. Reinhorn A M, Soong T T and Manolis G D 1986 Disaster Prevention of Deep Water Offshore Structures by Means of Active Control. *Proceedings of ASME Fifth International OMAE Conference*, Tokyo, Japan pp 39–44
16. Reinhorn A M, Manolis G D and Wen C Y 1987 Active Control of Inelastic Structures. *ASCE Journal of Engineering Mechanics* **113** pp 315–33
17. Roorda J 1980 Experiments in Feedback Control of Structures. In Leipholz H H E (ed) *Structural Control* North Holland, Amsterdam pp 629–61
18. Soong T T, Reinhorn A M and Yang J N 1987 A Standardized Model for Structural Control Experiments and Some Experimental Results. In Leipholz H H E (ed) *Structural Control* Martinus Nijhoff, Amsterdam pp 669–93
19. Miller R S, Krawinkler H and Gere J M 1979 *Model Tests on Earthquake Simulator Development and Implementation of Experimental Procedures* Report No. 39, Dept. of Civil Engineering, Stanford University, CA
20. Moncarz P D and Krawinkler H 1981 *Theory and Application of Experimental Model Analysis in Earthquake Engineering* Report No. 50, Dept. of Civil Engineering, Stanford University, CA
21. Chung L L, Reinhorn A M and Soong T T 1986 An Experimental Study of Active Structural Control. In Hart G C and Nelson R B (eds) *Dynamic Response of Structures* ASCE, New York pp 795–802
22. Chung L L, Reinhorn A M and Soong T T 1988 Experiments on Active Control of Seismic Structures. *ASCE Journal of Engineering Mechanics* **114** pp 241–56
23. Soong T T, Reinhorn A M and Yang J N 1988 Active Response Control of Building Structures Under Seismic Excitation. *Proceedings of 9th World Conference on Earthquake Engineering* **VIII** pp 453–8 Tokyo/Kyoto, Japan
24. Chung L L, Lin R C, Soong T T and Reinhorn A M 1989 Experimental Study of Active Control for MDOF Seismic Structures. *ASCE Journal of Engineering Mechanics* **115** pp 1609–27
25. Rodellar J, Chung L L, Soong T T and Reinhorn A M 1989 Experimental Digital Predictive Control of Structures. *ASCE Journal of Engineering Mechanics* **115** pp 1245–61
26. Reinhorn A M, Soong T T et al 1989 Experiments on Active Structural Control Under Seismic Loads. In Nelson J K Jr (ed) *Computer Utilization in Structural Engineering* ASCE, New York pp 101–10
27. McNamara R J 1977 Tuned Mass Damper for Buildings. *ASCE Journal of Structural Division* **103** pp 1785–98
28. Petersen N R 1980 Design of Large Scale Tuned Mass Dampers. In Leipholz H H E (ed) *Structural Control* North Holland, Amsterdam pp 581–96
29. Tuned Mass Damper Steady Sway of Skyscraper in Wind. *Engineering News Record* pp 28–9 August 1977

30. Abdel-Rohman M 1984 Effectiveness of Active TMD for Building Control. *Transactions of the Canadian Society of Mechanical Engineers* **8** pp 179–84
31. Chang J C H and Soong T T 1980 Structural Control Using Active Tuned Mass Dampers. *ASCE Journal of Engineering Mechanics Division* **106** pp 1091–8
32. Hrovat D, Barak P and Robins M 1983 Semi-Active vs. Passive or Active Tuned Mass Dampers for Structural Control. *ASCE Journal of Engineering Mechanics* **109** pp 691–701
33. Lund R A 1980 Active Damping of Large Structures in Winds. In Leipholz H H E (ed) *Structural Control* North Holland, Amsterdam pp 459–70
34. Kuroiwa H and Aizawa S 1987 Private Communication, May 1987
35. Kobori T, Kanayama H and Kamagata S 1987 Dynamic Intelligent Building as Active Seismic Response Controlled Structure. *Proceedings of Annual Metting of the Architectural Institute of Japan* Tokyo
36. Kobori T, Kanayama H and Kamagata S 1988 A Proposal of New Anti-seismic Structure with Active Seismic Response Control System — Dynamic Intelligent Building. *Proceedings of 9th World Conference on Earthquake Engineering* **VIII** pp 465–70 Tokyo/Kyoto, Japan
37. Sae-Ung S and Yao J T P 1978 Active Control of Building Structures. *ASCE Journal of Engineering Mechanics Division* **104** pp 335–50
38. Wiesner K B 1986 The Role of Damping Systems. *Proceedings of 3rd International Conference on Tall Buildings* Chicago
39. Masri S F, Bekey G A and Caughey T K 1982 On-line Control of Nonlinear Flexible Structures. *ASME Journal of Applied Mechanics* **49** pp 877–84
40. Miller R K, Masri S F, Dehghanyar T J and Caughey T K 1988 Active Vibration Control of Large Civil Structures. *ASCE Journal of Engineering Mechanics* **114** pp 1542–70
41. Traina M I et al 1988 An Experimental Study of the Earthquake Response of Building Models Provided with Active Damping Devices. *Proceedings of 9th World Conference on Earthquake Engineering* **VIII** pp 447–52 Tokyo/Kyoto, Japan
42. Agababian Assoc 1984 *Validation of Pulse Techniques for the Simulation of Earthquake Motions in Civil Structures.* AA Report No R-7824-5489 El Segondo CA
43. Agababian Assoc 1984 *Induced Earthquake Motion in Civil Structures by Pulse Method.* AA Report No R-8428-5764 El Segondo CA
44. Dehghamyar T J, Masri S F, Miller R K and Caughey T K 1987 On-line Parameter Control of Nonlinear Flexible Structures. In Leipholz H H E (ed) *Structural Control* Martinus Nijhoff, Amsterdam pp 141–59
45. Klein R E, Cusano C and Slukel J V 1972 Investigation of a Method to Stabilize Wind Induced Oscillations in Large Structures. Paper No 72-WA/AUT-11, 1972 ASME Annual Meeting, New York
46. Klein R E and Salhi H 1980 Time Optimal Control of Wind Induced Structural Vibrations Using Active Appendages. In Leipholz H H E (ed) *Structural Control* North Holland, Amsterdam pp 415–30
47. Abdel-Rohman M 1984 Optimal Control of Tall Buildings by Appendages. *ASCE Journal of Structural Engineering* **110** pp 937–46

48. Chang J C H and Soong T T 1980 The Use of Aerodynamic Appendages for Tall Building Control. In Leipholz H H E (ed) *Structural Control* North Holland, Amsterdam pp 199–210
49. Soong T T and Skinner G T 1981 Experimental Study of Active Structural Control. *ASCE Journal of Engineering Mechanics Division* **107** pp 1057–68
50. Abdel-Rohman M and Al-Zanaidi M 1987 Design of Appendages for Tall Building Control. *ASCE Journal of Structural Engineering* **113** pp 397–408
51. Soong T T, Bilgutay A, Schmitz G and Ben-Arroyo A F 1984 Aesthetics of Tall Structures with Aerodynamic Appendages. In Ramaswamy S D and Tam C T (eds) *Tall Buildings* TBRC pp 37–41
52. Murata M and Ito N 1971 Suppression of Wind-Induced Vibration of a Suspension Bridge by Means of a Gyroscope. *Proceedings of International Conference on Wind Effects on Building Structure* Tokyo pp 1057–66
53. Sirlin S, Paliou C, Longman R W, Shinozuka M and Samara E 1986 Active Control of Floating Structures. *ASCE Journal of Engineering Mechanics* **112** pp 947–65
54. Abdel-Rohman M and Nayfeh A H 1987 Active Control of Nonlinear Oscillations in Bridges. *ASCE Journal of Engineering Mechanics* **113** pp 335–48
55. Kelly J M, Leitmann G and Soldatos A G 1987 Robust Control of Base-Isolated Structures Under Earthquake Excitations. *Journal of Optimization Theory and Applications* **53** pp 159–80
56. Reinhorn A M, Soong T T and Wen C Y 1987 Base Isolated Structures with Active Control. *Proceedings of ASME PVD Conference*, San Diego CA

6 Optimization of Actively Controlled Structures

Much of the discussion presented in the preceding chapters has been concerned with structures equipped with active control devices. While not explicitly stated, active structural control has been addressed on the premise that, given a conventionally designed structure, it is supplemented by an active control device which is activated whenever necessary in order to enhance structural safety and serviceability under extraordinary loads. Thus, the structure and the active control system are individually designed and optimized.

To extend this concept further, it is of practical interest to view an actively controlled structure as an integrated whole and consider its related optimization problems. This consideration has led to the concept of 'active structures',[1] and this topic is briefly explored in this chapter.

We shall define an active structure as one consisting of two types of load resisting members: the traditional static (or passive) members that are designed to support basic design loads, and the dynamic (or active) members whose function is to augment the structure's capability in resisting extraordinary dynamic loads. Their integration is done in an optimal fashion and produces a structure that is adaptive to changing environmental loads and usages. As one can see, an active structure is conceptually and physically different from a structure that is actively controlled. Rather than individualized optimization of structure and control systems as in the case of an actively controlled structure, an active structure is one whose active and passive components are integrated and simultaneously optimized to produce a new strain of structural system. This important difference makes the concept of active structures exciting and potentially revolutionary.

The earliest germs of such an idea appear to be contained in Kirseh[2] and Kirsch and Moses.[3] In this study, a continuous beam is actively controlled by allowing the redundant supports to settle vertically. Actually, there is a one-to-one correspondence between redundants and controllers. The objective is either reduction in magnitude of the internal forces or minimization of the cross-sectional area under a given loading condition. A flexibility method of analysis that satisfies compatibility and equilibrium is used. Explicit stress constraints are satisfied, and an objective function that penalizes

cross-sectional dimensions, internal forces, and redundants is minimized. The basic limitation of their work is that it is a static approach.

Some aspects of simultaneous optimization of structure and control system have been considered in the design of space structures. In the work of Haftka *et al*,[4,5] the central thesis is that small changes in the configuration of a structure result in nontrivial changes in the control force requirements. The focus of their work, however, is on the sensitivity of control requirements for spacecraft to inadvertent variations in the spacecraft's dimensions. Nevertheless, they convincingly show that the magnitude of the control forces in a system that has been optimized can be substantially reduced either by minor changes in the thickness of key structural components or by adding small lumped masses to key locations.

The objective of this chapter is to lay down comprehensively the foundations of active structures so that this novel subject can be rigorously explored.[1,7] We begin by using two examples to demonstrate that the theory behind active structures is sound and that it can lead to truly optimal structures.

Example 6.1 Can substantial changes in structural configuration be realized by allowing some members of a structure to become active? To answer this question, consider first the design of a simple steel frame supporting a static load and subject to a horizontal base acceleration $\ddot{x}_0(t)$, as shown in Fig. 6.1(a). The frame consists of four identical columns with two sets of pretensioned diagonal tendons; it has dimensions $L = 48.0$ in, $h = 40.0$ in, and its mass $m = 16.70$ slugs.

Case A — passive structure: Consider first the case of determining k_p, the stiffness in the columns, necessary to limit the relative displacement $x(t)$ to $x_{lim} = 0.06$ in when

$$\ddot{x}_0(t) = 0.2g\sin 5\pi t \tag{6.1}$$

The equation of motion is

$$m\ddot{x}(t) + c\dot{x}(t) + k_p x(t) = -m\ddot{x}_0(t) \tag{6.2}$$

By taking a damping coefficient that corresponds to a damping factor of 1.24%, it is easy to show that the design value for k_p is equal to 32 667 lb/in. It is noted that the required stiffness k_s, simply for supporting the static load, is

$$k_s = 0.0006k_p \tag{6.3}$$

Case B — active structure: Consider now possible reduction in k_p by making the diagonal tendons active members while maintaining the original performance level. Both mass and damping remain unchanged. Active

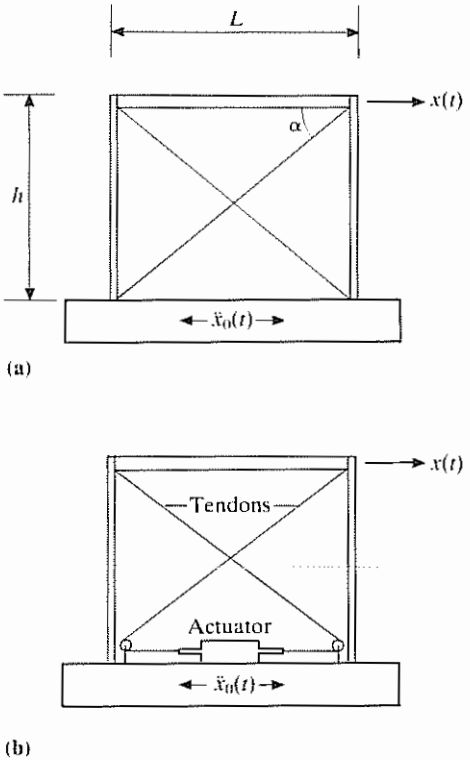

Figure 6.1 Passive and active steel frames under ground motions (a) passive; (b) active[1]

tendons imply that forces in the tendons can be generated and controlled by means of an external energy supply such as an electrohydraulic actuator. A possible structure configuration is shown in Fig. 6.1(b).

For the active structure, the equation of motion becomes

$$m\ddot{x}(t) + c\dot{x}(t) + k_a x(t) = -m\ddot{x}_0(t) - 4u(t)\cos\alpha \qquad (6.4)$$

where k_a is achievable stiffness in the columns of the active structure; and $u(t)$ is the control force in each tendon, which can be determined by using one of the control algorithms discussed in Chapter 3. For example, employing classical open-loop optimal control, Fig. 6.2 shows the value of k_a as a function of achievable maximum $|x(t)|$ and of corresponding required maximum $|u(t)|$. These results show that, without exceeding x_{lim}, the column stiffness can be reduced to an arbitrarily low level provided that the required control force is realizable. In particular, Fig. 6.2 shows that it is possible to fix k_a at a value equal to k_s for the passive case, while the dynamic requirements are satisfied entirely through activation of the tendons. In this particular case,

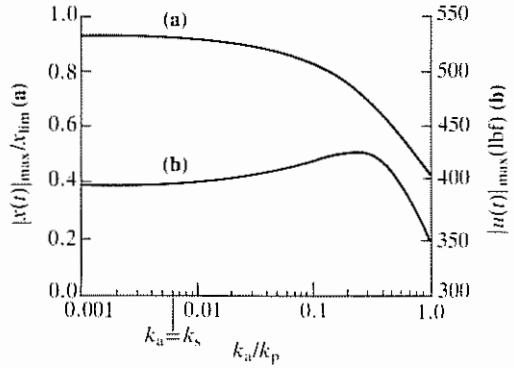

Figure 6.2 Normalized maximum displacement and maximum control force versus normalized structural stiffness[1]

the maximum $|u(t)|$ is 398 lb, and its time-dependent behaviour is shown in Fig. 6.3.

Example 6.2 An analysis of active control of cable-stayed bridges is given in Yang and Giannopoulos.[8,9] Some of the results presented in this study can be discussed in the context of active structures.

Case A — passive structure: As a more realistic example, consider the Sitka Harbor Bridge at Sitka, Alaska as the base passive structure. Design information on this suspension bridge[8,9] gives the fundamental natural frequency in flexure $\omega_g = 5.083$ rad/sec, the fundamental natural frequency in rotation $\omega_t = 8.589$ rad/sec, and the critical wind speed $\bar{u}_f = 155.5$ mph. For simplicity, the critical wind speed is considered here as the performance

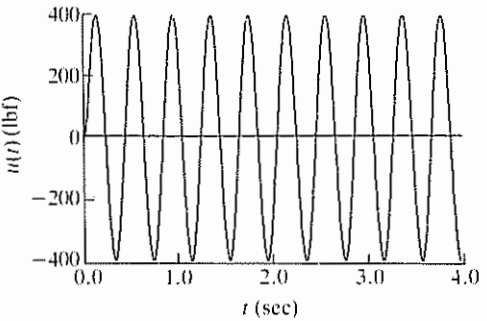

Figure 6.3 Control force in Example 6.1[1]

criterion. Wind speeds higher than the critical will cause aerodynamic instability in the bridge.

Case B — active structure: It is of interest to ask whether the value of $\bar{u}_f$ can be maintained or surpassed using a less conservative design when the existing suspension cables operate in an active mode. Specifically, a reduction in stiffness is considered in terms of a reduction in both the flexural and torsional frequencies. The reduced frequencies are now $\omega_g = 3.365$ rad/sec and $\omega_f = 5.686$ rad/sec. It is mentioned that the ratio ω_g/ω_f remains the same as before, i.e. $\omega_g/\omega_f = 0.60$.

As a possible configuration for active tendons, the bridge cables can be connected to electrohydraulic servomechanisms located at the points of anchorage. One transducer is installed at each anchorage point to sense the motion at that point. The sensed motion, in the form of electric voltage, is used to regulate the motion of a hydraulic ram, thus generating the required control force in each cable. For this configuration, the ram displacement $s(t)$ is related to the feedback voltage $v(t)$ by

$$\dot{s}(t) + R_1 s(t) = \frac{R_1 v(t)}{R} \tag{6.5}$$

where R_1 is the loop gain; and R is the feedback gain of the servomechanisms. The feedback voltage $v(t)$ is in turn proportional to the sensed motion. Suppose that the sensed motion is the flexure velocity $\dot{w}(t)$ at the anchorage. We then have

$$v(t) = p\dot{w}(t) \tag{6.6}$$

Let the two nondimensional control parameters be defined by

$$\varepsilon = \frac{R_1}{\omega_f}$$

and

$$\tau = \frac{p\omega_f^2}{R}$$

The critical wind speed $\bar{u}_f$ for the active structure thus becomes a function of ε and τ; the results are shown in Fig. 6.4. The case of $\varepsilon = 0$ corresponds to the passive structure. It is observed that the value of $\bar{u}_f$ increases as ε and τ increase, and this increase can be rather dramatic when certain values of ε and τ are chosen. Indeed, the critical wind speed for the active structure can be raised to any desirable level provided that the required control forces are realizable.

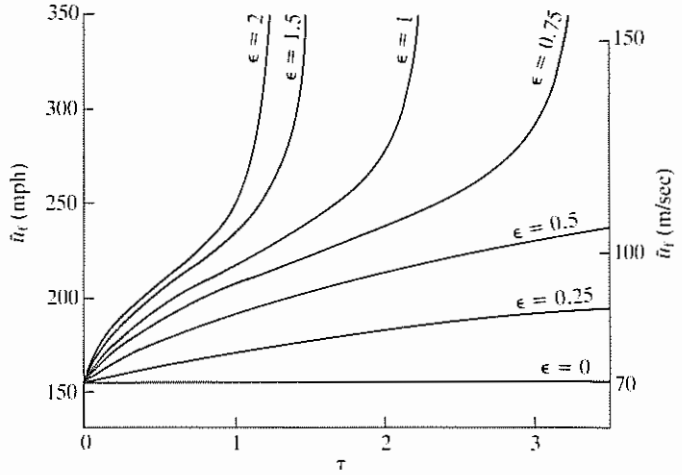

Figure 6.4 Critical wind velocity for active cable-stayed bridge[1]

6.1 Basic Equations

The basic state-space equation governing the optimal design of an active structure is again described by Eqs (3.1). However, it is now written in the form

$$\dot{z}(t) = A(\xi)z(t) + B(\xi)u(t) + H(\xi)f(t), \quad z(0) = z_0 \tag{6.7}$$

in which the structural parameters to be simultaneously optimized, denoted by ξ, are explicitly shown. In the above, $z(t)$ is defined as before by

$$z(t) = \begin{bmatrix} x(t) \\ \dot{x}(t) \end{bmatrix} \tag{6.8}$$

and [see Eqs (3.3) and (3.4)]

$$A(\xi) = \begin{bmatrix} \mathbf{0} & I \\ -M^{-1}(\xi)K(\xi) & -M^{-1}(\xi)C(\xi) \end{bmatrix} \tag{6.9}$$

$$B(\xi) = \begin{bmatrix} \mathbf{0} \\ M^{-1}(\xi)D(\xi) \end{bmatrix} \tag{6.10}$$

$$H(\xi) = \begin{bmatrix} \mathbf{0} \\ M^{-1}(\xi)E(\xi) \end{bmatrix} \tag{6.11}$$

The basic problem of active structural design is to determine ξ and $u(t)$ such that an appropriate objective functional is minimized. Following

classical quadratic performance criteria, for example, the performance index function J can be written in the form

$$J(z, \xi, u) = \int_0^{t_f} [z^T Q z + u^T R u + W(\xi)] \mathrm{d}t \tag{6.12}$$

where $W(\xi)$ represents a non-negative cost function depending on ξ but not on t in general. The matrices Q and R are the usual weighting matrices with appropriate dimensions. The structural parameter vector ξ satisfies

$$\xi \geqslant \xi_s \tag{6.13}$$

in which ξ_s represents values of the structural parameters corresponding to the base passive structure.

Extremization of the performance index function J given by Eq. (6.12) subject to the constraining Eqs (6.7) and (6.13) can be accomplished through the use of variational calculus. First, it will be noticed that the inequality constraints are simple enough to be handled explicitly. The differential equation constraint is included by forming a Lagrangian functional J^* as

$$J^*(z, \xi, u) = \int_0^{t_f} \{z^T Q z + u^T R u + W(\xi) + \lambda(t)[A(\xi)z(t) + B(\xi)u(t) + H(\xi)f(t) - \dot{z}(t)]\} \mathrm{d}t \tag{6.14}$$

where $\lambda(t)$ is the Lagrange vector multiplier. Note that the constraint has been integrated over time.

The conditions for minimizing J^* are

$$\delta^{(1)} J^* = 0 \tag{6.15}$$

$$\delta^{(2)} J^* > 0 \tag{6.16}$$

where $\delta^{(1)}$ and $\delta^{(2)}$ are, respectively, first and second variations. It is mathematically very difficult to ensure satisfaction of the condition on the second variation $\delta^{(2)}$. It can, however, be satisfied by arguing on physical grounds. Since Eq. (6.12) essentially is a composite quadratic performance index that contains a minimum error criterion, a minimum energy criterion and a minimum cost criterion, the first variation $\delta^{(1)}$ is with respect to z, u, and ξ. The Lagrange multiplier is also allowed to vary. Instead, the equation of motion (Eq. 6.7) must be retained. Taking the first variation of the Lagrangian functional results in

$$\delta^{(1)} J^* = \int_0^{t_f} \{2(\delta z^T Q z + \delta u^T R u) + \lambda^T (A\delta z + B\delta u - \delta \dot{z}) + \nabla_\xi W \delta\xi + \lambda^T (\nabla_\xi A z + \nabla_\xi B u + \nabla_\xi H f)\delta\xi + (Az + Bu + Hf - \dot{z})\delta\lambda\} \mathrm{d}t \tag{6.17}$$

In the above, ∇_ξ is a gradient operator with respect to the parameter vector ξ. Integrating the $\lambda^T \delta \dot{z}$ term by parts and rearranging, Eq. (6.17) gives

$$\int_0^{t_f} \{\delta z^T (2Qz + A^T\lambda + \dot{\lambda}) + \delta u^T (2Ru + B^T\lambda) + [\lambda^T(\nabla_\xi A z + \nabla_\xi B u + \nabla_\xi H f) + \nabla_\xi W]\delta\xi + (Az + Bu + Hf - \dot{z})\delta\lambda\}\,dt + \lambda^T \delta z\Big|_0^{t_f} = 0 \tag{6.18}$$

where the symmetry of M, C, and K has been taken into account. Since the variations in z, u, and ξ can take place independently of each other and in order to satisfy the necessary condition for minimizing J^*, i.e. $\delta J^* = 0$, we have the following system of equations:

$$\left.\begin{aligned} &Az + Bu + Hf - \dot{z} = 0, \quad z(0) = 0 \\ &2Qz + A^T\lambda + \dot{\lambda} = 0, \quad \lambda(t_f) = 0 \\ &2Ru + B^T\lambda = 0 \\ &\lambda^T(\nabla_\xi A z + \nabla_\xi B u + \nabla_\xi H f) + \nabla_\xi W = 0 \end{aligned}\right\} \tag{6.19}$$

over the time period $(0, t_f)$. The equations above represent a system of differential equations with four unknowns, namely, $z(t)$, $u(t)$, ξ, and $\lambda(t)$. Their solution determines the optimal configuration for the active structure.

6.2 Solution Procedure

Equations (6.19) represent, in general, a system of coupled nonlinear equations. Note that this nonlinearity is present even when the equations of motion represent linear elastic response, as is assumed here. (Material and/or geometric nonlinearities may be included, however, at the expense of making the system of equations computationally more involved.) Due to the complex nature of these equations, numerical techniques are usually required to obtain a solution.

An iterative sequential search procedure is studied[10] in which, at each iteration, the structural parameters are held constant until the performance index defined by Eq. (6.12) is minimized. The structural parameter values are then altered and the process is repeated until the global optimum is achieved. It is clear that, in terms of efficiency and convergence properties, a more desirable procedure is one in which the controller parameters and the structural parameters are optimized simultaneously. Simultaneous search procedures work in the full design space and update the structural and controller parameters simultaneously towards the final optimum design. Hence, these procedures not only can deal with high dimensional spaces with

fast convergence rates, but they may also avoid possible degeneracy into sub-spaces caused by sequential search methods.

Starting from prescribed initial values, the structural and controller parameters are updated at the kth iteration by ($k = 0, 1, 2, \ldots$)

$$\left.\begin{aligned} \xi^{k+1} &= \xi^k + \alpha^k d_\xi^k \\ u_t^{k+1} &= u_t^k + \alpha^k d_u^k \end{aligned}\right\} \tag{6.20}$$

In the above, d_ξ^k and d_u^k denote search directions in the scalar space and the functional space, respectively, whereas α^k is a unified scalar amplitude for both updating formulae and is selected so that the objective functional (Eq. 6.12) decreases with α^k along the search directions.

The search directions can be determined by, for example, the use of the conjugate gradient method.[11] In this case, the search direction calculations are based only upon the gradient information provided by

$$d^k = \nabla J^{*k} + \frac{\| \nabla J^{*k} \|^2}{\| \nabla J^{*k-1} \|^2} \nabla J^{*k-1} \tag{6.21}$$

The algorithm following this approach proceeds as follows:

1 Select initial values u_0 and ξ_0.
2 Solve the state and co-state equations (the first two of Eqs 6.19) for z^k and λ^k, $k = 0, 1, \ldots$.
3 Calculate the gradient with respect to u and ξ using

$$\nabla_u J_t^{*k} = \nabla_u \mathcal{H}(u^k, \xi^k, z^k, \lambda^k, t)$$

$$\nabla_\xi J^{*k} = \int_0^{t_f} \nabla_\xi \mathcal{H}(u^k, \xi^k, z^k, \lambda^k, \tau) \mathrm{d}\tau$$

where

$$\mathcal{H} = z^{\mathrm{T}} Q z + u^{\mathrm{T}} R u + W(\xi) + \lambda^{\mathrm{T}} [A(\xi) z + B(\xi) u + H(\xi) f]$$

4 Calculate the search directions, for $k \geqslant 1$,

$$d_u^k = -\nabla_u J_t^{*k} + \frac{\| \nabla J^{*k} \|^2}{\| \nabla J^{*k-1} \|^2} \nabla_u J_t^{*k-1}$$

$$d_\xi^k = -\nabla_\xi J^{*k} + \frac{\| \nabla J^{*k} \|^2}{\| \nabla J^{*k-1} \|^2} \nabla_\xi J^{*k-1}$$

and, for $k = 0$,

$$d_u^0 = -\nabla_u J_t^{*0}$$

$$d_\xi^0 = -\nabla_\xi J^{*0}$$

where

$$\|\nabla J^*\|^2 = (\nabla_\xi J^*)^T \nabla_\xi J^* + \|\nabla_u J^*\|^2$$

and

$$\|\nabla_u J^*\|^2 = \int_0^{t_f} (\nabla_u J_\tau^*)^T \nabla_u J_\tau^* \, d\tau$$

5 Update u and ξ by using Eqs (6.20).
6 Repeat steps 2–5 until Eqs (6.19) are satisfied with prescribed accuracy.

In the above, the state equation, the first of Eqs (6.19), and the costate equation, the second of Eqs (6.19), can be numerically integrated using, for example, Newmark's beta method[12] and Galerkin's two-point recurrence method,[13] respectively. The quadratic performance index, Eq. (6.12), can be integrated using similar procedures.

Unlike the sequential search procedure, where structural optimization is performed followed by control force optimization, the simultaneous procedure described here directs the solution towards a single final optimum design. Consequently, only one global optimization is performed. Furthermore, this procedure is not limited to linear structural behaviour or linear control laws.

Let us now look at some examples.

Example 6.3 Consider again the steel frame studied in Example 6.1. If the frame is modelled as a single-degree-of-freedom shear building, and if it is assumed that the columns are of rectangular cross section with base b, equalling twice the depth, then the stiffness k, mass m, and damping c can be expressed as

$$k = 32Eb^4/L^3$$

$$m = 8\rho Lb^2 + 16.52$$

$$c = 2\zeta m\sqrt{k/m}$$

where E is the elastic modulus, taken as 29×10^6 psi and ρ is the density, taken as 7.35×10^{-4} lb $-$ s^2/in^4. The damping ratio, ζ, is taken as 1.24%.

If one considers the base structure to be that which is just capable of supporting the static loads without assistance of the active members, then it is readily verified that, for a buckling mode of failure, the minimum structural parameter b is 0.34 in.

Consider now the structure with active tendons in place. For a support acceleration of

$$\ddot{x}_0(t) = 0.15g \sin 4\pi t, \tag{6.22}$$

the equation of motion has the form of Eq. (6.4). The time domain of interest is chosen to be 2 seconds with a step size of 0.005 sec and integration parameters of 1/6 for β and 1/3 for θ, where β and θ are the integration parameters for Newmark's beta method and Galerkin's method, respectively. The weighting matrices should be carefully chosen to reflect proper balance between the controlled response, input energy and structural weight (cost). If at all possible, the weights should reflect some physical parameter of the structure. In this example, the weight for the displacement response and the required control displacement are chosen to be proportional to the system stiffness. In particular, they are 3967 and 7934 for the displacement and control, respectively. For the velocity weight, a value of 16.52 is used which is proportional to the structure's dead mass. Note that these values have been chosen arbitrarily, consequently the minimum will be somewhat subjective.

Figure 6.5 shows the performance index versus the structural parameter b for both the active and passive systems. The active system is minimized when $b = 1.05$ in and PI (performance index) $= 124.15$ while the passive system is minimized when $b = 1.10$ in and PI $= 131.92$. For values of b in the range from 0.34 in to 1.4 in, it is clear from the reduced performance index that the active structure (active members and passive members) is superior to an equivalent passive structure (passive members only). As b is increased above 1.40 in, the required control force approaches zero. Clearly, no benefit is gained from having the active members in this range. Figure 6.6 shows the displacement response for the optimum b of 1.05 in. It is noted that the active members successfully reduce the response. The required control force in the tendons is shown in Fig. 6.7. Note that the stipulation on the final condition

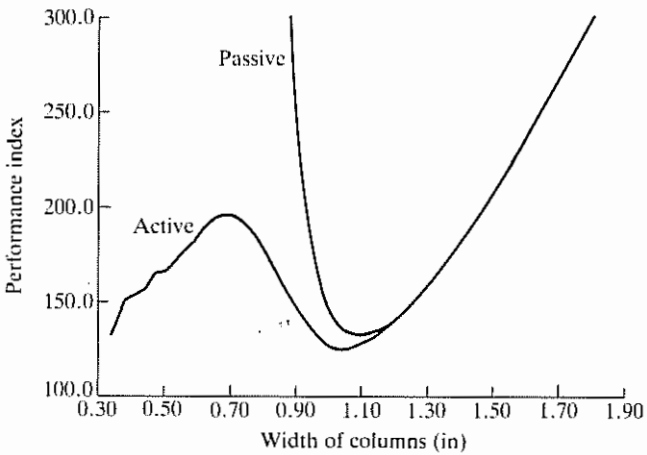

Figure 6.5 Performance index for steel frame[7]

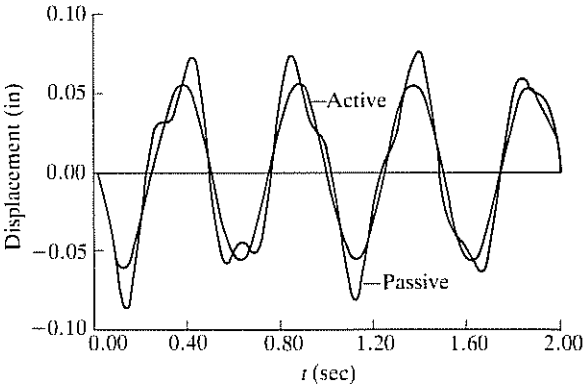

Figure 6.6 Displacement of steel frame[7]

of the co-state equation requires that the control force be driven to zero at the end of the time domain.

Example 6.4 In the preceding example, a relatively simple case with only one degree of freedom was considered. In what follows, a somewhat more realistic structure is investigated. Consider the king-post beam of Fig. 6.8. The two king-posts, serving as active members, are located along the beam and are capable of applying point forces directly to the beam. Sufficient pre-tensioning of the cables is assumed to allow both upward and downward control forces. A moving load of constant magnitude $p(x)$ and velocity $v(t)$ is applied to the beam.

The governing partial differential equation of motion is

$$EI\frac{\partial^4 y(x,t)}{\partial x^4}+\rho A\frac{\partial^2 y(x,t)}{\partial t^2}=p(x)+Du(t) \tag{6.23}$$

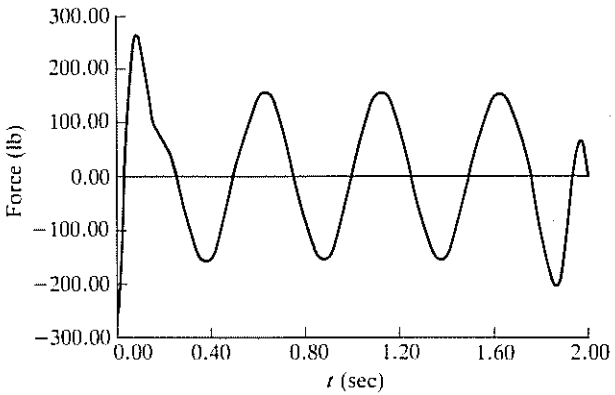

Figure 6.7 Control force in Example 6.3[7]

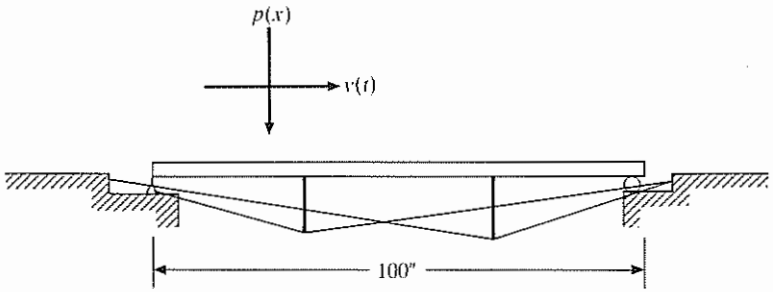

Figure 6.8 The king-post beam[7]

where EI is the flexural rigidity and ρA is the mass per unit length. Assuming that

$$y(x, t) = \sum_{i=1}^{\infty} \phi_i(x)\eta_i(t) \tag{6.24}$$

where ϕ_i are the mode shapes, Eq. (6.23) is transformed into an infinite number of second-order differential equations. The ith equation is expressed as

$$\ddot{\eta}_i + \omega_i^2 \eta_i = p_i + d_i u_i \tag{6.25}$$

where p_i and $d_i u_i$ are the modal counterparts of $p(x)$ and $Du(t)$. The natural frequency ω_i and the mode shape ϕ_i are given by

$$\omega_i = \left(\frac{\pi i}{L}\right)^2 \sqrt{EI/\rho A}$$

$$\phi_i = \sin\left(\frac{i\pi x}{L}\right)$$

Unfortunately, closed form solutions to the transformed equations of motion are not possible since the time variation of the control force is unknown a priori. By considering linear elastic response, however, the solution can be separated into two parts: (a) moving load solution, and (b) control force solution, with superposition of the two providing the total response. A closed form solution to the moving load is given in Timoshenko and Young.[14] So the problem is now reduced to finding the response due to the control force.

In practice, it is common to use only a finite number of modes when calculating the dynamic response. Letting n equal the number of modelled modes and m equal the number of independent control forces, we can define three classes of control: (a) $n < m$, (b) $n > m$, and (c) $n = m$. In the last case, the equations of motion can be written as n independent modal equations,

each with its own modal control force. Transformation from modal forces to physical forces is direct due to the one-to-one correspondence between n and m. As shown in Section 3.4, such an approach is referred to as independent modal space control (IMSC). Of the remaining two, case (a) is not considered here for essentially economic reasons, that is, the general trend is to have fewer control forces than modelled modes. Therefore, case (b) is the focus of this example. Since we are considering fewer control forces than modes, the transformation from modal to physical control forces involves the pseudo-inverse of an $n \times m$ matrix. This implies that the physical control forces may contain errors that lead to system degradation.[15] To avoid this problem, the control force vector is not transformed into modal space. Instead, the $m \times 1$ physical control vector is multiplied by the $n \times m$ modal participation matrix. The resulting modal differential equations of motion are externally coupled by the physical control force vector. The only requirement on the control force vector is that the system must be rendered controllable.

For the numerical analysis, the first five modes are considered. The integration parameters, β and θ, are taken as 1/6 and 1/3, respectively. Four hundred time steps each of duration 0.0005 sec are used. The moving load has a constant magnitude of 1000 lb and a horizontal velocity of 500 in/sec. The material and cross-sectional properties of the beam are the same as those used in Example 6.3. The weights for the performance index are chosen as follows: 5000 for displacements (all modes), zero for velocities (all modes) and 1000 for control forces (for each king-post).

In an effort to demonstrate both the optimal search method and the concept of an active structure, the king-post example is now investigated through a number of different cases. Specifically, the following four cases are identified.

Case 1: The structure is passive. The only design parameter considered is the beam width, b, subjected to the simple bounds:

$$0.10 \text{ in} \leqslant b \leqslant 10.0 \text{ in}$$

Case 2: Two active members (i.e. king-posts) located at $x/L = 0.30$ and 0.70, as well as the beam width are the design variables. The two active members are capable of generating both up and down control forces. No bounds are imposed on the magnitude of the control forces. The bounds on b are the same as in Case 1.

Case 3: Identical to Case 2 except that, along with the two active members and the width, the locations of the two active members are also considered as design variables. Hence, five design variables are considered with bounds on the active member locations specified by

$$x/L = 0.0 \leqslant XL \leqslant 1.00$$

$$x/L = 0.0 \leqslant XR \leqslant 1.00$$

Table 6.1 Performance comparisons

Case	PI	b (in)	y_{max} (in)	u_{max} (lb)	XL	XR	Iterations
1	145.23	1.45	−0.268	N/A	N/A	N/A	5
2	123.16	0.85	−0.108	608	0.30	0.70	27
3	102.44	0.93	−0.069	490	0.44	0.56	66
4	93.96	0.77	−0.036	496	Fig. 6.11	Fig. 6.11	87

which forces the two locations, XL for the left member and XR for the right, to be along the beam.

Case 4: In this variation, the effect of allowing the two active members to change position *with time* is considered. The simple bounds are identical to those of Case 3. Note that while this is a logical extension of the active structure concept, the realization of such a 'fully' active structure may be difficult.

The solutions to these four cases are obtained using the search procedure outlined above. The results are summarized in Table 6.1. The quantities listed in this table are the performance index (PI), the beam width (b), the maximum centreline deflection of the beam (y_{max}), the maximum control force (u_{max}), the active member location (XL and XR) and the number of iterations for convergence. Comparison of the centreline displacement response and required control force in the left king-post is shown in Figs 6.9 and 6.10, respectively. Also, the moving locations of the two king-posts for Case 4 are illustrated in Figs 6.11 and 6.12.

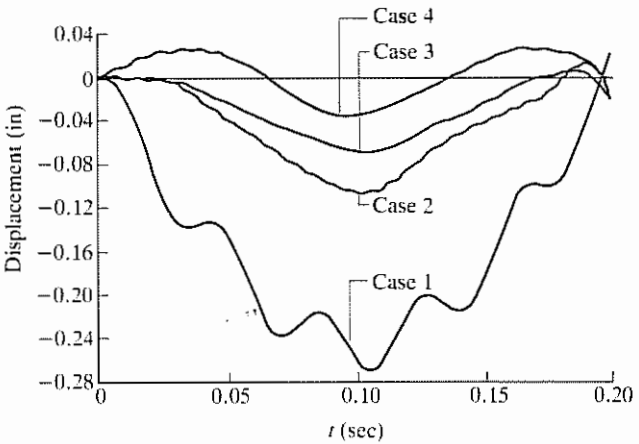

Figure 6.9 Maximum displacement of king-post beam[7]

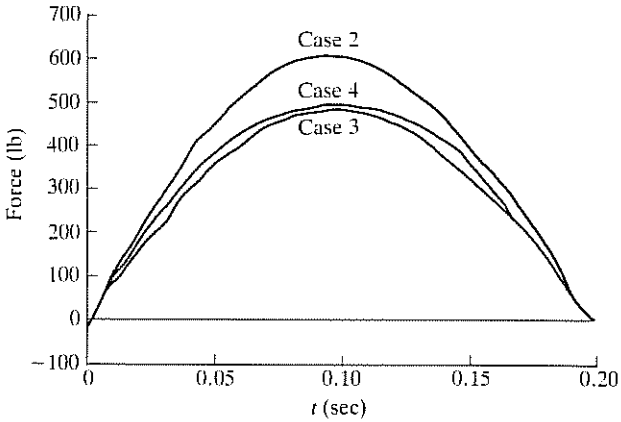

Figure 6.10 Maximum control force in Example 6.4[7]

It is seen from Table 6.1 and Figs 6.9 and 6.10 that Case 4, with a PI of 93.96, represents the optimum configuration of the king-post beam. This is expected since this case has the highest capacity to act as an active structure.

In closing, let us remark that, while a demonstration of active structure concept feasibility has been shown through examples, there are still many aspects that need to be examined. For instance, it is desirable to develop optimization procedures that not only allow time-dependent member characteristics but also time-varying structural configurations. Only then will they lead to truly optimal structures — optimal in geometry, in topology, and in utilization of material. Furthermore, critical comparisons between

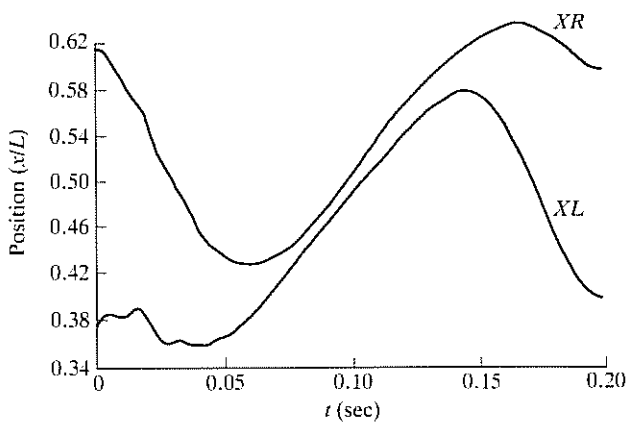

Figure 6.11 Location of active members in Case 4[7]

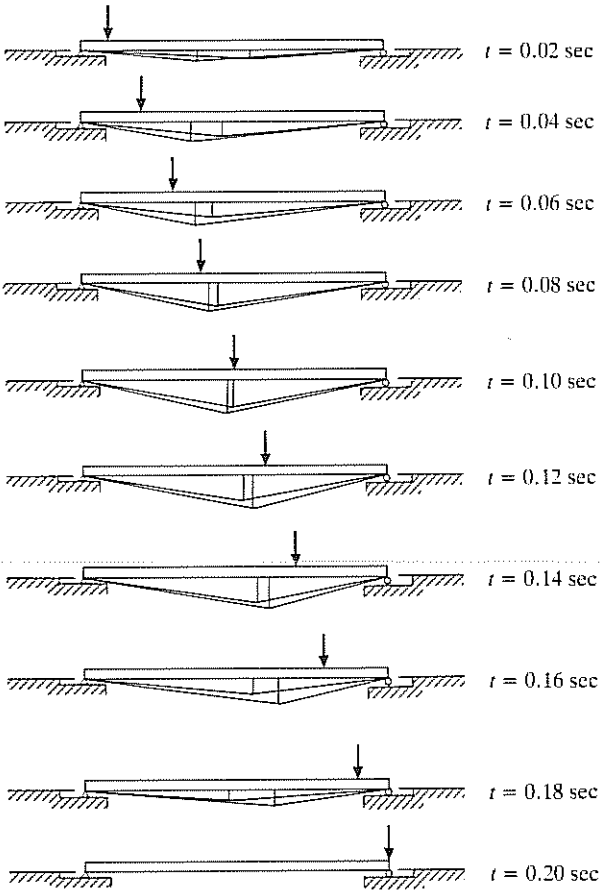

Figure 6.12 King-post configuration in Case 4[7]

active and traditional structures need to be carried out in order to establish the economic feasibility of active structures.

The concept of an active structure is a new and exciting one. Whether or not it can be implemented in the future depends to a great extent on parallel advances and successes in other technical areas, such as materials, electronics, and computers. Recent breakthroughs in all these areas are an encouraging sign and will help bring this concept closer to reality.

References

1. Soong T T and Manolis G D 1987 On Active Structures. *ASCE Journal of Structural Engineering* **113** pp 2290–301

2. Kirsch U 1976 Synthesis of Elastic Structures with Controlled Forces. *Computers and Structures* **6** pp 111–16
3. Kirsch U and Moses F 1977 Optimization of Structures with Control Forces and Displacements. *Engineering Optimization* **3** pp 37–44
4. Haftka R T, Martinovic Z N and Hallauer W L 1985 Enhanced Vibration Controllability by Minor Structural Modifications. *AIAA Journal* **23** pp 1260–66
5. Haftka R T et al 1986 Sensitivity of Optimized Control Systems to Minor Structural Modifications. *American Institute of Aeronautical Astronautics Paper No. 85-0801-CP* presented at AIAA/ASME/ASCE/AHS 26th Structures, Structural Dynamics, and Materials Conference, Orlando FL
6. Cheng F Y and Pantelides C P 1986 Optimal Control of Seismic Structures. In Hart G C and Nelson R B (eds) *Dynamic Response of Structures* ASCE, New York pp 764–71
7. Cha J Z, Pitarresi J M and Soong T T 1988 Optimal Design Procedures for Active Structures. *ASCE Journal of Structural Engineering* **114** pp 2710–23
8. Yang J N and Giannopoulos F 1979 Active Control and Stability of Cable-Stayed Bridge. *ASCE Journal of Engineering Mechanics Division* **105** pp 677–94
9. Yang J N and Giannopoulos F 1979 Active Control of Two-Cable-Stayed Bridge. *ASCE Journal of Engineering Mechanics Division* **105** pp 795–810
10. Soong T T and Pitarresi J M 1987 On Optimal Design of Active Structures. In Jenkins D R (ed) *Computer Applications in Structural Engineering* ASCE, New York pp 579–91
11. Fletcher R 1980 *Practical Methods of Optimization* Volume 1 John Wiley and Sons, New York, NY
12. Newmark N M 1959 A Method of Computation for Structural Dynamics. *ASCE Journal of Engineering Mechanics Division* **85** pp 67–94
13. Zienkiewicz O C 1977 *The Finite Element Method* 3rd edn McGraw-Hill, New York, NY
14. Timoshenko S and Young D H 1955 *Vibration Problems in Engineering* D. Van Nostrand Company Inc., Princeton, NJ
15. Meirovitch L, Barum M and Oz M 1983 A Comparison of Control Techniques for Large Flexible Systems. *Journal of Guidance, AIAA* 6 pp 302–10

Appendix A: Elements of Linear Control Systems

Summarized in this appendix are some basic results of modern control theory for linear systems with time-invariant parameters, on which much of the recent work on active structural control is based. Due to space limitation, the presentation is brief. The reader is referred to the general references cited at the end of this appendix for more details.

Most structural engineers are familiar with some of the results presented here in connection with structural dynamics. However, they may not be familiar with the *form* in which they are given. Indeed, the so-called state space approach in systems theory does not yet occupy a prominent place in structural dynamics. For our purposes, however, the state space approach is important because it is central to the development of modern control theory. Other advantages in using this approach include (a) adaptability to computer simulation and computation, (b) straightforward extensions from single input–single output to multiple input–multiple output systems and from low-order to high-order systems, and (c) easy generalization to more general system descriptions such as systems with time-varying parameters or stochastic systems.

Hence, we begin by introducing some results on the dynamics of linear systems using the state space formulation.

A.1 The State Equation

Central to the formulation and solution of a modern control problem is the so-called *state space* description of the underlying physical system. Many systems, including structural systems, can be described by a set of simultaneous first-order differential equations of the form

$$\dot{z}(t) = g(z(t), u(t), t) \tag{A.1}$$

where t is time, $z(t)$ is a time-varying vector denoting the *state* of the system and $u(t)$ is the *input* vector which represents externally applied forces and disturbances. In some cases, the input may be consciously controlled in an

effort to guide the behaviour of the system. In other cases, they may be fixed by the environment, but still retain an interpretation as input.

For linear systems with parameters which do not vary with time, Eq. (A.1) reduces to

$$\dot{z}(t) = Az(t) + Bu(t)$$

or simply

$$\dot{z} = Az + Bu \tag{A.2}$$

where A and B are constant matrices of appropriate dimensions.

Equation (A.2) represents the dynamics of a *time-invariant* linear system in the *state-space* form. Since most structural systems considered in this book are, when approximated by lumped-mass models, linear with time-invariant parameters, we consider only the linear time-invariant case in our development.

For many systems, the choice of the state vector z follows naturally from the physical structure as the following examples show.

Example A.1 Consider the horizontal translational vibration of a two-storey structure subjected to some lateral external excitation such as wind forces. Using a lumped-mass model as shown in Fig. A.1, the equations of motion in terms of $x_1(t)$ and $x_2(t)$, the horizontal displacements of the first and second floors, are

$$\left.\begin{aligned} &m_1\ddot{x}_1(t) + c_1\dot{x}_1(t) - c_2[\dot{x}_2(t) - \dot{x}_1(t)] + k_1x_1(t) \\ &\qquad - k_2[x_2(t) - x_1(t)] = u_1(t) \\ &m_2\ddot{x}_2(t) + c_2[\dot{x}_2(t) - \dot{x}_1(t)] + k_2[x_2(t) - x_1(t)] = u_2(t) \end{aligned}\right\} \tag{A.3}$$

where m_j, c_j and k_j are, respectively, the mass, damping and stiffness of the jth floor and $u_j(t)$ denotes the lateral force exerted on the jth floor.

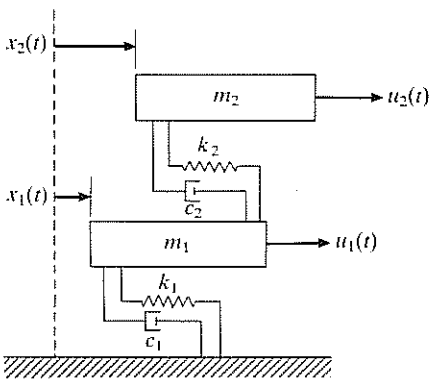

Figure A.1 An idealized two-storey structure

To write Eqs (A.3) in the state-space form, we set $\dot{x}_1(t) = y_1(t)$ and $\dot{x}_2(t) = y_2(t)$ and define the four dimensional state vector

$$z = \begin{bmatrix} x_1 \\ x_2 \\ y_1 \\ y_2 \end{bmatrix} \tag{A.4}$$

Equations (A.3) are now transformed into

$$\left.\begin{aligned} \dot{x}_1 &= y_1 \\ \dot{x}_2 &= y_2 \\ m_1\dot{y}_1 &= -c_1 y_1 + c_2(y_2 - y_1) - k_1 x_1 + k_2(x_2 - x_1) + u_1 \\ m_2\dot{y}_2 &= -c_2(y_2 - y_1) - k_2(x_2 - x_1) + u_2 \end{aligned}\right\} \tag{A.5}$$

In vector-matrix notation, they take the standard form of Eq. (A.2), i.e.

$$\dot{z} = Az + Bu \tag{A.6}$$

with

$$A = \begin{bmatrix} \mathbf{0}_2 & I_2 \\ K & C \end{bmatrix}, \qquad B = \begin{bmatrix} \mathbf{0}_2 \\ M^{-1} \end{bmatrix}, \qquad u = \begin{bmatrix} u_1 \\ u_2 \end{bmatrix} \tag{A.7}$$

where $\mathbf{0}_2$ is the 2×2 null matrix, I_2 is the 2×2 identity matrix,

$$K = \begin{bmatrix} -\dfrac{k_1 + k_2}{m_1} & \dfrac{k_2}{m_1} \\ \dfrac{k_2}{m_2} & -\dfrac{k_2}{m_2} \end{bmatrix} \tag{A.8}$$

$$C = \begin{bmatrix} -\dfrac{c_1 + c_2}{m_1} & \dfrac{c_2}{m_2} \\ \dfrac{c_2}{m_2} & -\dfrac{c_2}{m_2} \end{bmatrix} \tag{A.9}$$

$$M = \operatorname{diag}[m_1, m_2] \tag{A.10}$$

and M^{-1} denotes the inverse of M.

We see that extension to the case of an n-storey structure is straightforward using the similar lumped-mass approach. The state variable z in this example has a dimension of four; it is a $2n$-dimensional vector in the case of an n-storey structure.

As the next example shows, the components of a state vector need not represent physical displacements and velocities.

Example A.2 The deflection of a prismatic beam with flexural rigidity EI and mass density per unit length ρ is governed by the partial differential equation

$$\frac{\partial^4 y}{\partial x^4} + \frac{\rho}{EI}\frac{\partial^2 y}{\partial t^2} = \frac{1}{EI}w(x,t) \tag{A.11}$$

where $y(x,t)$ is the transverse displacement of a typical segment of the beam located at distance x from one end and $w(x,t)$ is the applied force distribution. Let us assume that

$$w(x,t) = \sum_{j=1}^{p} \delta(x - a_j)u_j(t) \tag{A.12}$$

where $\delta(\ )$ is the Dirac delta function. Thus, we have a system of p point forces exerted at points $a_j, j = 1, \ldots, p$, on the beam.

Using modal coordinates, it is well known that the solution to Eq. (A.11) can be represented by

$$y(x,t) = \sum_{j=1}^{n} \varphi_j(x)q_j(t) \tag{A.13}$$

where $q_j(t)$ are the modal amplitudes and $\varphi_j(x)$ are (normalized) mode shapes. While $n = \infty$ in theory, it is often assumed that the displacement $y(x,t)$ can be approximated with good fidelity by a truncated sum in which n is large but finite.

Form the $2n$-dimensional state vector

$$z = \begin{bmatrix} q_1 \\ \dot{q}_1 \\ \vdots \\ q_n \\ \dot{q}_n \end{bmatrix} \tag{A.14}$$

The substitution of Eqs. (A.12) and (A.13) into Eq. (A.11) leads to the state equation for the beam in the standard form

$$\dot{z} = Az + Bu \tag{A.15}$$

where the system matrix A is

$$A = \text{diag}[\Lambda_1, \Lambda_2, \ldots, \Lambda_n] \tag{A.16}$$

in which Λ_j is a 2×2 matrix of the form

$$\Lambda_j = \begin{bmatrix} 0 & 1 \\ -\omega_j^2 & 0 \end{bmatrix} \tag{A.17}$$

where $\omega_j^2 = j^4 \pi^4 EI/b^4 L$, L being the beam length;

$$\boldsymbol{B} = \begin{bmatrix} \boldsymbol{B}_1 \\ \boldsymbol{B}_2 \\ \vdots \\ \boldsymbol{B}_n \end{bmatrix} \tag{A.18}$$

where $\boldsymbol{B}_j$ is a $2 \times p$ matrix given by

$$\boldsymbol{B}_j = \frac{1}{EI} \begin{bmatrix} 0 & \cdots & 0 \\ \varphi_j(a_1) & \cdots & \varphi_j(a_p) \end{bmatrix} \tag{A.19}$$

and

$$\boldsymbol{u} = \begin{bmatrix} u_1 \\ \vdots \\ u_p \end{bmatrix} \tag{A.20}$$

It is seen in this example that the state vector z does not represent physical displacement or velocities but, with known mode shapes, the knowledge of z leads to a complete determination of $y(x,t)$ and hence the 'state of the system'. We have seen that this state-space representation is useful in structural modal control where certain critical modes are modified through the action of control forces.

A.2 Solution of the State Equation

Let us restrict ourselves to the linear time-invariant case and consider first the homogeneous equation

$$\dot{z} = Az \tag{A.21}$$

with initial condition

$$z(t_0) = z_0 \tag{A.22}$$

The solution to Eq. (A.21) always exists and it can be expressed as (see, for example the work by Zadeh and Desoer in the Bibliography)

$$z(t) = \Phi(t, t_0) z_0, \qquad t \geqslant t_0 \tag{A.23}$$

The *transition matrix* $\Phi(t, t_0)$ is the solution of the matrix differential equation

$$\dot{\Phi}(t, t_0) = A\Phi(t, t_0), \qquad \Phi(t_0, t_0) = I \tag{A.24}$$

which has the explicit form

$$\Phi(t, t_0) = \Phi(t - t_0) = e^{(t-t_0)A} = 1 + (t - t_0)A + \frac{1}{2!}[(t - t_0)A]^2 + \dots \tag{A.25}$$

This series converges for all A.

The elements of the transition matrix can be easily written down when the system matrix A is diagonalizable through a similarity transformation. The following result is useful (see, for example, the work by Noble in the Bibliography).

Theorem A.1 Let A be an $n \times n$ matrix having distinct eigenvalues λ_j, $j = 1, \dots, n$, and corresponding normalized eigenvectors η_j, $j = 1, \dots, n$, i.e.

$$\eta_j^T \eta_j = 1, \qquad j = 1, \dots, n \tag{A.26}$$

where the superscript T denotes vector or matrix transpose.

Define the $n \times n$ matrix T by

$$T = [\eta_1, \eta_2, \dots, \eta_n] \tag{A.27}$$

Then

$$A = T\Lambda T^{-1} \tag{A.28}$$

where Λ is the $n \times n$ diagonal matrix

$$\Lambda = \text{diag}[\lambda_1, \lambda_2, \dots, \lambda_n] \tag{A.29}$$

This result is useful because it allows us to write

$$\Phi(t - t_0) = e^{(t-t_0)A} = Te^{(t-t_0)\Lambda} T^{-1} \tag{A.30}$$

where

$$e^{(t-t_0)\Lambda} = \text{diag}[e^{(t-t_0)\lambda_1}, \dots, e^{(t-t_0)\lambda_n}] \tag{A.31}$$

Diagonalization is also possible when the transition matrix has multiple eigenvalues provided that the number of linearly independent eigenvectors for each eigenvalue is equal to its multiplicity. For more complicated cases, the transition matrix can be obtained through a reduction to the so-called Jordan form. We omit this discussion here since this situation is rare in dealing with structural systems.

Now, consider the state equation

$$\dot{z} = Az + Bu, \qquad z(t_0) = z_0 \tag{A.32}$$

If $u(t)$ is piecewise continuous for all t, we have

$$z(t) = \Phi(t - t_0)z_0 + \int_{t_0}^{t} \Phi(t - \tau)Bu(\tau)\,d\tau = e^{(t-t_0)A}z_0 + \int_{t_0}^{t} e^{(t-\tau)A}Bu(\tau)\,d\tau, \quad t \geqslant t_0 \tag{A.33}$$

This result can be easily verified by substituting it into Eq. (A.32) and with the aid of Eq. (A.25).

A.2.1 Impulse Response and Transfer Function Matrices

When $z_0 = \mathbf{0}$, Eq. (A.33) becomes

$$z(t) = \int_{t_0}^{t} K(t - \tau)u(\tau)\,d\tau, \qquad t \geqslant t_0 \tag{A.34}$$

where

$$K(t - \tau) = \Phi(t - \tau)B = e^{(t-\tau)A}B, \qquad t \geqslant \tau \tag{A.35}$$

is called the *impulse response matrix* of the system. It is seen from Eq. (A.34) that the ijth element of $K(t - \tau)$ corresponds to the response at time t of the ith component of the state vector to a unit impulse applied at the jth component of the input at time $\tau \geqslant t_0$, while all other components of the input vector and initial condition remain zero.

For linear time-invariant systems, it is often useful to seek solutions through Laplace transformation. Let

$$\mathscr{L}[z(t)] \equiv \int_{0}^{\infty} e^{-st}z(t)\,dt \equiv \bar{z}(s) \tag{A.36}$$

The Laplace transform of Eq. (A.32) leads to (with $t_0 = 0$)

$$\bar{z}(s) = (sI - A)^{-1}z(0) + (sI - A)^{-1}B\bar{u}(s) \tag{A.37}$$

When $z(0) = \mathbf{0}$, we have

$$\bar{z}(s) = H(s)\bar{u}(s) \tag{A.38}$$

where

$$H(s) = (sI - A)^{-1}B \tag{A.39}$$

is the *transfer matrix* of the system. It is noted that $H(s)$ and $K(t)$ for a given linear time-invariant system are Laplace transform pairs, i.e.

$$H(s) = \mathscr{L}[K(t)], \qquad K(t) = \mathscr{L}^{-1}[H(s)] \tag{A.40}$$

We also point out that $H(s)$ can be written in the form

$$H(s) = \frac{D(s)}{\mathrm{d}(s)} \tag{A.41}$$

where $D(s)$ is a matrix polynomial in s and

$$\mathrm{d}(s) = |sI - A| \tag{A.42}$$

is the characteristic polynomial of A if no cancellation occurs of factors of the form $s - \lambda_j$, where λ_j is an eigenvalue of A. The roots of $\mathrm{d}(s)$ are called the *poles* of the transfer function and they are the eigenvalues of A if no cancellation takes place.

A.2.2 Frequency Response Matrix

In the frequency domain, the response of a linear time-invariant system is characterized by the response to an input of the form

$$u(t) = ae^{j\omega t}, \qquad u(0) = 0, \qquad t \geqslant 0 \tag{A.43}$$

By direct substitution, a particular or steady-state solution of the state equation

$$\dot{z} = Az + Bu = Az + Bae^{j\omega t} \tag{A.44}$$

can be shown to be

$$z(t) = H(j\omega)ae^{j\omega t} \tag{A.45}$$

where

$$H(j\omega) = (j\omega I - A)^{-1}B \tag{A.46}$$

is the complex factor relating the response to the input and is called the *frequency response matrix* of the system. Equation (A.45) shows that, with $u(t)$ given by Eq. (A.43), the steady-state response $z(t)$ oscillates with the same frequency ω but in general with a change in amplitude and a phase shift.

Since inputs can in general be represented as a sum of sinusoidal terms and since the superposition principle applies in the linear case, the knowledge of the frequency response matrix leads directly to the solution to the state equation for linear time-invariant systems.

A comparison of Eq. (A.46) and Eq. (A.39) shows that $H(j\omega)$ is simply the transfer function $H(s)$ with s replaced by $j\omega$.

A.2.3 The Case of Stochastic Input

Since many of the system inputs in the study of structural control are stochastic in nature, we give in this section some results on the response of linear time-invariant systems to stochastic inputs. The reader is referred to the general references cited at the end of this appendix for a review of the fundamentals in stochastic processes and for details of the derivations of the results presented herein (see, for example, the works by Lin and Soong in the Bibliography).

In the linear time-invariant case, Eq. (A.33) gives the general solution representation which is also valid when the input vector $\boldsymbol{u}(t)$ is a stochastic vector process. Using capital letters to denote stochastic quantities (except $\boldsymbol{A}$ and $\boldsymbol{B}$), Eq. (A.33) can now be written as

$$\boldsymbol{Z}(t) = \mathrm{e}^{(t-t_0)\boldsymbol{A}}\boldsymbol{z}_0 + \int_{t_0}^{t} \boldsymbol{\Phi}(t-\tau)\boldsymbol{B}\boldsymbol{U}(\tau)\,\mathrm{d}\tau, \qquad t \geqslant t_0 \tag{A.47}$$

where $\boldsymbol{Z}(t)$, being a function of the stochastic vector process $\boldsymbol{U}(t)$, is also stochastic. We see that the first term on the right-hand side of Eq. (A.47) is at most a deterministic contribution to $\boldsymbol{Z}(t)$. For expediency, we shall assume $\boldsymbol{z}_0 = \boldsymbol{0}$ in what follows.

Let the mean and correlation function matrix of $\boldsymbol{U}(t)$ be denoted by, respectively,

$$\boldsymbol{m}_U(t) = E[\boldsymbol{U}(t)], \qquad \boldsymbol{R}_{UU}(s,t) = E[\boldsymbol{U}(s)\boldsymbol{U}^{\mathrm{T}}(t)] \tag{A.48}$$

We are primarily interested in the mean and correlation function matrix of the response $\boldsymbol{Z}(t)$.

Taking the expectation of Eq. (A.47) (with $\boldsymbol{z}_0 = \boldsymbol{0}$), we easily see that

$$\boldsymbol{m}_Z(t) \equiv E[\boldsymbol{Z}(t)] = \int_{t_0}^{t} \boldsymbol{\Phi}(t-\tau)\boldsymbol{B}\boldsymbol{m}_U(\tau)\,\mathrm{d}\tau, \qquad t \geqslant t_0 \tag{A.49}$$

The correlation function matrix $\boldsymbol{R}_{ZZ}(s,t)$ of $\boldsymbol{Z}(t)$ is found in a similar fashion. We have

$$\begin{aligned}
\boldsymbol{R}_{ZZ}(s,t) &\equiv E[\boldsymbol{Z}(s)\boldsymbol{Z}^{\mathrm{T}}(t)] \\
&= E\left\{\left[\int_{t_0}^{s} \boldsymbol{\Phi}(u-s)\boldsymbol{U}(u)\,\mathrm{d}u\right]\left[\int_{t_0}^{t} \boldsymbol{\Phi}(v-t)\boldsymbol{U}(v)\,\mathrm{d}v\right]^{\mathrm{T}}\right\} \\
&= \int_{t_0}^{t}\int_{t_0}^{s} \boldsymbol{\Phi}(u-s)\boldsymbol{R}_{UU}(u,v)\boldsymbol{\Phi}^{\mathrm{T}}(v-t)\,\mathrm{d}u\,\mathrm{d}v
\end{aligned} \tag{A.50}$$

Equations (A.49) and (A.50) show that the knowledge of the first two moments of $\boldsymbol{U}(t)$ leads to the determination of the first two moments of $\boldsymbol{Z}(t)$. In theory, the probability distribution of $\boldsymbol{Z}(t)$ can also be found in terms of the

probability distribution of $\boldsymbol{U}(t)$; this, however, is much more involved. A special case, however, is worth mentioning, namely, with $\boldsymbol{Z}(t)$ and $\boldsymbol{U}(t)$ related as given by Eq. (A.47), $\boldsymbol{Z}(t)$ is Gaussian if $\boldsymbol{U}(t)$ is Gaussian.

The integrals in Eqs (A.49) and (A.50) can be simplified somewhat when $\boldsymbol{U}(t)$ is second-order stationary. In this case, $\boldsymbol{m}_U(t)$ is a constant and

$$\boldsymbol{R}_{UU}(s,t)=\boldsymbol{R}_{UU}(t-s)$$

and, in particular, Eq. (A.50) with $t_0=-\infty$ (input applied at time $-\infty$) reduces to, after some change of variables,

$$\boldsymbol{R}_{ZZ}(t-s)=\int_0^\infty\int_0^\infty \boldsymbol{\Phi}(u)\boldsymbol{R}_{UU}(t-s+v-u)\boldsymbol{\Phi}^{\mathrm{T}}(v)\,\mathrm{d}u\,\mathrm{d}v \qquad \text{(A.51)}$$

which is also seen to be a function of $(t-s)$ only.

The second-order stationarity of the solution process $\boldsymbol{Z}(t)$ in this case implies the existence of its associated power spectral density. As we recall, the power spectral density $\boldsymbol{S}_{ZZ}(\omega)$ of a second-order stationary process is defined by

$$\boldsymbol{S}_{ZZ}(\omega)=\frac{1}{2\pi}\int_{-\infty}^{\infty}\mathrm{e}^{-j\omega\tau}\boldsymbol{R}_{ZZ}(\tau)\,\mathrm{d}\tau \qquad \text{(A.52)}$$

Applying this definition to Eq. (A.51), we obtain the following important result:

$$\boldsymbol{S}_{ZZ}(\omega)=\boldsymbol{H}^*(j\omega)\boldsymbol{S}_{UU}(\omega)\boldsymbol{H}^{\mathrm{T}}(j\omega) \qquad \text{(A.53)}$$

where $\boldsymbol{H}(j\omega)$ is the frequency response matrix of the system and $\boldsymbol{H}^*(j\omega)$ is its complex conjugate. Equation (A.53) gives a simple relation between the spectral density matrix of the input $\boldsymbol{U}(t)$ and that of the response $\boldsymbol{Z}(t)$. This simple input–output relationship is one of the primary reasons for the use of spectral densities in the analysis of linear time-invariant systems. We also note that the second moments of $\boldsymbol{Z}(t)$ can be computed from Eq. (A.53) by means of a single integral

$$\begin{aligned}E[\boldsymbol{Z}(t)\boldsymbol{Z}^{\mathrm{T}}(t)]\equiv\boldsymbol{R}_{ZZ}(0)&=\int_{-\infty}^{\infty}\boldsymbol{S}_{ZZ}(\omega)\,\mathrm{d}\omega\\&=\int_{-\infty}^{\infty}\boldsymbol{H}^*(j\omega)\boldsymbol{S}_{UU}(\omega)\boldsymbol{H}^{\mathrm{T}}(j\omega)\,\mathrm{d}\omega\end{aligned} \qquad \text{(A.54)}$$

A.3 Stability

Stability of a dynamic system pertains to, roughly stated, the boundedness to some degree of the solution of its state equation. It is one of the most

important performance qualities of a system in analysis and control. For our purposes, it is adequate to consider the homogeneous state equation of the form

$$\dot{z}(t) = Az(t), \qquad z(t_0) = z_0 \tag{A.55}$$

and consider its *equilibrium state* z_e. An equilibrium state of the system described by Eq. (A.55) is a solution satisfying

$$Az_e = \mathbf{0} \tag{A.56}$$

clearly, $z_e = \mathbf{0}$ is an equilibrium state in this case and is unique if A is nonsingular.

Definition An equilibrium system state z_e is said to be *stable* (in the sense of Lyapunov) if, for any t_0 and any $\varepsilon > 0$, there exists a real number $\delta(\varepsilon, t_0) > 0$ such that

$$\|z_0 - z_e\| \leqslant \delta$$

implies

$$\|z(t) - z_e\| < \varepsilon$$

for all $t \geqslant t_0$. If δ does not depend on t_0, the equilibrium state is said to be *uniformly stable.*

In the above, the Euclidean norm can be used for $\|z\|$, i.e.

$$\|z\| = \left[\sum_j z_j^2\right]^{1/2} \tag{A.57}$$

although other norms are also possible.

In words, the (Lyapunov) stability guarantees that the system state at any $t \geqslant t_0$ stays close to the equilibrium state by choosing the initial state close enough to the equilibrium state, a rather weak condition of boundedness. Stronger stability criteria are given below.

Definition An equilibrium system state z_e is *asymptotically stable* if it is stable and if, for any t_0, there is a $\delta > 0$ (possibly dependent on t_0) such that

$$\|z_0 - z_e\| \leqslant \delta$$

implies

$$\|z(t) - z_e\| \to 0$$

as $t \to \infty$. We see that, in addition to being stable, the solution in this case always converges to z_e when the initial condition is chosen close enough to the equilibrium state.

Definition An equilibrium system state z_e is *exponentially stable* if there exist real numbers $\alpha > 0$ and $\beta > 0$ such that

$$\|z(t) - z_e\| \leqslant \alpha e^{-\beta(t-t_0)} \|z_0\|, \qquad t \geqslant t_0$$

for every z_0. Thus, under exponential stability, the state converges to the equilibrium state in an exponential fashion independent of the initial condition.

We have thus far addressed stability of the equilibrium state. For linear systems, however, stability of the equilbrium state implies stability in any other solution. To see this, let $z(t)$ be any other solution of Eq. (A.55). Since both $z(t)$ and z_e satisfy Eq. (A.55), $z(t) - z_e$ is also a solution, i.e. it satisfies the state equation

$$\frac{d}{dt}(z - z_e) = A(z - z_e)$$

Hence, stability in z_e implies stability in any solution. For this reason, we consider *stability of the system* to be synonymous with stability of the equilibrium state. Furthermore, $z_e \equiv \mathbf{0}$.

Conditions for various forms of system stability can be easily established for linear time-invariant systems. As already shown in Section A.2, for a system described by Eq. (A.55) whose system matrix A has distinct eigenvalues λ_j and eigenvectors η_j, $j = 1, 2, \ldots$, the solution $z(t)$ can be written as

$$z(t) = \sum_j g_j e^{\lambda_j t} \eta_j \tag{A.58}$$

where g_j, $j = 1, 2, \ldots$, are scalars whose values are functions of z_0. Hence, the stability properties are determined by the eigenvalues λ_j: this is true also in the case where A is not diagonalizable. The following theorems are direct results of this observation and we omit their proofs.

Theorem A.3 (Stability) The linear time-invariant system given by Eq. (A.55) is stable if and only if (a) all eigenvalues of A have nonpositive real parts, and (b) to any eigenvalue of zero real part with multiplicity k there correspond exactly k linearly independent eigenvectors. Condition (b) is needed to ensure that no terms in the solution grow as $t, t^2, \ldots$.

Theorem A.4 (Asymptotic Stability) The linear time-invariant system given by Eq. (A.55) is asymptotically stable if and only if all eigenvalues of A have strictly negative real parts.

We easily see from Eq. (A.58) that, if a linear time-invariant system is asymptotically stable, it is exponentially stable. This result is formalized in the following theorem.

Theorem A.5 (Exponential Stability) The linear time-invariant system given by Eq. (A.55) is exponentially stable if and only if it is asymptotically stable.

A.4 Controllability and Observability

Due to various reasons, a dynamic system designed to perform in a certain fashion does not always do so in a completely satisfactory manner. As an example, the actual load supported by a structure may exceed the design load. Corrective actions are thus necessary sometimes and control theory offers one of the possible approaches to this end.

A *control system* is a dynamic system which, through the action of an external *manipulatable* input $\boldsymbol{u}(t)$, operates in a certain prescribed fashion as time evolves. In design and synthesis of control systems, it is fruitful to first pose a number of basic equations concerning their ability to perform as required. *Controllability* is concerned with the question of whether or not the state of a given system can be transferred from any given state to any other given state under the action of a control input. The important result given below is stated without proof, which can be found in most of the standard control texts.

Definition The linear time-invariant system

$$\dot{z}(t) = \boldsymbol{A}z(t) + \boldsymbol{B}u(t), \qquad z(t_0) = z_0 \tag{A.59}$$

is said to be *completely controllable* if, under the action of a piecewise continuous input $\boldsymbol{u}(t)$, $t_0 \leqslant t \leqslant t_1$, the state of the system can be brought from any z_0 at any t_0 to any terminal state z_1 at time t_1 within a finite time $t_1 - t_0$.

Theorem A.6 Let the dimension of $z(t)$ be n and the dimension of $\boldsymbol{u}(t)$ be m. Then the system (A.59) is completely controllable if and only if the $n \times nm$ matrix $\boldsymbol{P}$ defined by

$$\boldsymbol{P} = [\boldsymbol{B} \mid \boldsymbol{AB} \mid \cdots \mid \boldsymbol{A}^{n-1}\boldsymbol{B}] \tag{A.60}$$

has rank n.

The second question has to do with observability, namely, whether or not a system has the property that its state can be determined from the knowledge of the input and output information. We give the following definition.

Definition The linear time-invariant control system

$$\left.\begin{aligned} \dot{z}(t) &= \boldsymbol{A}z(t) + \boldsymbol{B}u(t), \qquad z(t_0) = z_0 \\ y(t) &= \boldsymbol{C}z(t) + \boldsymbol{D}u(t) \end{aligned}\right\} \tag{A.61}$$

is said to be *completely observable* if the knowledge of control input $u(t)$ and output $y(t)$ over a finite time interval $t_0 < t \leqslant t_1$ completely determines the state $z(t_1)$ for all t_1.

Theorem A.7 Let the dimensions of $z(t)$ and $y(t)$ be, respectively, n and r. Then the system (A.61) is completely observable if and only if the $rn \times n$ matrix Q defined by

$$Q = \begin{bmatrix} C \\ \hline CA \\ \hline \vdots \\ \hline CA^{n-1} \end{bmatrix} \tag{A.62}$$

has rank n.

Bibliography

The reader is referred to the following books for amplification and further reading.

Theory of Linear Systems

Luenberger D G 1979 *Introduction to Dynamic Systems* Wiley, NY

Noble B 1969 *Applied Linear Algebra* Prentice-Hall, Englewood Cliffs NJ

Polak E and Wong E 1970 *Notes for a First Course on Linear Systems* Van Norstrand, NY

Wiberg D W 1971 *State Space and Linear Systems* Schaum's Outline Series, McGraw-Hill, NY

Zadeh L A and Desoer C A 1963 *Linear System Theory: The State Space Approach* McGraw-Hill, NY

Stochastic Processes and Linear Systems

Crandall S H and Mark W D 1963 *Random Vibration in Mechanical Systems* Academic Press, NY

Dinca F and Teodosiu C 1973 *Nonlinear and Random Vibrations* Academic Press, NY

Lin Y K 1967 *Probabilistic Theory of Structural Dynamics* McGraw-Hill, NY
Papoulis A 1965 *Probability, Random Variables, and Stochastic Processes* McGraw-Hill, NY
Soong T T 1973 *Random Differential Equations in Science and Engineering* Academic Press, NY

Linear Control Systems

Anderson B D O and Moore J B 1971 *Linear Optimal Control* Prentice-Hall, Englewood Cliffs NJ
Athans M and Falb P L 1966 *Optimal Control* McGraw-Hill, NY
Bryson A E Jr and Ho Y C 1969 *Applied Optimal Control* Ginn Blaisdell, Waltham MA
Kwakernaak H and Sivan R 1972 *Linear Optimal Control Systems* Wiley, NY
Ogata K 1967 *State Space Analysis of Control Systems* Prentice-Hall, Englewood Cliffs NJ
Sage A P and White C C III 1977 *Optimum Systems Control 2nd edn* Prentice-Hall, Englewood Cliffs NJ
Wonham W M 1974 *Linear Multivariable Control* Lecture Notes in Economics and Mathematical Systems, Vol. 101, Springer-Verlag, NY

Appendix B: Conversion Table: English Units to SI Units

Appendix B Conversion table: English units to SI units

To convert from	To	Multiply by
Acceleration		
foot/second^2 (ft/sec^2)	metre/second^2 (m/sec^2)	3.048×10^{-1}*
inch/second^2 (in/sec^2)	metre/second^2 (m/sec^2)	2.54×10^{-2}*
Area		
foot^2 (ft^2)	metre^2 (m^2)	9.2903×10^{-2}
inch^2 (in^2)	metre^2 (m^2)	6.4516×10^{-4}*
Density		
pound mass/inch^3 (lbm/in^3)	kilogram/metre^3 (kg/m^3)	2.7680×10^4
pound mass/foot^3 (lbm/ft^3)	kilogram/metre^3 (kg/m^3)	1.6018×10
Energy, work		
British thermal unit (Btu)	joule (J)	1.0544×10^3
foot-pound force (ft-lbf)	joule (J)	1.3558
kilowatt-hour (kw-h)	joule (J)	3.60×10^6*
Force		
kip (1000 lbf)	newton (N)	4.4482×10^3
pound force (lbf)	newton (N)	4.4482
Length		
foot (ft)	metre (m)	3.048×10^{-1}*
inch (in)	metre (m)	2.54×10^{-2}*
Mass		
slug (lbf-sec^2/ft)	kilogram (kg)	1.4594×10
ton (2000 lbm)	kilogram (kg)	9.0718×10^2
Power		
foot-pound/minute (ft-lbf/min)	watt (W)	2.2597×10^{-2}
horsepower (550 ft-lbf/sec)	watt (W)	7.4570×10^2
Pressure, stress		
atmosphere (std) (14.7 lbf/in^2)	newton/metre^2 (N/m^2 or Pa)	1.0133×10^5
pound/inch^2 (lbf/in^2 or psi)	newton/metre^2 (N/m^2 or Pa)	6.8948×10^3
Velocity		
foot/minute (ft/min)	metre/second (m/sec)	5.08×10^{-3}*
foot/second (ft/sec)	metre/second (m/sec)	3.048×10^{-1}*
Viscosity		
foot^2/second (ft^2/sec)	metre^2/second (m^2/sec)	9.2903×10^{-2}
pound-mass/foot-second (lbm/ft-sec)	pascal-second (Pa-sec)	1.4882
pound-force-second/foot^2 (lbf-sec/ft^2)	pascal-second (Pa-sec)	4.788×10

* Exact value

Index